APOLLO

GUIDANCE AND NAVIGATION

Approved: Milton B. Trageser Date: 7/15/64
Milton B. Trageser, Director
Apollo Guidance and Navigation Program

Approved: Roger B. Woodbury Date: 8/1/64
Roger B. Woodbury, Deputy Director
Instrumentation Laboratory

R-446

(Unclassified Title)

PRIMARY G&N SYSTEM LUNAR ORBIT OPERATIONS

Vol. II of II

Edited by
Norman E. Sears

April 1964

[redacted] INSTRUMENTATION LABORATORY
CAMBRIDGE 39, MASSACHUSETTS

ACKNOWLEDGMENT

This report was prepared under DSR Project 55-191, sponsored by the Manned Spacecraft Center of the National Aeronautics and Space Administration through Contract NAS 9-153.

The following Space Guidance Analysis group personnel contributed to the preparation of this report.

D. S. Baker
R. D. Brown
G. W. Cherry
P. G. Felleman
R. D. Goss
E. S. Muller - Raytheon Resident Engineer
R. J. Phaneuf
N. E. Sears
R. L. White
J. B. Young

R-446

VOLUMES I AND II

PRIMARY G&N SYSTEM LUNAR ORBIT OPERATIONS

ABSTRACT

This report summarizes the primary G&N system operation and performance during the lunar orbit phases of the Apollo lunar landing mission. The lunar orbit phases include orbit navigation, descent, landing, surface operations, launch and ascent, rendezvous and LEM aborts. These phases are primarily concerned with the LEM primary G&N operation, but CSM operations of orbit navigation, LEM back-up guidance capability, and LEM retrieval are included. Each lunar orbit phase is described with respect to:

1) Primary G&N system objectives and operating modes.
2) Current guidance equations.
3) Typical trajectories.
4) Primary G&N performance and error analysis.

A general description and performance specification is included for the basic units of the primary G&N system.

Edited by

Norman E. Sears

April 1964

TABLE OF CONTENTS

VOLUME I OF II

TABLE OF CONTENTS (Cont)

TABLE OF CONTENTS (Cont)

TABLE OF CONTENTS (Cont)

TABLE OF CONTENTS (Cont)

TABLE OF CONTENTS (Cont)

VOLUME II OF II

CHAPTER 5

SURFACE AND PRELAUNCH OPERATIONS

5.1 General Objectives

This phase of the landing mission starts at terminal landing and touchdown when the LEM descent engine is shut down, and ends when the LEM ascent engine is ignited for the powered ascent phase. The time interval involved may vary between 6 to 24 hours, depending upon the mission plan and objectives. The primary G&N system objectives during this phase are as follows:

1. Update the CSM orbital parameters
2. Determine or update the LEM landing position
3. Determine an appropriate aim point on the CSM orbit for control of the launch and rendezvous phases
4. Determine three launch timing factors:
    a) Desired launch time for the direct ascent trajectory
    b) Latest launch time for the direct ascent trajectory
    c) Latest launch time for a parking orbit launch.

Under normal operations, when the powered ascent can be initiated within a determined launch window, direct ascent trajectories are used for the rendezvous phase (Chapter 7). A direct ascent is defined as a trajectory that would intercept the CSM after powered ascent injection assuming no errors. This is contrasted to a parking orbit operation which would involve injecting the LEM into an intermediate, or parking orbit, from which a transfer trajectory must be initiated to place the LEM on an intercept

course with respect to the CSM. The LEM primary G&N system has the capability of both direct ascent and parking orbit operations (Chapter 6). As mentioned above, direct ascents are used if launch timing can be achieved within a determined launch window. Launches after this interval will require parking orbit injection up to a point where the launch is rescheduled until the next CSM orbital pass.

5.2 Primary G&N Operations

After landing and engine cutoff, the LEM primary G&N system is maintained in an operating mode for some interval of time. This interval is presently undefined, but may be in the order of 15 to 30 minutes. During this interval, a launch or emergency abort could be initiated under G&N control if there were some reason not to remain on the lunar surface. The primary G&N system would control such surface aborts in the same manner as aborts initiated during the landing maneuver (Section 8.3), up to a point where direct ascent trajectories cannot be made. After this time, parking orbit operation would be required.

The primary G&N system will be designed to have emergency launch capability. Emergency launches are defined as conditions which require immediate launch from the lunar surface regardless of the CSM position relative to the landing site. The primary cause of emergency launch is ascent stage propulsion system contingencies, such as potential loss of propellant or pressurization due to punctures, leaks, etc. The objective of the G&N system, in such cases, is to inject the LEM into a clear perilune orbit in the shortest time possible. Standard IMU alignments using the AOT are not attempted in this case. During the G&N system operating period after landing, the IMU gimbal angles relative to the LEM are stored in the LGC. In emergency launch the IMU gimbals are commanded to this previous position by the LGC. This constitutes a coarse alignment only (fine alignment mode with AOT being omitted due to time) and will be in error by

the amount of IMU drift during the landing maneuver (typically 1 to 2 mr) plus any settling of the LEM on the surface after the 15 to 30 minute post landing interval.

Under normal operating conditions, the LEM IMU is aligned using the AOT as described in Section 1.3. This alignment is made and the system maintained in an operating mode before the CSM overpass prior to desired launch overpass. The LEM rendezvous radar tracking data is used to update or check the CSM orbit and landing site parameters as described in the following section. The primary G&N system is maintained in the operation mode during the next two hours prior to launch. During this interval, the desired launch aim point and timing is computed and checked with that relayed to the LEM from CSM over the intervehicle communication or data link. The aim point determination procedure is described in Section 5.4.

A final LEM IMU fine alignment using the AOT is made within 15 minutes of the predicted launch time to limit ascent injection uncertainties (Section 6.5).

5.3 LEM CSM Tracking Operations

As stated in Section 5.1, two of the objectives of the primary G&N system during this phase of the mission are to update the CSM orbital parameters and determine the position of the final LEM landing site. The primary G&N systems on both CSM and LEM can perform these objectives by tracking each other as the CSM passes over the LEM landing site. The Manned Space Flight Network (MSFN), incorporating DSIF tracking stations, may also be an additional source of this information. The normal operating procedure would involve the CSM and LEM G&N systems to determine independently the objectives of this phase and then compare the results with each other and MSFN data if available. The most accurate of the three systems would naturally be used as the source for the standard parameters for launch and aim point determination.

The tracking angle sector during which radar data is used in primary G&N systems on both CSM and LEM is shown in Fig. 5.1. This is a ±45 degree sector centered about the landing site vertical. The CSM traverses the sector in about three minutes as shown. The maximum range and range rate values encountered are also included in Fig. 5.1.

5.3.1 CSM Tracking Operation

The CSM will normally track the LEM on the lunar surface, at least on the orbital pass after descent and landing, and on the overpass prior to launch to determine and check the landing site position vector. This tracking could be done either optically with the SCT or with the rendezvous radar. SCT tracking would normally require a cooperative optical beacon on the LEM, or some type of flare ignited on the lunar surface by the astronaut, if the landing was made in earth shine conditions. Sunlight landing conditions would also require some reflective aid or active device that could be seen with the SCT, if optical tracking is desired. The CSM procedure in the optical tracking case is identical to that described in Section 2.4 for original landing site determination. Landing site determination is possible to an rms accuracy of 1500 feet for the level of orbital uncertainty and optical tracking accuracies described in Section 2.4.

Since it is uncertain at the present time whether there will be cooperative optical beacons on the LEM that could be detected under sunlight landing conditions, the primary mode of operation on CSM for LEM landing site determination uses rendezvous radar tracking data against the LEM transponder. The CSM G&N system operation would be identical to that described in Sections 2.2 and 2.4, except that radar tracking angles, and range rate or range signals would be used instead of optical angles. The CSM radar tracking angles must be compensated for angular biases, due to structure deformations as described in Section 7.2. This is done by estimating the angle biases in the same manner the orbital

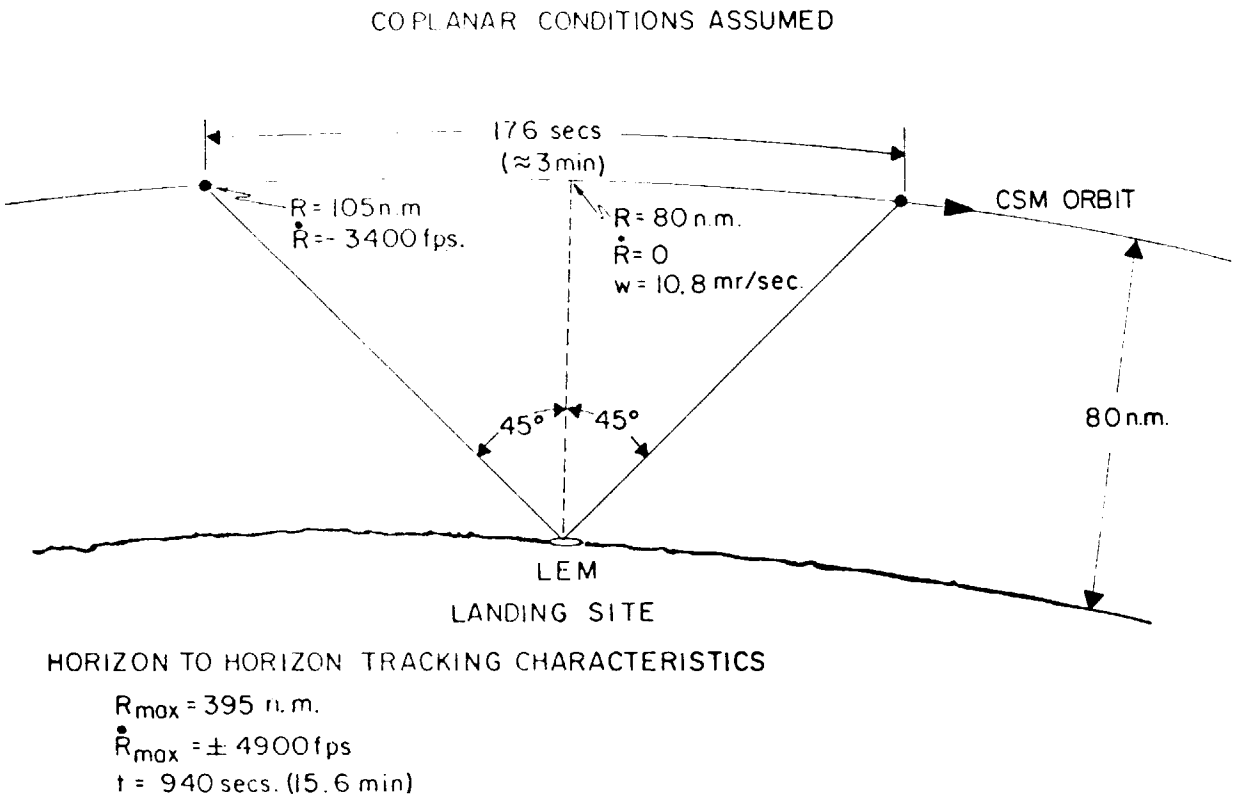

Fig. 5.1 Pre-launch minimum desired tracking sector.

parameters are estimated, and involves 9 x 9 matrix operation.

An example of CSM landing site performance is summarized for several tracking conditions in Table 5.1. In this case, a noncoplanar situation was assumed in which the CSM orbital track passes within 8 nm ($\approx 0.5^{\circ}$ central angle) of the LEM landing site at an altitude of 80 nm. As the CSM traversed the ±45 degree sector of Fig. 5.1, five measurements of each tracking parameter were taken at approximately equal angle intervals, (i.e., 45°, 22°,0°, -22°, -45°). The initial uncertainty of the LEM landing site was assumed to be 7500 feet in both horizontal directions, and 1500 feet in altitude resulting in an initial rms position uncertainty of 10,700 feet. The CSM orbital uncertainty, during the tracking interval, was taken from typical orbital navigation models of Chapter 2 involving landmark sightings prior to LEM tracking on the surface. The CSM orbital one sigma uncertainties used in this example were 1485 feet in position and 1.3 fps in velocity. With these initial conditions, the final LEM position uncertainty on the lunar surface at the end of the tracking sector is summarized for various tracking combinations and performance levels in Table 5.1.

Item 1 of Table 5.1 lists the results of using the three tracking parameters (two angles and range rate) that are normally used in the midcourse rendezvous operation (Chapter 7). The accuracies listed for Item 1 are those currently specified for the rendezvous radar (Section 1.2) under the assumption that angle biases have been estimated and effectively compensated for in navigation technique. Case 2 of Table 5.1 lists the results of using range rather than range rate. There is little difference in Cases 1 or 2 because the angle measurements alone can provide essentially the same accuracy as illustrated in Item 3 and repeated from Section 2.4, Table 2.6.

In a case where radar angle biases cannot be compensated for, due to a completely unpredictable structure alignment stability, range, or range rate only, signals could be used for LEM landing

TABLE 5.1

CSM Determination of LEM Landing Site

Initial LEM Position Uncertainty: 10,700 ft (1σ)
CSM Orbital Uncertainties: 1485 ft, 1.3 fps (1σ)

	Tracking Parameter	Accuracy (1σ)	Number of Measurements	Final LEM Site Uncertainty
1	Angle	1 mr	5	
	Range Rate	0.33%	5	1445 ft
2	Angle	1 mr	5	
	Range	0.33%	5	1511 ft
3	Angles Only	1 mr	5	1550 ft
4	Range Rate Only	0.33%	5	7655 ft
5	Range Rate Only	2.0%	5	8275 ft
6	Range Only	0.33%	5	7705 ft
7	Range Only	2.0%	5	9745 ft

site determination. It might be noted that the CSM structure stability between the CM G&N navigation base and proposed rendezvous radar installation locations on the SM is currently being studied by NAA. Cases 4 and 5 of Table 5.1 summarize the results using range rate data only at the two accuracy levels listed, while Cases 6 and 7 list the results for range data only. It might be noted that the final LEM uncertainties of Cases 4 through 7 of Table 5.1 are primarily in a direction normal to the CSM orbital plane, (Z direction) where the final uncertainties of Items 1 to 3 are more evenly distributed between the three component directions. As might be expected, range, and range rate only, data provides good in-plane information, but relatively poor out-of-plane information.

For normal CSM G&N operation, the performance listed under Cases 1 through 3 of Table 5.1 is expected for LEM landing site vector determination. The CSM continues the orbit navigation procedure, described in Chapter 2, and updates its orbital parameters. The updated orbital parameters and landing site vector could then be used in the aim point and timing determination described in Section 5.4 in the CSM and relayed to the LEM over the communication or data link.

5.3.2 LEM Tracking Operations

The previous section described the CSM G&N operation in determining or updating the CSM orbital parameters and LEM landing site, and transferring this information over the communication or data link to the LEM. In case the communication link or a part of the CSM G&N system has failed so that this information is not available, the LEM G&N system has the capability of determining the required parameters independently. The LEM primary G&N system, of course, estimated the final touchdown and landing site position within the G&N performance capability during the previous landing maneuver phase (Section 4.4). The LEM G&N system also knew the CSM orbital parameters at the

time of descent injection. The uncertainties in these orbital parameters will propagate from this time until the time the LEM rendezvous radar commences CSM tracking, if the CSM cannot update this data over the communication link. The objective of the LEM surface tracking operation is to update the CSM orbit or check this information with that relayed to the LEM.

An example of the LEM G&N system operating independently of the CSM system is summarized in Table 5.2 for various tracking parameter combinations and performance. The LEM landing site uncertainties are those which developed during the descent and landing maneuvers. The δX and δZ uncertainties are the hover point uncertainties of Fig. 4.26. A landing site altitude uncertainty of 1500 feet was assumed for a case in which the terrain elevation could not be determined any more accurately in the original orbit navigation phase (Section 2.4). The LEM inertial velocity uncertainty exists because of the altitude uncertainty of the landing site, however, the rss value of this uncertainty is typically less than 0.5 fps, and has negligible effect on the LEM tracking operation. The level of initial CSM orbital uncertainties listed in Table 5.2 were determined by taking the CSM uncertainties at LEM surface landing, and propagating these uncertainties one more orbital period. As indicated in Chapter 2, the magnitude of the initial uncertainty is not too important, provided a sufficient number of measurements are made since these uncertainties are reduced very rapidly by the first few measurements.

The normal LEM rendezvous radar tracking parameters and performance are listed in Case 1 of Table 5.2. In the model used for this particular analysis, one measurement parameter (angle or range rate) was made at angles of 37^{o}, 24^{o}, 5^{o}, -15^{o}, -31^{o} and -41^{o} from the LEM vertical (Fig. 5.1). The rss CSM uncertainties at the end of tracking over the first 90^{o} sector are listed in Tabel 5.2. If these uncertainties were allowed to propagate one more orbit, and the LEM then track the CSM over half

Table 5.2

LEM Determination of CSM Orbital Parameters

LEM Landing Site Parameter Uncertainties

δX = 3060 ft
δY = 1500 ft
δZ = 1420 ft
RSS = 3700 ft
Velocity < 0.5 fps RSS

Initial CSM Uncertainties

δX = 31,780 ft	$\delta \dot{X}$ = 0.8 fps
δY = 1712 ft	$\delta \dot{Y}$ = 27.9 fps
δZ = 685 ft	$\delta \dot{Z}$ = 1.4 fps
RSS = 31,800 fps	RSS = 28.0 fps

	Tracking Parameter	Accuracy (1σ)	Number of Measurements 1st pass	Number of Measurements 2nd pass	CSM Orbit Uncertainty (RSS) End of 1st tracking sector	CSM Orbit Uncertainty (RSS) Overhead at launch
1	Angle	1 mr	3	1	2650 ft	3890
	Range Rate	0.33%	3	2	3.0 fps	4.1 fps
2	Angle	1 mr	3	1	2830 ft	3770 ft
	Range	0.33 %	3	2	3.1 fps	3.8 fps
3	Range Rate	0.33%	6	3	2650 ft 2.7 fps	4050 ft 3.8 fps
4	Range Rate	2.0%	6	3	3230 ft 3.2 fps	5690 ft 5.2 fps
5	Range	0.33%	6	3	4340 ft 3.5 fps	3760 ft 3.6 fps
6	Range	2.0%	6	3	11,030 ft 9.9 fps	13,250 ft 11.6 fps

the sector on the second pass until it was directly overhead (typical launch phasing conditions), the CSM orbital uncertainties existing at that time are summarized in the last column of Table 5.2. Case 2 of this table summarizes a similar tracking schedule using range data, rather than range rate data, with the tracking angle measurements. Items 3 to 6 of Table 3.2 are included to show the effects of range or range rate data only. It should be pointed out that Cases 3 to 6 were included for general interest only, since it is very unlikely that tracking bias angle compensation cannot be achieved in the LEM due to relatively close installation of the rendezvous radar antenna to the IMU (Fig. 1.5), and the radar tracking and alignment accuracy specification (Ref 5.1).

5.4 Launch Aim Point and Timing Determination

The launch conditions from which the powered ascent and rendezvous must be made will normally require noncoplanar trajectories relative to CSM orbit. The most extreme noncoplanar launch conditions considered in the primary G&N analysis are illustrated in Fig. 5.2. In this figure, it was assumed that the CSM orbit was inclined to the lunar equator by 10^{o}, and that the desired landing site was on the equator at Point A. The lunar rotation will move the landing site along the equatorial plane to Point B during the time the LEM is on the lunar surface. The lunar rotation is approximately 13^{o} per day, and since the CSM orbit is retrograde with a nodal precession of about 1^{o} per day (Ref 5.2) in the same direction as the lunar rotation, the landing site will rotate relative to the CSM orbital node at a rate of 12^{o} per day. In a 24 hour landing mission, the landing site at Point B of Fig. 5.2 would be 2.2^{o} central angle measured between Points B and C (about 36 nm) away from the track of the CSM orbit at the time of launch. This represents the maximum noncoplanar launch condition for the model of Fig. 5.2. It should be pointed out that the noncoplanar launch condition can be restricted to lower values by orienting the CSM orbit at lunar orbit injection such

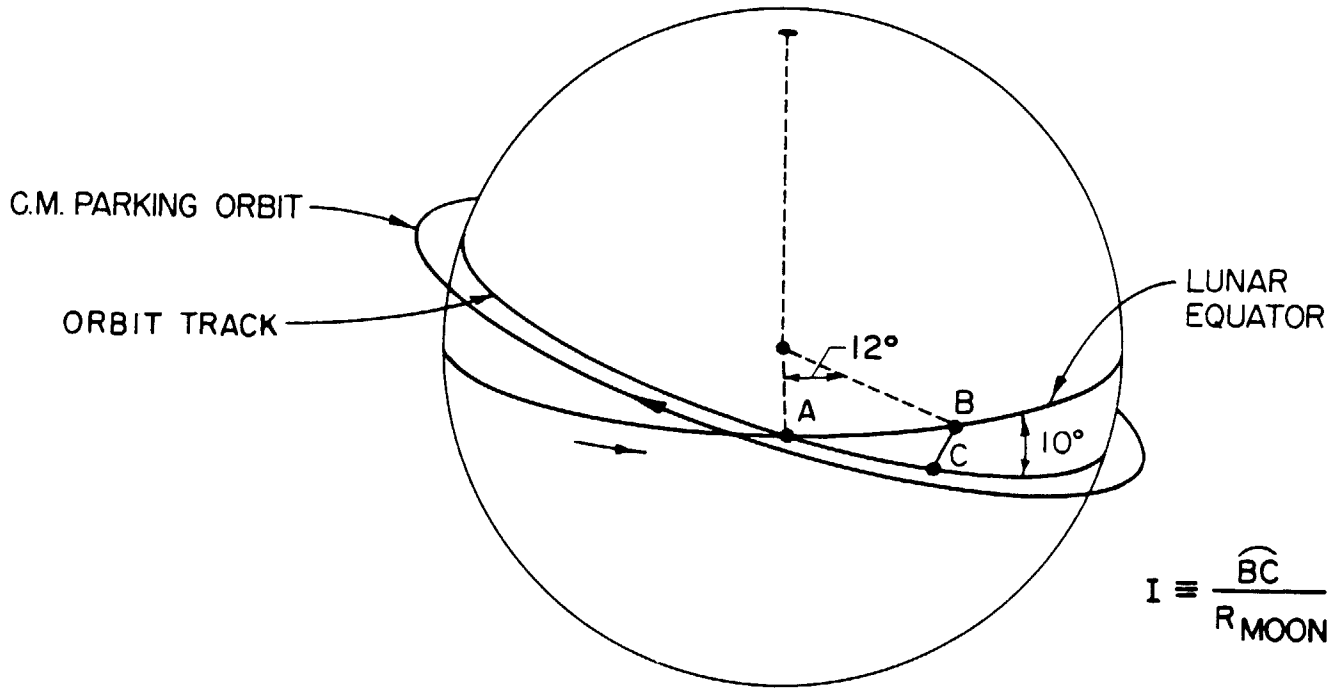

Fig. 5.2 Launch conditions relative to the C.M. orbit.

that the maximum latitude excursion of the orbit is near, or just beyond, the desired landing site, or by restricting the CSM orbit and landing sites to near equatorial conditions. Current mission profiles and analysis restrict the out of plane launch conditions to about 0.5 degrees. Out of plane launch conditions ranging from 0.5 degrees to 2.2 degrees will be presented in examples of the following mission phases (Chapter 6 and 7).

Typical characteristics of ascent trajectories for rendezvous with various out of plane launch conditions are summarized in Fig. 5.3. The trajectory parameters listed in this figure are for the unpowered or coast phase of the ascent trajectories from injection to the intercept aim point. The ΔV_2 column indicates the relative terminal closing velocity assuming a perfect trajectory had been achieved. The sum of the injection velocity, V_1, and ideal rendezvous velocity, ΔV_2, are then summed to indicate the ideal ΔV requirement independent of gravity loss effects. The time listed in Fig. 5.3 is the trajectory time from injection to aim point. The perilune altitude of the ascent trajectory is listed in the final column. It can be seen from Fig. 5.3 that there are two ΔV minimum direct ascent trajectories for noncoplanar launch conditions, one less than 180° central angle, and one greater than 180°. The characteristics of these two possible ascent trajectories will be described later. The major effect of noncoplanar launch conditions is on the terminal rendezvous closing velocity, as indicated in the ΔV_2 column of Fig. 5.3. The terminal rendezvous maneuver (Section 7.6) both rotates and increases the LEM velocity vector to match that of the CSM.

The required input data for the aim point and timing determination is:

$\underline{R}_{CM}$	CSM position vector
$\underline{V}_{CM}$	CSM velocity vector
t_{ref}	reference time
$\underline{R}_{LEM}$	LEM landing site vector

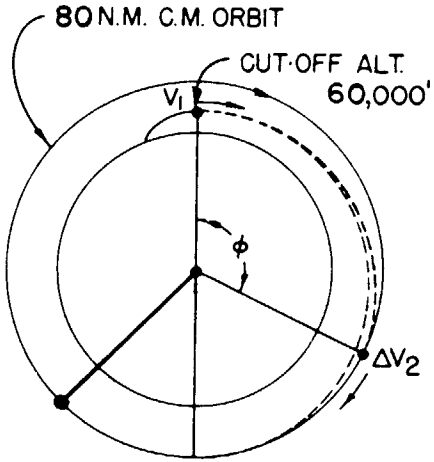

	I (DEG)	ϕ (DEG)	ΔV_2 (FPS)	$V_1 + \Delta V_2$ (FPS)	TIME (SEC)	H PER (NM)
1	0	140	151	5724	2604	9.6
2	0	180	97	5677	3486	9.8
3	0.5	153.5	140	5716	2963	9.6
4	0.5	213.5	148	5728	4190	9.7
5	2.0	123	246	5834	2350	8.7
6	2.0	235	240	5822	4598	8.0

Fig. 5.3 Lunar ascent trajectories.

These inputs were obtained from the procedure described in Section 5.3. The required outputs of the prelaunch computation are:

$\underline{R}_{CM}(t_A)$	aim point or position of the CSM at time t_A
t_{ndl}	nominal direct launch time
t_{ldl}	latest direct launch time
t_{lpo}	latest parking orbit launch time

These times are shown graphically in Fig. 5.4, when the reference time, $t = 0$, has been set at the nominal launch time. As indicated in Fig. 5.4, the normal launch procedure will involve direct ascents if launch timing is achieved during the first interval indicated, followed by parking orbit injection if the launch time is between t_{ldl} and t_{lpo}. The latest possible launch time, t_{lpo}, is about 12 minutes after t_{ndl}, since a rendezvous can be achieved faster by waiting for the next CSM orbital pass if the launch time has slipped beyond this time. Since t_{lpo} is known for a given CSM orbit, the primary objective of this part of the prelaunch computation is to determine $\underline{R}_{CM}(t_A)$, t_{ndl}, and t_{ldl}.

The important parameters required for the aim point determination are illustrated in Fig. 5.5. The LEM landing site, $\underline{R}_{LEM}(t_0)$, and CSM orbit parameters are known. The normal LEM powered ascent trajectory characteristics are also known (Chapter 6). These include the central angle covered (indicated as 10^{o}), the injection altitude (50,000 feet) and the normal ascent maneuver time (typically 420 seconds). The LEM position vector at injection can then be estimated at injection time, t_1, indicated as $\underline{R}'_{LEM}$ in Fig. 5.5. The procedure for determining the desired aim point $\underline{R}_{CM}(t_A)$ is then an iterative operation involving the initial phasing angle, θ_0, which is directly related to the launch time, and the central angle, ϕ, which is a function of the time of arrival t_A and θ_0.

The aim point determination procedure is outlined in Fig. 5.6.

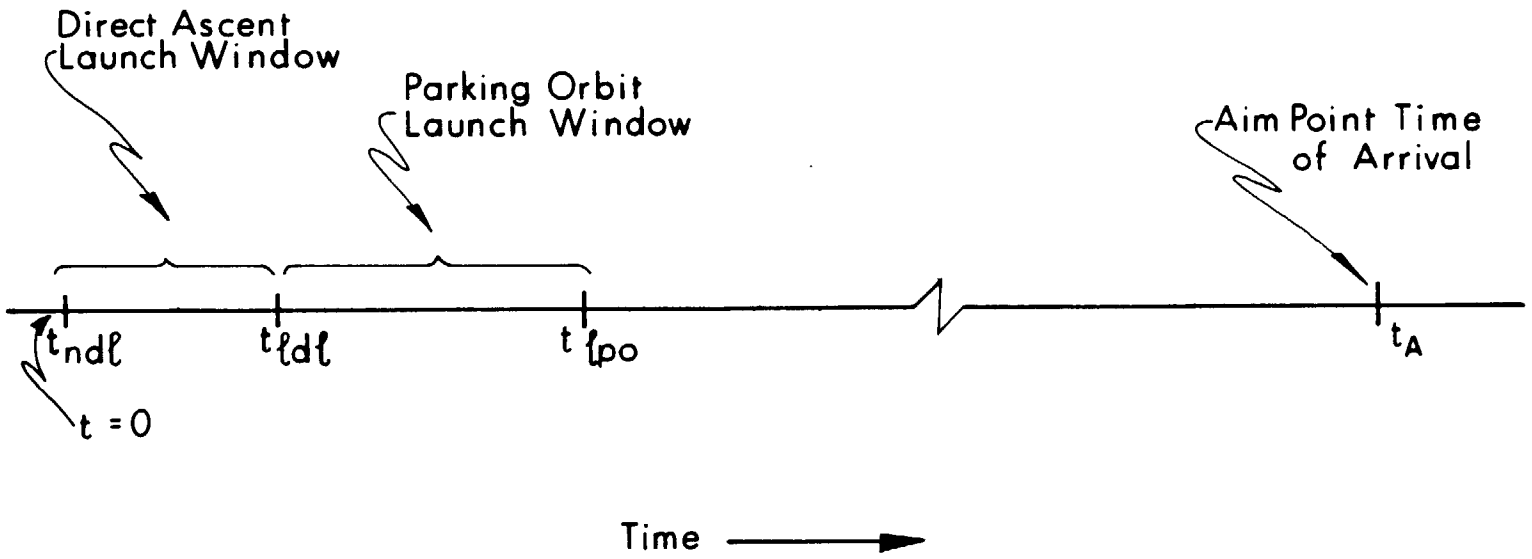

Fig. 5.4 Ascent time points.

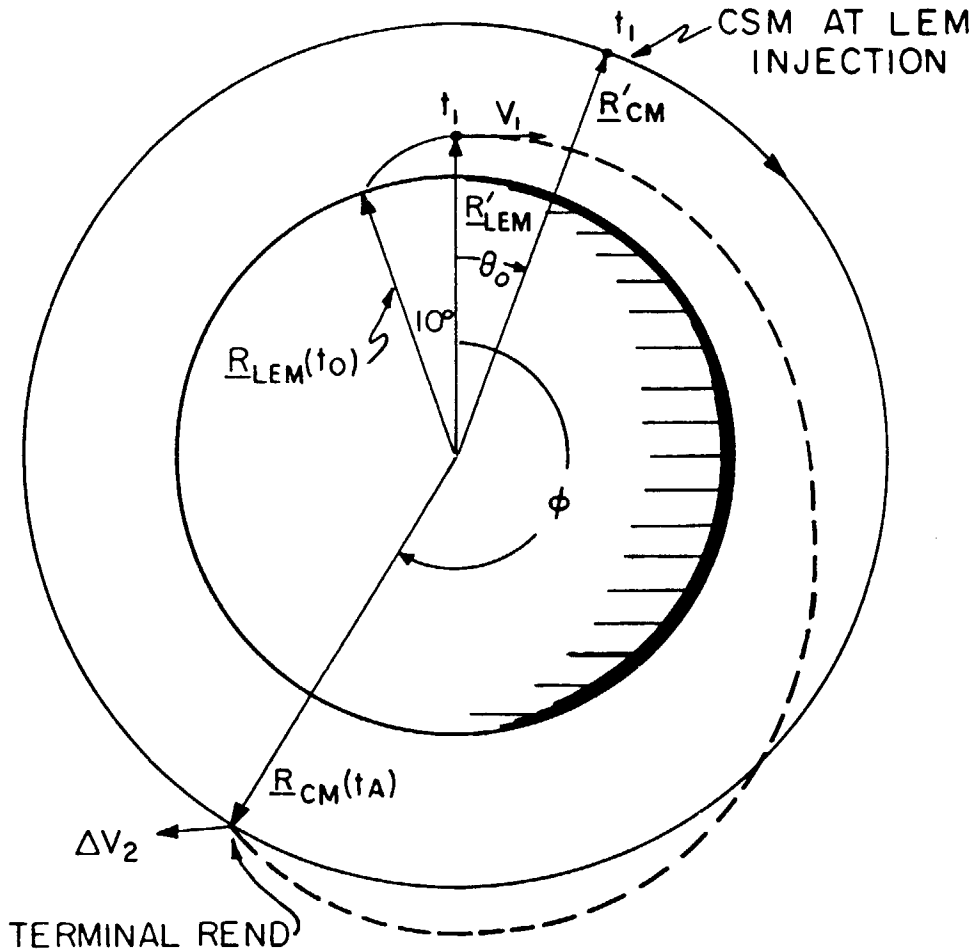

Fig. 5.5 Launch aim point determination.

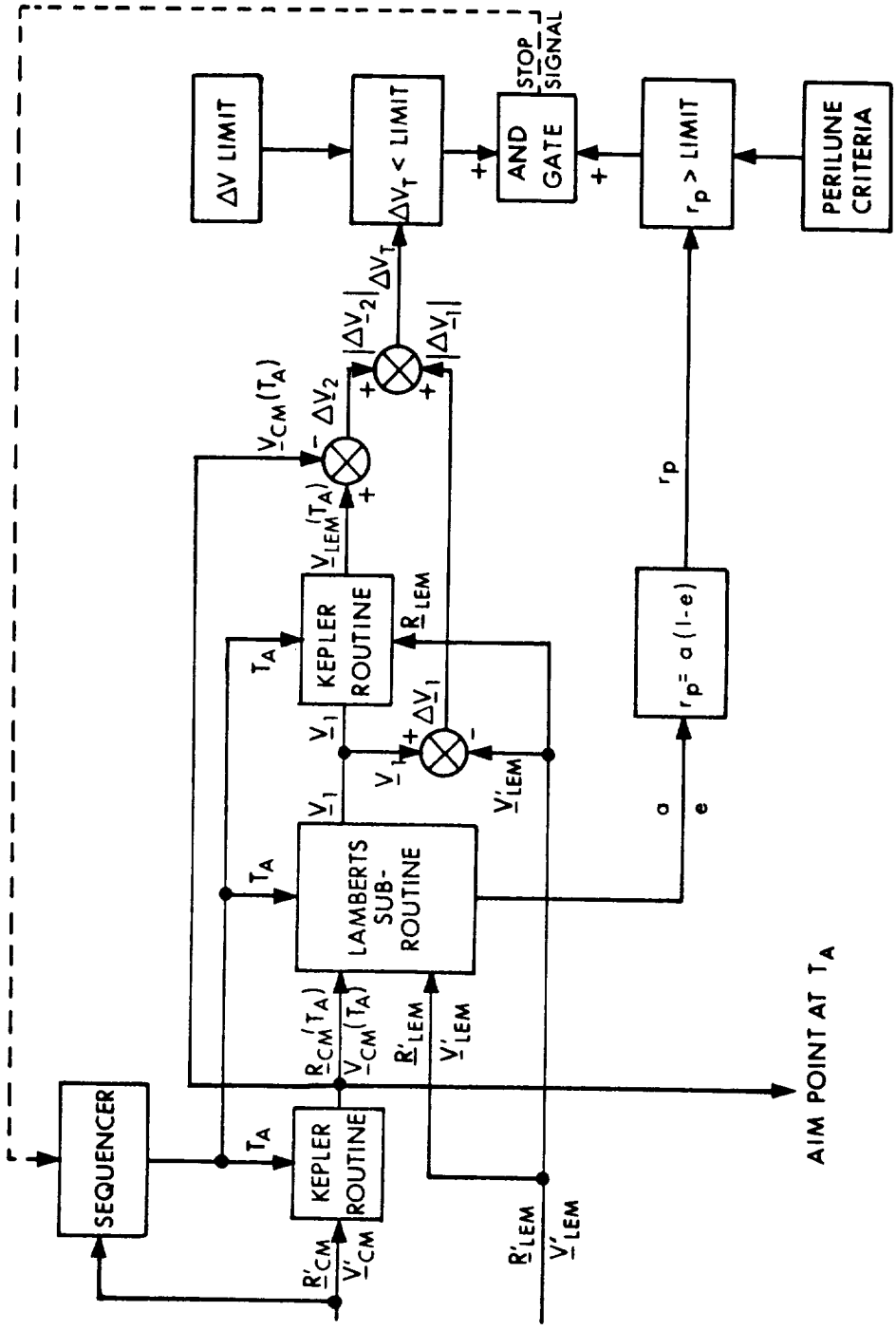

Fig. 5.6 Aim point determination.

An initial separation angle, θ_0, is assumed (typically 8 to 9 degrees) at a reference time, t_1, in Fig. 5.5 with the associated CSM and LEM position vectors $\underline{R}'_{CM}$ and $\underline{R}'_{LEM}$ respectively. An initial time of arrival t_A measured from t_1 is supplied by a stored program referenced as a sequencer in Fig. 5.6. This initial t_A will be larger than the expected value for ascents covering central angles greater than 180 degrees or less than that expected for ascent trajectories of less than 180 degrees. A Kepler routine is then used to advance the position and velocity of the CSM by the time interval t_A resulting in $\underline{R}_{CM}(t_A)$ and $\underline{V}_{CM}(t_A)$. A Lambert routine is then used to determine the required LEM injection velocity, $\underline{V}_1$ in Figs. 5.5 and 5.6, for a trajectory that passes between the LEM injection position $\underline{R}'_{LEM}$, and the CSM aim point position $\underline{R}_{CM}(t_A)$ under test in the given interval t_A. The diagram of Fig. 5.6 is general in the sense that the procedure could be used for transfer trajectory determination when the LEM is in a parking orbit. In the case of surface launch, however, the velocity $\underline{V}'_{LEM}$ is assumed zero, and the required injection velocity $\underline{V}_1$ is equal to $\Delta\underline{V}_1$. The next step indicated in Fig. 5.6 is to advance the LEM from the injection point, assuming it has the required velocity $\underline{V}_1$, by a time, t_A, to determine the LEM velocity at intercept or aim point $\underline{V}_{LEM}(t_A)$. It might be noted that there are several ways or equations by which this step could be done using outputs of the Lambert routine. The procedure shown in Fig. 5.6 uses a Kepler routine since this program is already stored in the LGC for other phases of the mission. The LEM and CSM velocity vectors at the aim point are then subtracted to determine the terminal rendezvous closing velocity, $\Delta\underline{V}_2$. The total characteristic velocity requirement ΔV_T is then the sum of the injection velocity $|\Delta\underline{V}_1|$ and rendezvous velocity $|\Delta\underline{V}_2|$. ΔV_T is compared with a preset ΔV limit, as shown. The ascent trajectory perilune altitude is computed from the semimajor axis, a, and eccentricity, e, from the Lambert routine. The resulting perilune altitude, or radius vector r_p, is then compared with a

limiting perilune criteria. If either the ΔV_T or perilune check is not met, the sequencer changes the t_A to a lower value and the process is repeated until both criteria are satisfied, as will be indicated by the stop signal in Fig. 5.6. The sequencer then continues to change the t_A until a minimum ΔV_T condition is found. This will be represented by a t_A with an associated central angle ϕ from $\underline{R}'_{LEM}$ for the assumed separation angle θ_0. The sequencer next holds the central angle ϕ fixed, and varies the injection separation angle θ_0, which is directly related to launch time through the known characteristics of the powered ascent maneuver. The separation angle is varied until the ΔV_T or perilune limits have been established for the selected central angle ϕ. The desired direct ascent launch times t_{ndl} and t_{ldl} are determined directly from the limits of the separation angle θ_0. This procedure is more clearly illustrated in Fig. 5.7. This is the same type of figure and similar analysis as presented in Reference 5.3.

As indicated in Fig. 5.6, the two criteria that the ascent trajectory must meet are a ΔV limit and perilune altitude limit. The perilune altitude limit has arbitrarily been set at 35,000 feet for the present examples. The characteristic velocity limit for injection and terminal rendezvous was also arbitrarily chosen to be 5900 fps, as listed in Fig. 5.7, by the following ΔV allocations:

1)	Normal injection velocity	5600 fps
2)	Typical terminal rendezvous velocity for 0.5^o noncoplanar launch	150 fps
3)	Contingency ΔV for late launch, etc.	150 fps
4)	ΔV Limit Criteria	5900 fps
5)	Typical ascent trajectory losses	460 fps
6)	Midcourse rendezvous corrections	50 fps
7)	Docking requirements	25 fps
	TOTAL	6435 fps

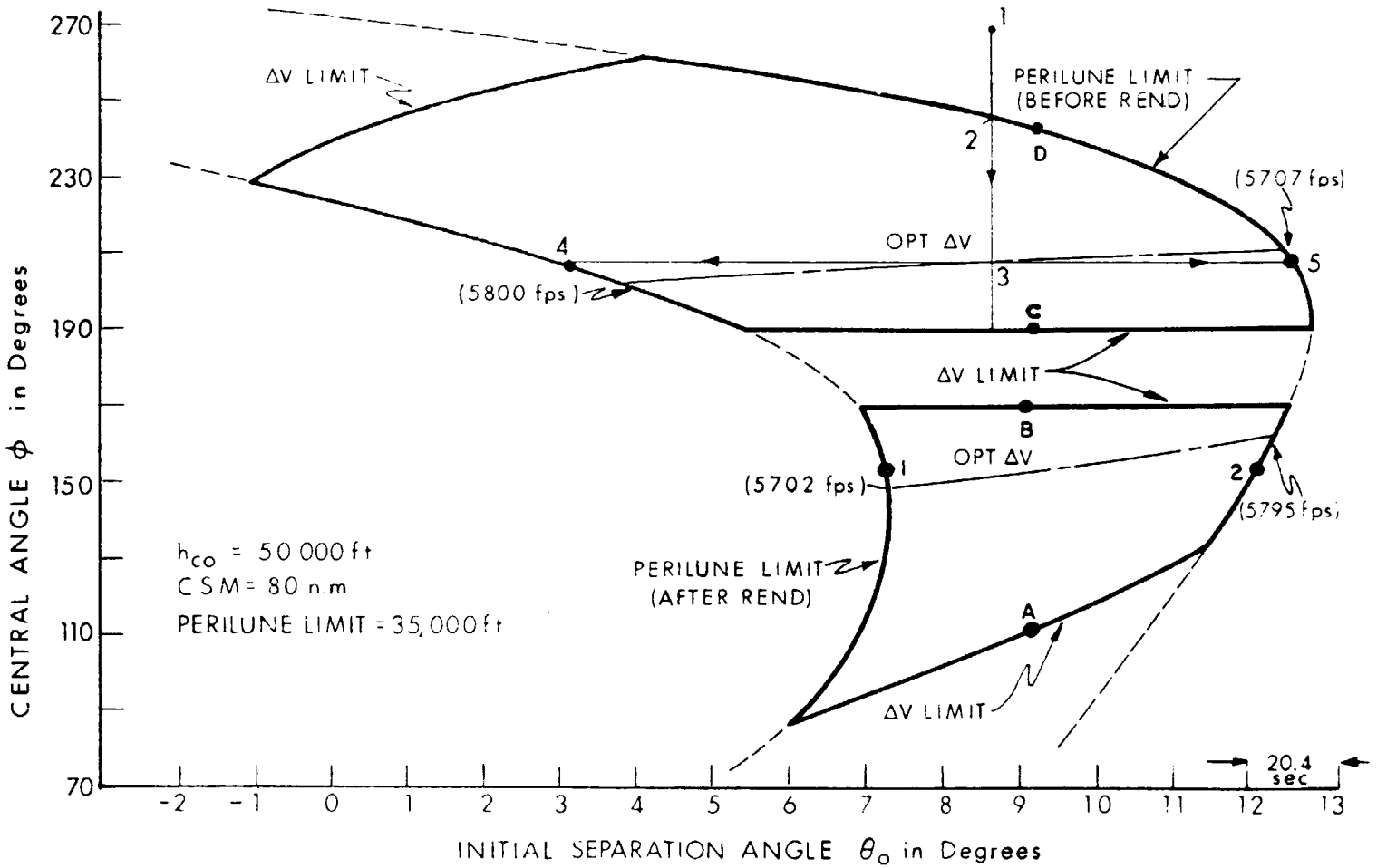

Fig. 5.7 Lunar launch window, $I_o = 0.5^o$.

This total compares closely with current LEM ascent stage ΔV capability ($\approx$ 6450 fps). It should be noted that the ΔV criterion of 5900 fps, illustrated in Fig. 5.7, is arbitrary and could be set at any desired value.

The example illustrated in Fig. 5.7 is for a 0.5^{o} noncoplanar launch condition. The ΔV and perilune limit conditions are plotted against the central angle ϕ and the initial separation angle θ_0 at ascent injection. Time of arrival t_A is directly related to ϕ and θ_0. Two acceptable aim point sectors are indicated in this figure, one greater than 180^{o} and one less than 180^{o}. The aim point determination procedure described above can be illustrated on Fig. 5.7 as follows. Assume that an aim point greater than 180^{o} is desired, and that the initial separation angle θ_0 is set at 8.5 degrees (CSM ahead of the LEM). The sequencer initial t_A will require a ϕ of 270 degrees as shown by Point 1 of Fig. 5.7. The Point 1 conditions are then operated on by the procedure of Fig. 5.6, and it is found that the perilune condition is not met. In this case, the perilune would be below the surface of the moon and lie between the injection point and the aim point, a totally unacceptable condition. The sequencer of Fig. 5.6 would then reduce t_A or ϕ, until the perilune criteria were met at Point 2 of Fig. 5.7, since the ΔV_T criteria is satisfied. Point 2 then represents the first acceptable aim point so far determined. The sequencer then continues varying ϕ until the minimum ΔV condition is found at Point 3. The central angle corresponding to Point 3 is then fixed (209 degrees), and the separation angle θ_0 is varied until Points 4 and 5 are determined. θ_0 is varied by changing $\underline{R}'_{CM}$ by $\delta\theta_0$, which has the effect of varying the initial launch time and the time of arrival t_A. Points 4 and 5 indicate a possible direct ascent launch window that is close to the minimum ΔV requirement for rendezvous from the 0.5 degree noncoplanar launch condition. Since every degree of θ_0 represents 20.4 seconds of launch delay, the interval represented by Points 4 and 5 is equivalent to a possible launch window of 184 seconds. Point 4 represents the initial

lauch time, t_{ndl}, and is determined by subtracting powered ascent time (420 seconds) from the time the CSM reaches a position 13.2 degrees (10^{o} plus θ_0 of 3.2^{o}) ahead of the launch site. A similar procedure determines t_{ldl} from Point 5.

The boundary conditions for acceptable aim points in the 0.5^{o} noncoplanar launch case of Fig. 5.7 are set by the perilune criterion along the ϕ coordinate, and by the ΔV criterion along the θ_0 coordinate. The initial minimum ΔV point for the trajectories covering more than 180^{o} (just below Point 4 of Fig. 5.7) requires an injection velocity of 5596 fps at a positive flight path angle of 0.82 degrees relative to the local horizontal. The terminal rendezvous closing velocity is 204 fps, in this case giving a total ΔV requirement of 5800 fps as indicated. As the launch time is delayed (θ_0 increases) the ascent trajectory perilune altitude increases until it reaches 50,000 feet at zero injection flight path angle, then decreases until the 35,000 foot perilune criteria is exceeded near Point 5. The required injection velocity at this last point of the launch window is 5578 fps at a negative flight path angle of -0.76 degrees. The rendezvous terminal velocity in this case is 129 fps, resulting in a total ΔV requirement of 5707 fps. The optimum ΔV_T condition for the greater than 180 degree case, therefore, slopes such that the lowest possible ΔV condition exists at the end of the direct launch window. The reverse condition exists for the central angle zone less than 180 degrees as indicated in Fig. 5.7. The injection and rendezvous velocities are approximately reversed for the cases described above for the greater than 180 degree case. It might be noted that the minimum ΔV_T condition occurs for the less than 180 case of Fig. 5.7 at a θ_0 of 2.5^{o}, $\phi = 102^{o}$ for a ΔV of 5686 fps. This condition falls outside the perilune criteria, which occurs after rendezvous, and indicates the theoretical ΔV penalty for the clear perilune criteria for this out of plane launch condition.

The launch windows provided by the optimum ΔV condition are 163 seconds for the greater than 180^{o} case, and 100 seconds for the less than 180^{o} case in Fig. 5.7. The optimum ΔV condition for the greater than 180^{o} case is also slightly more constant with respect to central angle ϕ. The maximum possible launch window for the greater than 180^{o} case would cover the greatest θ_0 range possible equivalent to 282 seconds, as opposed to 120 seconds for the lower than 180 degree case. The procedure and example previously outlined for determining the direct ascent launch window is simplified in the sense that no attempt was made to exactly follow the minimum or optimum ΔV condition, nor was the maximum possible launch window determined. At the present time, the minimum launch window requirements for LEM ascent have not been specified. A more elaborate iterative and search technique in the LGC is possible to essentially establish the maximum limits of the launch window or aim point zones shown in Fig. 5.7. At the present time, however, it is felt that the simplified procedure outlined above in which a single ΔV minimum point is first established, and the launch window then determined for a constant value of central angle ϕ, will provide sufficient direct ascent launch time limits.

The direct ascent launch window limits for 2 degree noncoplanar launch conditions are shown in Fig. 5.8, for the same ΔV and perilune criteria. The perilune limit lines of Figs. 5.7 and 5.8 are virtually identical. The ΔV limit boundaries are much less for the 2 degree noncoplanar case as would be expected from the higher rendezvous closing velocity conditions (Fig. 5.3). It can be seen from Fig. 5.8, that the aim point zones are bounded by the perilune conditions on one side only, and the others by the ΔV limit criterion. The launch window for the greater than 180 degree case for ΔV optimum condition in Fig. 5.8 is 140 seconds as opposed to 60 seconds for the less than 180 degree case. It should be noted that for this out of plane launch condition, the initial launch time for greater than 180 degree ascents would require the full ΔV allotment of 5900 fps if the the launch were

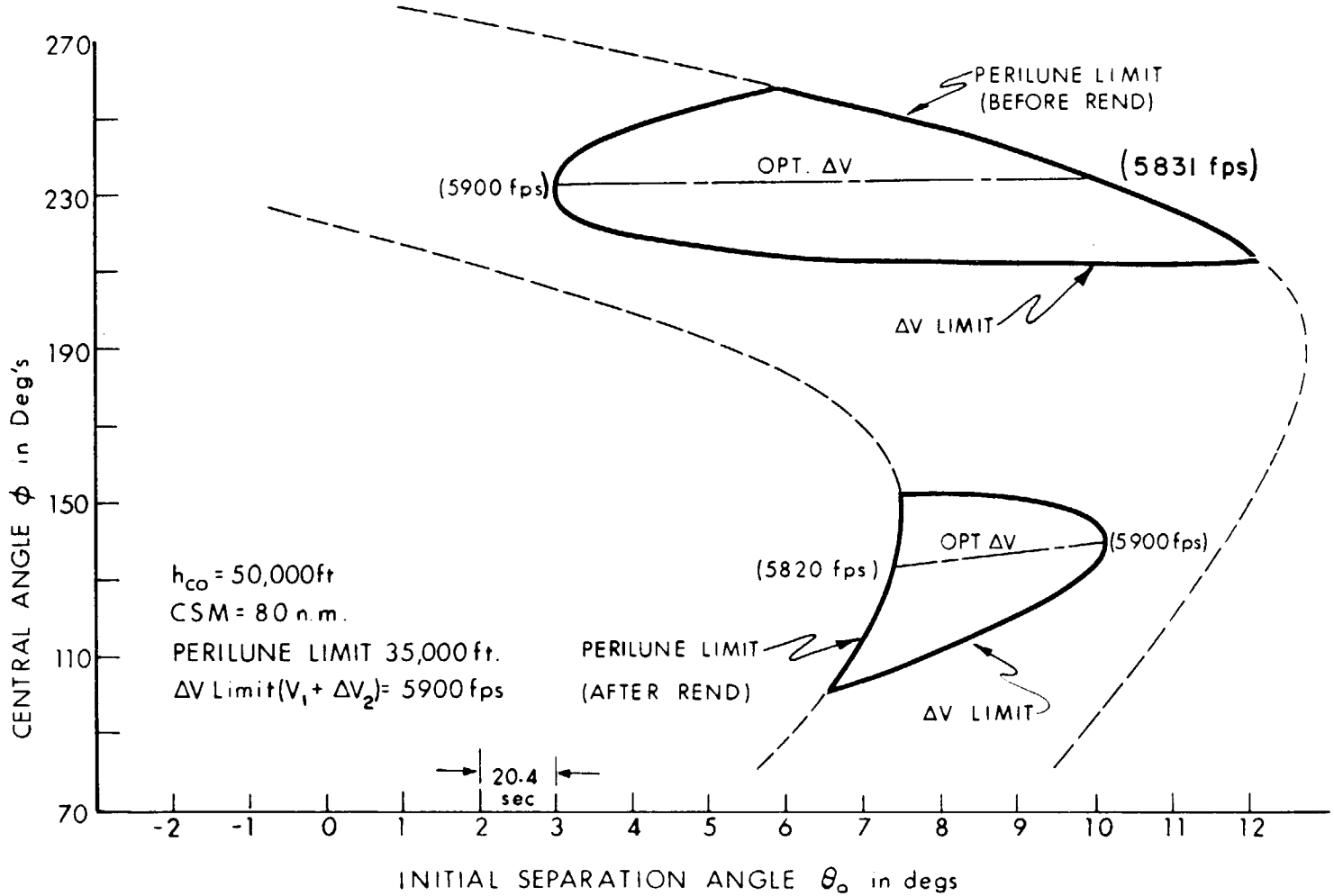

Fig. 5.8 Lunar launch window, $I_o = 2.0^o$.

achieved on time, and that this ΔV requirement would decrease as launch time was delayed until the perilune limit was reached. For the ascent trajectories covering less than 180 degrees, however, the lowest ΔV requirement would be achieved if the launch was made on time and delayed launches would progressively require more ΔV until the 5900 fps limit was reached after 60 seconds of delay.

In the case of launch times after t_{ldl}, but before t_{lpo}, the LEM would be injected into a parking orbit. The simplest primary G&N system operation in this case would use the same ascent trajectory plane planned for the desired launch. After the LEM was injected into an orbit in this plane, radar tracking between the two vehicles would be established, and a procedure virtually identical to that outlined in Fig. 5.6 would be used to determine the timing (vehicle phasing θ_0) and aim point for the transfer trajectory to the CSM orbit.

Launch delays within the direct ascent launch window are compensated for during the powered ascent so that LEM will arrive at the chosen aim point at the prescribed time of arrival. The powered ascent guidance is described in Chapter 6. After ascent injection, midcourse velocity corrections are made at the longest possible range to establish an intercept trajectory (Chapter 7). It might be noted that the aim point determined in the prelaunch phase to which the LEM ascent trajectory is controlled in the powered ascent and midcourse rendezvous phases, would be the intercept point on the CSM orbit if no terminal rendezvous maneuver were made. This intercept trajectory is actually changed when the range between the two vehicles closes to 5 nm to other aim points further along the CSM so that a relatively slow terminal rendezvous can be monitored by the astronaut (Section 7.6).

CHAPTER 6

LAUNCH AND POWERED ASCENT PHASE

6.1 Primary G&N System Objectives.

This phase of the mission involves the powered ascent maneuver which starts when the ascent engine is ignited at launch and terminates with injection cutoff. The G&N objectives during this maneuver are to achieve desired injection conditions that will result in a LEM trajectory that intercepts the designated aim point on the CSM orbit at the specified time of arrival. If the launch maneuver is initiated within the direct ascent launch window (Section 5.4), the primary G&N system controls the powered ascent maneuver such that a direct ascent trajectory is achieved. For cases involving delayed launches beyond the direct launch window, but prior to the final parking orbit launch limit, the primary G&N system controls the ascent maneuver to result in a clear perilune parking orbit. In cases of emergency launch in which it is required to initiate the ascent maneuver at any time, the G&N system will control the ascent maneuver to a clear perilune parking orbit. The guidance concept used to achieve these three types of ascent maneuvers is discussed in Section 6.2.

The primary G&N system configuration used for the launch and powered ascent phase is a pure inertial system as illustrated in Fig. 6.1. This G&N configuration is essentially the same as that used during the first phase of the powered landing maneuver (Fig. 3.21), except that the G&N system controls the LEM thrust direction of the constant thrust ascent engine. As indicated in Fig. 6.1, the LEM attitude commands and engine-on-off signals are commanded through the CDUs and LGC, respectively to the LEM SCS.

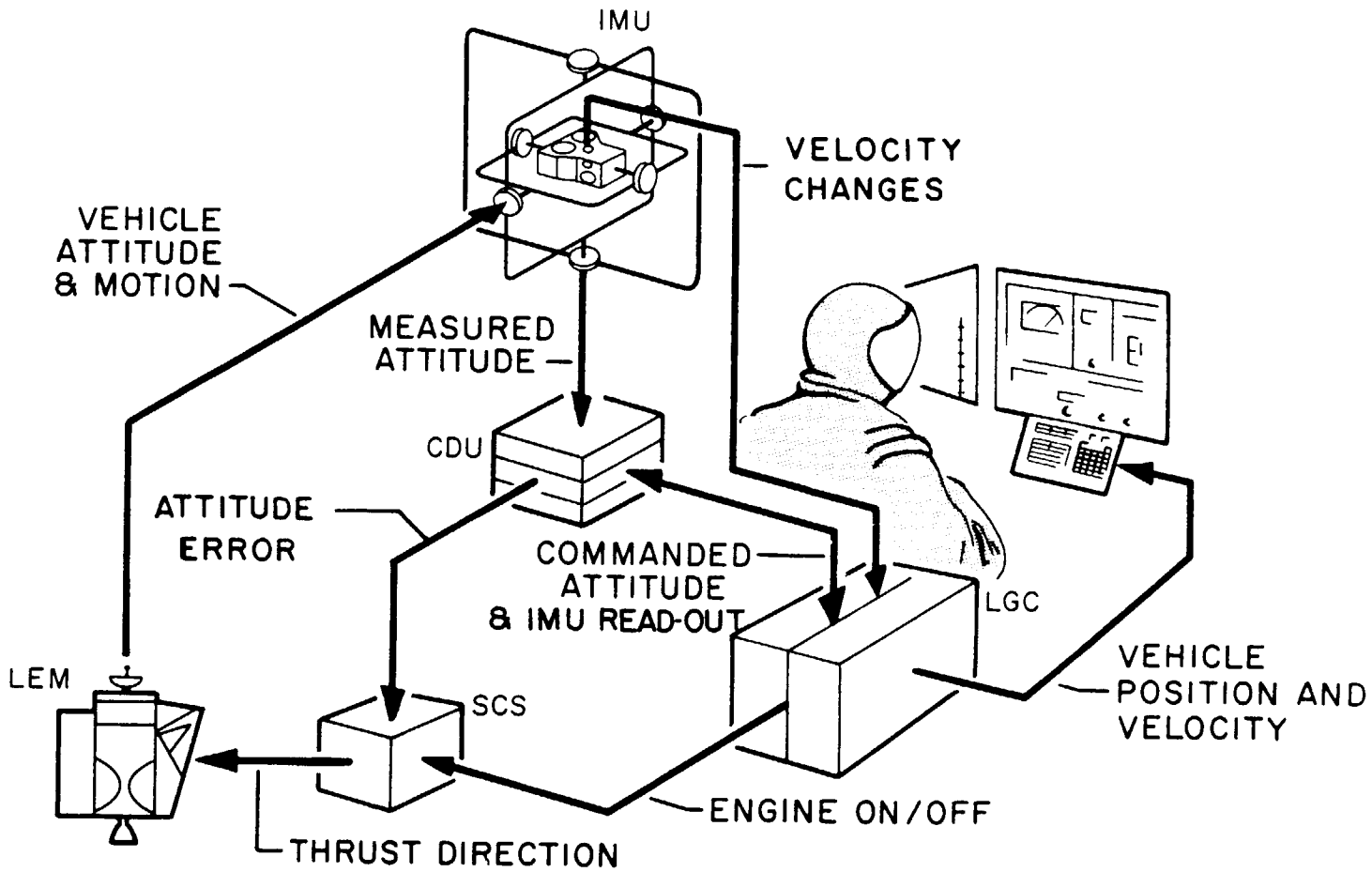

Fig. 6.1 Powered ascent maneuver.

6.2 Powered Ascent Guidance Equations

6.2.1 General

The LEM-powered ascent guidance equations compute thrust vector orientation and thrust termination commands. These commands cause the spacecraft to attain a specified velocity vector. The equations can also control, when such control is necessary, the burnout altitude of the spacecraft. Altitude control can help to assure 1) local terrain clearance during launch from the lunar surface, and 2) a clear perilune trajectory following a thrust termination command. The guidance system commands also constrain the spacecraft burnout position and velocity vectors to lie in a specified plane. Figures 6.2 and 6.3 illustrate the controlled quantities in the coordinate system in which the guidance computations are performed. Figure 6.2 also illustrates the angle θ_{BO}. This is the angle between a reference line in the specified plane of motion and the LEM burnout position vector. The guidance equations predict θ_{BO} throughout a powered ascent. The purpose of predicting θ_{BO} is explained in a following section which concerns Lambert's problem and the ascent-to-rendezvous guidance procedure.

As mentioned, the control of burnout altitude of the spacecraft is not a necessary feature of the guidance equations, and the guidance system can be operated in a mode which permits the acquisition of a specified velocity vector without the explicit control of burnout altitude. When burnout altitude is not controlled, it is predicted. The prediction of burnout altitude is performed for the same reason that θ_{BO} is predicted.

Another feature of the guidance technique is that the burnout attitude of the vehicle can be constrained to a specified orientation. This feature may be of use during the terminal rendezvous maneuver (Section 7.6).

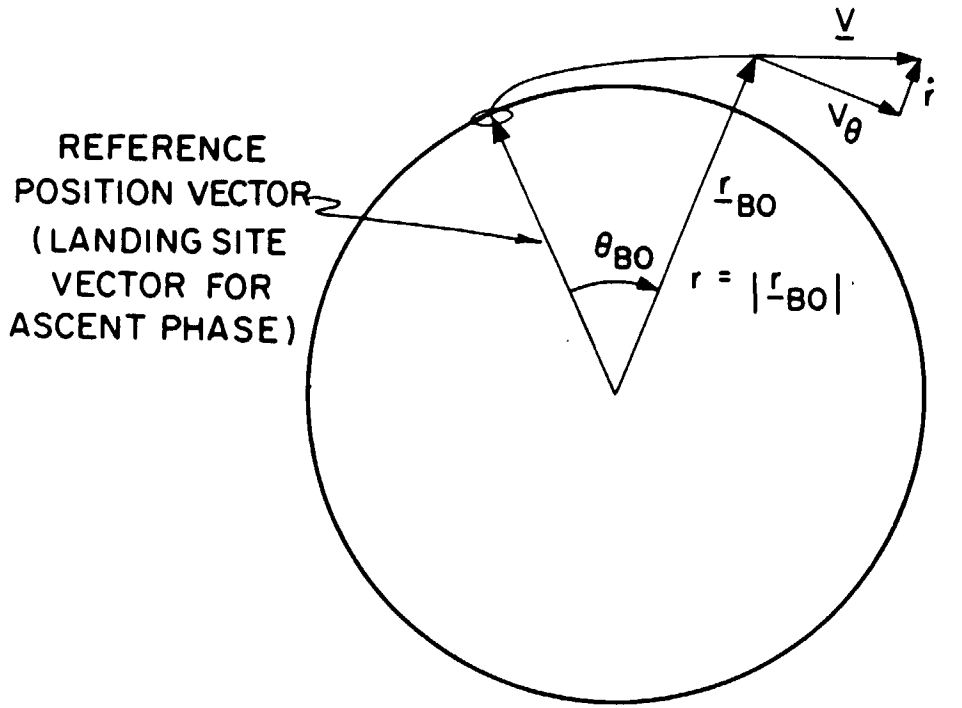

CONTROLLED IN PLANE QUANTITIES ARE:

1) r
2) V_θ
3) $\dot{r}$

Fig. 6.2 Trajectory plane controlled quantities.

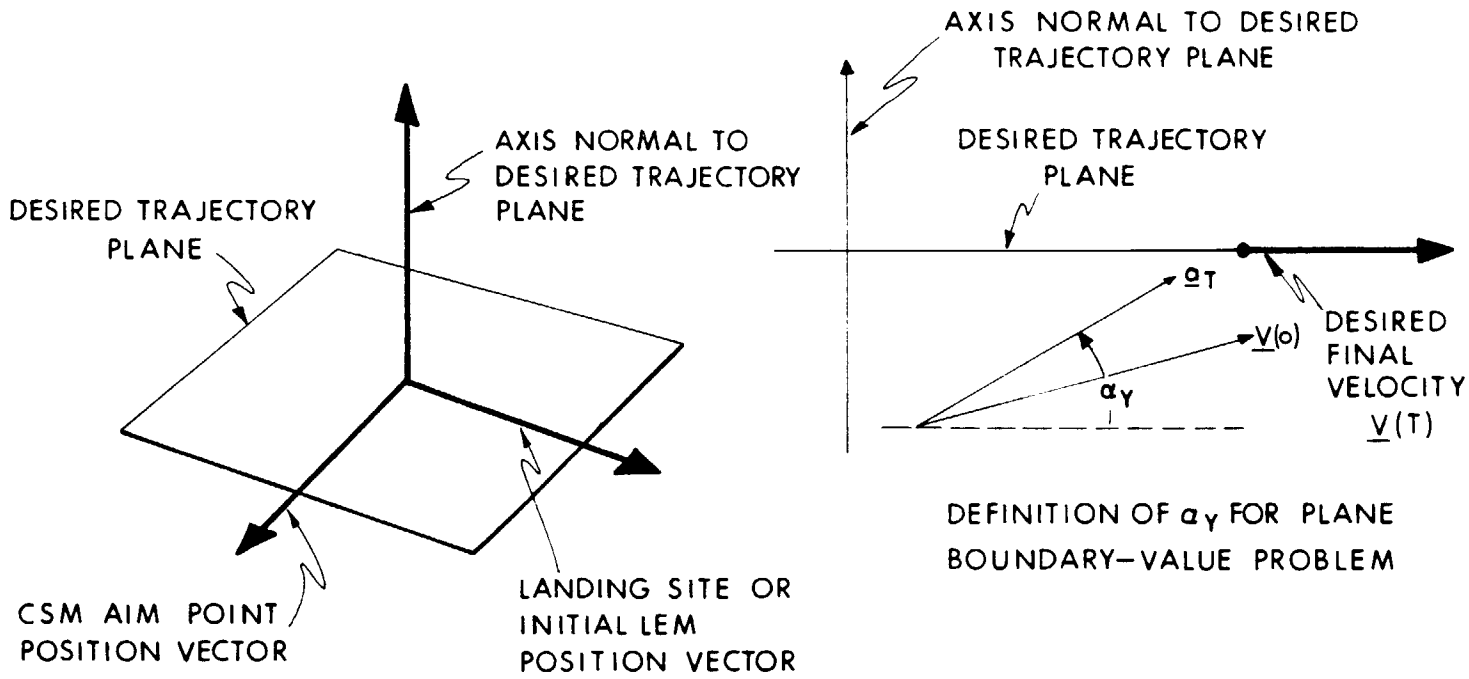

Fig. 6.3 Trajectory plane control.

The ascent guidance equations are quite flexible because they are completely explicit and can be operated in either a controlled burnout altitude mode or a free burnout altitude mode. In the constrained burnout altitude mode, the burnout altitude can be arbitrarily specified - with the limitation, of course, that the resulting boundary-value problem be physically reasonable.

It is interesting to list the LEM-powered flight phases during which the ascent equations can be used and then determine whether burnout altitude control is required, and if so what a reasonable specification of burnout altitude might be.

The ascent guidance equations could be used for the LEM Hohmann descent injection maneuver of Section 3.3 if no engine throttling is performed. No burnout altitude control is required for this maneuver.

The ascent equations are used for aborts during a lunar landing maneuver. The abort powered maneuver would have the objective of a direct ascent-to-rendezvous with the CSM (Chapter 8). It is probably not necessary to provide burnout altitude control for aborts which occur early in the landing phase. In fact, it is rather difficult to change the altitude very much when the burning period is short. The burning time would be short for aborts which occur early after the landing maneuver is initiated. If burnout altitude control is exercised for aborts early in the landing phase, altitude increases could be accomplished by an initial "vertical rise" period in which the thrust is initially pointed along the radius vector to the vehicle. While such thrust regimes are fuel inefficient, a great deal of propellant is available for early abort conditions.

For aborts which occur late in the landing maneuver, altitude control is definitely required. Furthermore, burnout altitude for an abort late in the landing maneuver might be specified to be higher than for a normal ascent from the lunar surface if

the phase angle between the two vehicles is large and a direct abort trajectory is required with a minimum specified perilune condition. Approximately one foot is added to the perilune altitude for every foot of added burnout altitude. There is, however, ΔV a penalty for burning out at higher altitudes.

Emergency launches from the surface of the moon - in particular emergency launches which occur before any re-alignment of the IMU - require burnout altitude control for a safe perilune. A higher than normal burnout altitude might be advisable. If the emergency ascent is into a waiting orbit (the usual case), a slight overspeed terminal velocity could be explicitly specified to further guarantee a safe perilune trajectory.

There are two kinds of "non-emergency" ascents from the lunar surface. The first is the direct ascent-to-rendezvous trajectory, which is guided if the launch takes place within the direct-ascent launch window. The second is the parking-orbit ascent trajectory, which is used when it is too late for a direct ascent. Direct ascent trajectories almost always have non-zero cut-off flight path angles. The perilune location is sometimes between the burnout position and the CSM intercept point, and sometimes after the CSM intercept point. It appears reasonable to regard the former kind of trajectory - the one in which the sequence of events is burnout, perilune, and interception - as being much more critical in respect to the perilune altitude than the latter kind of trajectory - the one in which the events are burnout, interception, and, if rendezvous is not accomplished, perilune. For the latter kind of trajectory, either the LEM main ascent engine or the RCS engines could be used in order to rendezvous, and if rendezvous must be postponed for a reason that does not involve the failure of both propulsion units, the perilune altitude can be raised by increasing apolune speed. It may therefore be advisable to increase the specified burnout altitude for the critical direct ascent case in which the sequence

of events is burnout, perilune, and intercept.

Finally, the ascent equations are used for ascent-to-rendezvous from an intermediate parking orbit, if one is used, for implementation of midcourse corrections, and for terminal rendezvous maneuvers (Chapter 7). Burnout altitude control is not necessary for any of these maneuvers.

6.2.2 Derivation of E Guidance Equations

The guidance equations for attaining specified values of r, $\dot{r}$, and v_θ (Fig 6.2) are first derived in this section. The method of controlling r and v_θ without restricting the final radius, r, is then illustrated. Finally the prediction of the burnout position vector $\underline{r}_{BO}$ is described.

The acquisition of the desired terminal values of radius and radial rate is achieved by calculating an appropriate thrust angle regime. The formula for the thrust angle regime contains the terminal time T as a parameter. For each value of T a solution thrust angle regime can be computed. If the spacecraft were flown according to this thrust angle regime, the radius and radial rate would attain the specified values at t = T. The precise value of T which also makes the terminal value of v_θ equal to its desired value must be selected. The formula which contains T as a parameter is first derived for computing the thrust angle regime which satisfies the radius and radial rate boundary-value requirements. The algorithm is then developed for finding the value of T which simultaneously makes v_θ (T) equal to the desired value of v_θ.

The steering law or guidance equation is a direct solution to the equations of motion, and so the starting point for deriving the radius and radial rate control law is the differential equation of radial motion:

$$\ddot{r} = -\mu/r^2 + v_\theta{}^2/r + a_T \sin\alpha \qquad (6.1)$$

The angle α is defined in Fig. 6.4. Equation (6.1) states that the total (kinematic) radial acceleration is equal to the sum of the gravitational acceleration, centrifugal acceleration, and radial component of thrust acceleration. Since a_T (t) is a function of time and not directly controllable in the LEM ascent stage, α (t) must be chosen so that it makes the terminal radius and radial rate equal to their specified values at time T.

$$r\,(T) = r_D \tag{6.2}$$

$$\dot{r}\,(T) = \dot{r}_D \tag{6.3}$$

In deriving an α (t) program which satisfies Eqs. 6.2 and 6.3, it is convenient to initially concentrate on $\ddot{r}$ (t). The current radius and radial rate are denoted at the present time, t_o, by

$$\left.\begin{matrix} r\,(t_o) \\ \dot{r}\,(t_o) \end{matrix}\right\} = \begin{matrix} \text{given current values} \\ \text{of radius and radial rate} \end{matrix} \tag{6.4}$$

Equations (6.1 - 6.4) constitute a two-point boundary-value problem. It is required to find an efficient $\ddot{r}$ (t) which causes the vehicle to move from the initial boundary point, represented by Eq. (6.4), to the desired terminal boundary point, represented by Eqs. (6.2 - 6.3). Having computed this solution, $\ddot{r}$ (t), α (t) is chosen so that the sum of the three sources of radial acceleration, namely gravitational, centrifugal, and a_T sin α (t), is equal to the solution $\ddot{r}$ (t).

The solution $\ddot{r}$ (t) must satisfy the following pair of integral equations which are obtained by simply integrating $\ddot{r}$ (t) between the current time t_o and the terminal time T, and substituting the initial and final boundary conditions into the resulting integral equations.

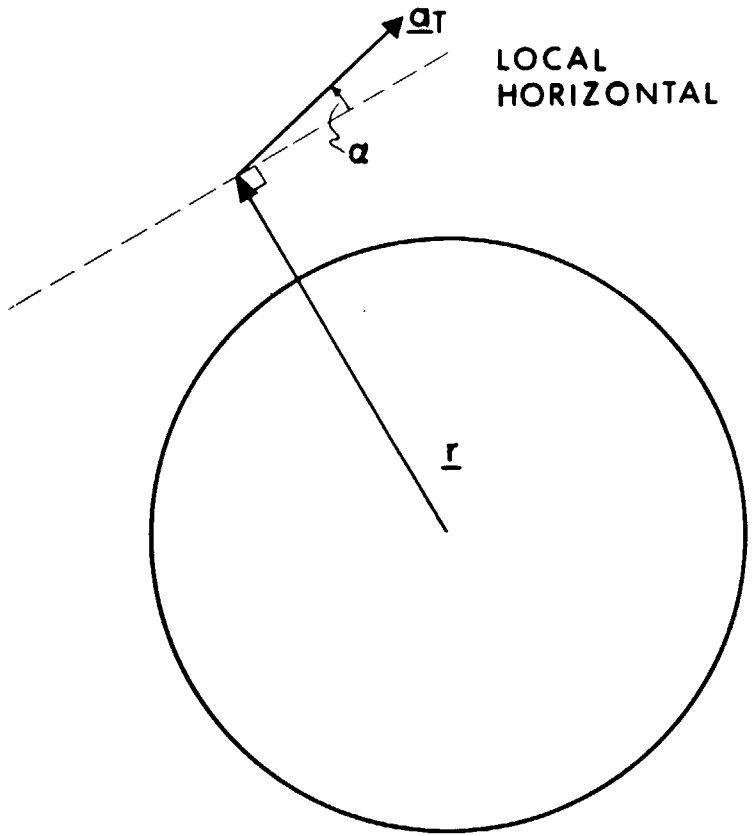

Fig. 6.4 Definition of α for the radius and radial rate boundary-value problem.

$$\dot{r}_D - \dot{r}_o = \int_{t_o}^{T} \ddot{r}\,(t)\,dt \tag{6.5}$$

$$r_D - r_o - \dot{r}_o\,T_{go} = \int_{t_o}^{T}\left[\int_{t_o}^{t} \ddot{r}\,(s)\,ds\right]dt \tag{6.6}$$

The following notation has been introduced in Eqs. (6.5) and (6.6)

$$\dot{r}_o = \dot{r}\,(t_o) \tag{6.7}$$

$$r_o = r\,(t_o) \tag{6.8}$$

$$T_{go} = T - t_o \tag{6.9}$$

The description of the boundary-value problem had a second-order differential equation, Eq. (6.1), which was coupled with the differential equation for v_θ through the centrifugal acceleration term and four auxiliary boundary conditions, Eq. 6.2-6.4. Equations (6.5 and 6.6) are superior in the sense that they are self-contained; the boundary conditions are inherently contained in this pair of equations. These equations constitute a pair of simultaneous linear integral equations from which the solution function of time, $\ddot{r}\,(t)$, must be determined. The solution of a pair of simultaneous integral equations is not simple. In fact Eqs. (6.5 and 6.6) do not even uniquely determine $\ddot{r}\,(t)$. There are an infinite number of functions, $\ddot{r}\,(t)$, which can satisfy Eqs. (6.5 and 6.6); and some other condition or conditions must be imposed before $\ddot{r}\,(t)$ is uniquely determined. The additional conditions desired are

$$\int_{t_o}^{T} a_T\,(t)\,dt = \text{Minimum} \tag{6.10}$$

and

$$v_\theta (T) = v_{\theta, D} \tag{6.11}$$

This formulation of the problem is too difficult to solve directly. The problem, so posed, belongs to a very difficult class of problems known as multidimensional, non-linear, variational, two-point boundary-value problems. Many researchers are attacking these problems. So far, the most fruitful results have been in the area of numerical optimization techniques based on the method of steepest ascent. These methods are not presently applicable to real-time explicit guidance of space vehicles, however, for the construction of one steepest ascent steering program might require a half-hour of computation time on a large scale, high-speed digital computer. A relatively simple steering law can be synthesized which satisfies Eq. (6.11) and comes very close to satisfying Eq. (6.10). Consideration of Eqs. (6.10) and (6.11), is deferred for the present time and some other means of making Eqs. (6.5) and (6.6) uniquely determine a solution $\ddot{r}(t)$ is attempted.

The difficulty of using Eqs. (6.5) and (6.6) for directly solving for $\ddot{r}(t)$ is that $\ddot{r}(t)$, regarded as expanded in a generalized Fourier series, has a infinite number of degrees of freedom. Equations (6.5) and (6.6) can determine only two of the undetermined coefficients, leaving an infinite number of undetermined Fourier coefficients. If the form of $\ddot{r}(t)$ could be restricted to two degrees of freedom, Eqs. (6.5) and (6.6) would uniquely determine the solution $\ddot{r}(t)$. By specifying that

$$\ddot{r}(t) = c_1 p_1(t) + c_2 p_2(t) \tag{6.12}$$

where c_1 and c_2 are two undetermined coefficients and $p_1(t)$ and $p_2(t)$ are two pre-specified linearly independent functions of time, $\ddot{r}(t)$ is restricted to two degrees of freedom, and Eqs. (6.5) and (6.6)

become a pair of simultaneous linear algebraic equations, which can be readily solved for c_1 and c_2. It might be noted that $\ddot{r}(t)$, as defined in Eq. (6.12), has two degrees of freedom because the determination of two arbitrary constants, c_1 and c_2, completely fixes and determines $\ddot{r}(t)$. Substituting the two-degree-of-freedom $\ddot{r}(t)$ into Eqs. (6.5) and (6.6) yields

$$\dot{r}_D - \dot{r}_o = f_{11}\, c_1 + f_{12}\, c_2 \tag{6.13}$$

$$r_D - r_o - \dot{r}_o\, T_{go} = f_{21}\, c_1 + f_{22}\, c_2 \tag{6.14}$$

where

$$f_{11} = \int_{t_o}^{T} p_1(t)\, dt \tag{6.15}$$

$$f_{12} = \int_{t_o}^{T} p_2(t)\, dt \tag{6.16}$$

$$f_{21} = \int_{t_o}^{T} \left[\int_{t_o}^{t} p_1(s)\, ds \right] dt \tag{6.17}$$

$$f_{22} = \int_{t_o}^{T} \left[\int_{t_o}^{t} p_2(s)\, ds \right] dt \tag{6.18}$$

For example, if $p_1(t)$ and $p_2(t)$ are specified as follows:

$$p_1(t) = 1 \tag{6.19}$$

$$p_2(t) = T - t\ , \tag{6.20}$$

Eqs. (6.13) and (6.14) become simply:

$$\dot{r}_D - \dot{r}_o = T_{go}\, c_1 + (T_{go}^2/2)\, c_2 \qquad (6.21)$$

$$r_D - r_o - \dot{r}_o\, T_{go} = (T_{go}^2/2)\, c_1 + (T_{go}^3/3)\, c_2 \qquad (6.22)$$

Then, in vector-matrix notation, the solution for c_1 and c_2 is:

$$\begin{bmatrix} c_1 \\ c_2 \end{bmatrix} = \begin{bmatrix} 4/T_{go} & -6/T_{go}^2 \\ -6/T_{go}^2 & 12/T_{go}^3 \end{bmatrix} \begin{bmatrix} (\dot{r}_D - \dot{r}_o) \\ (r_D - r_o - \dot{r}_o\, T_{go}) \end{bmatrix} \qquad (6.23)$$

It should be noted that the time-to-go, T_{go}, is the terminal time T minus the current time t_o:

$$T_{go} = T - t_o \qquad (6.24)$$

The quantity $(\dot{r}_D - \dot{r}_o)$ is the current deviation of the radial velocity from its desired value. The quantity $(r_D - r_o - \dot{r}_o\, T_{go})$ can be regarded as the "effective" deviation of the radial displacement. Both of these quantities must be driven to zero by t = T. The matrix in Eq. (6.23) whose elements are functions of T_{go} maps the separation between the current and desired boundary conditions into the coefficients c_1 and c_2. From Eq. (6.1) and Eq. (6.12), it is required that

$$c_1\, p_1(t) + c_2\, p_2(t) = -\mu/r^2 + v_\theta^2/r + a_T \sin\alpha \qquad (6.25)$$

since the sum of all the radial acceleration terms must be equal to the solution $\ddot{r}$ (t). Since only $\alpha(t)$ is directly controllable, $\alpha(t)$ must be chosen to satisfy Eq. (6.25). Thus:

$$\alpha(t) = \sin^{-1}\left\{\left[\mu/r^2 - v_\theta^2/r + c_1(t) + c_2 p_2(t)\right] \Big/ a_T\right\} \qquad (6.26)$$

Equation (6.26) yields the solution thrust angle regime. The coefficients c_1 and c_2 are computed from Eq. (6.23).

The matrix which maps the deviations in the boundary conditions into the coefficients c_1 and c_2 plays a very important role in the formulation and computation of the solution thrust angle regime. This matrix has been called the E matrix, because it allows the solution thrust angle program to be expressed as an explicit function of the separation between the current values of the boundary conditions and the desired values of the boundary conditions. The designation E Guidance results from this E matrix.

The form of the elements of the E matrix depends on the functions chosen for p_1 (t) and p_2 (t). The functions chosen for p_1 (t) and p_2 (t) in Eqs. (6.19) and (6.20) were for illustrative purposes. Thus the E matrix in Eq. (6.23) is only an example, and the choices made in Eqs. (6.19) and (6.20) are not necessarily the final or best choices.

The choice of functions for p_1 (t) and p_2 (t) is based on two considerations: 1) The fuel efficiency of the resulting steering law, and 2) the computational simplicity of the resulting E matrix. The elements of the E matrix in Eq. (6.23), which arose from choosing the p_1 (t) and p_2 (t) in Eqs. (6.19) and (6.20), are seen to be extremely simple. The simplicity is not surprising, since a constant and a linear function of time are very simple linearly independent functions of time. The functions that were used for the examples presented in this section were not as simple

as those in Eqs. (6.19)and(6.20), but they have been shown to be very satisfactory from the viewpoint of the fuel efficiency of the resulting steering law.

It might be noted that as T_{go} becomes vanishingly small, the elements of the E matrix increase without bound. Of course, under ideal conditions, the separations in the boundary values simultaneously disappear and c_1 and c_2 do not "blow up". Under practical conditions, the separation in the computed boundary values becomes negligible, but does not approach zero as T_{go} becomes vanishingly small. Consequently, as T_{go} becomes vanishingly small, the negligible but non-vanishing errors in the boundary conditions require an infinite thrust effort for correction, and c_1 and c_2 do blow up. This undesired behaviour of the E matrix and c_1 and c_2 is avoided by simply not recomputing the E matrix and c_1 and c_2 during the last few seconds of powered flight.

Equations (6.23)and(6.26) are repeatedly computed during a powered maneuver. The values c_1 and c_2 do not change, however, if the thrust vector orientation command is perfectly implemented and if the initial prediction of T is never altered. Even under practical conditions, if certain key quantities are properly smoothed, if the rocket thrust is nearly constant, and if the control system is functioning properly, the coefficients change rather slowly. Thus Eq. (6.26) can be used for many seconds without updating of c_1 and c_2. Because of the validity of this procedure, it is acceptable to omit recomputation of c_1 and c_2 in the terminal seconds of powered flight.

Before leaving the subject of radius and radial rate control, an illustration is presented of how the choice of an appropriate $\ddot{R}(t)$ program can control the terminal values of R and $\dot{R}$. Figure 6.5 illustrates a hypothetical boundary-value problem where:

$$\left.\begin{aligned} R(0) &= 1 \\ \dot{R}(0) &= 2 \end{aligned}\right\} \text{ Initial Boundary Condition} \qquad (6.27)$$

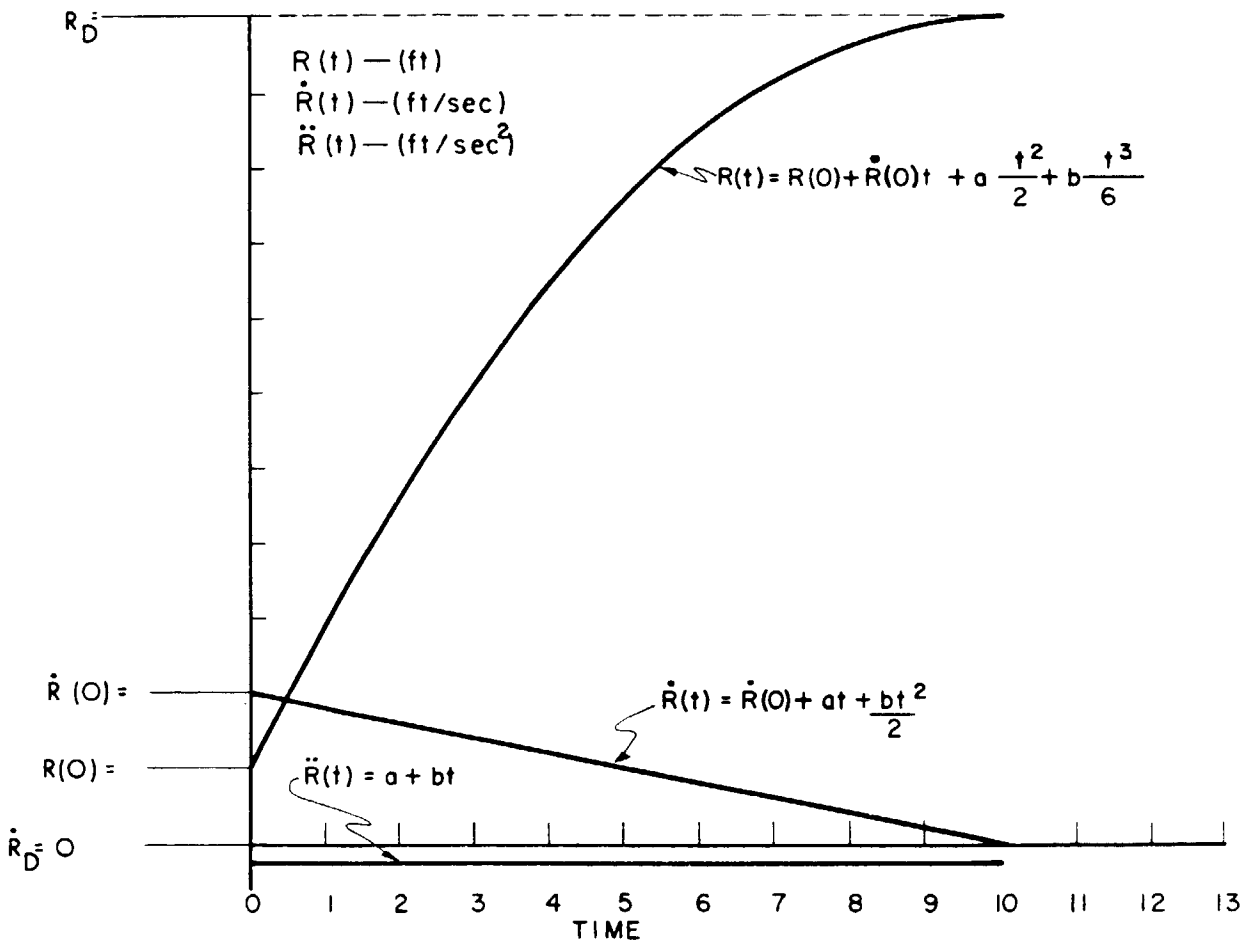

Fig. 6.5 Controlling R(t) and $\dot{R}$(t) with $\ddot{R}$(t).

$$R(T) = R_D = 11$$
$$\dot{R}(T) = \dot{R}_D = 0 \quad \left\{ \text{Desired Terminal Boundary Condition} \right. \tag{6.28}$$

If it is specified that

$$R(t) = a + bt \quad , \tag{6.29}$$

the coefficients a and b can be selected to satisfy Eqs. (6.27)and (6.28). These coefficients are evaluated by substituting T, which in this case is 10, into the equations for R (t) and $\dot{R}$ (t) and solving the resulting equations for a and b. It can be verified that for this particular boundary-value problem, b should be zero and the value of a should be a small negative number. The resulting R (t) and $\dot{R}$ (t) curves are shown in Fig. 6.5.

6.2.3 The Determination of T

An algorithm is required for computing the required value of terminal time T. T is chosen to satisfy the following equation:

$$v_\theta(T) = v_{\theta D} \tag{6.30}$$

Figure 6.6 indicates that the terminal value of specific angular momentum h is used as the basis for choosing T, rather than the terminal value of v_θ. The two quantities are really equivalent since

$$h = r\, v_\theta \tag{6.31a}$$

and the terminal value of r is either controlled or predicted. It is preferred to work with h rather than v_θ because the specific angular momentum is described by a simpler differential equation than the horizontal component of velocity.

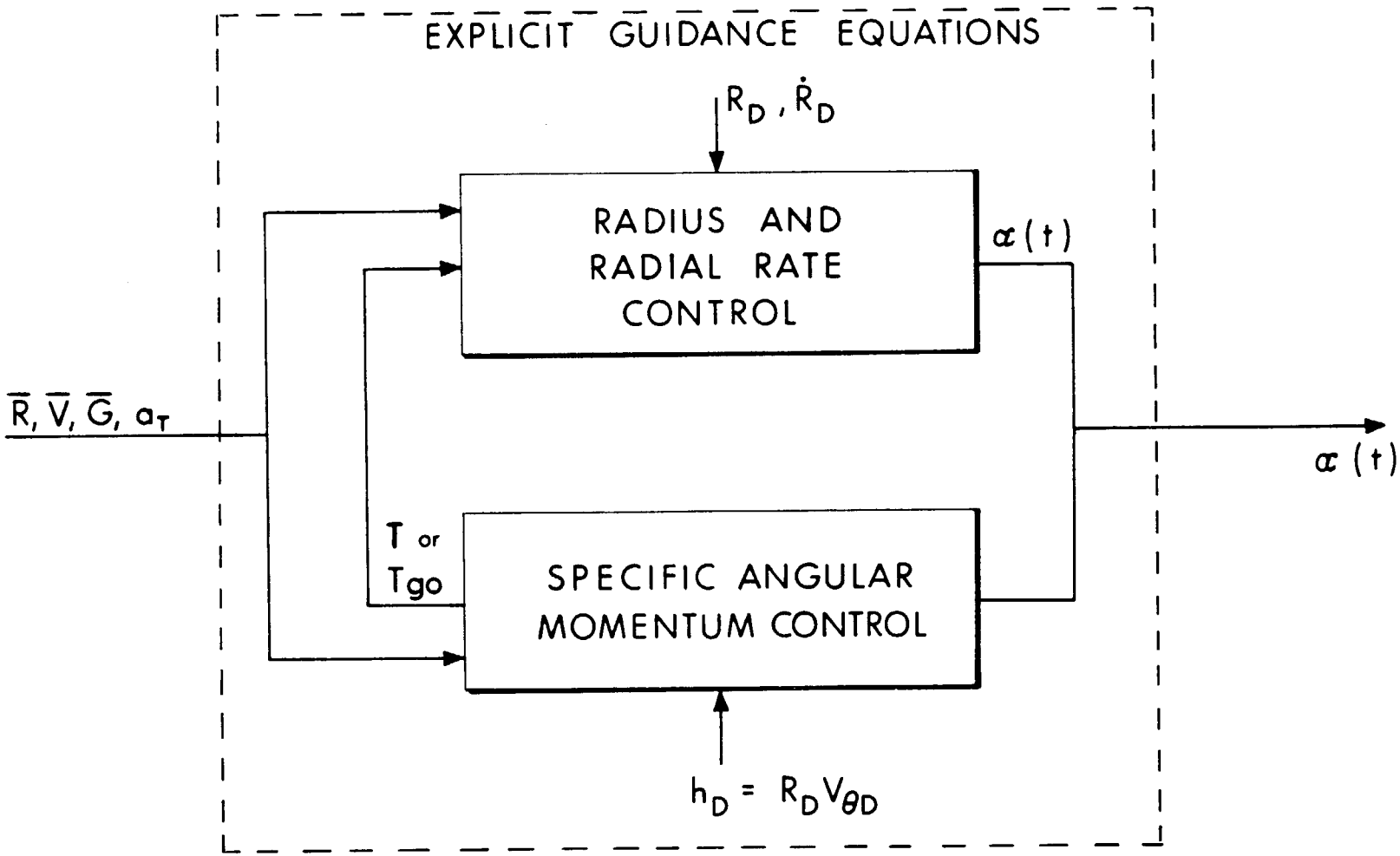

Fig. 6.6 The computation loop for finding α (t) and T_{go}.

Figure 6.6 shows that the computation of $\alpha(t)$ and T constitutes an iterative loop. The computation loop is started by guessing a value for T. The radius and radial rate control equations, Eqs. (6.23) and (6.26) for example, are then used to compute $\alpha(t)$. On the basis of $\alpha(t)$, T and the differential equation for h, an improved value of T, is computed in the block labeled "Specific Angular Momentum Control". In practice, an accurate value for T is established in one or two passes through the entire loop. It is the contents of the block labeled "Specific Angular Momentum Control" that is now described in detail.

The determination of T is, of course, equivalent to the determination of T_{go}. It is sometimes more convenient to think in terms of T_{go} rather than T, and whichever concept is more convenient is used in the following description.

The differential equation of specific angular momentum is particularly simple:

$$dh/dt = r\, a_T \cos\alpha \quad , \tag{6.31b}$$

but it is still difficult to integrate directly. Integrating Eq.(6.31b) would be helpful, if it were possible to perform the integration. Such an integration would be between the current time t_o and the proper terminal time T.

$$h(T) - h_o = \int_{t_o}^{T} r\, a_T \cos\alpha \, dt \tag{6.32}$$

But if T is the correct terminal time:

$$h(T) = h_D \quad , \tag{6.33a}$$

and

$$h_D - h_o = \int_{t_o}^{T} r\, a_T \cos\alpha \, dt \tag{6.33b}$$

If all the factors in the function under the integral sign in Eq. (6.33b) for $t_o \leq t \leq T$ are known, and direct integration of this function is possible, the resulting algebraic equation for T can be solved. Unfortunately, all these conditions cannot be satisfied.

The primary difficulty in integrating the specific torque is the factor $\cos\alpha(t)$. This factor is very complicated.

$$\cos\alpha(t) = \sqrt{1 - \left\{ \left[\mu/r^2 - v_0^2/r + c_1 p_1(t) + c_2 p_2(t) \right] / a_T \right\}^2} \qquad (6.34)$$

To permit at least a step toward integrating the specific torque, Eq. (6.34) is defined as the difference between an easily integrable term and a correction term.

$$r\cos\alpha\, a_T = r_D a_T - M_c \qquad (6.35)$$

Then the differential equation for specific angular momentum becomes:

$$dh/dt = r_D a_T - M_c \qquad (6.36)$$

A simplification will result in the ensuing derivation if the origin of the computation time axis is considered to be located at the current instant. Thus $t = 0$ is the present time. Integrating Eq. (6.36) between $t = 0$ (the current time) and $t = T_{go}$ (the correct terminal time on the present computation time axis) results in:

$$h_D - h_o = - r_D v_e \ln(1 - T_{go}/\tau) - h_c \,, \qquad (6.37)$$

where

$$h_c = \int_0^{T_{go}} M_c \, dt \qquad (6.38)$$

and

$$\tau = v_e / a_T(0) \qquad (6.39)$$

A more detailed derivation of Eqs. (6.36) through (6.39) is presented in Appendix B. Eq. (6.37) is next solved for the T_{go} which occurs in the argument of the natural logarithm in Eq. (6.37). The result has the following form:

$$T_{go} = \tau \left\{ 1 - \exp \left[- (h_D - h_o + h_c)/r_D v_e \right] \right\} \qquad (6.40)$$

The only unknown term on the right-hand side of Eq. (6.40) is h_c. A method for accurately estimating h_c is next developed. A rough estimate of h_c, ($h_{c,n}$ where initially $h_{c,1} = 0$), is used in Eq. (6.40) to obtain an estimate of T_{go}, referred to as $T_{go,n}$. The subscript "n" indicates the nth estimate in an iterative loop. Thus, the next improved value of T_{go} will be $T_{go,n+1}$. This estimate of T_{go} is used to determine a thrust angle regime which satisfies the specified radius and radial rate boundary conditions. The spacecraft is then flown (mathematically), for $T_{go,n}$ seconds according to the calculated thrust angle regime, and the final specific angular momentum, $h_{f,n}$ is observed. If $h_{f,n}$ is not equal to h_D, $h_{c,n}$ is modified to obtain a better estimate of the correct h_c. A logical equation for computing an improved estimate of h_c is:

$$h_{c,n+1} = h_D - h_{f,n} + h_{c,n} \qquad (6.41)$$

With the improved estimate of h_c obtained from Eq. (6.41), an improved estimate of T_{go} is computed from Eq. (6.40) along with a new thrust angle regime using the new estimate, $T_{go,n+1}$, for T_{go}. After another hypothetical flight of the spacecraft, the new final specific angular momentum, $h_{f,n+1}$, is computed and the process of obtaining an improved estimate of h_c and T_{go} is repeated. The eventual convergence of this process depends on the derivative of the right-hand side of Eq. (6.40) with respect to T_{go}. The magnitude of this derivative must be less than one for convergence. Since h_c is the only term on the right-hand

side of Eq. (6.40) which is a function of T_{go}, the convergence and speed of convergence of the iterative process depend on the derivative of h_c with respect to T_{go}. It has been found that h_c varies only slightly with respect to T_{go}, and consequently the process just described converges very rapidly. Thus:

$$h_{f,n} \rightarrow h_D \text{ (for } n = 1, 2, \ldots) \quad , \tag{6.42}$$

and the correct value of T_{go} is finally established.

A physical interpretation of this numerical process is illustrative. Assume that the rate of change of specific angular momentum had been approximated as follows:

$$dh/dt \approx r_D \, a_T \tag{6.43}$$

Evidently, the specific torque in Eq. (6.43) is overestimated since

$$r \cos\alpha < r_D \text{ (in general)} \tag{6.44}$$

That is, the torque lever arm is in general shorter than the estimate, r_D, in Eq. (6.43). The most important effect comes from the fact that:

$$\cos\alpha < 1 \text{ (generally)}, \tag{6.45}$$

and thus torque is "lost". Nevertheless, Eq. (6.43) is integrated and T_{go} determined:

$$T_{go} \approx \tau \left\{ 1 - \exp\left[-(h_D - h_o)/r_D v_e \right] \right\} \tag{6.46}$$

Equation (6.46) computes too short a time-to-go because it is based on a torque lever arm of r_D, which is greater than the actual torque lever arm. Torque is "lost", principally because α is not zero (note Eq. (6.45)). Since specific torque is lost,

the integral of specific torque, specific angular momentum, is also lost. Eq. (6.46) can be corrected by adding an estimate of the loss of specific angular momentum to the term $(h_D - h_o)$. The loss of specific angular momentum is defined as the deficiency in specific angular momentum due to the fact that the actual torque lever arm is less than r_D. If the estimate of the loss of specific angular momentum is denoted by $h_{c,n}$ and added to $(h_D - h_o)$ in Eq. (6.46), the T_{go} becomes:

$$T_{go} \approx \tau \left[1 - \exp\left(-(h_D - h_o + h_{c,n})/r_D v_e\right)\right] \quad (6.47)$$

This time-to-go is then used in order to determine the vehicle trajectory for the computed number of seconds using the thrust angle regime calculated for this particular value of time-to-go. In addition, assume that the resulting final specific angular momentum is not equal to h_D. It is then concluded that the estimate of how much specific angular momentum would be lost was incorrect. Denoting the final specific angular momentum by $h_{f,n}$ the error in final specific angular momentum is calculated. The error in the final specific angular momentum is:

$$h_D - h_{f,n} \quad (6.48)$$

Evidently the momentum loss was not estimated correctly and was off by approximately the value in Eq. (6.48). This "loss" found in Eq. (6.48) is then added to the first guess at the loss to obtain a better guess:

$$h_{c,n+1} = h_D - h_{f,n} + h_{c,n} \quad (6.49)$$

Equation (6.49) is seen to be the same as Eq. (6.41).

If an algorithm can be synthesized for predicting the final specific angular momentum which would result from a given guess at T_{go}, then an improved estimate of T_{go} can be

computed. There are many possible approaches to designing a final-specific-angular-momentum predictor. The approach developed here offers certain computational advantages, can be made almost arbitrarily accurate, and also is relatively simple. The development is based on a Taylor's series expansion. This function appears nearly linear when plotted, and consequently the series expansion can be truncated after a few terms. Consider the function:

$$H(t) = \exp\left[-\left(h(t) - h_o\right) / r_D v_e \right] \tag{6.50}$$

This can be expanded in a Taylor's series expansion about $t = 0$, the current time:

$$H(t) = H(0) + \dot{H}(0)t + \ddot{H}(0)t^2/2 + H^{(3)}(0)t^3/6 + H^{(4)}(0)t^4/24 + \ldots \tag{6.51}$$

If this expansion is evaluated for $t = T_{go,n}$, then the following is obtained:

$$H(T_{go,n}) \equiv \exp\left[-(h_{f,n} - h_o) / r_D v_e \right] \tag{6.52}$$

The coefficients of the powers of $T_{go,n}$ are evaluated in Appendix C.

Next consider the following expression:

$$\exp\left[-(h_D - h_o + h_{c,n}) / r_D v_e \right] = \exp\left[-(h_D - h_o) / r_D v_e \right] \exp\left[-h_{c,n} / r_D v_e \right] \tag{6.53}$$

The equality in Eq. (6.53) is due to the law of multiplication of exponential functions:

$$e^{x+y} = e^x e^y \tag{6.54}$$

Eq. (6.53) is now divided by Eq. (6.52):

$$\exp\left[-(h_D - h_o + h_{c,n})/r_D v_e\right] / H(T_{go,n}) = \exp\left[-(h_D - h_{f,n} + h_{c,n})/r_D v_e\right] \quad (6.55)$$

The right-hand side of Eq. (6.55) is also:

$$\exp\left[-(h_D - h_{f,n} + h_{c,n})/r_D v_e\right] = \exp(-h_{c,n+1}/r_D v_e) \quad (6.56)$$

A better estimate of T_{go}, $T_{go,n+1}$, can now be calculated from:

$$T_{go,n+1} = \tau \left\{1 - \exp\left[-(h_D - h_o)/r_D v_e\right] \exp(-h_{c,n+1}/r_D v_e)\right\} \quad (6.57)$$

From $T_{go,n+1}$, a new thrust angle regime can be determined along with the new coefficients $H(0)$, $\dot{H}(0)$, $\ddot{H}(0)$, etc. $H(T_{go,n+1})$ is next calculated and Eq. (6.55) and Eq. (6.57) again used in order to obtain $T_{go,n+2}$.

While other means of predicting $h_{f,n}$ and obtaining $T_{go,n+1}$ are feasible, the procedure presented here has the following three advantages:

1) The function expanded in a Taylor's series is nearly linear, and consequently, abrupt truncation of the series is permissible. This would not true if h(t), for example, were expanded.

2) By expanding H(t) as it is defined in Eq. (6.50), the right-hand side of Eq. (6.52) is obtained when the expansion is evaluated for T_{go}. Note that the exponential in Eq. (6.52) is obtained directly and it is not necessary to evaluate an exponential function.

3) After an accurate value of T_{go} is found, a good estimate of the value of $\exp(-h_c/r_D v_e)$ at some succeeding time (one computation cycle later, for example) can be found by decrementing T_{go} by the elapsed time, δT_{go}, and performing the following calculation:

$$\exp\left(-h_c/r_D v_e\right) = \left[1 - (T_{go} - \delta T_{go})/\tau\right] / \exp\left[-(h_D - h_o)/r_D v_e\right] \tag{6.58}$$

where h_o is the new (present) specific angular momentum. Eq. (6.58) is obtained by algebraic manipulation of Eq. (6.57) while dropping the subscript notation. The fact that at any instant following the initial accurate estimation of T_{go}, a good estimate of $\exp\left(-h_c/r_D v_e\right)$ can be obtained is very important. It means, in practice, that after the initiation of powered flight only a pass and a half through the iterative loop is necessary. In order to describe clearly the steps which occur in the guidance computer during any computation cycle following the first, the following sequence of steps is summarized.

The Computational Steps Involved in Computing $\alpha(t)$ and T_{go}

1. Compute the present state vector, $\underline{r}$ and $\underline{v}$.
2. Perform the computation in Eq. (6.58).
3. Compute the required thrust angle regime, $\alpha(t)$, using $T_{go} - \delta T_{go}$ for the current T_{go}. The thrust angle regime $\alpha(t)$ is obtained from Eqs. (6.23) and (6.26).
4. Calculate the coefficients in Eq. (6.51), namely $H(0)$, $\dot{H}(0)$, etc., as shown in Appendix C.
5. Evaluate the right-hand side of Eq. (6.51), using $T = T_{go} - \delta T_{go}$ and obtaining $\exp\left[-(h_f - h_o)/r_D v_e\right]$ (Note Eq. (6.52)).
6. Perform the calculation illustrated in Eq. (6.55), obtaining thereby a better estimate of $\exp\left(-h_c/r_D v_e\right)$ (Note Eq. (6.56)).
7. Use the better estimate of $\exp\left(-h_c/r_D v_e\right)$ in Eq. (6.57) in order to obtain an accurate value for T_{go}.
8. Using this accurate estimate of T_{go}, find the thrust angle regime corresponding to the accurate T_{go}.
9. Finally, compute the pitch command on the basis of this last computed $\alpha(t)$. If T_{go} is smaller than ϵ, count down the time and issue the thrust termination command.

6.2.4 Controlling the Injection Velocity Vector Without Controlling The Injection Altitude

The derivation of the radius and radial rate control equations required satisfying both Eqs. (6.5) and (6.6). Evidently, Eq. (6.6) does not have to be satisfied if it is not necessary to control injection altitude. Since Eq. (6.5) can determine only one degree-of-freedom, the appropriate definition of $\ddot{r}(t)$ is:

$$\ddot{r}(t) = c_1 p_1(t) \tag{6.59}$$

Substituting this definition of $\ddot{r}(t)$ into Eq. (6.5) yields:

$$\dot{r}_D - \dot{r}_0 = c_1 \int_{t_0}^{T} p_1(t)\, dt \tag{6.60}$$

Consequently:

$$c_1 = (\dot{r}_D - \dot{r}_0) \Big/ \int_{t_0}^{T} p_1(t)\, dt \tag{6.61}$$

If $p_1(t)$ is defined as follows:

$$p_1(t) = 1 \tag{6.62}$$

c_1 becomes

$$c_1 = (\dot{r}_D - \dot{r}_0) \Big/ T_{go} \tag{6.63}$$

Another possible choice for $p_1(t)$ is:

$$p_1(t) = a_0 + a_1(T - t) \tag{6.64}$$

where a_0 and a_1 are arbitrary pre-specified constants. Then:

$$c_1 = (\dot{r}_D - \dot{r}_0) \Big/ (a_0 T_{go} + a_1 T_{go}^2 / 2) \tag{6.65}$$

This is an interesting choice of $p_1(t)$ because a_0 and a_1 can be adjusted in pre-flight simulations in order to optimize fuel consumption.

The definition of $p_1(t)$ can be generalized to:

$$p_1(t) = a_0 + a_1(T - t) + a_2(T - t)^2 + \ldots + a_n(T - t)^n \quad (6.66)$$

The appropriate c_1 is then:

$$c_1 = (\dot{r}_D - \dot{r}_0) \Big/ \left[a_0 T_{go} + a_1 T_{go}^2/2 + \ldots + a_n T_{go}^{n+1}/(n+1) \right] \quad (6.67)$$

It should be evident that $p_1(t)$ can be developed in pre-flight simulations in order to make the in-flight performance arbitrarily close to optimum. Furthermore, the in-flight boundary-value solution is always exact. (The present discussion on optimization also applies to the case where radius is controlled.)

A review of the computation steps performed in the computer when $\underline{V}_{BO}$ only is controlled is as follows:

1. An initial guess at T_{go} is made.
2. c_1 is computed from Eq. (6.67)
3. The thrust angle with respect to the local horizontal is computed using:

$$\alpha(t) = \sin^{-1}\left\{ \left[\mu/r^2 - V_\theta^2/r + c_1 p_1(t) \right] / a_T \right\} \quad (6.68)$$

4. The burnout radius of the spacecraft is predicted. (The prediction equation was derived by finding the second integral of Eq. (6.59) with p_1 defined as in Eq. (6.66).)

$$r_{BO} = r_0 + T_{go}\dot{r}_0 + c_1 \left[a_0 T_{go}^2/2 \ldots + a_n T_{go}^{n+2}/(n+2) \right] \quad (6.69)$$

5. The estimate of T_{go} is refined by the equations which control the final value of specific angular momentum.

6.2.5 Powered Ascent-to-Intercept Guidance

The steering equations described in Section 6.2.4 are used in order to inject the LEM into a parking orbit. These equations are also employed in order to establish the appropriate initial conditions for a coasting trajectory which intercepts the CSM. The velocity vector, required for a spacecraft to free-fall from point A to a given point B in a specified time is called the Lambert velocity vector. Evidently, at any point A where the LEM thrust is terminated, the LEM must possess the Lambert velocity vector and the CSM must be on an orbit such that it will also arrive at point B in T_{ff} seconds. Point A is not constrained, but it must be known because of the fact that the Lambert velocity vector is a function of A, B, and T_{ff}. In vector notation, the burnout position vector of the LEM at point A is denoted by $\underline{r}_{BO}$, and the point at which the LEM will intercept the CSM is denoted by $\underline{r}_{CM}$ (TOF). The time of LEM free-fall from $\underline{r}_{BO}$ to $\underline{r}_{CSM}$(TOF) is denoted by T_{ff}.

It is convenient to locate the origin of the time-axis at the instant of nominal (intended) engine ignition, i.e., at the beginning of the direct-ascent-to-intercept window. Measured on this time-axis, the time-of-intercept is TOF seconds (hence the terminology that the point of intercept is $\underline{r}_{CSM}$(TOF)). Note that because of this convention:

TOF	=	engine ignition delay +
		duration of powered flight +
		duration of free-fall

The above equation must be constrained to be true if the LEM is to arrive at $\underline{r}_{CSM}$ at the right time. There is another equation for TOF which is more convenient. This alternative equation explicitly contains the remaining time of rocket burning, T_{go}, at any instant of the powered flight.

TOF	=	time elapsed since the instant of nominal engine ignition + time-to-go till thrust termination + duration of free-fall

The aim point $\underline{r}_{CM}(TOF)$ is chosen during the pre-launch procedures as described in Section 5.4. The desired time of arrival, TOF, and the time of nominal engine ignition are known and related by:

$$TOF = t + T_{go} + T_{ff} \quad , \tag{6.70}$$

where:

t = time that has elapsed since the instant of nominal (intended) engine ignition

T_{go} = time-to-go until burnout

During the powered ascent maneuver, T_{go} and T_{ff} are chosen in order to satisfy Eq. (6.70). There is no direct constraint on the duration of powered flight, now is there any direct constraint on the duration of free-fall; but the sum of these times and the engine ignition delay (if any) is constrained according to Eq. (6.70). It should also be noted that:

$t + T_{go}$ = engine ignition delay (if any) + duration of powered flight

When the rocket thrust is terminated, the vehicle is by definition at $\underline{r}_{BO}$. The vehicle must then coast to $\underline{r}_{CM}(TOF)$, and Eq. (6.70) must be satisfied. Suppose that at any instant t during powered flight the vector $\underline{r}_{BO}$ could be predicted. If the remaining time of rocket burning T_{go} could also be predicted, then Eq. (6.70) could be solved for T_{ff}, the only remaining unknown in the equation:

$$T_{ff} = TOF - (t + T_{go}) \tag{6.71}$$

All the quantities required to make the solution to Lambert's problem well-defined are now available. These quantities are $\underline{r}_{BO}$, $\underline{r}_{CSM}(TOF)$ and T_{ff} . A subroutine which gives the solution to Lambert's problem can be interrogated in order to find the vertical and horizontal components of the Lambert velocity vector. The E guidance equations can be used to achieve the required Lambert velocity vector. Of course, the E guidance equations are also used to predict T_{go} . The only computational elements required in addition to the E guidance equations are the Lambert subroutine and the $\underline{r}_{BO}$ predictor. The $\underline{r}_{BO}$ predictor turns out to be quite simple as described in Section 6.2.6.

Since $\underline{r}_{BO}$ is not initially known, it must be estimated. The present position $\underline{r}(t)$ can serve for the first guess. The time-to-go is also initially guessed. The starting value is not critical. Then Eq. (6.70) can be evaluated for T_{ff} and the Lambert subroutine interrogated to find the required intercept velocity vector. In the next step the E guidance equations develop the correct thrust angle regime and T_{go} to achieve the Lambert velocity vector. The outputs of the E guidance equations are used as inputs to the $\underline{r}_{BO}$ predictor in order to predict $\underline{r}_{BO}$ accurately. Note, that all these steps constitute one complete cycle through an iterative loop. Several cycles through this loop develop mutually consistent and accurate values of $\underline{r}_{BO}$, $\dot{r}_{\lambda}$, $v_{\theta\lambda}$, T_{go} and $\alpha(t)$. Figure 6.7 depicts in block diagram from the ascent guidance system and guidance computation loop.

6.2.6 Burnout Position Prediction

In order to compute $v_{\theta\lambda}$ and $\dot{r}_{\lambda}$, the horizontal and vertical components of the Lambert velocity vector, it is necessary to predict the burnout position vector of the spacecraft. Since the vehicle is constrained to lie in a specific plane, the burnout position vector prediction is a planar problem. If

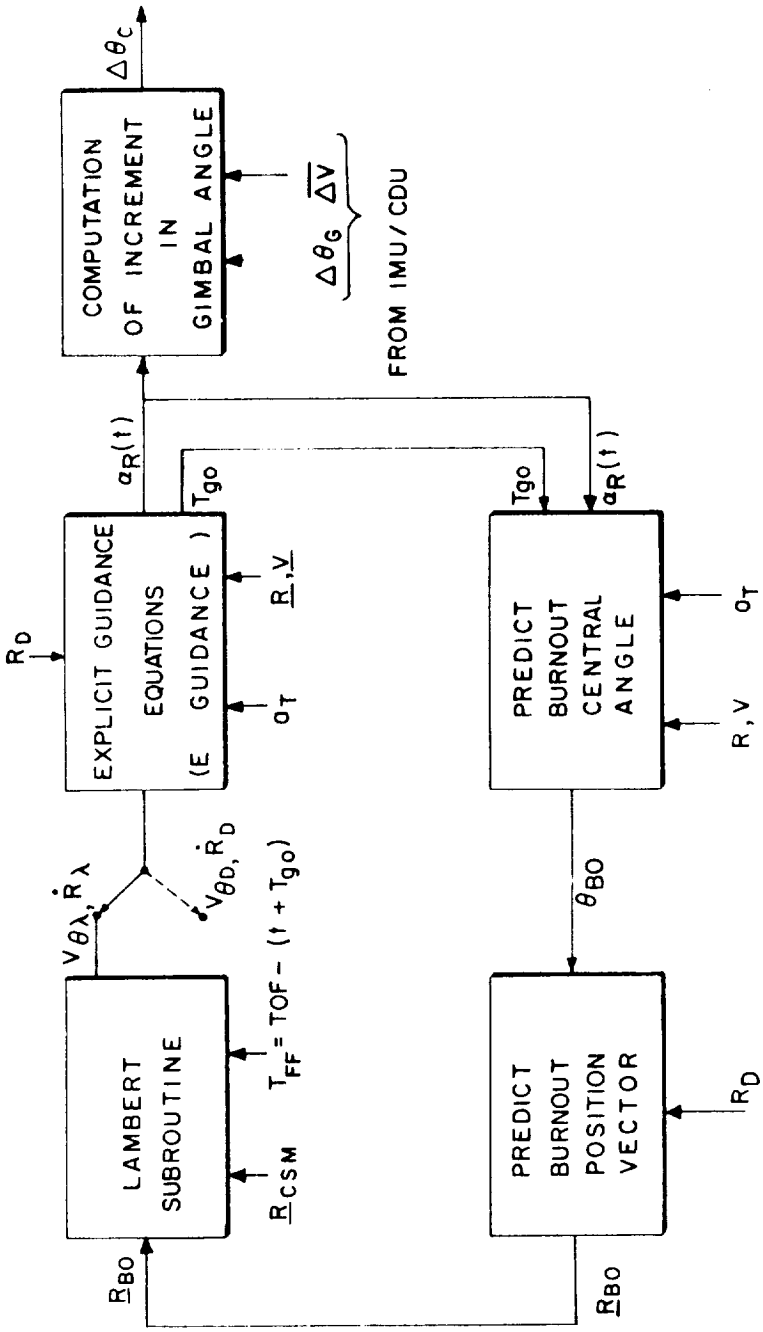

Fig. 6.7 Ascent guidance system.

burnout altitude is constrained, only θ_{BO} or, equivalently, θ_{go} need be predicted. If burnout altitude is not constrained, then both r_{BO} and θ_{BO} must be predicted. The equations for predicting r_{BO} have been developed in Section 6.2.2. The equations for predicting θ_{go}, the central angle which will be traveled during the remaining time of burning, will be developed in this section.

The θ_{go} prediction equations can be made almost arbitrarily accurate. There is no point,however, making the mathematical analysis more accurate than the assumed model for the vehicle on which the prediction is based. The following predictor is biased toward simplicity.

For this derivation, the origin of the time axis is assumed located at the current instant. Suppose that $\dot{\theta}(t)$ is represented as a quadratic function of time:

$$\dot{\theta}(t) = a_0 + a_1 t + a_2 t^2 \tag{6.72}$$

and that it is desired to evaluate the a_i's so that $\dot{\theta}(t)$, as defined in Eq. (6.72), is satisfied by the known values of $\dot{\theta}_o$, $\ddot{\theta}_o$, and $\dot{\theta}_f$. The quantities $\dot{\theta}_o$, $\ddot{\theta}_o$, and $\dot{\theta}_f$ are respectively the current value of angular rate, the current value of angular acceleration, and the burnout (final) value of angular rate. It can be shown that:

$$a_0 = \dot{\theta}_o \tag{6.73}$$

$$a_1 = \ddot{\theta}_o \tag{6.74}$$

$$a_2 = (\dot{\theta}_f - \dot{\theta}_o - \ddot{\theta}_o T_{go})/T_{go}^2 \tag{6.75}$$

The right-hand sides of these equations are easily evaluated.

$$\dot{\theta}_o = h_o / r_o^2 \tag{6.76}$$

$$\ddot{\theta}_o = \dot{h}_o / r_o^2 - 2\dot{r}_o h_o / r_o^3 \tag{6.77}$$

$$\dot{\theta}_f = h_D / r_D^2 \tag{6.78}$$

Equation (6.72) can be integrated between the current time t = 0 and the terminal time $t = T_{go}$ as follows:

$$\theta_f - \theta_o = a_0 T_{go} + a_1 T_{go}^2 / 2 + a_2 T_{go}^2 / 3 \tag{6.79}$$

$$\theta_{go} = \theta_f - \theta_o \tag{6.80}$$

These equations for predicting θ_{go} are seen to be quite simple. A more accurate, slightly more complicated, θ_{go} predictor can be designed by defining $\theta(t)$ as follows:

$$\dot{\theta}(t) = a_0 + a_1 t + a_2 t^2 + a_3 t^3 \tag{6.81}$$

and using the known value of $\theta_o^{(3)}$ or $\ddot{\theta}_f$ in order to evaluate the additional a_i. It is evident that the prediction of θ_{go} can be made arbitrarily accurate by assuming higher and higher order polynomials for $\dot{\theta}(t)$.

6.2.7 Control of Spacecraft Burnout Attitude

It is possible to synthesize a thrust angle regime which results in the attainment of specified values of burnout radius, radial rate, and radial acceleration. Controlling the terminal value of radial acceleration is equivalent to controlling the burnout attitude of the vehicle.

During the terminal rendezvous maneuvers (Section 7.6) it may be desirable to control the burnout attitude as well as the burnout velocity vector of the vehicle. The equations for performing these functions are derived as follows.

The differential equation of radial motion is:

$$\ddot{r} = -\mu/r^2 + V_\theta^2/r + a_T \sin\alpha \qquad (6.82)$$

It is necessary to satisfy this equation as well as the two terminal constraints:

$$\dot{r}(T) = \dot{r}_D \qquad (6.83)$$

$$\alpha(T) = \alpha_D \qquad (6.84)$$

Since there are two equations of constraint, a two-degree-of-freedom $\ddot{r}(t)$ is in order:

$$\ddot{r}(t) = c_1 p_1(t) + c_2 p_2(t) \quad , \qquad (6.85)$$

where, as before, $p_1(t)$ and $p_2(t)$ are simple, pre-specified, linearly independent functions of time, and c_1 and c_2 must be chosen to satisfy Eqs. (6.83) and (6.84). With reference to Eq. (6.82), evaluating each side of the equation at t = T, yields:

$$\ddot{r}(T) = -\mu/r_{BO}^2 + V_{\theta D}^2/r_{BO} + a_T(T) \sin\alpha_D \qquad (6.86)$$

All the quantities on the right-hand side of Eq. (6.86) are known. It is convenient to use the symbol $\ddot{r}_D$ for the right-hand side of Eq. (6.86). Then Eq. (6.86) is equivalent to:

$$\ddot{r}(T) = \ddot{r}_D \qquad (6.87)$$

Thus the two equations of constraint for $\ddot{r}(t)$ are:

$$\ddot{r}_D = c_1 p_1(T) + c_2 p_2(T) \qquad (6.88)$$

$$\dot{r}_D - \dot{r}_0 = c_1 \int_{t_0}^{T} p_1(t)\, dt + c_2 \int_{t_0}^{T} p_2(t)\, dt \qquad (6.89)$$

Suppose $p_1(t)$ and $p_2(t)$ are chosen as follows:

$$p_1(t) = 1 \tag{6.90}$$

$$p_2(t) = T - t \tag{6.91}$$

Then Eqs. (6.88) and (6.89) become:

$$\ddot{r}_D = c_1 \tag{6.92}$$

$$\dot{r}_D - \dot{r}_0 = T_{go}c_1 + (T_{go}^2/2)c_2 \tag{6.93}$$

Solving these equations for c_1 and c_2 yields:

$$c_1 = \ddot{r}_D \tag{6.94}$$

$$c_2 = (\dot{r}_D - \dot{r}_0 - T_{go}\ddot{r}_D)/(T_{go}^2/2) \tag{6.95}$$

The desired thrust angle profile is:

$$\alpha(t) = \sin^{-1}\left\{\left[\mu/r^2 - V_\theta^2/r + c_1p_1(t) + c_2p_2(t)\right]/a_T\right\} \tag{6.96}$$

This expression now appears the same as the expression derived in Section 6.2.2 on radius and radial rate control. The c_1 and c_2 are different, of course.

6.3 Typical Powered Ascent Trajectories

The characteristics of typical powered ascent maneuvers, controlled by the explicit guidance equations presented in the previous section, are illustrated in Figs. 6.8 through 6.11. The trajectory characteristics shown in Figs. 6.8 and 6.9 are for an aim point condition less than 180 degrees from the landing site (Section 5.4). After a 10 second vertical rise period, the

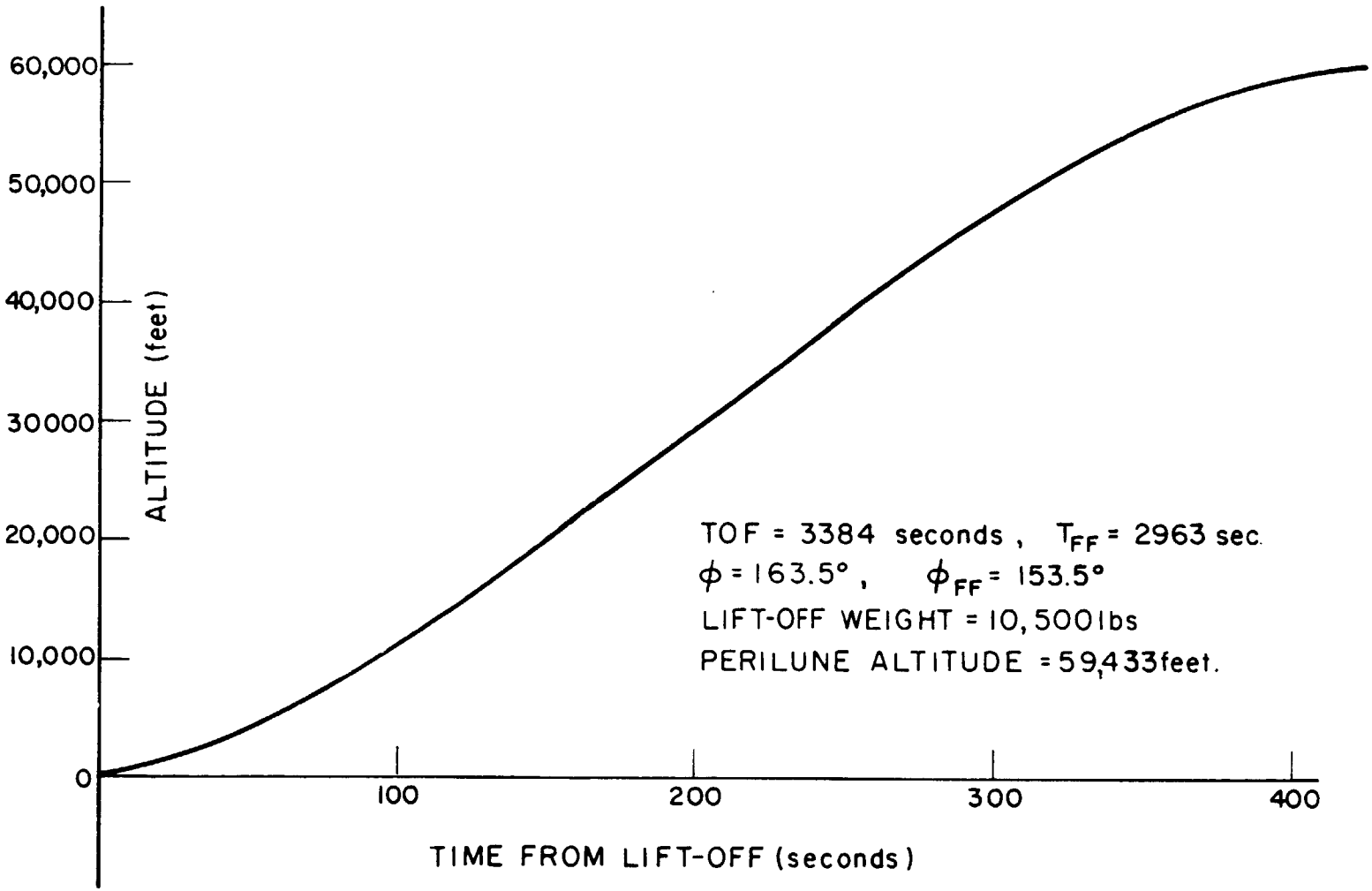

Fig. 6.8 Altitude versus time for ascent trajectory.

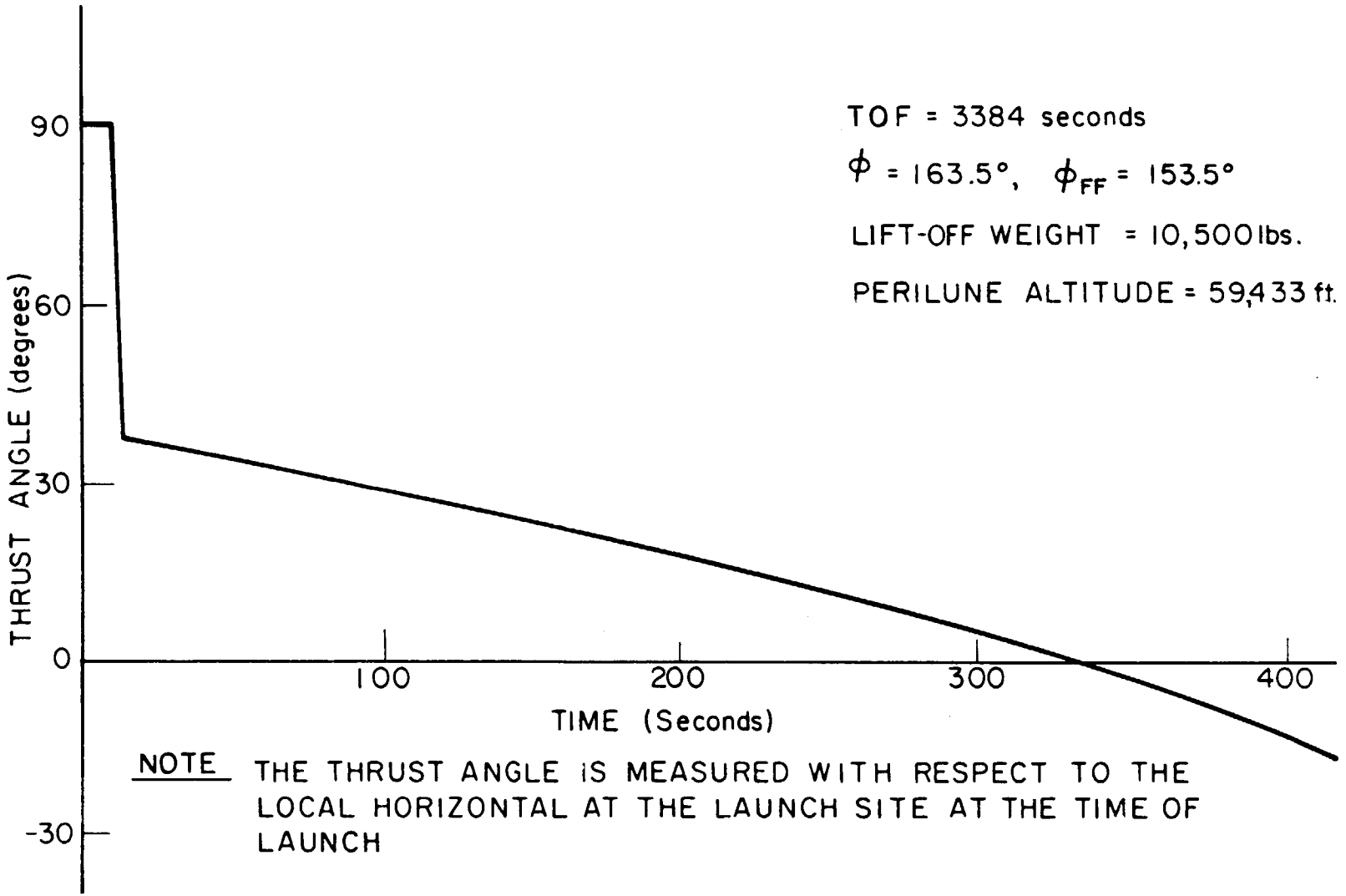

Fig. 6.9 Inertial thrust angle versus time (for ascent trajectory).

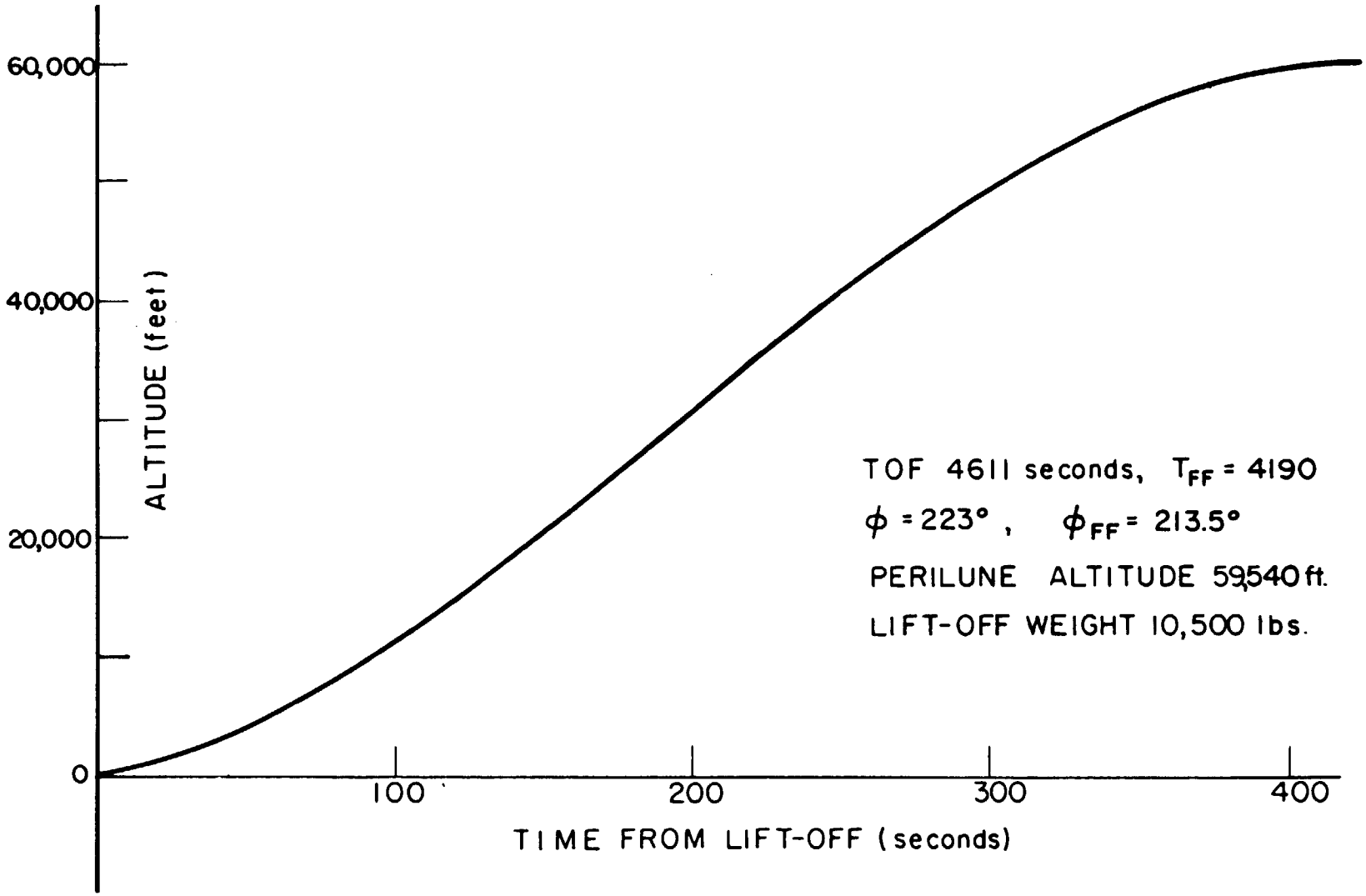

Fig. 6.10 Altitude versus time for ascent trajectory.

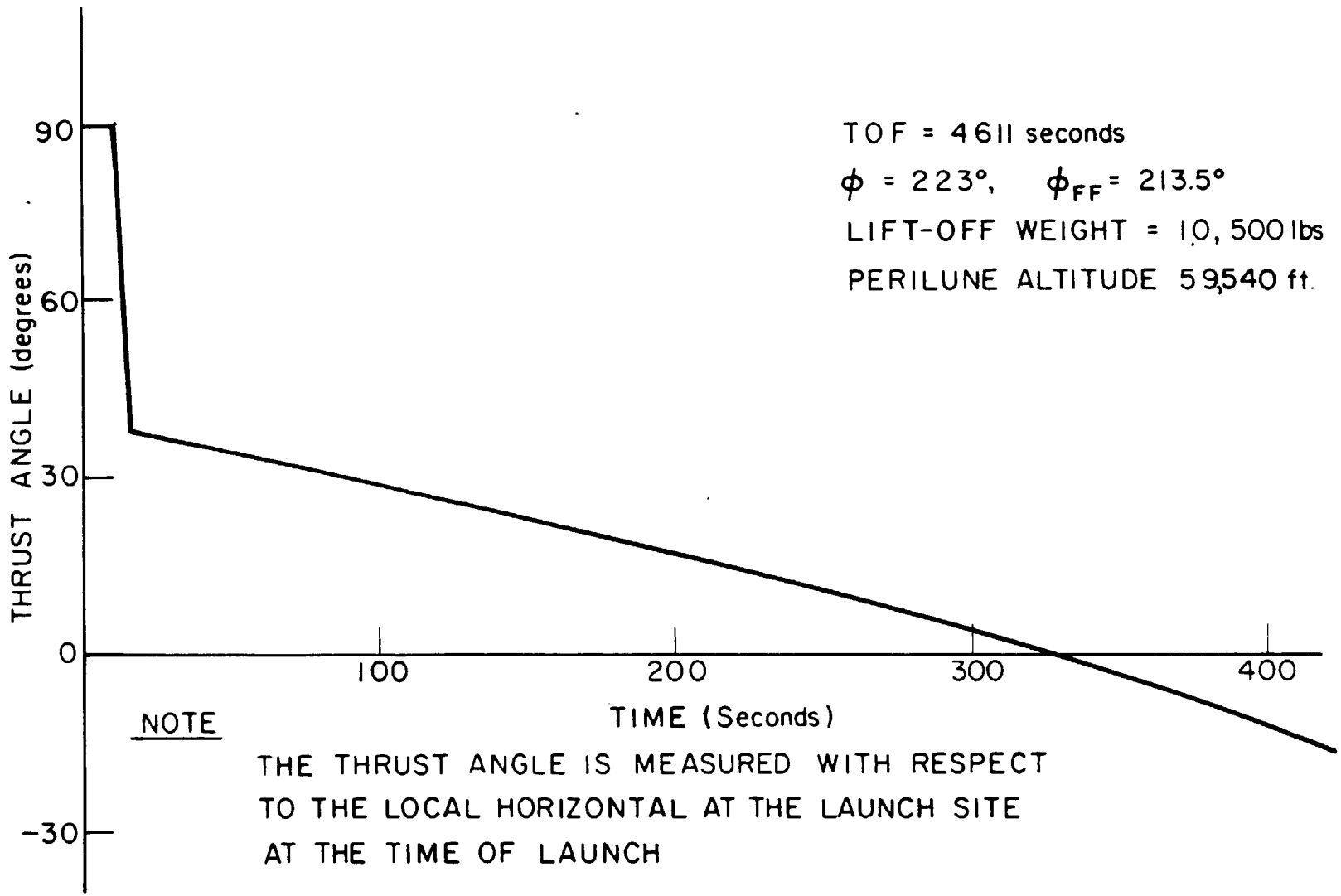

Fig. 6.11 Inertial thrust angle versus time (for ascent trajectory).

powered ascent maneuver was controlled to a burnout altitude of 60,000 feet with an injection velocity that would place the LEM on an intercept trajectory with an aim point 163.5 degrees from the landing site. Figure 6.8 is an altitude-time profile of the powered ascent maneuver. This maneuver lasted 421 seconds and covered a 164 nm ground range from launch point to injection. The injection velocity was 5576 ft/sec at a flight path angle of 0.26 degrees above the local horizontal. The initial LEM weight was assumed to be 10,500 pounds for this maneuver. The maneuver was controlled by the non-gimballed ascent engine which had a constant thrust of 3500 pounds at a specific impulse of 306 seconds. The commanded thrust angle profile is illustrated in Fig. 6.9. After the initial 10 second vertical rise, the LEM was pitched at its maximum attitude rate (10 degrees/second) until the thrust attitude commanded by the explicit ascent guidance equations was achieved. As shown in Fig. 6.9, the commanded thrust attitude was slowly varied relative to the initial coordinates at launch until injection. Since the powered ascent trajectory covers a central angle of 10 degrees, the thrust attitude at burnout is about 10 degrees below the local horizontal. The ascent trajectory after cutoff covers a central angle of 153.5 degrees to the desired aim point on the CSM orbit with a free fall flight time, t_{FF}, of 2963 seconds. The relative closing velocity between the CSM and LEM vehicles at the rendezvous aim point is 140 ft/sec for this particular ascent trajectory. The perilune altitude of the ascent trajectory is at 59,433 feet and occurs after the rendezvous aim point since the injection flight path angle was positive. It might be noted that this ascent trajectory would be located in about the middle of the possible direct ascent launch window for the trajectory case of less than 180 degree central angle as described in Section 5.4. The phasing angle θ_o between the two vehicles at ascent injection was 8.5 degrees for the maneuvers presented in this section.

Figures 6.10 and 6.11 illustrate similar powered ascent maneuver characteristics for an ascent trajectory that covers a central angle of greater than 180 degrees. The maneuver of Fig. 6.10 has a slightly different altitude-time profile than that of Fig. 6.8, since the injection velocity is 5580 ft/sec at a negative flight path angle of 0.18 degrees. The commanded thrust angle profile of Fig. 6.11 is virtually identical to that of Fig. 6.9 for the scales involved. Both ascent maneuvers required essentially the same time (421 seconds). The 213.5 degree ascent trajectory resulted in a final rendezvous relative velocity of 148 ft/sec. A perilune altitude of 59,540 feet occured between the injection and rendezvous maneuver in this case. The particular aim point chosen for the trajectory of Figs. 4.10 and 4.11 was again near the mid point of the direct ascent launch window.

It should be noted that the powered ascent maneuvers presented in this section assumed no LEM vehicle attitude dynamics other than the maximum 10 degree/second attitude rate. The resulting unpowered ascent trajectories from the two powered ascent maneuvers of Figs. 6.8 through 6.11 will be described in Section 7.4.3 for the following rendezvous midcourse correction phase.

Figure 6.12 illustrates typical relative phasing conditions between the CSM and LEM vehicles at the ascent ignition and cutoff points of the powered ascent maneuver. The injection phase angle, θ_0, of 8.5 degrees was chosen to represent launch conditions approximately in the center of the possible direct ascent launch window.

6.4 Effects of Delayed Launch Time.

Figures 6.13 and 6.14 summarize the ascent trajectory ΔV and perilune effects resulting from delayed launch times from that illustrated in Fig. 6.12. Figure 6.13 is for the 153.5 degree ascent trajectory of Figs. 6.8 and 6.9. With reference to Fig. 6.13, it can be seen that as the launch time is delayed, the required

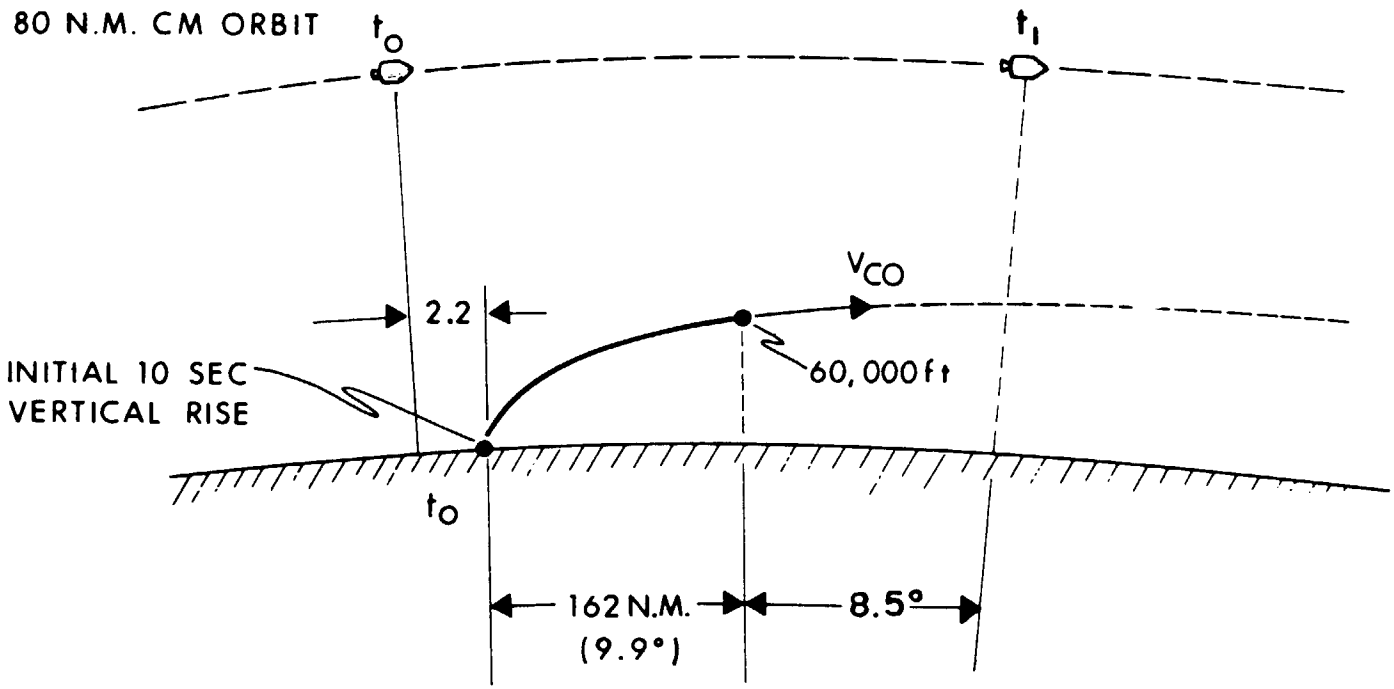

POWERED ASCENT TIME	421.5 SEC.
INITIAL WEIGHT	10,500 LBS.
I_{sp}	306 SEC.
INITIAL ACCELERATION	10.8 fps^2
FINAL ACCELERATION	19.8 fps^2
CUT-OFF VELOCITY	5500 fps - 5600 fps

Fig. 6.12 General characteristics of the powered ascent trajectory.

FIXED TIME OF ARRIVAL CONCEPT

ASCENT TRAJECTORY CHARACTERISTICS

ϕ_{FF} = 153.5°

I_o = 0.5°

h_{co} = 60,000'

θ_o = 8.5° (ZERO LAUNCH DELAY CASE)

LAUNCH DELAY (sec)	T_{FF} (sec)	V_1 (fps)	α_1 (deg)	ΔV_2 (fps)	$V_1 + \Delta V_2$ (fps)	ΔV_T (fps)	H_{per} (ft)	PERILUNE LOCATION w.r.t REND.
0	2963	5576	0.26	140	5716	6182	59,400	AFTER
20	2943	5579	-0.07	155	5735	6202	59,800	BEFORE
40	2923	5584	-0.40	176	5760	6230	56,200	BEFORE
60	2903	5588	-0.74	200	5788	6260	48,100	BEFORE
80	2883	5593	-1.08	227	5819	6294	36,200	BEFORE
100	2863	5598	-1.42	255	5853	6330	21,200	BEFORE

Fig. 6.13 Launch delay effects.

FIXED TIME OF ARRIVAL CONCEPT

ASCENT TRAJECTORY CHARACTERISTICS

ϕ_{FF} = 213.5°

I_o = 0.5°

h_{co} = 60,000'

θ = 8.5° (ZERO LAUNCH DELAY CASE)

LAUNCH DELAY (sec)	T_{FF} (sec)	V_I (fps)	α_I (deg)	ΔV_2 (fps)	$V_I + \Delta V_2$ (fps)	ΔV_T (fps)	H_{per} (ft)	PERILUNE LOCATION w.r.t RENDEZ.
0	1490	5580	-0.18	148	5728	6196	59,500	BEFORE
20	4170	5577	-0.35	140	5716	6185	56,800	BEFORE
40	4150	5575	-0.53	132	5707	6177	53,000	BEFORE
60	4130	5572	-0.70	126	5699	6171	47,500	BEFORE
80	4110	5570	-0.87	123	5693	6166	40,500	BEFORE
100	4090	5567	-1.06	122	5689	6164	31,600	BEFORE

Fig. 6.14 Launch delay effects.

injection velocity, V_1, increases slightly at progressively more negative injection flight path angles, α_1. The results shown in Fig. 6.13 are for a fixed time of arrival concept so that the free fall time from injection to aim point is progressively reduced by the amount of the launch delay. The terminal rendezvous velocity, ΔV_2, of Fig. 6.13 increases more rapidly than V_1 with launch delay time. The total launch and terminal rendezvous velocity, ΔV_T, of Fig. 6.13 is the sum of the injection velocity V_1, terminal rendezvous velocity ΔV_2, and the ΔV loss during the powered ascent maneuver which achieves the desired injection velocity. The additional characteristic velocity required during the powered ascent maneuver is summarized in Fig. 6.15 as a function of injection flight path angle or final radial velocity, $\dot{R}$. The ΔV_{Lost} in this figure is defined as the difference between the required injection velocity, V_1, and the integral of the thrust acceleration during the powered ascent maneuver controlled by the equations of Section 6.2. Figure 6.15 indicates that there is approximately a 10 ft/sec difference for positive and negative injection flight path angles over a normal direct ascent launch window. The ΔV_T column of Fig. 6.13 indicates the increase of the total ascent characteristic velocity requirement as a function of launch delay. For the initial launch time chosen ($\theta_0 = 8.5^{\circ}$), an 80 second launch delay approaches the 35,000 foot perilune limit of Section 5.4 with a ΔV penalty of 112 ft/sec for the 0.5 degree out of plane launch condition assumed in Fig. 6.13.

Figure 6.14 illustrates the effects of launch delays for the ascent trajectory of Fig. 6.10 and 6.11. Figs. 6.10 and 6.11 result in a free fall central angle of 213.5 degrees from a 0.5 degree out of plane launch condition. With reference to Fig. 6.14, it can be seen that the required injection velocity V_1 and a terminal rendezvous velocity ΔV_2 both decrease as the launch delay increases. This is consistent with the examples of Section 5.4 since the increases in injection phasing angle due to launch delays for a central angle greater than 180 degrees is approaching

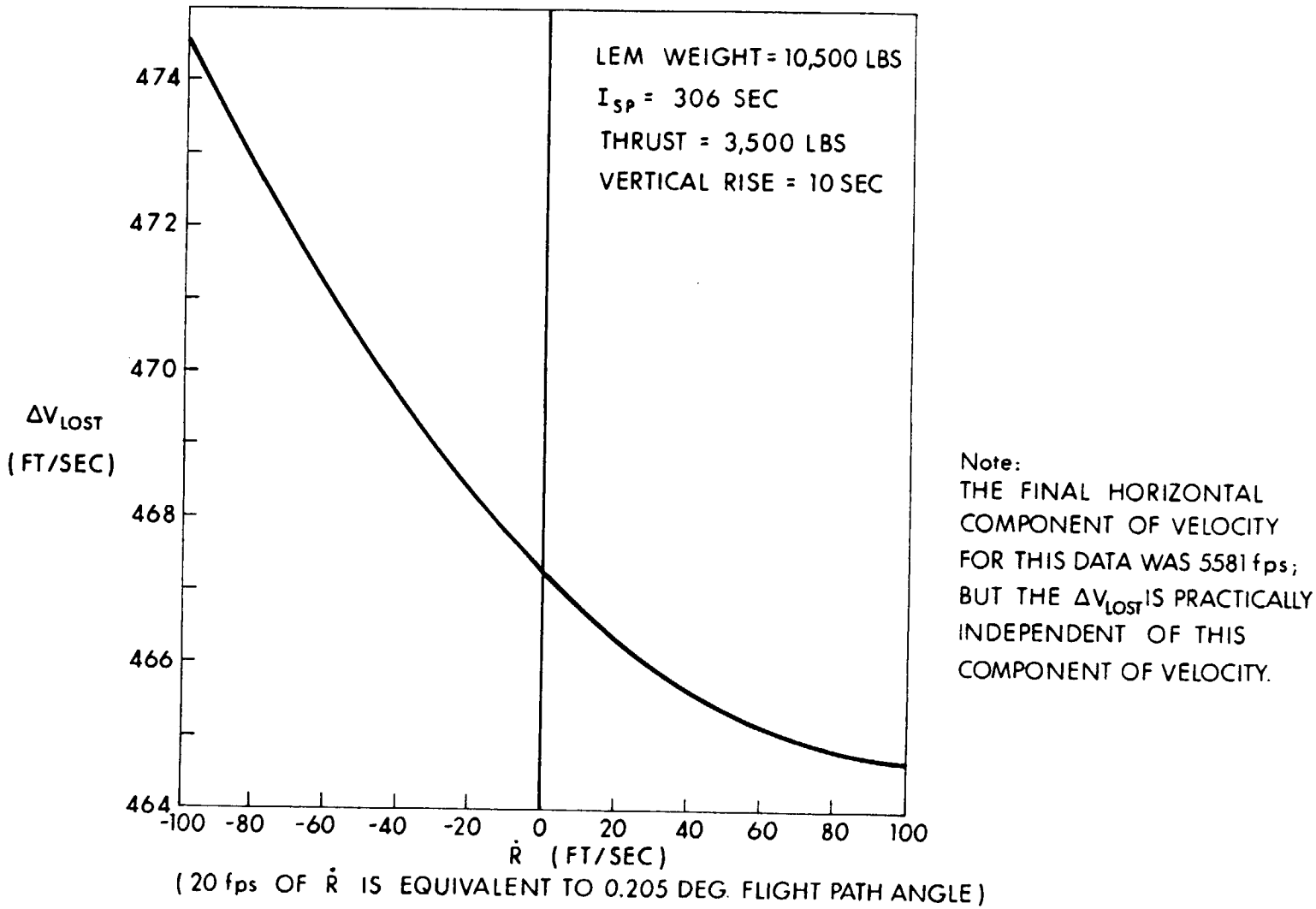

Fig. 6.15 Characteristic velocity lost as a function of burnout altitude rate and flight path angle.

the minimum ΔV requirement. The minimum ΔV condition is not reached, however, before the 35,000 foot perilune altitude condition is reached at a launch delay of about 90 seconds from the initial launch time chosen. It can be seen from Fig. 6.14 that the launch delay interval involved for this particular trajectory is near the minimum ΔV case since a launch delay of 90 seconds involves a difference in total ΔV of only 31 ft/sec.

6.5 G&N System Performance.

The one sigma injection uncertainties in the various position and velocity components for typical powered ascent maneuvers are illustrated in Fig. 6.16. The first row in this figure summarize the uncertainties due to IMU alignment and performance errors. The final row summarizes the rss of IMU and initial condition uncertainties.

The major factors contributing to the uncertainties of Fig. 6.16 are listed in Fig. 6.17. Items 1 and 2 of Fig. 6.17 summarize the initial position and velocity uncertainties of the landing site. Items 3 through 6 summarize the performance of the IMU accelerometers and gyros. Item 7 indicates that launch timing was compensated for by the ascent guidance system when it achieved the desired aim point injection conditions. A thrust termination uncertainty of 0.5 ft/sec was assumed for the ascent engine termination conditions.

The IMU performance during the powered ascent trajectory for the performance levels listed in Fig. 6.17 are summarized in Fig. 6.18. The major sources of IMU error for this phase are due to Items 1 and 2, initial platform misalignment and accelerometer bias. It was assumed in this example that the initial rss alignment uncertainty, due to the lunar surface alignment and drift after alignment prior to launch, was at a level of 1 mr at the time of launch. The total rss of all IMU errors shown in Fig. 6.18 are those listed in Fig. 6.16 for IMU

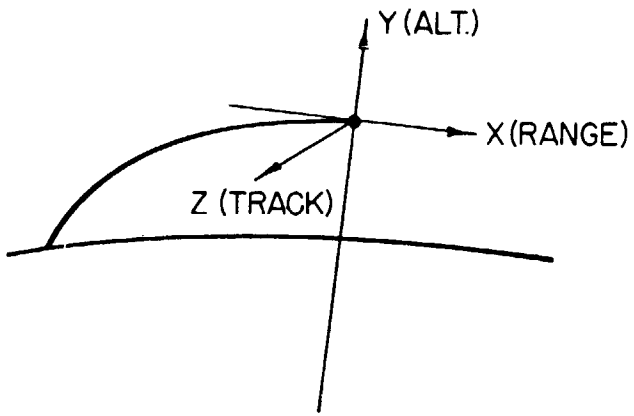

SOURCE	ΔX (FT)	ΔY (FT)	ΔZ (FT)	$\Delta\dot{X}$ (FPS)	$\Delta\dot{Y}$ (FPS)	$\Delta\dot{Z}$ (FPS)
RSS ALIGNMENT AND IMU ERRORS	638	1015	1086	3.5	6.5	6.6
RSS INITIAL CONDITIONS AND IMU ERRORS	2100	1810	2284	4.0	6.6	6.9

Fig. 6.16 Typical ascent trajectory injection errors.

1. INITIAL POSITION UNCERT. W.R.T. C.M. ORBIT	2000 FT. (RANGE & TRACK) 1500 FT. (ALT.)
2. INITIAL VELOCITY UNCERT. W.R.T. C.M. ORBIT	< 1 FPS (RANGE & TRACK) <0.1 FPS (ALT.)
3. INITIAL I.M.U. ALIGNMENT UNCERT.	1 MR
4. ACCEL. IA NON-ORTHOGONALITY	0.1 MR
5. ACCELEROMETER ERRORS	
BIAS	0.2 CM/SEC^2
SCALE FACTOR ERROR	100 PPM
ACCEL. SENS. S.F. ERROR	10 PPM/g
6. GYRO ERRORS	
BIAS DRIFT	10 MERU
ACCEL. SENS. DRIFT	10 MERU/g
ACCEL. SQUARED SENS. DRIFT	1 MERU/g^2
7. TIMING ERRORS	COMPENSATED FOR BY ASCENT GUIDANCE
8. THRUST TERMINATION UNCERT.	0.5 FPS

Fig. 6.17 Summary of ascent trajectory injection error factors.

No. 092678	POSITION			VELOCITY		
IMU ERROR SOURCE	RANGE (ft)	ALT (ft)	TRACK (ft)	RANGE (fps)	ALT (fps)	TRACK (fps)
1. INITIAL PLATFORM MISALIGNMENT (1 mr: uncertainty at launch)	467	907	990	2.5	5.9	5.9
2. ACCELEROMETER BIAS (0.2 cm/sec^2)	415	428	421	2.3	2.3	2.4
3. ACCELEROMETER SCALE FACTOR (100 ppm)	93	32		0.6	0.1	
4. ACCELEROMETER MISALIGNMENT (0.1 mr)	16	96			0.6	
5. GYRO FIXED DRIFT (0.15 deg/hr)	41	89	93	0.1	0.8	0.1
6. GYRO MASS UNBALANCE (0.15 deg/hr/g)	17	39	15		0.4	
R.S.S. OF ALL SOURCES	638	1015	1086	3.5	6.5	6.6

Fig. 6.18 IMU powered ascent trajectory uncertainties.

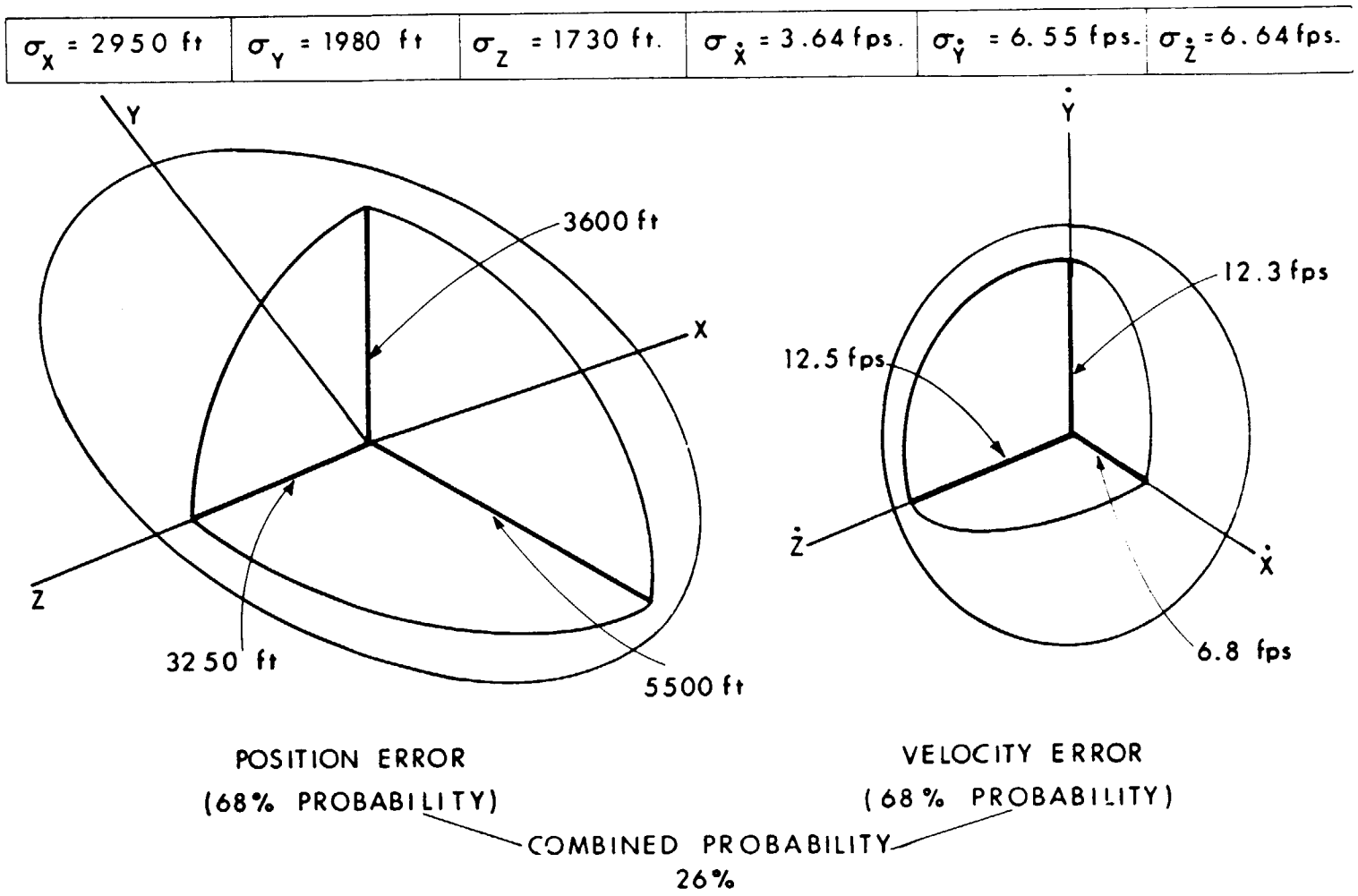

Fig. 6.19 Error volume at burnout of ascent.

performance.

The position and velocity error volumes at ascent injection are illustrated in Fig. 6.19. These error volumes were generated from the correlation matrix at injection resulting from initial condition and IMU performance uncertainties. The one sigma component values listed at the top of Fig. 6.19 are the square roots of the diagonal terms of the final correlation matrix and are essentially equal to the overall rss injection uncertainties listed in Fig. 6.16. The injection uncertainty shown in Figs. 6.16 and 6.19 will be used as standard ascent injection uncertainties in evaluating the rendezvous guidance technique described in the following chapter.

CHAPTER 7

RENDEZVOUS PHASE

7.1 Rendezvous Phase Description and Objectives

The rendezvous maneuver consists of two phases, midcourse and terminal. The midcourse rendezvous phase is initiated immediately after a powered injection from a surface launch or aborted landing maneuver at typical ranges of 200 nm. The objective of the primary G&N system for this phase is to establish a collision or intercept trajectory between the two vehicles by a series of velocity corrections initiated at the longest possible range. The terminal rendezvous phase controls the acceleration of the rendezvousing vehicle such that the relative velocity between the two vehicles is reduced to essentially zero, as the relative range decreases to a desired terminal separation distance. The terminal rendezvous phase typically starts at a relative range of 5 nm, and ends at the docking conditions currently chosen to be a 500 ft separation distance with a closing velocity of 5 fps.

The midcourse rendezvous phase is also referred to as the long range rendezvous phase, and the various computational networks available to achieve the objective of this phase are illustrated in Fig. 7.1. Under normal conditions, the LEM is the active rendezvousing vehicle controlled by the primary G&N units consisting of the rendezvous radar, the LGC and the IMU as illustrated by the heavy lined network in Fig. 7.1. An identical G&N network exists in the CSM which is used to monitor the rendezvous trajectory and as a back-up guidance system if there is a failure in the LEM primary G&N system. With reference to Fig. 7.1, the optics on the LEM (AOT), or the scanning tele-

scope (SCT) on the CSM, can be used with the primary G&N rendezvous technique as a back-up to the rendezvous radars. The two primary G&N systems are linked between the two vehicles by the communication or data link system as shown for monitoring and back-up purposes. The third network shown in Fig. 7.1, consisting of the Manned Spaceflight Network (DSIF) and star occultations with the communication system to earth, provides a further back-up system to the LEM or CSM for establishing an intercept trajectory between the two vehicles such that terminal rendezvous could be accomplished by on-board systems. An analysis of the performance of this third level back-up network is described in Ref. 7.1.

The terminal rendezvous guidance networks existing on both the LEM and CSM are illustrated in Fig. 7.2. The primary G&N system on both vehicles is essentially identical to that used for the long range or midcourse rendezvous phase. The back-up guidance networks, consisting of the rendezvous radar with manual control, or visual and manual control from extended docking conditions, represent further back-up modes of operation and will not be discussed in this report. The guidance equations and rendezvous technique considered for the primary G&N computation network in both the CSM and LEM of Figs. 7.1 and 7.2 are presented in the following sections.

The guidance equations presented in Section 7.2 are used to control both the midcourse and terminal rendezvous maneuvers. The basic guidance and navigation technique is the same as that used during the translunar midcourse phases of the Apollo Lunar Mission. This guidance technique is described in Ref. 7.2, and was chosen for the rendezvous phases for the following reasons:

1. It is extremely flexible in that all ascent and abort trajectories, (including CSM retrieval trajectories) can be handled with any valid tracking data between the two vehicles provided by radar or optics.

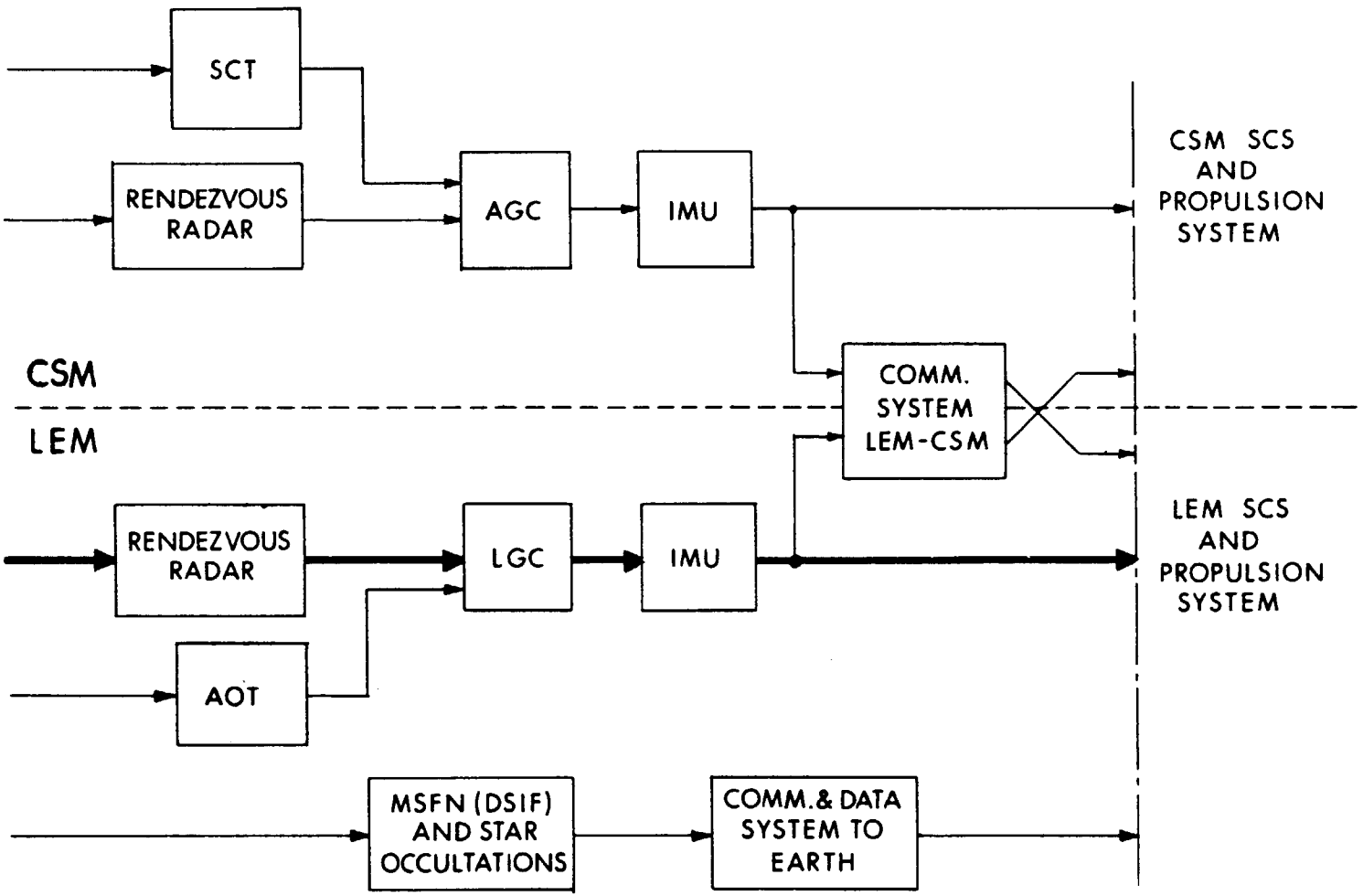

Fig. 7.1 Long range rendezvous mid-course correction computation networks.

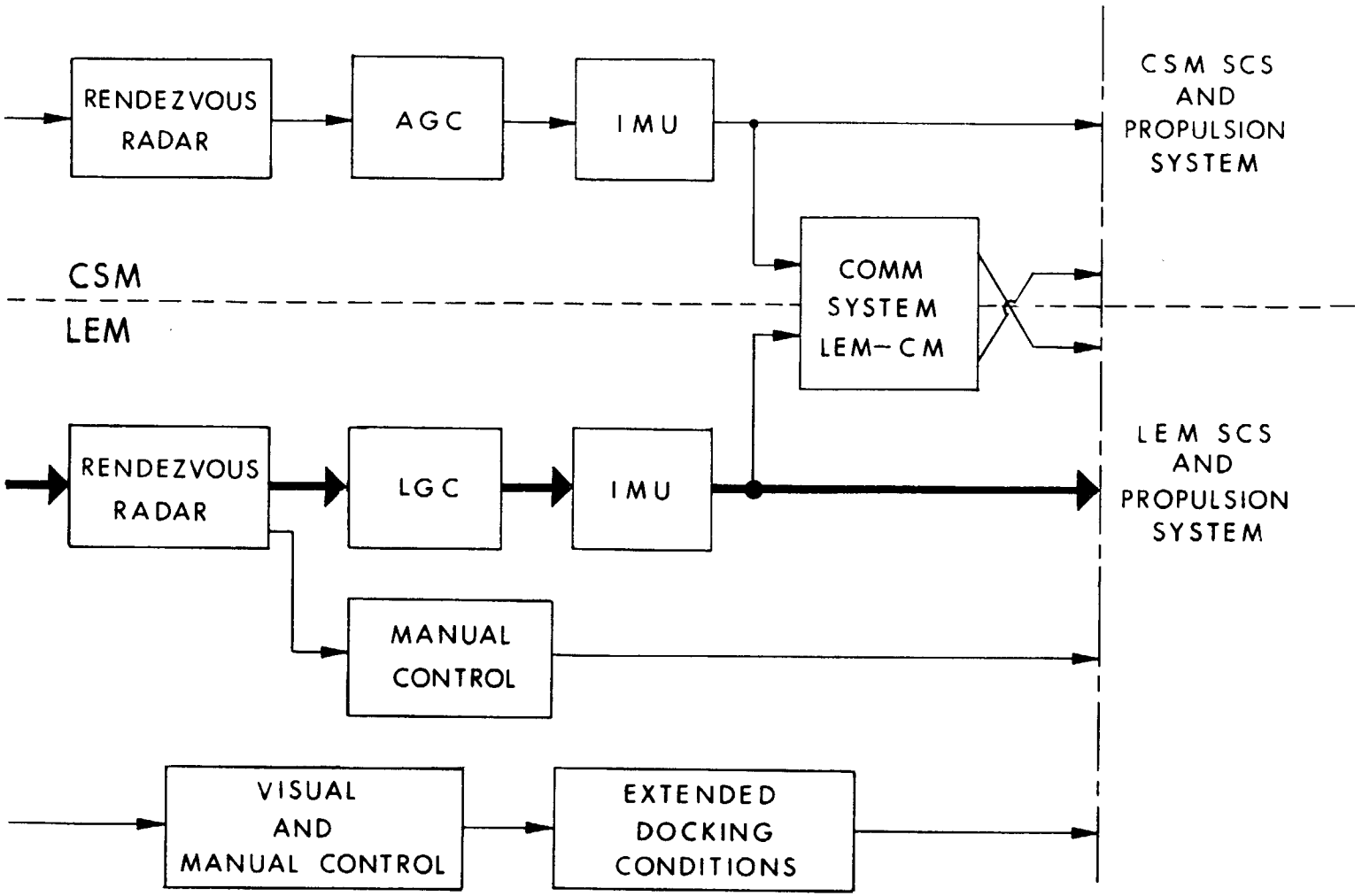

Fig. 7.2 Terminal rendezvous guidance networks.

2. Of the guidance techniques investigated, it provided the best performance in achieving effective velocity corrections at long ranges using the currently specified rendezvous radar (Ref. 7.3). The first midcourse velocity correction is typically applied between 5 and 10 minutes after ascent or abort injection, thereby limiting the required midcourse and terminal rendezvous propellant requirements.

3. Most of the guidance equations or computer subroutines required for this system exist in the AGC as programs required for other phases of the Apollo Mission such as translunar midcourse and orbital navigation phases.

There are two major differences between the guidance technique for the rendezvous and translunar phases. The first concerns the input tracking or observation measurements. Tracking radar data between the two vehicles is used in the rendezvous phase rather than the optical star horizon or landmark measurements used in the translunar navigation phase. For the specified radar performance (Ref. 7.3), the tracking parameters that have proved most useful in the rendezvous phase are range rate ($\dot{R}$) or range (R), and the two tracking angles measured with respect to the IMU. Other combinations of the six tracking parameters are possible, but generally result in higher ΔV requirements. This includes optical tracking angle data which can be used as back-up to the rendezvous tracking radars, as indicated in Figs. 7.1 and 7.2. The second difference between guidance technique for the rendezvous and translunar phases is the necessity for estimating tracking radar angle biases for the current performance and installation tolerances in the long range midcourse rendezvous phase. The estimating technique for these biases is the same as that used for the navigation position and velocity deviations, as described in Section 7.2.

In this chapter, a nominal mission is assumed in which

the LEM is the active rendezvous vehicle controlling the maneuver to the CSM. It should be noted, that the guidance and navigation equations presented in Section 7.2 are used in both CSM and LEM. Either vehicle could be the active vehicle controlling the rendezvous maneuver, and under normal operations, each would solve the same midcourse and terminal rendezvous problem so that system operation could be monitored, and one guidance system take over in the case of an indicated failure in the other. This type of operation is used primarily in the rendezvous phase of the mission, but as pointed out in Chapters 3 and 5, this navigation technique is planned for all unpowered phases of the LEM mission. This included the descent orbit phase in which the initial descent trajectory and perilune conditions are checked by both vehicles (Chapter 3), and the LEM lunar surface phase (Chapter 5) in which the CSM orbit relative to the LEM landing site is determined by radar tracking by both vehicles in order to determine the launch trajectory aim point and timing.

7.2 Rendezvous Guidance Equations

7.2.1 General Comments

The block diagram in Fig. 7.3 represents three major subdivisions of the midcourse rendezvous guidance system. Each of these subdivisions will be considered separately. The guidance equations appropriate to each block will be presented along with the respective inputs and outputs necessary to interconnect the three blocks into an integrated system.

The basic notation used in the guidance equations is shown in Fig. 7.4. Some additional comment on this notation is appropriate here. All vectors are three-dimensional, except $\delta\underline{x}$, $\underline{e}$, $\underline{b}$ and $\underline{W}$, which are nine-dimensional. (It should be noted that letters representing vectors are underscored to distinguish them from statistical averages which have a bar above.) An extrapolated vector (or matrix), noted by a prime, is the value of the vector

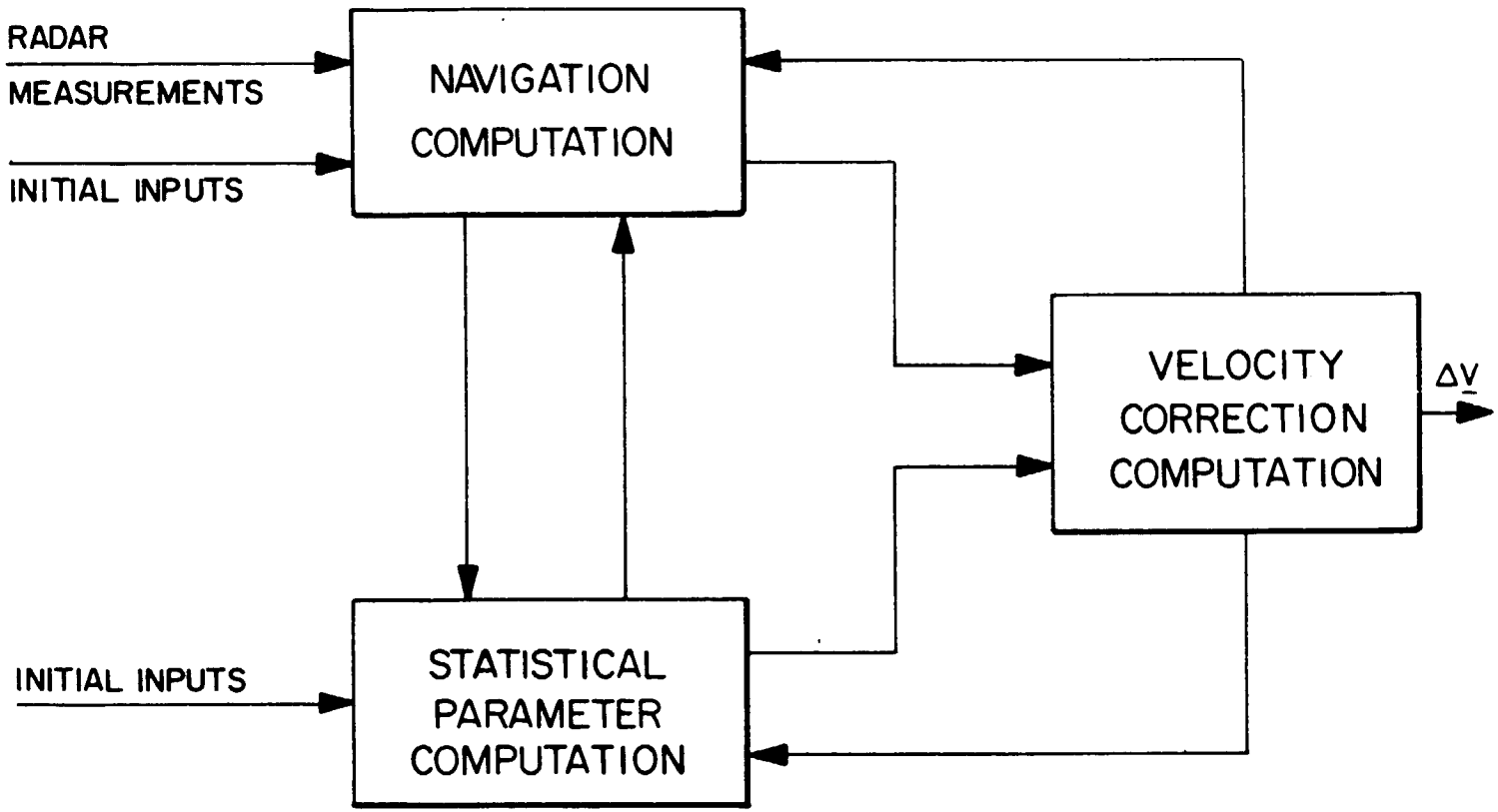

Fig. 7.3 Rendezvous guidance flow diagram.

1. GENERAL

A = SCALAR

$\underline{A}$ = n-DIMENSIONAL VECTOR

$\hat{\underline{A}}$ = ESTIMATED VECTOR

$\underline{A}'$ = EXTRAPOLATED VECTOR FROM LAST MEASUREMENT

$A_{(n \times m)}$ = MATRIX (n BY m)

$A^T_{(n \times m)}$ = TRANSPOSE OF MATRIX

$\bar{A}$ = STATISTICAL AVERAGE

$[A]_0$ = INITIAL CONDITION

2. SUB-SCRIPTS

LEM : LUNAR EXCUSION MODULE

CM : COMMAND MODULE

CL : RELATIVE CM-LEM QUANTITY

Fig. 7.4 Guidance equation notation.

at time t_n computed from: first, the knowledge of its value at time t_{n-1}; second, the time elapsed $t_n - t_{n-1}$; and third, the equations governing its variation with time. The transpose of a vector $\underline{A}$ appears in the equations as $\underline{A}^T$.

Some general definitions are listed in Fig. 7.5. These definitions are consistent with those of Ref. 7.2. The only difference is the inclusion of measurement bias estimates $\underline{\hat{B}}$IAS in the estimate of the state deviation vector $\delta\underline{\hat{x}}$ with its associated error in the bias estimate $\underline{\gamma}$. This results in the augmentation of the original covariance matrix (noted as E in Ref. 7.2) from a six by six matrix to a nine by nine matrix, and the augmentation of the original transition matrix (noted as Φ) from a six by six matrix to a nine by nine matrix P. It can thus be seen that the bias estimates are treated as additional state variables in the same manner as position $\delta\underline{r}$ and velocity $\delta\underline{v}$ deviations. It is necessary to have only a priori statistical knowledge of the biases to be estimated, and a knowledge of the manner in which the biases vary with time. This additional input data is represented by the bias covariance matrix $(E_{BIAS})_{0_{\hat{\lambda}}}$ and the bias transition matrix Φ_{BIAS}. The bias estimate $\underline{B}$IAS is a 3-dimensional vector, thus allowing for the estimate of three quantities in addition to the state deviation vectors $\delta\underline{r}$ and $\delta\underline{v}$, e.g., the estimate of the bias in each of three independent measurements, or possibly the estimate of 3 Euler angles representing the platform or radar axes misalignment.

In the present system configuration, the error model chosen was one in which the measurements had constant biases. This error model is valid for the LEM installation in which rendezvous radar is mounted relatively close to the IMU (Fig. 1.3), and installation and structure designs are sufficient to hold the bias tolerances specified in Ref. 7.3. The CSM radar installation is currently under study by NAA and MIT to determine possible structure alignment tolerances. In the rendezvous guidance concept presented in this section, the knowledge of the stability of the alignment bias is more important than the magnitude of the bias.

The initial bias covariance matrix in Fig. 7.5 is a diagonal matrix, each term on the diagonal being mean square value (on an ensemble basis) of the bias in each of the three independent measurements used. The bias transition matrix becomes an identity matrix since the biases are constant. It should be noted again that this error model is arbitrary. For example, if the biases were known to vary in some prescribed manner with time (e.g., linearly or exponentially), the only change required would be in the bias transition matrix.

The coordinate system used for the radar measurement is shown in Fig. 7.6, where β represents elevation angle, θ is the azimuth angle, and the X_I - Y_I - Z_I frame is inertial.

7.2.2 Rendezvous Navigation Computation

In this portion of the system, the position and velocity of the LEM in inertial space are estimated along with the measurement biases. Basically, this is accomplished by tracking the CM and utilizing this tracking data, at discrete time intervals, along with a priori statistical knowledge (LEM position and velocity deviations from a reference trajectory, measurement random errors and measurement biases) to obtain an optimum linear estimate. It is inherently assumed, that the ephemeris of the CM is precisely known in inertial space so that determining the LEM's position and velocity, with respect to the CM, determines the LEM's inertial position and velocity. The fact that the CM ephemeris is not exactly known in no way affects the determination of the LEM's relative position and velocity which is of first order importance in the rendezvous problem. The estimate of the LEM's inertial position and velocity will be in error, but this is a second order effect, with negligible influence on mid-course and rendezvous guidance.

The details of the navigation scheme may be more readily explained with the aid of the block diagram in Fig. 7.7. The concept of a reference trajectory is utilized to permit the use of per-

$$\delta \underline{X} = \begin{bmatrix} \delta \underline{r} \\ \delta \underline{v} \\ \underline{\text{Bias}} \end{bmatrix} : \text{(STATE DEVIATION VECTOR)}$$

$$\underline{e} = \delta \hat{\underline{X}} - \delta \underline{X} = \begin{bmatrix} \underline{\epsilon}\ \text{(POS.)} \\ \underline{\delta}\ \text{(VEL.)} \\ \underline{\gamma}\ \text{(BIAS)} \end{bmatrix} : \text{(ERROR IN ESTIMATED } \delta \underline{X}\text{)}$$

$$E_{\substack{\text{LEM} \\ (9X9)}} = \overline{\underline{e}\,\underline{e}^T} = \left[\begin{array}{c:c:c} \overline{\underline{\epsilon}\,\underline{\epsilon}^T} & \overline{\underline{\epsilon}\,\underline{\delta}^T} & \overline{\underline{\epsilon}\,\underline{\gamma}^T} \\ \hdashline \overline{\underline{\delta}\,\underline{\epsilon}^T} & \overline{\underline{\delta}\,\underline{\delta}^T} & \overline{\underline{\delta}\,\underline{\gamma}^T} \\ \hline \overline{\underline{\gamma}\,\underline{\epsilon}^T} & \overline{\underline{\gamma}\,\underline{\delta}^T} & \overline{\underline{\gamma}\,\underline{\gamma}^T} \end{array}\right] = \left[\begin{array}{c:c} E_{\substack{\text{LEM} \\ (6X6)}} & \\ \hline & E_{\substack{\text{Bias} \\ (3X3)}} \end{array}\right] : \begin{array}{l}\text{COVARIANCE MATRIX} \\ \text{OF} \\ \text{ESTIMATION ERRORS}\end{array}$$

$$X_{\substack{(6X6)}} = \overline{\begin{bmatrix} \delta \underline{r} \\ \delta \underline{v} \end{bmatrix} \begin{bmatrix} \delta \underline{r} \\ \delta \underline{v} \end{bmatrix}^T} : \text{(COVARIANCE MATRIX OF DEVIATIONS)}$$

$$\text{GENERAL EXTRAPOLATION: } \delta X' = \underset{(9X9)}{P}\, \delta X \; ; \quad \begin{bmatrix} \delta \underline{r} \\ \delta \underline{v} \end{bmatrix}' = \underset{(6X6)}{\Phi} \begin{bmatrix} \delta \underline{r} \\ \delta \underline{v} \end{bmatrix}$$

$$P_{\substack{(9X9)}} = \left[\begin{array}{c:c:c} \multicolumn{2}{c:}{\multirow{2}{*}{$\underset{(6X6)}{\Phi}$}} & \begin{matrix} 0 \\ \hdashline 0 \end{matrix} \\ & & \\ \hline 0 & 0 & \Phi_{\substack{\text{Bias} \\ (3X3)}} \end{array}\right]$$

Fig. 7.5 General definitions.

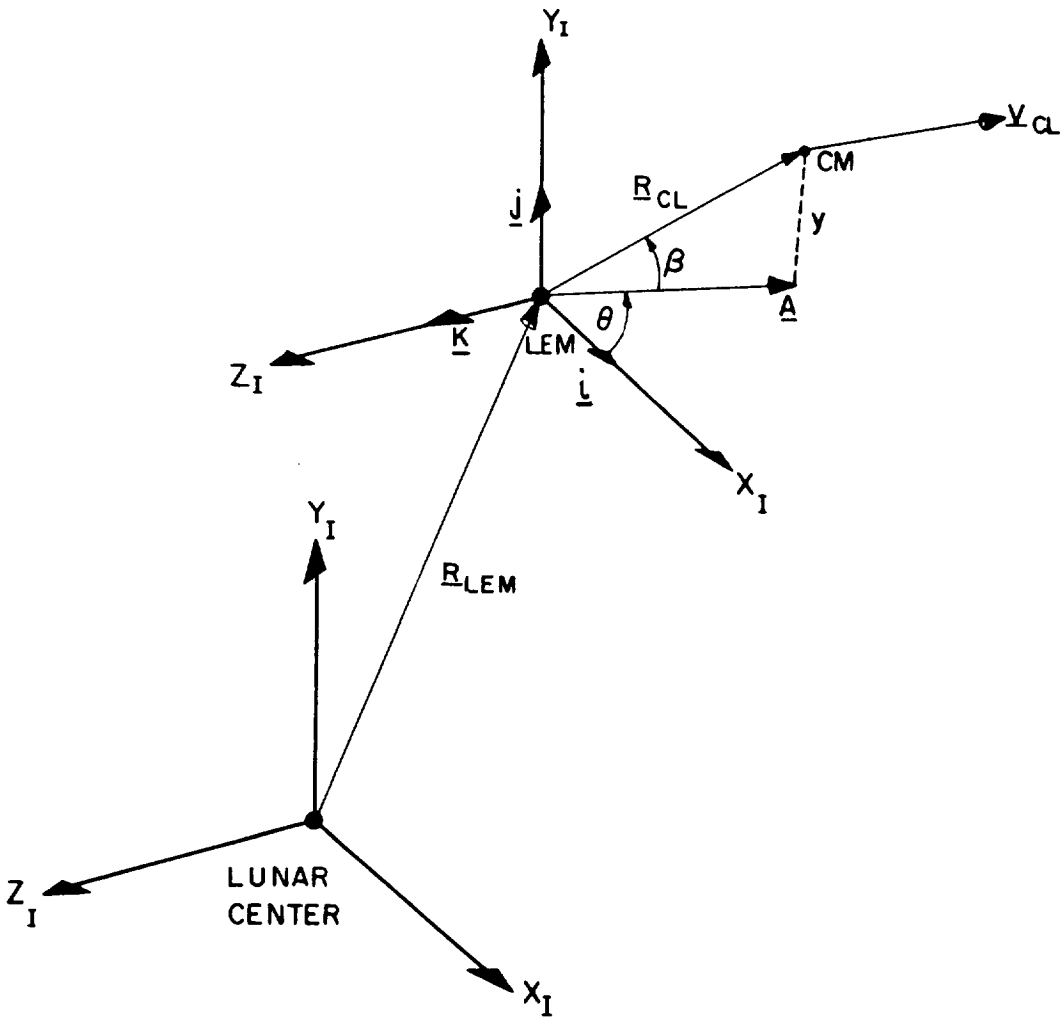

Fig. 7.6 Measurement coordinate system.

turbation theory, i.e., estimates are made of position and velocity deviations from a reference trajectory. To further assure the validity of the perturbation theory, the reference trajectory used is that of the current estimated trajectory, so that deviations from this reference are always small.

Measurements are utilized and the estimates updated at discrete times (typically every 60 seconds during the mid-course phase), thus allowing time for some preliminary measurement smoothing and navigation computation time. The following initial inputs are required, after which, at the specified time intervals, the LEM's position and velocity estimates are updated, as are the measurement bias estimates:

Required Initial and Tracking Inputs

A. Statistical Initial Inputs

1. covariance matrix of LEM initial position and velocity errors $(E_{LEM})_0$ 6×6

2. covariance matrix of initial bias estimation errors $(E_{BIAS})_0$* 3×3

3. variance of tracking measurement errors. (for each type of measurement used).

B. Reference Trajectory Inputs

1. LEM inertial position and velocity vectors $(\underline{R}_{LEM})_0$, $(\underline{V}_{LEM})_0$.

2. CM inertial position and velocity vectors $(\underline{R}_{CM})_0$, $(\underline{V}_{CM})_0$.

3. aim point vector $\underline{R}_{CM}(T_A)$.

* Since there is no correlation between initial deviations and biases, these correlation terms in the nine by nine initial covariance matrix $(E_{LEM})_{9 \times 9}$ are set equal to zero.

4. nominal arrival time T_A.

5. velocity correction criteria ratio (described in Section 7.2.4)

C. Tracking Measurements

1. type of measurements to be used: Range (R), Range Rate ($\dot{R}$), Elevation Angle (β), Elevation Angle Rate ($\dot{\beta}$), Azimuth Angle (θ), or Azimuth Angle Rate ($\dot{\theta}$).*

2. time interval to be employed for estimate update.

D. Initial Estimates

1. position and velocity deviations = 0.

2. bias = 0.

With reference to Fig. 7.7, the estimation procedure at the first time point, t_1 (e.g., 60 seconds from burnout injection) may be traced through the diagram starting at the initial reference trajectory parameters. The equations of motion (Fig. 7.8) are integrated to yield LEM and CM position and velocities at t_1 ($\hat{\underline{R}}'_{LEM}$, $\hat{\underline{V}}'_{LEM}$, $\underline{R}'_{CM}$, $\underline{V}'_{CM}$). $\hat{\underline{R}}'_{LEM}$ is required in the statistical computation section of the system as explained in the following section. Since the reference trajectory is defined as the current estimated LEM trajectory, "hats" appear over $\hat{\underline{R}}'_{LEM}$ and $\hat{\underline{V}}'_{LEM}$ to indicate estimates. Subtracting the LEM parameters from the CM parameters yields the current estimate of the relative trajectory parameters ($\hat{\underline{R}}'_{CL}$, $\hat{\underline{V}}'_{CL}$). These relative parameters are used for two computations: one, the measurement geometry vector (b-vector); and two, the estimate of the measurement to be made ($\hat{q}'$). Each type of measurement

* Any combination of these measurements may be employed, but as presently configured, the system can estimate biases in only 3 measurements.

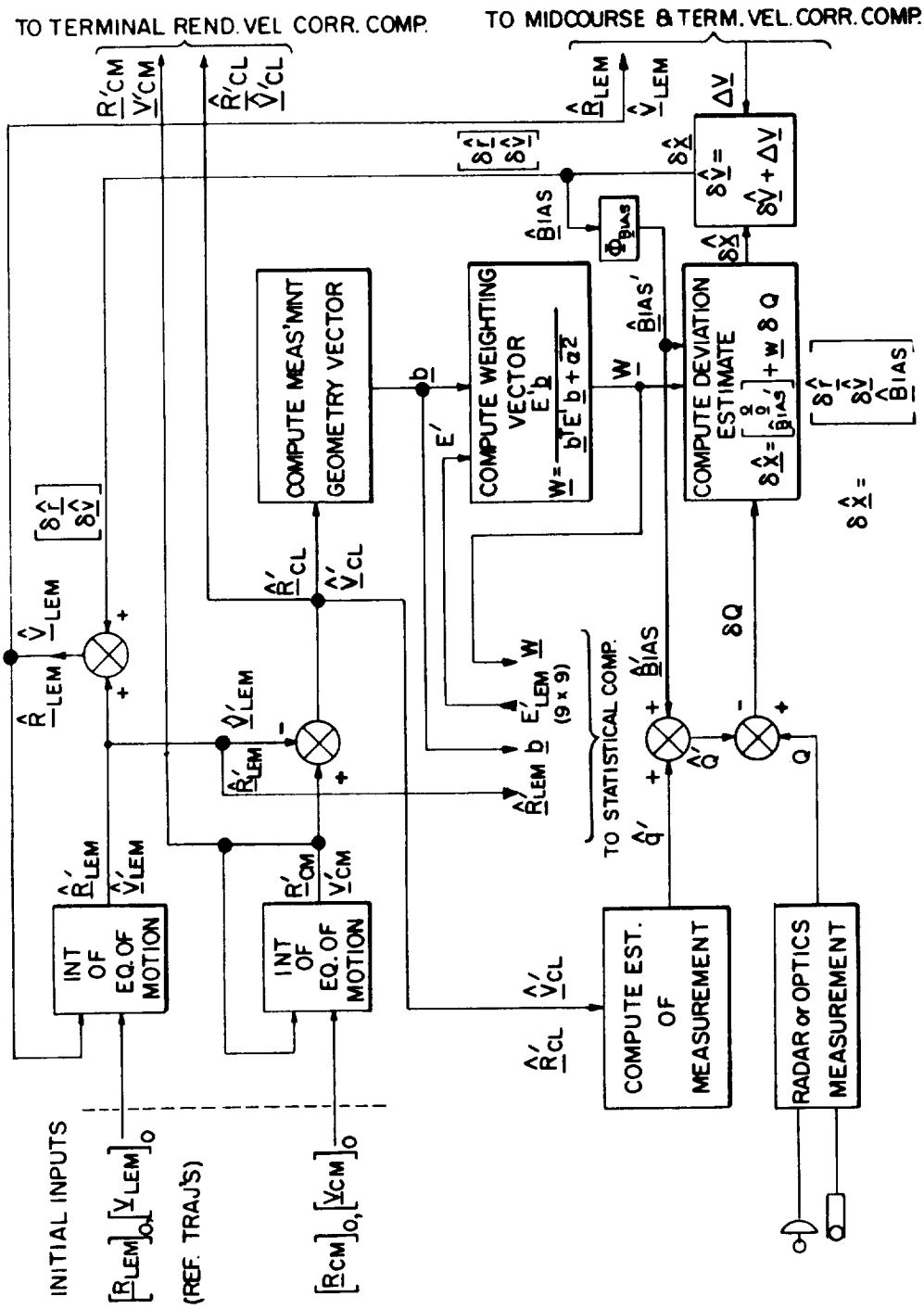

Fig. 7.7 Rendezvous navigation computation.

INTEGRATION OF EQUATIONS OF MOTION:

$$\ddot{\underline{R}} = \dot{\underline{V}} = -\frac{\mu}{R^3}\,\underline{R}$$

MEASUREMENT GEOMETRY VECTOR $\underline{b}$:

DEFINED AS: $\delta q = \underline{b} \cdot \delta \underline{X}$ = DEVIATION OF MEASUREMENT FROM REF.

$$\underline{b} = \begin{bmatrix} \underline{b}_0 \\ \underline{b}_3 \\ \underline{b}_6 \end{bmatrix}$$

MEASUREMENT:		$\underline{b}_0$	$\underline{b}_3$	$\underline{b}_6$
RANGE RATE	$\frac{1}{R_{CL}^3}\left[\underline{R}_{CL} \times (\underline{V}_{CL} \times \underline{R}_{CL})\right]$	$\underline{R}_{CL}/R_{CL}$	(1, 0, 0)	
ANGLE (β)	$\frac{1}{R_{CL}^2 A_y}\left[A^2 \underline{R}_{CL} - R_{CL}^2 \underline{A}\right]$	(0, 0, 0)	(0, 1, 0)	
ANGLE (θ)	$\frac{1}{A^2 y}\left[\underline{R}_{CL} \times \underline{A}\right]$	(0, 0, 0)	(0, 0, 1)	

$\overline{\alpha^2}$ = RADAR OR OPTICAL TRACKING VARIANCE

Fig. 7.8 Navigation guidance equations.

has its appropriate b-vector, which is the quantity relating the deviation in the measurement to the deviation in the state vector. Typical b-vectors are given in Fig. 7.8 for the set of three measurements ($\dot{R}$, β, θ) normally used (b-vectors for all six radar measurements, R, $\dot{R}$, β, θ, $\dot{\beta}$, $\dot{\theta}$ may be found in Ref. 7.4). The estimate of the value of the measurement to be made is computed using the appropriate equation in Fig. 7.9 for $\dot{R}_{CL}$, β or θ. (It should be noted here that when more than one type of measurement is utilized, each measurement is processed independently. Although the measurements are made simultaneously at time t_1, they are utilized sequentially in the computations to update the estimate of the LEM position and velocity.)

With reference to Fig. 7.7 the b-vector is used in two computations: first, the weighting vector $\underline{W}$; and second, statistical computation S-C section of the system. $\underline{W}$ is computed as shown in Fig. 7.7 using $\underline{b}$, the extrapolated covariance matrix $E'_{\substack{LEM \\ 9\times9}}$ which comes from the statistical computation section, and the variance of the random measurement error $\bar{\alpha}^2$. Then $\underline{W}$ is: one, fed back into the S-C section to be used in updating $E'_{\substack{LEM \\ 9\times9}}$ for the next time point; and two, used to compute the optimum estimate of the state deviation vector $\delta\hat{\underline{x}}$.

The optimum linear estimator requires four quantities at time t_1: first, the weighting vector $\underline{W}$; second, the estimate of the measured quantity $\hat{q}'$; third, the actual measurement Q; and fourth, the current bias estimate $\hat{\underline{B}}$IAS. Initially, the bias estimate is zero, but after t_1, there will exist a value for this parameter which has been extrapolated from the last time point. With these quantities, the current estimate of the state deviation vector $\delta\hat{\underline{x}}$ is computed. (i.e., the position and velocity deviation from the current estimated position and velocity plus the bias estimate in <u>each</u> of the measurements).

Once $\delta\hat{\underline{x}}$ has been computed at t_1, the new reference trajectory is formed by adding $\delta\hat{\underline{r}}$ to $\hat{\underline{R}}'_{LEM}$ and $\delta\hat{\underline{v}}$ to $\hat{\underline{V}}'_{LEM}$. These new parameters are fed to the velocity correction section of the system. The bias estimate portion of $\delta\hat{\underline{x}}$, $\hat{\underline{B}}IAS$, is stored until needed at the next time point. If the velocity correction logic has called for a velocity correction, the value of the correction applied $\Delta\underline{V}$ in terms of IMU accelerometer output is used to further update the new reference trajectory. (NOTE: In Fig. 7.7, $\Delta\underline{V}$ is shown to be added impulsively to $\delta\hat{\underline{v}}$ for convenience.)

The entire procedure discussed above yields the best current estimate at time t_1 of the following parameters: one, the LEM's position and velocity; and second, the measurement biases. This procedure is repeated at each of the predetermined time intervals through the rendezvous phase. A slight modification is made at the start of terminal rendezvous maneuver. The bias estimate at that time is fixed, and no further bias estimates are made. This is done to reduce some of the computations and does not affect accuracy since a satisfactory estimate of bias has been achieved before the terminal rendezvous phase.

7.2.3 Rendezvous Statistical Computation

The section of the system shown in block diagram form in Fig. 7.10 has three major functions: first, computation of the transition matrix $\underset{6\times6}{\Phi}$; two, extrapolation of the matrices $\underset{9\times9}{E_{LEM}}$ and $\underset{6\times6}{X}$; and three, updating $\underset{9\times9}{E_{LEM}}$ after a measurement and updating $\underset{6\times6}{X}$ after a velocity correction. The $\underset{6\times6}{E_{LEM}}$ matrix may also be updated after a velocity correction, if a substantial error is expected in applying a velocity correction. For the expected errors in application, this has been found to be unnecessary. The equations required for the extrapolation and updating functions are listed in Fig. 7.11. The differential equation which is integrated

EXTRAPOLATED ESTIMATE OF MEASUREMENTS:

$$q = \dot{R}_{CL}, \beta, \theta$$

$$\dot{R}_{CL} = \frac{\underline{R}_{CL}}{R_{CL}} \cdot \underline{V}_{CL}$$

$$\beta = \sin^{-1}\left(\frac{\underline{R}_{CL}}{R_{CL}} \cdot \underline{j}\right)$$

$$\theta = \sin^{-1}\left(-\underline{R}_{CL} \cdot \underline{k}/A\right)$$

TRANSITION MATRIX P:

$$\underset{(6X6)}{\dot{\Phi}} = \underset{(6X6)}{F}\ \underset{(6X6)}{\Phi} \quad ; \quad \left[\underset{6X6}{\Phi}\right]_0 = \begin{bmatrix} I & 0 \\ 0 & I \end{bmatrix}$$

$$\underset{(6X6)}{F} = \begin{bmatrix} 0 & I \\ G & 0 \end{bmatrix} \quad ; \quad \underset{(3X3)}{G} = \nabla \underline{g} \quad ; \quad \nabla = \left\| \frac{\partial}{\partial \underline{R}} \right\|$$

$$\underset{(3X3)}{\Phi_{Bias}} = I$$

Fig. 7.9 Navigation guidance equations (cont.).

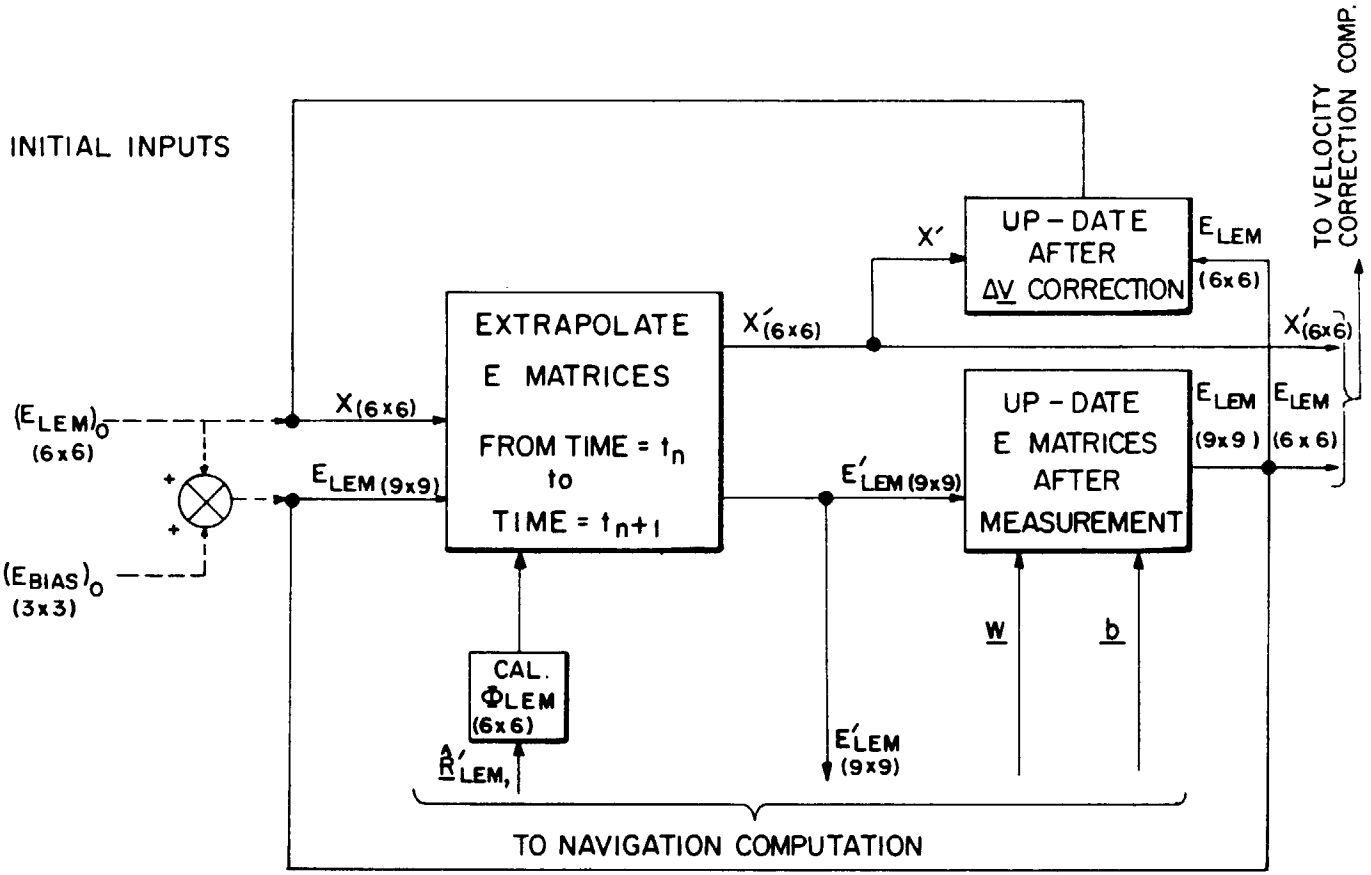

Fig. 7.10 Rendezvous statistical computation.

EXTRAPOLATION OF E MATRICES

$$\underset{(9X9)}{E'_{LEM}} = \underset{(9X9)}{P}\ \underset{(9X9)}{E_{LEM}}\ \underset{(9X9)}{P^T}$$

$$\underset{(6X6)}{X'} = \underset{(6X6)}{\Phi_{LEM}}\ \underset{(6X6)}{X}\ \underset{(6X6)}{\Phi^T_{LEM}}$$

UP-DATING E MATRICES (9X9):

$$E = \left(I - \underline{w}\ \underline{b}^T\right) E'$$

UP-DATING OF X MATRIX (6X6):

$$X = \left(I + JB\right)\left(X' - \underset{(6X6)}{E'_{LEM}}\right)\left(I+JB\right) + \underset{(6X6)}{E'_{LEM}}; \qquad \underset{(6X3)}{J} = \begin{bmatrix} 0 \\ \hline I \\ (3X3) \end{bmatrix}$$

Fig. 7.11 Statistical equations.

for the computation of $_{6\times6}\Phi$ is given in Fig. 7.9, together with the initial condition for $_{6\times6}\Phi$. The explicit expression for the three by three G matrix (gradient of gravity with respect to position) is:

$$G = \frac{\mu}{R^5}\begin{bmatrix} 3R_x^2 - R^2 & 3R_xR_y & 3R_xR_z \\ 3R_yR_x & 3R_y^2 - R^2 & 3R_yR_z \\ 3R_zR_x & 3R_zR_y & 3R_z^2 - R^2 \end{bmatrix}$$

where

R = magnitude of $\underline{\hat{R}}_{LEM}$

μ = gravitational constant

R_x, R_y, R_z = components of $\underline{\hat{R}}_{LEM}$

The initial E_{LEM} and E_{BIAS} are initial input data (as explained previously) which are combined to give $(E_{LEM})_0$. This initial nine by nine matrix is extrapolated to yield the required E'_{LEM} to be used in computing $\underline{W}$ in the navigation section. Then, together with $\underline{b}$ and $\underline{W}$ (from the navigation section), E'_{LEM} is used to update itself, yielding E_{LEM} at time t_1. E_{LEM} is then fed back in Fig. 7.10 and extrapolated to the next point for the subsequent estimate update. The six by six portion of E_{LEM} is sent to the velocity correction section to be used in the statistical correction logic. The X matrix, the covariance matrix of true deviations, is also required in the statistical correction logic. Since the initial deviation estimate is zero, the error in the estimate is just the true deviation. Thus, the initial value of X is $(E_{LEM})_0$ as indicated in Fig. 7.10. If a velocity

correction is made, the extrapolated value of the X matrix at that time must be updated since the true velocity deviation has been changed. (This is assumed to be an impulsive velocity correction and introduces very little error.)

7.2.4 Velocity Correction Computation and Decision

This section of the system is subdivided into the mid-course velocity correction, and terminal rendezvous velocity correction since a modification to the logic is made when the terminal rendezvous phase is initiated.

7.2.4.1 Midcourse Velocity Correction

Two separate logic schemes have been considered for determining when a velocity correction should be applied during the midcourse rendezvous phase. One would be simply to have predetermined times along the trajectory at which the estimated correction $\Delta\hat{\underline{V}}$ would be applied. In such a system, the final correction could always be applied at some predetermined range (e.g., 25 nm) which would limit the miss distance at the nominal arrival time to a reasonable value. If the trajectories to be flown were fairly well established; this scheme would allow for a degree of optimization by properly selecting the correction times to minimize the total ΔV. However, in order to have a logic which is satisfactory for a wide variety of trajectories, though not necessarily optimum for any one, a statistical velocity correction SVC, logic has been incorporated. A comparison of these two mid-course correction criteria is made in Section 7.5.

The SVC logic utilizes a priori statistical knowledge of the LEM's position and velocity deviations, $\underset{6\times6}{X}$ matrix, and the updated statistical knowledge of errors in the estimates of these deviations, $\underset{6\times6}{E_{LEM}}$, to determine the mean squared estimate of the required velocity correction DELV, and the mean squared uncertainty in this estimate, DELU. When the square root of

the ratio of DELU to DELV is below a predetermined level, RATIO, the estimated velocity correction $\Delta\hat{\underline{V}}$ is applied. Figure 7.12 illustrates this system. Utilizing only the initial reference trajectory $(\underline{R}_{LEM})_0$, $(\underline{V}_{LEM})_0$ and the time of arrival, T_A, for which the velocity correction will achieve an intercept trajectory, the C* matrix is calculated at each measurement time point along the trajectory. The C* matrix contains partial derivatives of required velocity for an intercept at T_A with respect to position deviations at the present time. General equations for C* are given in Fig. 7.13 and more specifically, in Ref. 7.2 under perturbation matrices. DELV and DELU are then calculated using equations in Fig. 7.13. A small degree of error is introduced since only the original reference trajectory is used, whereas E_{LEM} and X' are propagated along the estimated trajectory. Since the deviations between these trajectories is always quite small, however, this error produces negligible effect on the values of DELV and DELU.

The estimate of the velocity correction required, $\Delta\hat{\underline{V}}$ is made on the basis of a constant arrival time, T_A. This computation is shown in Fig. 7.12. The position vector of the command module, $R_{CM}(T_A)$ at time $= T_A$ is available as initial data. This vector, together with the current estimate of the LEM position vector, $\hat{\underline{R}}_{LEM}$, and the time desired for an intercept (the difference between the initial desired arrival time, T_A, and the present time, TIME) are fed into a computational scheme for solving Lambert's problem. The velocity required by the LEM to intercept the CM at $t = T_A$ is computed as $\underline{V}_C$. By subtracting the current estimate of the LEM's velocity, $\hat{\underline{V}}_{LEM}$, from $\underline{V}_C$, $\Delta\hat{\underline{V}}$ is obtained. When the velocity correction logic demands application, $\Delta\hat{\underline{V}}$ is commanded and the output of the IMU yields the actually applied $\Delta\underline{V}$ which is returned to the navigation computation section to update the LEM's estimated trajectory.

Mention should be made of the effect of errors in the

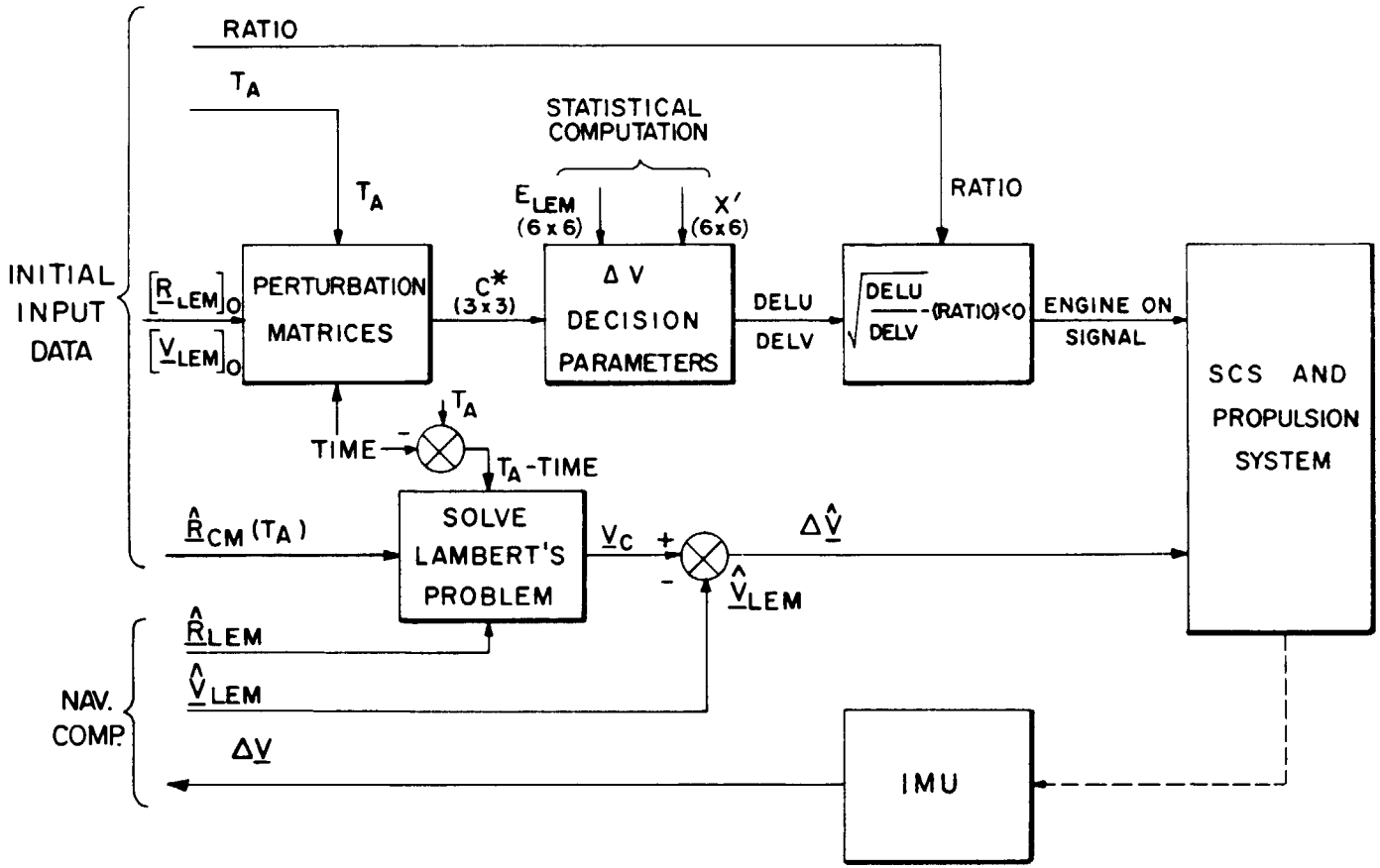

Fig. 7.12 Mid-course rendezvous velocity correction computation and decision.

PERTURBATION MATRICES:

$$\underset{(3X3)}{\nabla} = \left\| \frac{\partial}{\partial \underline{V}_{T_A}} \right\|$$

$$\underset{(3X3)}{R^*} = \nabla \underline{R}_{LEM}$$

$$\underset{(3X3)}{V^*} = \nabla \underline{V}_{LEM}$$

$$\underset{(3X3)}{C^*} = \underset{(3X3)}{V^*}\ \underset{(3X3)}{R^{*-1}}$$

ΔV DECISION PARAMETERS:

$$\underset{(3X6)}{B} = \left[\underset{(3X3)}{C^*} \,\vdots\, \underset{(3X3)}{-I} \right]$$

$$DELU = TRACE\left[\underset{(3X6)}{B}\ \underset{(6X6)}{E_{LEM}}\ \underset{(6X3)}{B^T} \right]$$

$$DELV = TRACE\left[\underset{(3X6)}{B}\ \underset{(6X6)}{(X' - E_{LEM})}\ \underset{(6X3)}{B^T} \right]$$

Fig. 7.13 Mid-course rendezvous velocity correction equations.

knowledge of the aim point - $\underline{R}_{CM}(t_A)$, caused by uncertainties in the CM ephemeris. In a rendezvous problem where the vehicle being tracked is also the target, aim point errors are small second order effects. It was mentioned previously that the navigation system accurately defines the relative position and velocity of the LEM with respect to the CM, although the estimates of inertial position and velocity may be in error due to CM ephemeris uncertainties. Thus, the inertial estimate is degraded in order to place the LEM in a correct relative position to the CM. Then for the relatively short flight time trajectories involved, the estimated $\Delta\hat{\underline{V}}$ required to intercept using incorrect inertial data for both vehicles is negligibly different from that required using true inertial data.

A special situation must be accounted for during the midcourse velocity correction phase. This is when a velocity correction is called for and the central angle from $\hat{\underline{R}}_{LEM}$ to the aim point vector $\underline{R}_{CM}(T_A)$ is in the vicinity of 180 degrees. If the $\hat{\underline{R}}_{LEM}$ is not exactly in the plane of $\underline{R}_{CM}(T_A)$ and $(\underline{V}_{LEM})_0$ (the original trajectory plane), the velocity correction computed by solving Lambert's problem may be prohibitively high. Logic must be provided, therefore, to prevent application of the correction until the central angle becomes smaller than 180 degrees. For the expected rms position and velocity errors at injection combined with measurement errors, preventing midcourse velocity corrections in a band ±20 degrees about 180 degrees proved satisfactory when the SVC criterion was used. A method of handling this singularity condition is described in Section 7.5 for a fixed time correction criteria.

7.2.4.2 Terminal Rendezvous Velocity Correction

A slight modification to the basic guidance and navigation scheme discussed for the midcourse phase is made in the terminal rendezvous phase. This amounts simply to a redefinition of the aim point and the desired time of arrival (Fig. 7.14).

- MID-COURSE GUIDANCE WITH THE FOLLOWING MODIFICATIONS:

1. REDEFINE AIM POINT AND TIME OF ARRIVAL ON TERMINAL $R - \dot{R}$ CONCEPT

$$T_{GO} = \frac{R \text{ (PRESENT RANGE)}}{\dot{R}_d \text{ (DESIRED RANGE RATE)}}$$

$$T_A' = \text{TIME} + T_{GO}$$

INTEGRATE CM POSITION AHEAD BY T_{GO} FOR NEW AIM POINT

2. FIX ANGLE BIAS ESTIMATE AT PRESENT VALUE

Fig. 7-14 Terminal rendezvous guidance.

The objective of the terminal rendezvous phase is to control the relative closing velocity to zero or some prescribed value as the range between the two vehicles closes to a desired terminal separation range from which docking can be achieved. Since the midcourse rendezvous phase established an intercept trajectory between the two vehicles, the relative velocity can be considered to be range rate as measured by the rendezvous radar. Under these conditions, the terminal rendezvous maneuver can be described in a range-range rate, $R\text{-}\dot{R}$, phase plane by some criteria which controls the closing velocity ($\dot{R}$) as some function of range (R) so that the desired terminal conditions can be established. There are many terminal $R\text{-}\dot{R}$ criteria or schedules that could be used. These generally fall into categories such as parabolic, linear, or a fixed range-range rate schedule. The guidance scheme shown in Fig. 7.14 is general in the sense that it could be used with any terminal $R\text{-}\dot{R}$ criteria provided tracking measurements (at least one), could be made between thrust periods. The type of terminal $R\text{-}\dot{R}$ criteria used in the primary G&N system will depend upon the following factors:

1. The maximum closing relative velocities expected for rendezvous trajectories initiated from noncoplanar launch conditions, or direct abort trajectories from any point after separation.
2. The propulsion system or systems that must be used to effect the terminal rendezvous maneuver for either the LEM or CSM.
3. Monitoring requirements (visual and system displays), of the astronauts from both LEM and CSM and the degree of desired similarity or compatibility.
4. Back-up guidance requirements (possibly manually controlled in the CSM and visually and/or manually controlled in the LEM).

At the present time, an "accepted"terminal $R\text{-}\dot{R}$ criteria covering

all of these factors has not been extablished. Some typical criteria that have been used in the analysis of the primary G&N system for both LEM and CSM controlled rendezvous are as follows:

LEM controlled terminal rendezvous

Parabolic R-$\dot{R}$ criteria starting at R=5 nm

Engine on: $\dot{R}^2/2R \geqq 1/3$ fps^2

Engine off: $\dot{R}^2/2R \leqq 1/6$ fps^2

Fixed Range-Range rate schedule

Range	Desired range rate
5 nm	-100 fps
1.5 nm	-20 fps
0.25 nm	-5 fps

The terminal rendezvous maneuver is nominally controlled by the LEM RCS jets provided that the terminal trajectory initial conditions are within the RCS capability. This RCS capability for terminal rendezvous has recently been defined (Ref. 7.5) for nominal launches as 200 fps. The ascent engine would be used to reduce the final closing velocity to within this range if the particular launch trajectory resulted in higher final closing conditions. The ascent or descent engine would be used to establish velocities within the RCS capability for the LEM weight conditions resulting from various abort times during the landing maneuver. The LEM controlled terminal rendezvous maneuver is illustrated in more detail in Section 7.6.

CSM controlled terminal rendezvous

Fixed Range-Range rate schedule

Range	Desired range rate
5 nm	-80 fps
0.5 nm	-5 fps

These two terminal velocity corrections are made with the SM propulsion system. The SM RCS has been assumed capable of

correcting the terminal closing velocity of -5 fps to within 1 fps. These criteria result in 3 to 7 thrust periods for the LEM controlled rendezvous, while the CSM rendezvous is restricted to 2 thrust maneuvers in order to limit SM engine restarts. The time required for the terminal rendezvous maneuver using the above LEM $R\text{-}\dot{R}$ criteria ranges from 7 to 11 minutes over the last 5 nm while the CM criteria results in a terminal phase of 5-6 minutes. The desired docking conditions at the end of the guidance controlled terminal rendezvous maneuver have been a separation range of 500 feet with closing velocity of -5 fps ± 1 fps. The primary point to be made here is that the primary G&N rendezvous technique in both vehicles is capable of performing virtually any terminal $R\text{-}\dot{R}$ criteria that may be specified.

As indicated in the diagram of Fig. 7.15 and equations of Fig. 7.14 the terminal $R\text{-}\dot{R}$ criteria programmed in the AGC is used to compute a new time to go, T_{GO}, to the intercept point. This intercept is defined by a new aim point along the CM orbit $\underline{R}_{CM}(T'_A)$ computed by integrating the CM equations of motion ahead by T_{GO} seconds from the present CM conditions, $\underline{R}'_{CM}$, $\underline{V}'_{CM}$. As indicated in Figs. 7.14 and 7.15, the new time of arrival, T'_A is simply T_{GO} added to the present time. Then, as in the mid-course rendezvous velocity correction of Fig. 7.12, the new arrival time, T'_A, the new aim point and current estimate of the LEM's position vector, $\hat{\underline{R}}_{LEM}$, are applied to a routine which solves Lambert's problem to yield the required LEM velocity, V_c, which will result in an intercept at T'_A. The $\Delta\hat{\underline{V}}$ is again $\underline{V}_c$ minus the current estimate of the LEM's velocity, $\hat{\underline{V}}_{LEM}$. This entire procedure is illustrated in Fig. 7.15. It is apparent that this scheme, besides taking out the required $\dot{R}$, also makes appropriate corrections normal to the line of sight to maintain the vehicles on a collision course.

It should be noted that the manner in which T_{GO} is calculated $(R/\dot{R}_d)$ assumes an impulsive thrust. This follows since the solution to Lambert's problem requires an impulsive velocity

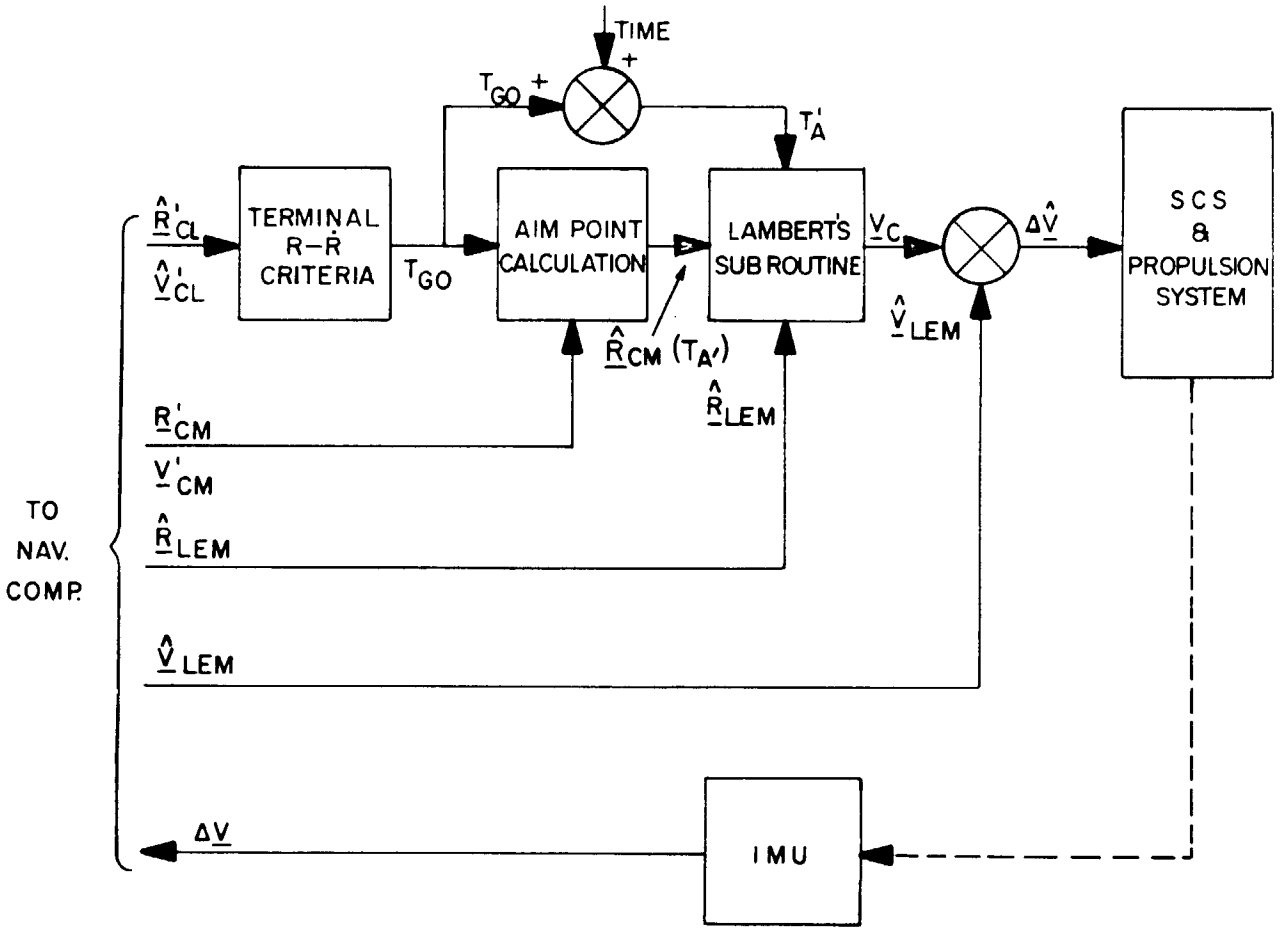

Fig. 7.15 Terminal rendezvous velocity correction computation.

correction. Since the thrust is applied in a finite time, the actual time to rendezvous will be shorter than the computed T_{GO}. However, T_{GO} is redefined at subsequent velocity correction points until the final $\dot{R}$ cancellation requires a small velocity application resulting in a small error in T_{GO} due to finite thrust times. In addition, the closing velocity will also be small at this time, making small errors in T_{GO} negligible.

The navigation scheme used during the midcourse phase continues right into the terminal rendezvous phase computing $\hat{\underline{R}}_{LEM}$ and $\hat{\underline{V}}_{LEM}$. One slight modification mentioned previously is the fixing of the last estimate of the measurement biases at the start of this phase. Two other modifications which substantially improve the navigation accuracy are initiated at the start of the terminal phase. The first is the replacement of range rate measurements by range measurements. Since range rate is essentially constant during this phase, the measurement of this quantity provides very little information except possibly after thrust periods. However, the small errors in thrust application will not alter the estimate of range rate appreciably. On the other hand, relative range is changing rapidly and measurements of this parameter improve the estimate of position and velocity.

The second modification is to increase the magnitude of the covariance matrix E_{LEM}. This has the effect of increasing the sensitivity of the estimation process by effectively increasing the "gain" of the system. (A similar procedure is followed in the translunar midcourse navigation phase.) The theory behind this is that after many measurements have been taken, the estimation errors (in a statistical sense), will have become very small, i.e., E_{LEM} becomes very small. The effect of this on the estimation process is to place little weight on any additionally received measurements, and rely heavily on the current estimates. Thus, by increasing the magnitude of E_{LEM}, the measurements currently

received, which happen to be extremely good because of the small range, are given added weight and may substantially enhance the accuracy of the estimates. The manner in which this modification is presently being employed is as follows: At the start of the terminal phase (or possibly earlier when the range = 25 nm.), the position components of E_{LEM} are multiplied by 100, the velocity components are multiplied by 9, and the cross correlation terms are multiplied by 30. This has the effect of increasing the statistical position error by an order of magnitude and the statistical velocity error by a factor of 3. Greater weight is given to the position components since the three measurements utilized (range and two angles) are basically position measurements and will rapidly decrease the position terms in the covariance matrix. The results to date have been quite satisfactory.

It should be pointed out that the diagrams of Figs. 7.12 and 7.15 are computational flow diagrams and do not represent detailed schematics of the interface between the primary G&N system and the spacecraft SCS and propulsion systems. The $\Delta\underline{V}$ signals in these figures are commanded vector velocity corrections. In the spacecraft, this commanded velocity correction would be presented to SCS and the propulsion systems as an attitude command, an engine-on signal, followed by an engine-off signal after the desired velocity correction had been achieved as measured by the IMU. The engine-on signal in Fig. 7.12 merely represents the output of the velocity correction criteria and is not necessarily the same engine-on signal from the AGC to the spacecraft flight control system.

7.3 Rendezvous Statistical Parameter Study

In the analysis of the primary G&N rendezvous technique, several system parameters are important. The frequency or time interval between rendezvous navigation computations (Section 7.2) is one such parameter. Figure 7.16 illustrates the effect of the time interval between computations in the rendezvous technique for typical injection velocity uncertainties for a one sigma tracking parameter accuracy of 0.5% in range rate and

1 mr for the two line of sight angles relative to the IMU. From this figure, it can be seen that there is little difference between measurement intervals of 30 to 120 seconds over the initial phases of the rendezvous trajectory. In the G&N analysis to date, a measurement interval of 60 seconds has been commonly used.

For a measurement or computation interval of 60 seconds during a coplanar ascent trajectory, Figs. 7.17 and 7.18 summarize the effects of various tracking parameter performance in terms of LEM velocity uncertainty. In Fig. 7.17, the velocity uncertainty at the end of a 10 minute tracking period (10 measurements) is illustrated for one sigma range rate accuracies varying from 0.01% to 0.5% over a tracking angle accuracy of 1 to 5 mr. Figure 7.18 illustrates the rms velocity uncertainty at the end of a 20 minute tracking period for the same initial injection uncertainties, computation interval, and similar range of tracking performance parameters. The effect of a 120 second computation or measurement cycle for a 20 minute tracking interval is shown in Fig. 7.19 as a function of varying range rate performance when used with a 1 mr angle accuracy, and as a function of tracking angle accuracy when used with a range rate accuracy of 0.5%.

The effects of uncompensated angular bias on the rms velocity uncertainty over a typical ascent trajectory are illustrated in Fig. 7.20. In this figure, an uncompensated or non-estimated 5 mr bias can be seen to result in large velocity uncertainties compared with a 0 bias or pure random tracking case. When the 5 mr bias is estimated, as described in Section 7.2.2, the system performance is very similar to the ideal zero bias case of Fig. 7.20. The effects and importance of estimating tracking angle biases will be further illustrated in Section 7.4.2.

The statistical criteria parameter $(DELU/DELV)^{1/2}$, (Section 7.2.4.1) for applying midcourse velocity corrections is illustrated as a function of time over an abort trajectory in

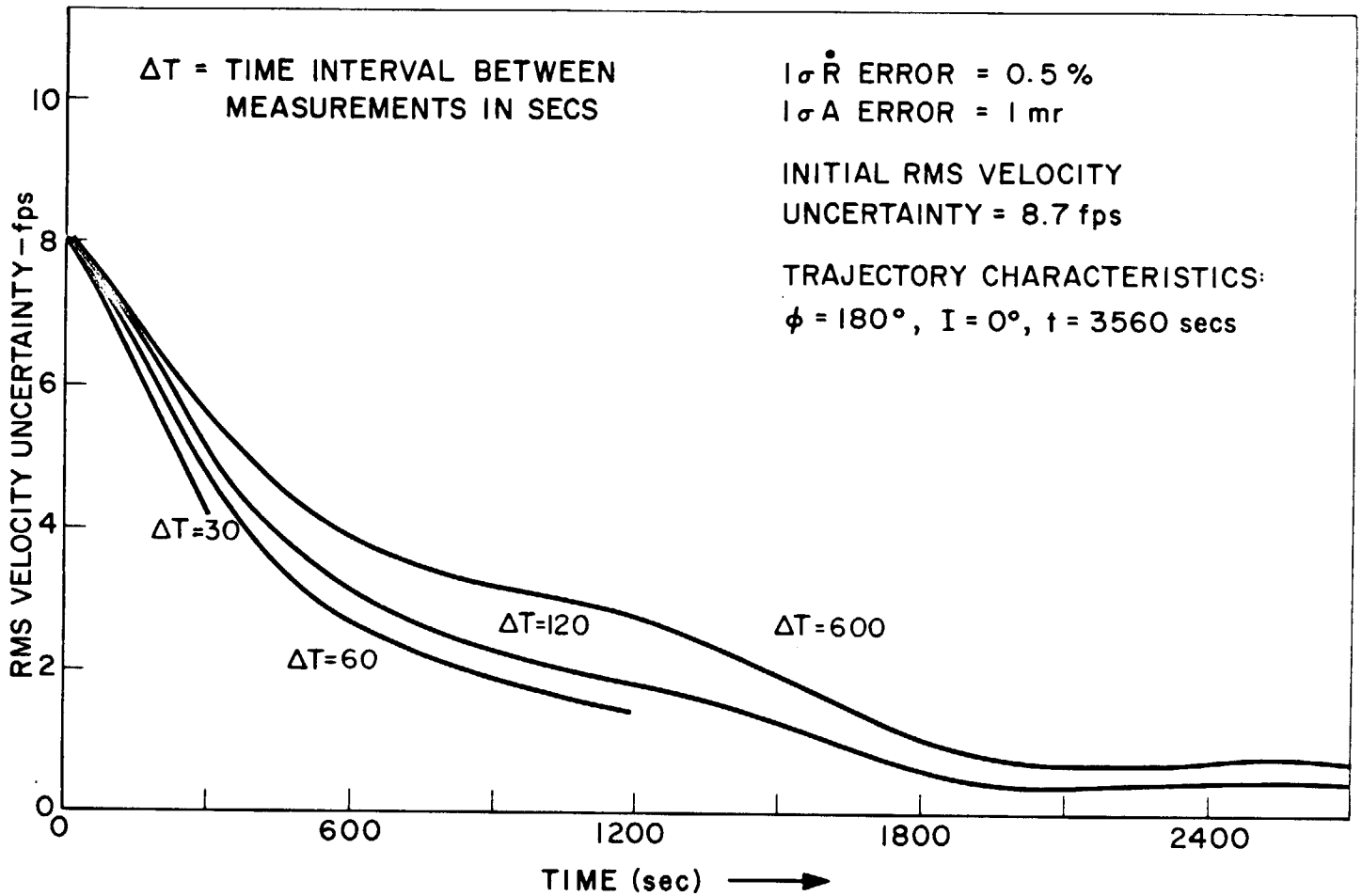

Fig. 7.16 LEM velocity uncertainty analysis during ascent trajectory.

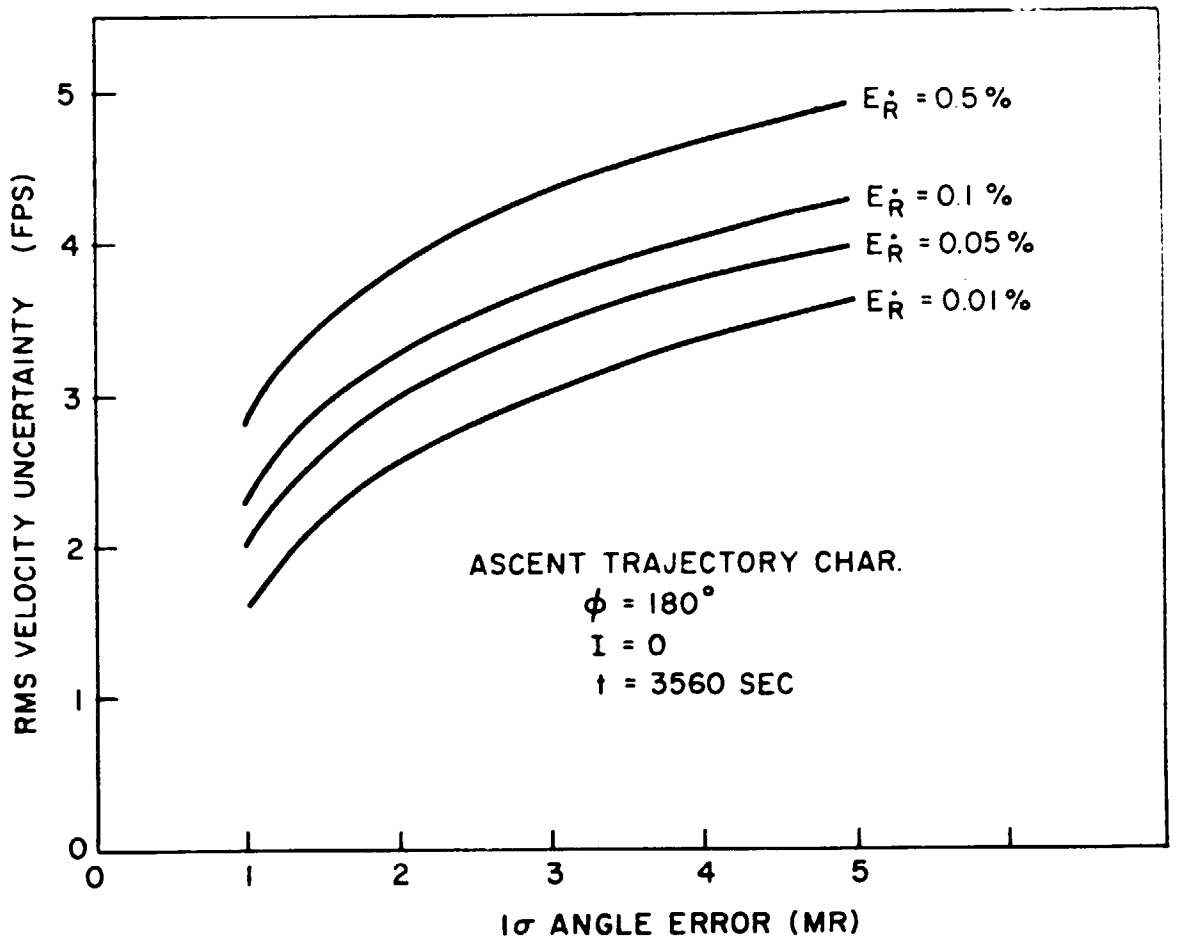

Fig. 7.17 Rendezvous trajectory correction analysis (10 minute tracking period).

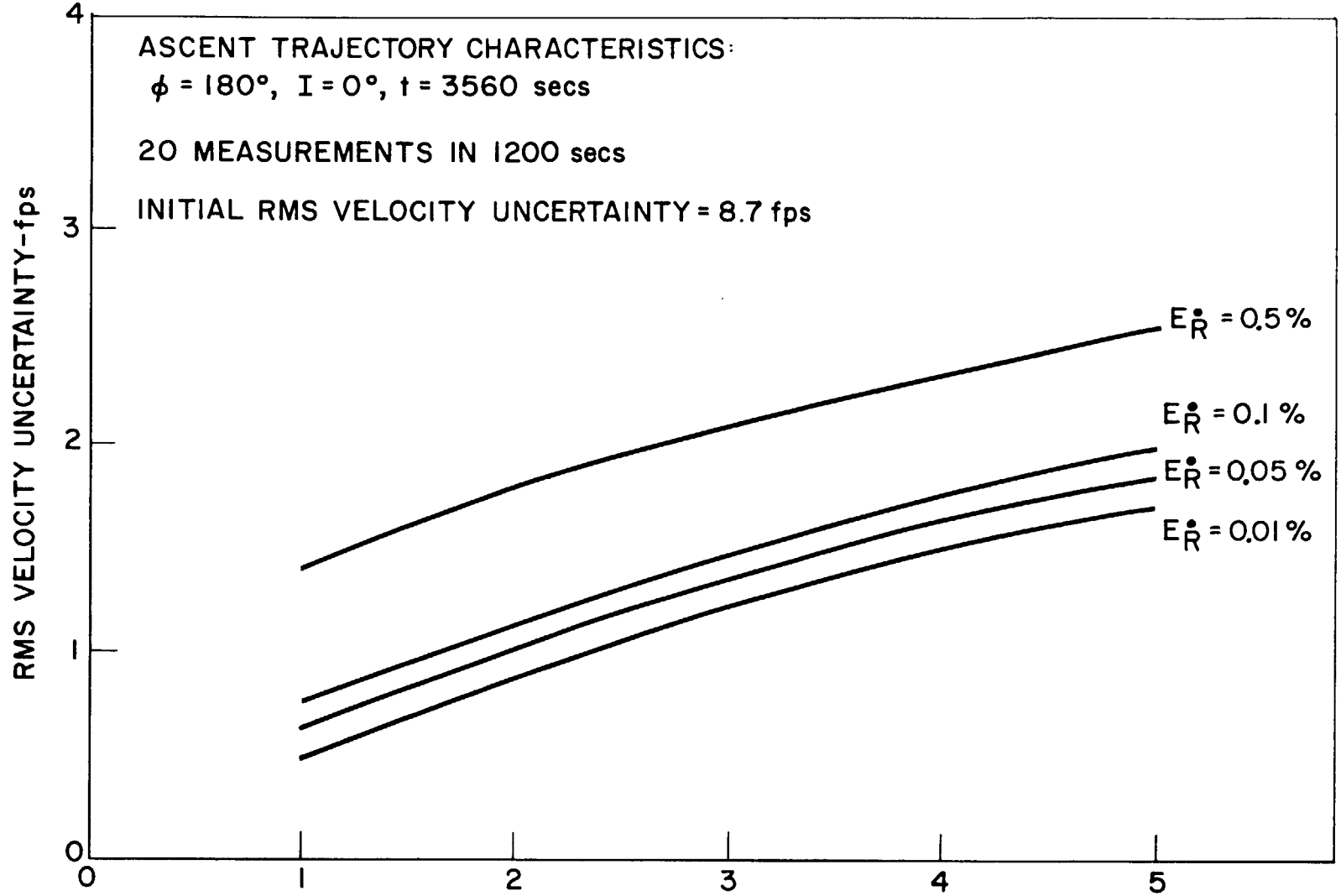

Fig. 7.18 Rendezvous trajectory correction analysis (20 minute tracking period).

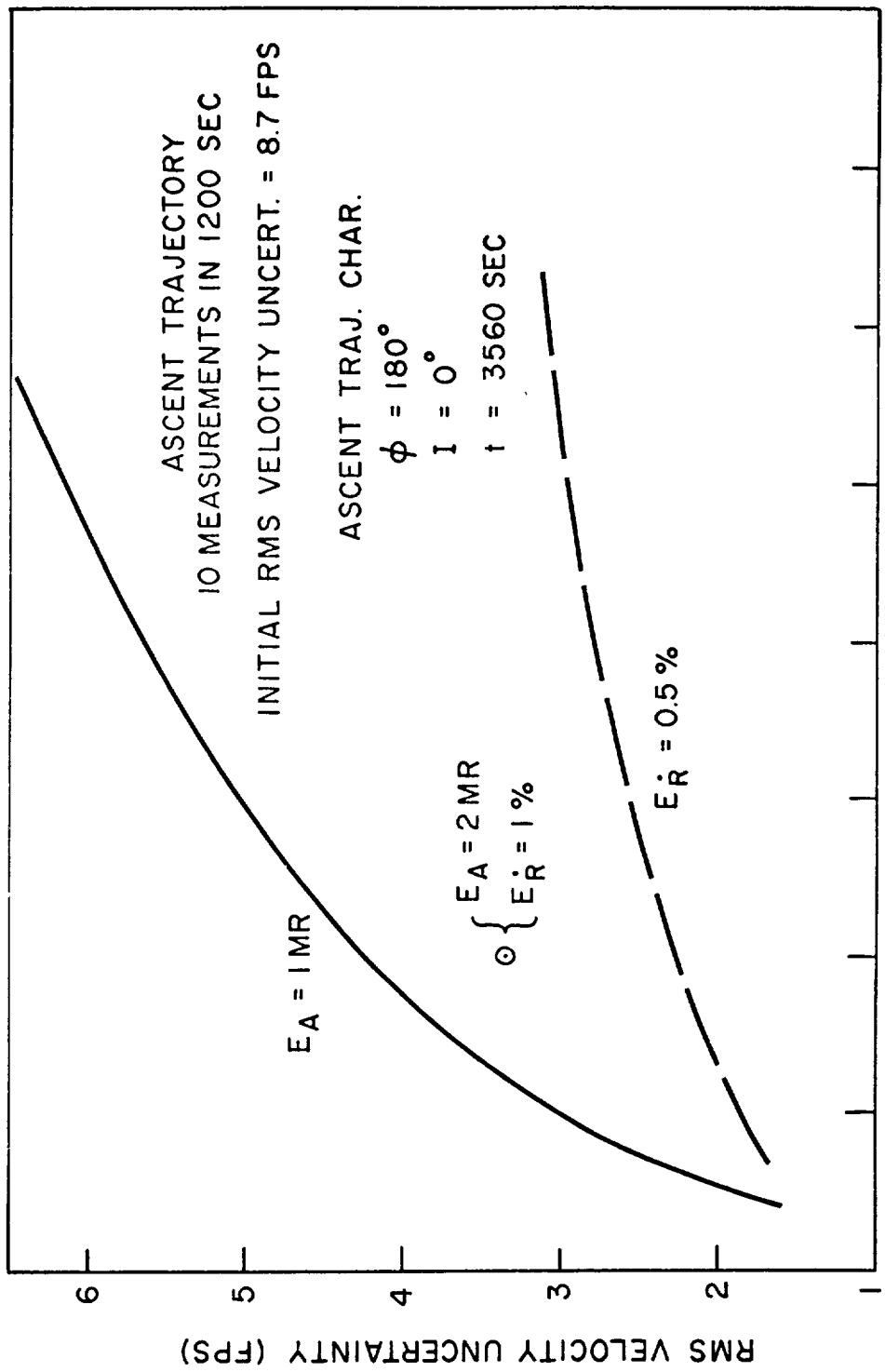

Fig. 7.19 Rendezvous trajectory correction analysis.

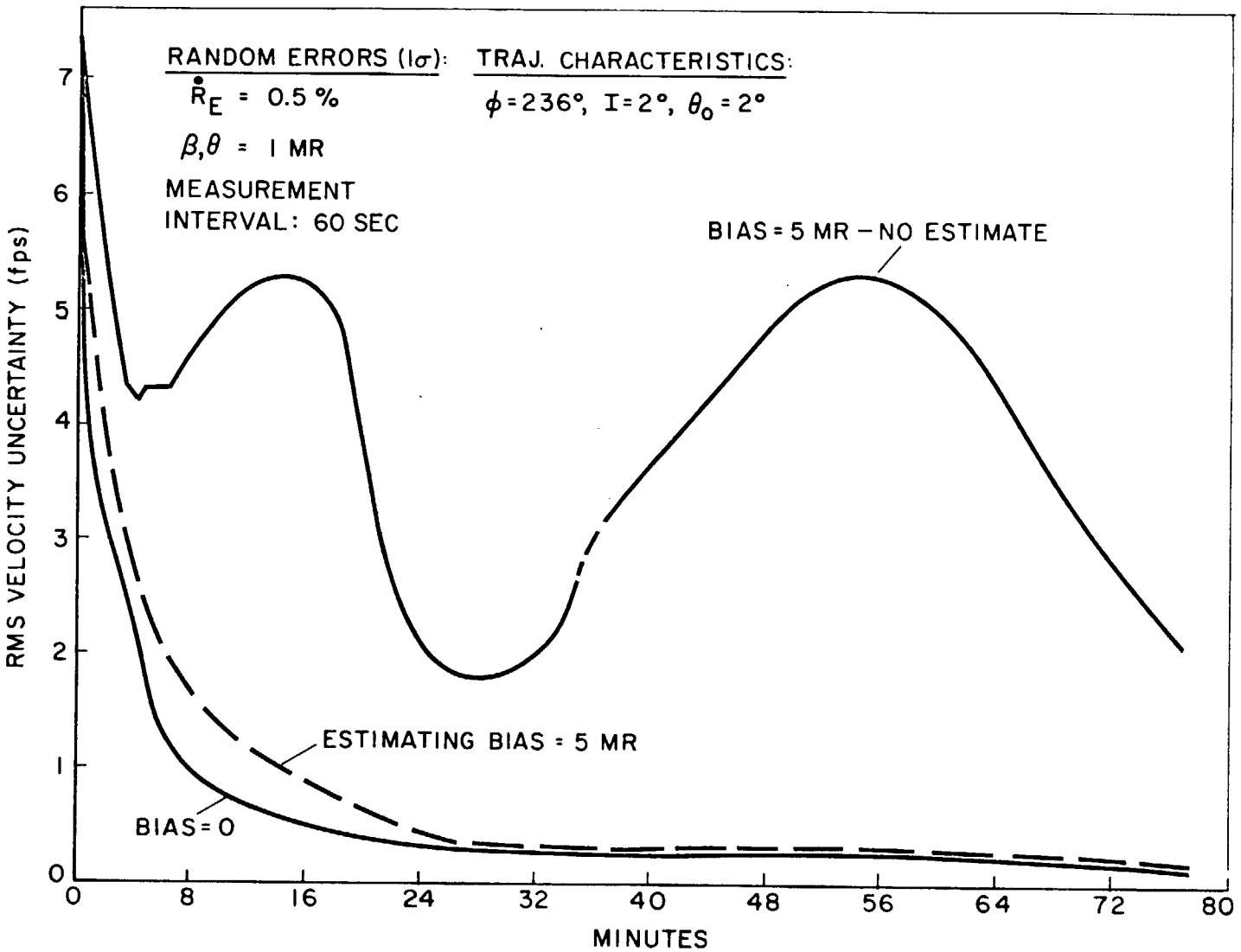

Fig. 7.20 LEM velocity uncertainty analysis during abort trajectory.

Fig. 7.21. In this figure, 3 midcourse corrections were applied when the statistical ratio was set at 0.3. After each correction, the DELU/DELV ratio increases to near infinity since the desired velocity correction essentially forces DELV to zero. The ratio is then decreased due to tracking measurements until the set value of 0.3 is reached and another velocity correction is applied. In this figure, a fourth and final midcourse correction was almost applied before the terminal rendezvous phase, but in this case the final trajectory correction would have to be incorporated in the terminal rendezvous maneuver.

Several values of the $(DELU/DELV)^{1/2}$ ratio have been investigated for the mid-course rendezvous phase. The lower this ratio, the fewer midcourse velocity corrections called for. In order to restrict or minimize the ΔV midcourse requirement, it is desirable to apply the first velocity correction as soon as possible after ascent or abort injection. The limiting factors affecting the earliest time for the first velocity correction are radar tracking accuracy, bias compensation, range, and magnitude of injection errors. The $(DELU/DELV)^{1/2}$ ratio of 0.3 has proven to be a reasonable compromise between these factors, and typically requires 3 midcourse velocity corrections for ascent trajectories, and between 1 to 5 corrections for LEM abort trajectories.

The statistical performance of the midcourse rendezvous phase is summarized in terms of midcourse velocity correction ΔV for a typical ascent trajectory in Fig. 7.22. This particular ascent trajectory covers a central angle of 132 degrees and is illustrated in more detail in Section 7.4.2. The effects of various combinations of angle and range rate tracking performance are shown in this figure. The average velocity correction required to establish an intercept course at range of 25 nm, in the absence of any midcourse corrections, was 70 fps as indicated in the total velocity correction column. Assuming standard ascent injection

uncertainties (Section 6.4) in the case of a range rate accuracy of 0.33% and angle tracking accuracy of 1 mr, three midcourse corrections were required at the times indicated with a total ΔV requirement of 27 fps. The velocity corrections required for decreasing angle accuracy, when used with two levels of range rate tracking performance, are summarized in this figure.

Figure 7.23 is a summary for a similar parametric study made for a typical abort trajectory. This abort trajectory resulted from an abort initiated during the hover phase of the landing maneuver, and covered a central angle of 206 degrees from injection to terminal aim point (Section 8.5). In this case, a total average velocity correction of 74 fps would have been required in the absence of any midcourse correction at a range of 25 nm in order to establish an intercept trajectory. The results summarized in Fig. 7.23 are the required average velocity corrections for various levels of tracking parameter accuracy. In comparing the results of Figs. 7.22 and 7.23, it can be seen that the midcourse velocity corrections reduced the required ΔV to achieve an intercept trajectory by greater than a factor of two, compared with making a single trajectory correction at a range of 25 nm.

The parametric effects listed in Fig. 7.24 compare the results of angle tracking only in the absence of range or range data during the midcourse rendezvous phase for the ascent trajectory of Fig. 7.22. From Fig. 7.24, it can be seen that for 1 mr tracking accuracies, the angle only case (optical tracking) required essentially 7 fps more ΔV than the standard tracking case of angles and range rate data of Fig. 7.22. A similar comparison for range rate only performance is also listed in Fig. 7.24. In this case, the tracking data is insufficient to reduce the uncertainties enough to allow a midcourse velocity correction before the 25 nm range point. It is concluded, therefore, that the range rate data alone is not satisfactory for midcourse navi-

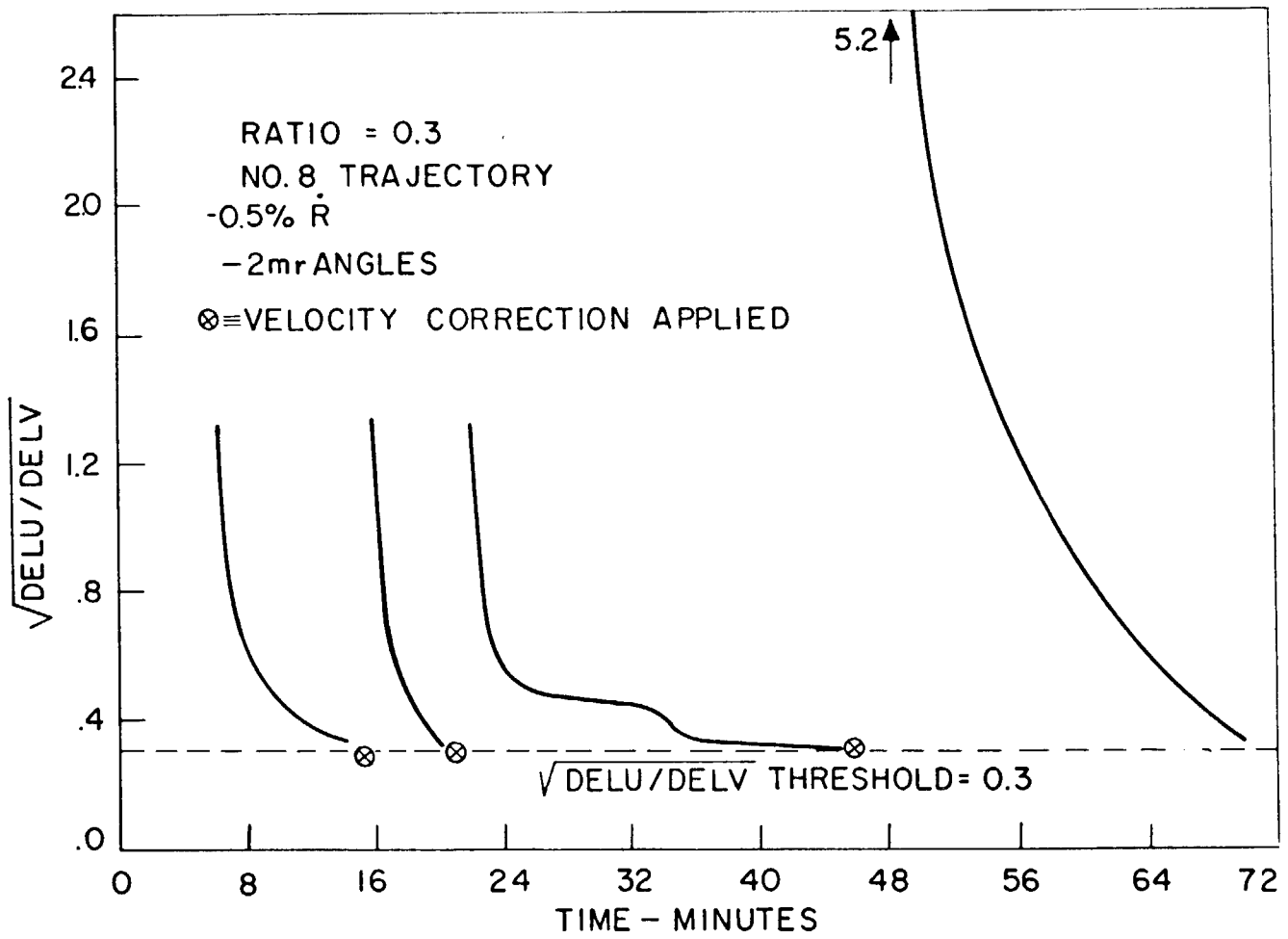

Fig. 7.21 Mid-course velocity correction criteria.

- MEASUREMENTS TAKEN EVERY 60 secs UP TO 2050 secs (25 n.m. RANGE)
- TRAJECTORY CENTRAL ANGLE = 132.5°

	MEAS: UNCERTAINTY (1 σ)	VEL. RATIO THRESHOLD $\left[\frac{DELU}{DELV}\right]^{1/2}$	No. OF CORRECTIONS	TIME OF EACH VEL. CORR (sec)	MAGNITUDE OF VEL. CORR. (fps)	TOTAL ΔV REQUIREMENT (fps)
		0	0	—	—	70*
+	0.33 % $\dot{R}$ 1 mr ∠	0.3	3	540 1380 2050	13.8 7.7 5.5	27
	0.33% $\dot{R}$ 2 mr ∠	0.3	3	660 1440 2050	15.1 9.1 5.9	30.1
	0.33 % $\dot{R}$ 4 mr ∠	0.3	3	900 1680 2050	18.8 11.5 4.6	34.9
	1 % $\dot{R}$ 1 mr ∠	0.3	3	600 1440 2052	14.4 8.9 5.5	28.8
	1 % $\dot{R}$ 2 mr ∠	0.3	3	720 1560 2052	15.9 10.6 5.7	32.2
	1% $\dot{R}$ 4 mr ∠	0.3	3	900 1740 2050	18.7 13.7 4.7	37.1

* ΔV REQUIRED AT 25 n.m. RANGE IF NO MIDCOURSE CORRECTIONS WERE MADE
\+ CURRENT RENDEZVOUS RADAR SPECIFICATIONS

Fig. 7.22 Ascent trajectory mid-course rendezvous phase.

- MEASUREMENTS TAKEN EVERY 60 secs UP TO 2520 secs (25 nm RANGE)
- TRAJECTORY D-8 CENTRAL ANGLE = 206°
- ABORT INITIATED DURING HOVER

MEAS: UNCERTAINTY (1σ)	VEL RATIO THRESHOLD $\left[\frac{DELU}{DELV}\right]^{1/2}$	No. OF CORRECTIONS	TIME OF EACH VEL.CORR (sec)	MAGNITUDE OF VEL.CORR. (fps)	TOTAL ΔV REQUIREMENT (fps)
	0	0	—	—	74*
0.33% $\dot{R}$ 1 mr $\angle$	0.3	3	840 1860 2520	27.1 5.8 2.4	35.3
0.33% $\dot{R}$ 2 mr $\angle$	0.3	3	840 1860 2526	26.7 8.3 3.5	38.5
0.33% $\dot{R}$ 4 mr $\angle$	0.3	3	960 1860 2525	26.1 9.6 4.1	39.8
1 % $\dot{R}$ 1 mr $\angle$	0.3	3	840 1800 2529	27.0 7.4 3.4	37.8
1% $\dot{R}$ 2 mr $\angle$	0.3	3	840 1860 2532	26.6 9.8 4.5	40.9
1% $\dot{R}$ 4 mr $\angle$	0.3	3	960 1980 2522	25.9 12.5 4.7	43.1

* ΔV REQUIRED AT 25 n.m. RANGE IF NO MIDCOURSE CORRECTIONS WERE MADE
+ CURRENT RENDEZVOUS RADAR SPECIFICATIONS

Fig. 7.23 Abort trajectory mid-course rendezvous phase.

ASCENT TRAJECTORY CENTRAL ANGLE = 132.5°

MEASUREMENTS TAKEN EVERY 60 secs UP TO 2050 sec (25 n.m. RANGE)

MEAS: UNCERTAINTY (1σ)	VEL. RATIO THRESHOLD $\left[\frac{DELU}{DELV}\right]^{1/2}$	No. OF CORRECTIONS	TIME OF EACH VEL.CORR (sec)	MAGNITUDE OF VEL.CORR. (fps)	TOTAL Δ V REQUIREMENT (fps)
	0	0	—	—	70 *
1mr	0.3	3	840 1440 2052	17.7 9.9 6.7	34.3
2mr	0.3	3	1020 1680 2046	21.0 12.9 5.6	39.5
4 mr	0.3	2	1200 2037	25.0 20.2	45.2
0.33% $\dot{R}$	0.3	1	2018 *	8 2	8 2
1% $\dot{R}$	0.3	1	2021*	9 5	9 5

* ΔV REQUIRED AT 25 nm RANGE IF NO MIDCOURSE CORRECTIONS WERE MADE

Fig. 7.24 Partial tracking data condition - mid-course rendezvous phase.

gation. The relative importance of angle and range rate tracking data is dependent upon the particular trajectory under consideration. Generally, the tracking angle data is always the more effective for the tracking accuracies currently specified. The contribution of the range rate data to angle tracking is more pronounced in early abort trajectories in which there are wide variations of operating and closing velocities along the line of sight. Range rate data is also very important during the bias angle estimation period during a typical ascent trajectory of Fig. 7.22. Studies of this type have indicated that there is a slight advantage in using range rate tracking data instead of range tracking data of the same accuracy. There is little advantage in using both range and range rate data in this navigation technique. Since the range rate data is somewhat superior in performance and controllable bias, this tracking parameter, in combination with tracking angle data, has been used in all midcourse rendezvous analysis.

7.4 Typical Long Range Rendezvous Trajectories and Primary G&N Performance

7.4.1 Primary G&N Operation

Immediately after ascent injection, the LGC will command the rendezvous radar through the radar CDU's to point along the computed line of sight to the CSM. In normal operation, the CSM should lie within the beam width, $\approx 4^{o}$, of the rendezvous radar and radar lock-on is automatic. If radar tracking acquisition is not established after directing the antenna along the computed line of sight, the LGC generates a spiral type search pattern about this position to achieve lock-on. In the case where radar lock-on is not achieved along the initial computed line of sight, a performance or system failure is indicated in LEM rendezvous radar, the CSM transponder, or the primary G&N computed CSM position. If radar lock-on cannot be achieved, the CSM must provide the required midcourse correction data over the inter-vehicle communication system or retrieve the

LEM (Section 8). In some cases, rendezvous radar tracking may be established prior to launch, and be maintained throughout the powered ascent phase thereby avoiding the acquisition procedure.

After radar acquisition and tracking are established, the computation procedure of Section 7.2 is cycled every 60 seconds until the first midcourse velocity correction is required. The basic G&N units required for this computation are the rendezvous radar, LGC, IMU and CDU's as shown previously in Fig. 7.1, and presented in general schematic form in Fig. 7.25. The attitude control of the LEM during the unpowered ascent is not controlled by the G&N system other than to keep the line of sight within the radar gimbal angle coverage. The astronaut would probably manually orient the vehicle so the line of sight is within his window coverage. At the time of a midcourse correction, the vehicle is oriented by the LGC to the desired attitude and the RCS jets controlled to provide the desired velocity correction monitored by the IMU in the same manner that the powered ascent maneuver was controlled in the previous chapter. As indicated in Section 7.3, any single midcourse velocity correction is normally below 27 fps. The vehicle control during a midcourse correction can be done with either the $\underline{V}_G \times \dot{\underline{V}}_G$ steering of Section 3.2.2.1, or the explicit equations of Section 6.2. Since a midcourse velocity correction can be in any direction, rendezvous radar tracking may have to be interrupted during the velocity correction maneuver due to limited radar gimbal coverage. Reaquisition in these cases is the same procedure as previously described. The rendezvous computation and midcourse correction is repeated until the terminal rendezvous maneuver starting at a range of 5 nm.

7.4.2 Simulation Results

The statistical parameter studies of Section 7.3 were checked with an actual trajectory digital simulation for ascent

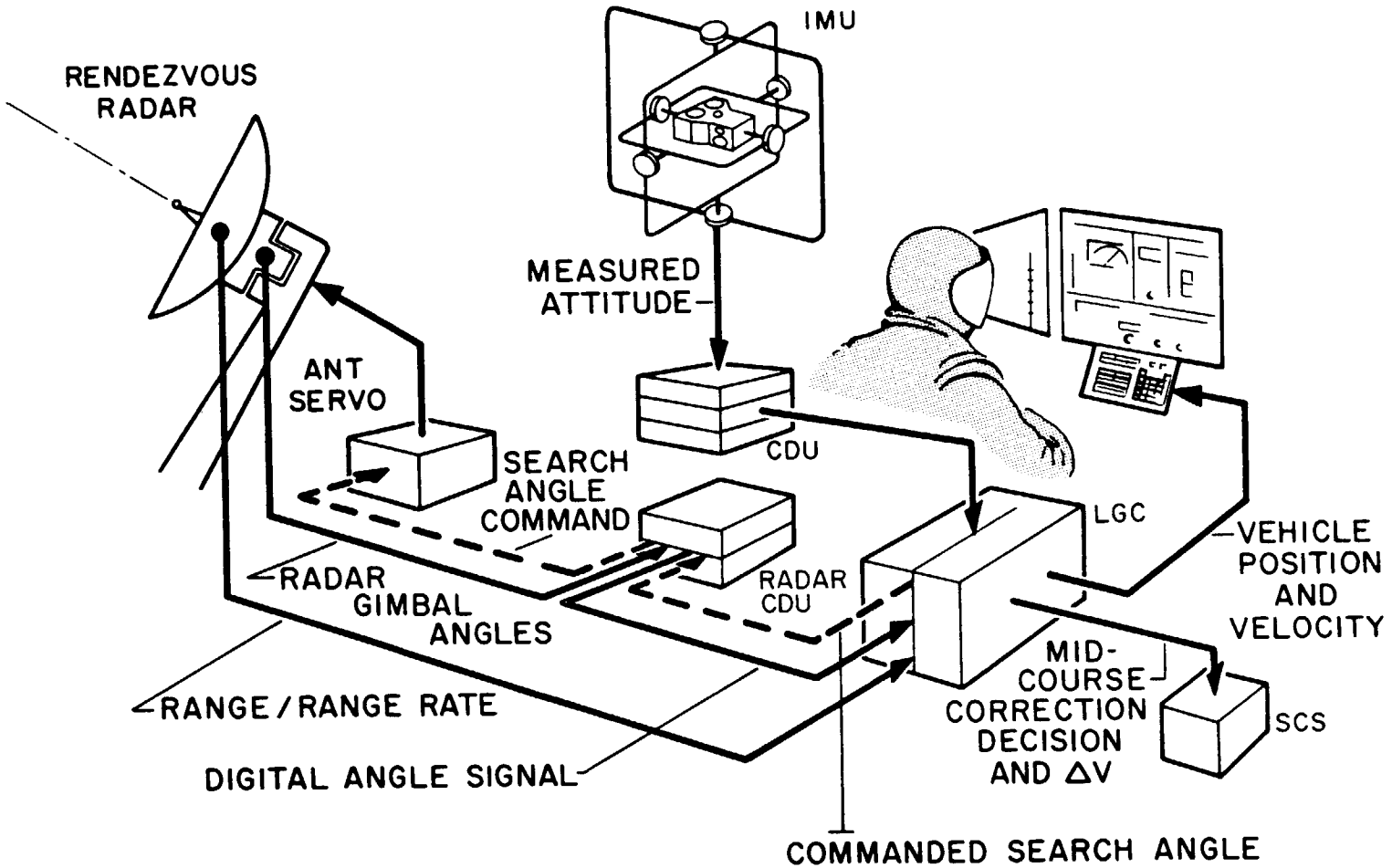

Fig. 7.25 Rendezvous computation phase.

and abort trajectories using the rendezvous guidance technique described in Section 7.2. The initial injection errors for the ascent trajectories studied are summarized in Fig. 7.26. The ascent trajectory considered was initiated from noncoplanar conditions of 2.2°, and covered a central angle of 132.5° from the injection point to the desired aim point on the CSM orbit. As indicated in Fig. 7.26, the initial separation between the two vehicles at injection was 8.5° (CSM ahead of LEM), and the resulting trajectory had a perilune of 49,000 ft. The IMU uncertainties during the powered ascent trajectory are essentially those shown in Section 6.5. These are summarized in this figure and combined with the initial condition uncertainties of the launch site to provide a total rss uncertainty in position of 4160 ft and a velocity uncertainty at injection of 9.9 fps.

The initial conditions for the guidance technique used to control the long range or midcourse rendezvous phase for ascents are summarized in Fig. 7.27. These initial conditions will be called standard conditions in following examples. The important parameters summarized in Fig. 7.27 are: the 60 second measurement or computation interval used during the midcourse guidance phase; the 0.3 value for the ΔV correction criteria ratio; velocity corrections were assumed to be applied with an angle uncertainty of 10 mr; and the radar performance used during the long range rendezvous phase is as listed in this figure and corresponds to the radar performance specified in Ref. 7.3. The initial condition injection position and velocity errors listed in Fig. 7.27 are those summarized in Fig. 7.26 all with a positive sign. This choice of sign results in a miss distance or point of closest approach that is about average, but not the most severe that can be chosen. The results of these initial conditions and the particular choice of sign are illustrated in following trajectory examples. The initial covariance matrices required in the guidance technique described in Section 7.2, are summarized in Fig. 7.27 for the digital simulation.

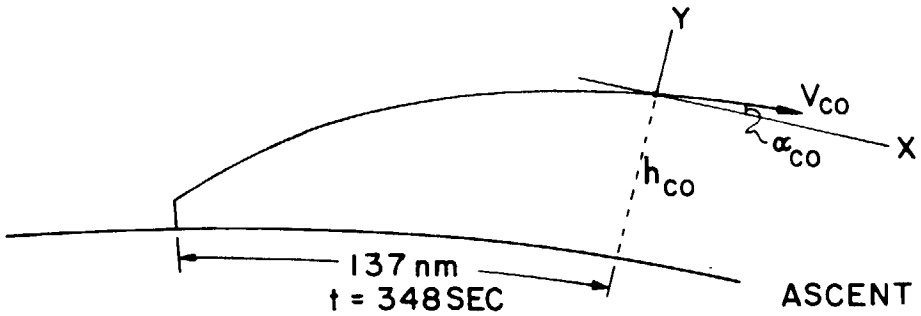

POWERED ASCENT CHAR.

V_{co} = 5594 fps

α_{co} = 0.26°

h_{co} = 50,600 FT

ASCENT TRAJ. CHAR.

I = 2.2°

ϕ = 132.5°

θ = 8.5°

$\dot{R}_f$ = -319 fps

h_{per} = 49,000 FT

INJECTION UNCERTAINTIES

	X (FT)	Y (FT)	Z FT	$\dot{X}$ (fps)	$\dot{Y}$ (fps)	$\dot{Z}$ (fps)
IMU UNCERTAINTIES (Imr ALIGNMENT ACC)	638	1015	1086	3.5	6.5	6.6
INITIAL CONDITION UNCERTAINTIES	2500	1500	2500	<0.1	<0.1	< 0.1
R. S. S.	2580	1810	2730	3.5	6.5	6.6

δr_0 = 4160 FT $\quad$ δV_0 = 9.9 fps

Fig. 7.26 Ascent trajectory and rss injection errors.

GENERAL PARAMETERS:

MEASUREMENT INTERVAL: 60 SEC

ΔV DECISION RATIO: 0.3

VELOCITY CORRECTION ANGLE UNCERTAINTY (IMU+SCS): 10mr

RADAR PERFORMANCE:

	RANDOM TRACKING (1σ)	FIXED BIAS	$\dot{R}$ (1σ)
ACTUAL :	1 mr	5 mr	0.33% ± 1 fps
ESTIMATED:	1 mr	10 mr	0.33% ± 1 fps

INITIAL CONDITION ERRORS:

δX	δY	δZ	$\delta \dot{X}$	$\delta \dot{Y}$	$\delta \dot{Z}$
+2580FT	+1810FT	+2730FT	+3.5 fps	+6.5fps	+6.6 fps

INITIAL COVARIANCE MATRICES OF ESTIMATION ERRORS:

$$\left[E_{\substack{LEM \\ (6X6)}}\right]_0 = \begin{bmatrix} 6.66\times10^6 & 0 & 0 & 2010 & 0 & 0 \\ 0 & 3.28\times10^6 & 0 & 0 & 5938 & 0 \\ 0 & 0 & 7.43\times10^6 & 0 & 0 & 6451 \\ 2010 & 0 & 0 & 12.25 & 0 & 0 \\ 0 & 5938 & 0 & 0 & 42.25 & 0 \\ 0 & 0 & 6451 & 0 & 0 & 43.56 \end{bmatrix}_0 \text{(FT, fps)}$$

$$\left[E_{Bias}\right]_0 = \begin{bmatrix} 0 & 0 & 0 \\ 0 & 100 & 0 \\ 0 & 0 & 100 \end{bmatrix} \text{(mr)} \; ; \quad \left[E_{\substack{CM \\ (6X6)}}\right] = 0$$

Fig. 7.27 Standard simulation run-ascent rendezvous.

The initial LEM covariance matrix is essentially that of the uncertainties listed in Fig. 7.26 with a correlation between respective position and velocity coordinates, i.e., $X, \dot{X}$. The initial rms bias estimation error was 0 for range rate and 10 mr for each tracking angle component. It might be noted that the initial radar angle bias estimate will normally be determined during the prelaunch phase as a result of tracking the CSM overpass. (Section 5.3). As indicated in Fig. 7.27, the initial uncertainty of the CSM orbit was assumed to be zero. It might be noted that the effects of actual CM orbital uncertainties will be illustrated in a following example, but it is assumed that in the guidance technique no CM orbital uncertainties are known.

A typical ascent trajectory controlled by the rendezvous guidance system is illustrated in Figs. 7.28 and 7.29. This trajectory is plotted in local vertical coordinate system centered on the CSM. The projection of the ascent trajectory into the XY, or CM orbital plane, is illustrated in Fig. 7.28, and the trajectory projection in the XZ, or horizontal plane, is illustrated in Fig. 7.29. In these two figures, the uncorrected trajectory resulting from the particular injection errors of Fig. 7.26 is illustrated as the dotted trajectory which has a miss or point of closest approach to the CSM of 8.4 nm at a time approximately 100 seconds sooner than the reference ascent trajectory. The primary G&N rendezvous system required 3 midcourse corrections, as illustrated in these figures. The time, ranges and velocity components of these corrections are listed in the two figures. In this case, the total midcourse velocity corrections required 27 fps to compensate for the 9.9 fps uncertainty at ascent injection. A statistical analysis of this trajectory and injection velocity uncertainty condition, $(E_{LEM})_0$ of Fig. 7.27, resulted in an average midcourse ΔV requirement of 27 fps indicating that the particular injection errors of Figs. 7.27 and 7.28 result in ΔV requirements and uncorrected miss distances that are essentially a one sigma case. The third and final midcourse cor-

rection in Fig. 7.28 was applied at a range of 25 nm, and resulted in a miss distance of less than 250 ft. During this trajectory, an actual fixed angle bias of 5 mr was assumed as noted in Fig. 7.27, and the initial rms estimate of the fixed bias was 10 mr. This ascent trajectory will be referred to as the standard ascent and is summarized in Case 1 of Fig. 7.30. The terminal phase over the last 20 mile range of this standard trajectory is illustrated in more detail in Fig. 7.31 for the XY plane projection. It can be seen from this figure, that the actual trajectory of the standard ascent labeled #1 closely approximates the reference trajectory over the final phase of this maneuver. If the initial injection errors were increased by a factor of 3, the resulting uncorrected trajectory is shown in Fig. 7.31, as trajectory #2, with a point of closest approach of 22.7 nm. If this trajectory were controlled with the primary G&N guidance system, a total of 3 corrections would be required with a total midcourse ΔV requirement of 78 fps as summarized in Case 5 of Fig. 7.30. The final correction of this trajectory is shown in Fig. 7.31, and again the actual trajectory closely approximates the reference trajectory over the final phase of the rendezvous maneuver.

With reference to Fig. 7.30, the effects of the currently specified radar performance are illustrated in Case 2. In this case, it was assumed that the LEM was injected on a perfect ascent trajectory which would intercept the CSM if no further correction were made. Using the primary G&N rendezvous system, 3 corrections were required due to the uncertainties in the radar tracking performance and required a total ΔV of 13.4 fps.

The effects of not estimating the tracking angle biases in the rendezvous radar is illustrated in Case 3 of Fig. 7.30. In this case, it was assumed that a 15 mr fixed bias existed in the two tracking angles of the rendezvous radar. Assuming the standard injection uncertainties, a total of 3 midcourse correc-

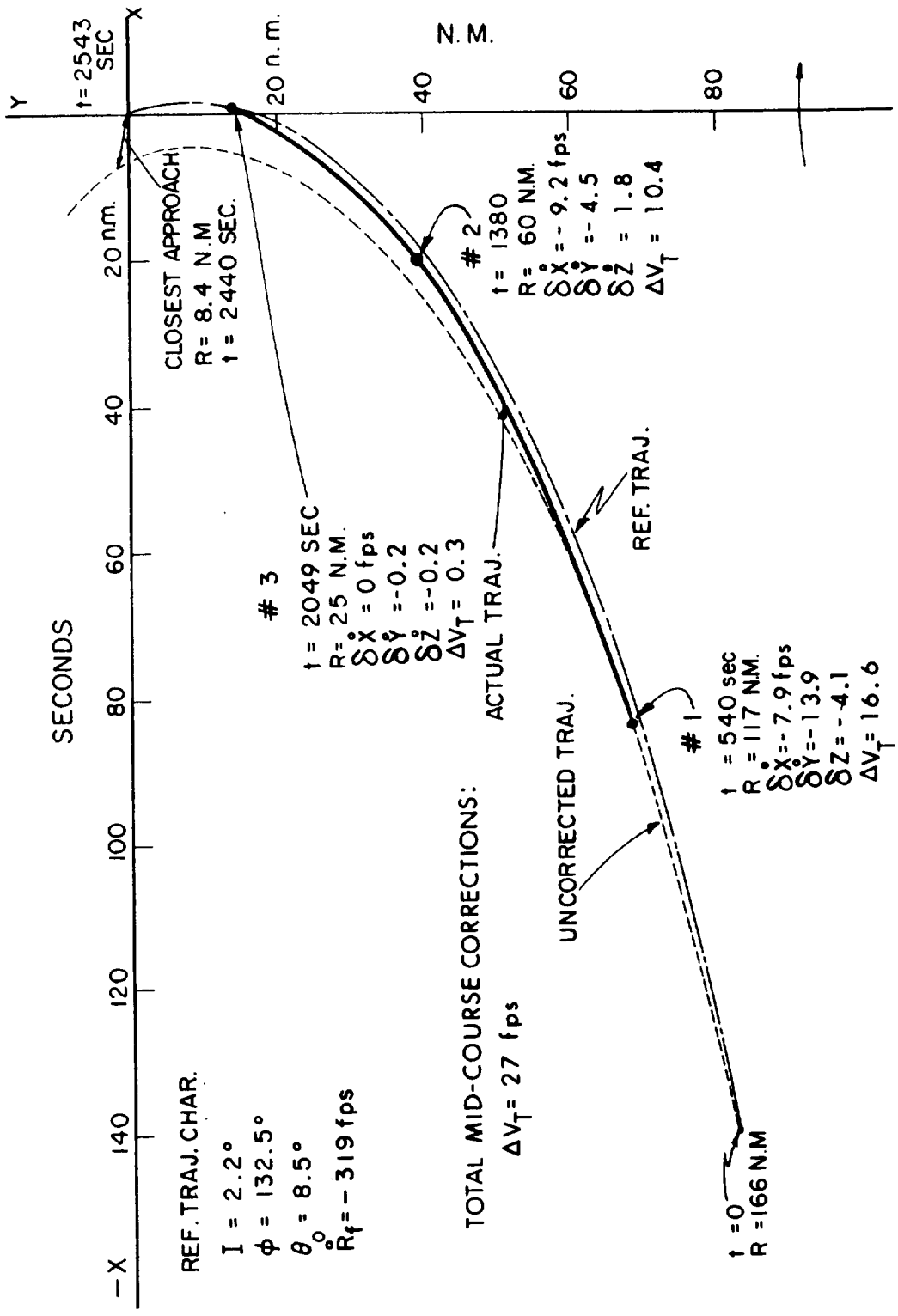

Fig. 7.28 Rendezvous from ascent (x-y plane trajectory projection).

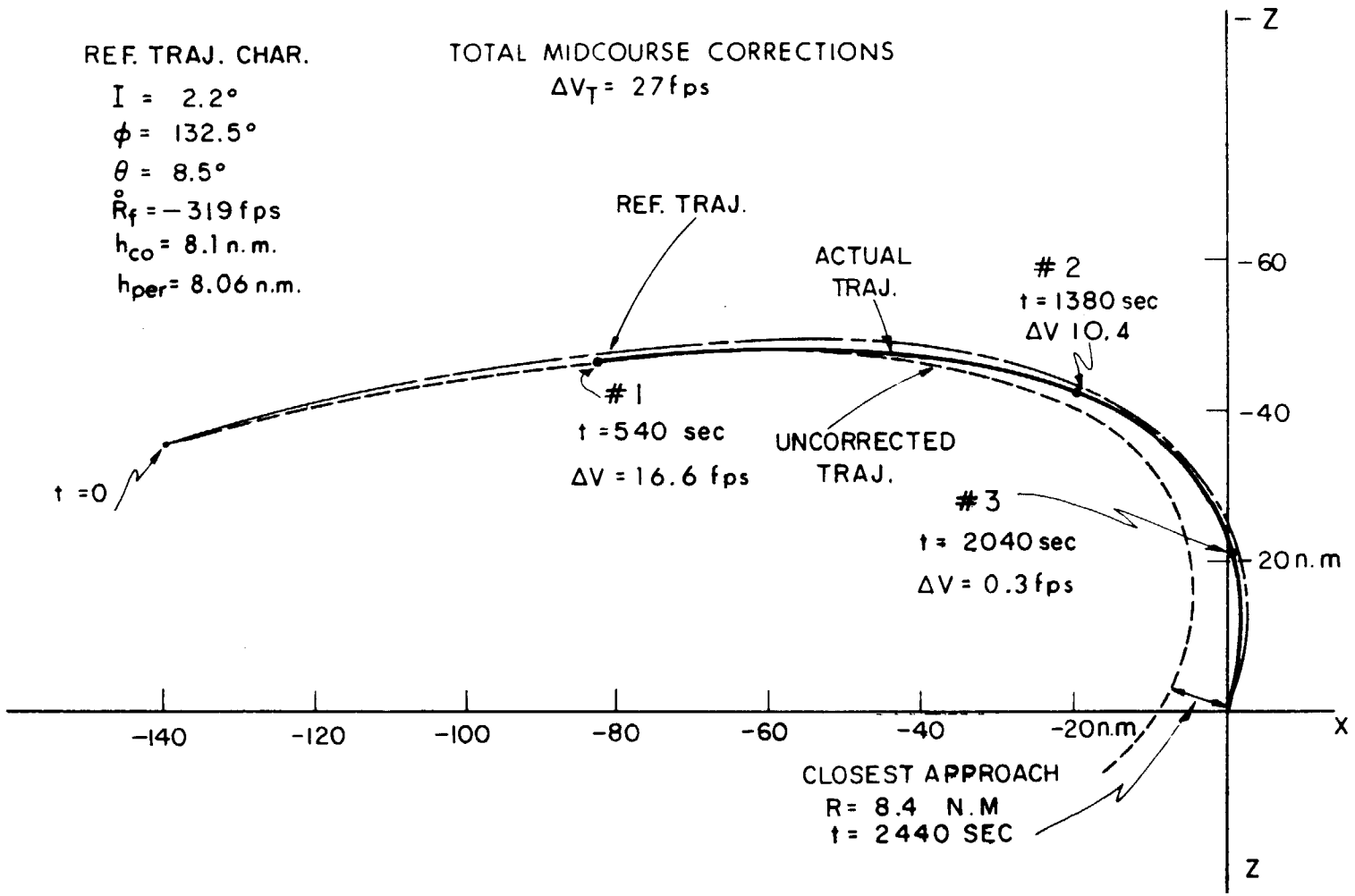

Fig. 7.29 Rendezvous from ascent (x-z plane trajectory projection).

	SIMULATION COMMENTS	$[\delta V_{LEM}]_0$ (fps)	UNCORRECTED MISS (nm)	NUMBER OF CORRECTIONS	FINAL MISS (FT)	TOTAL VELOCITY CORRECTION (fps)
1.	STANDARD ASCENT SIMULATION	9.9	8.4	3	225	27
2.	EFFECT OF RADAR UNCERT'S ONLY	0	0	3	150	13.4
3.	NO RADAR BIAS EST. (Bias=15mr)	9.9	8.4	3	3720	90.4
4.	EST. BIAS (Bias = 30mr)	9.9	8.4	3	220	30.6
5.	LARGE LEM INITIAL COND. ERRORS $\binom{3X}{STD}$	29.7	22.7	3	395	78
6.	I.C.= 3 X STD., Bias= 30mr	29.7	22.7	3	390	80
7.	$[E_{LEM}]_{6X6_0}$= 10 X STD.	9.9	8.4	4	425	60.6
8.	RADAR TRACKING ACC.= 3mr (1σ)	9.9	8.4	3	600	43.7
9.	NO IMU + SCS ALIGNMENT ERROR FOR ΔV CORRECTIONS	9.9	8.4	3	200	28.3

Fig. 7.30 Long range rendezvous summary.

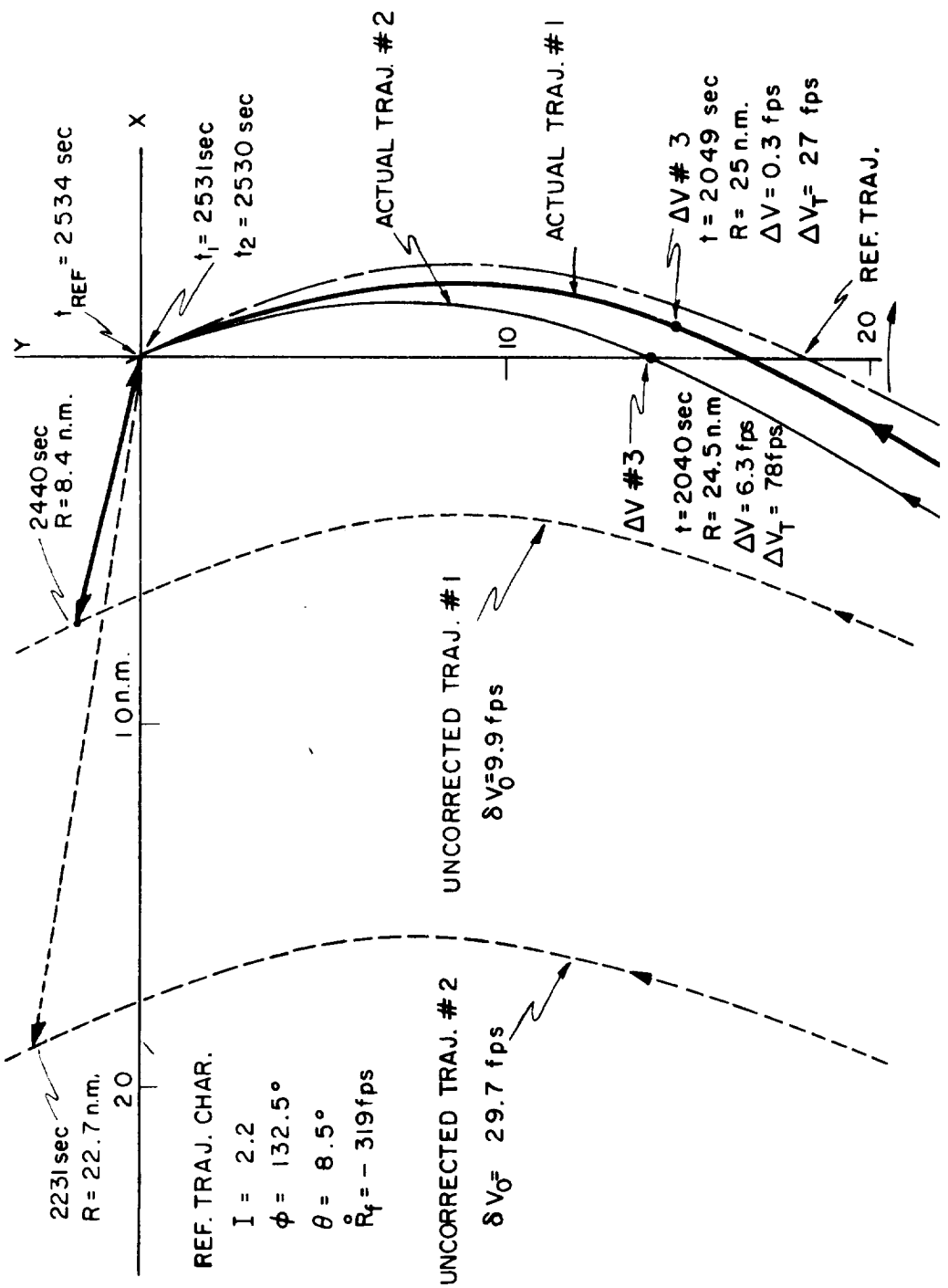

Fig. 7.31 Rendezvous from ascent (x-y plane trajectory projection)

tions were again required resulting in a ΔV requirement of 90.4 fps and a point of closest approach of over 1/2 nm. Case 4 of Fig. 7.30 illustrates the effect of estimating a bias in the tracking angles when the actual bias has a magnitude of 30 mr, twice that currently specified for the LEM installation. In this case, with a standard injection uncertainty, the total midcourse guidance ΔV requirement was 30.6 fps or only slightly greater than that of the standard ascent Case 1. The importance of estimating the tracking angle biases is illustrated by comparing the results of Cases 3 and 4 in Fig. 7.30.

Case 6 of Fig. 7.30 illustrates the effect of large injection errors, three times that of the standard run of Case 1, and with an angle bias of 30 mr which would be estimated or compensated for in a guidance technique. By comparing the results of Cases 5 and 6, it can be seen that when the initial injection errors are three times those estimated, and the initial bias in the tracking angle is three times that estimated, the resultant ΔV requirement is only 2 fps greater than that case illustrated in Case 5 for small bias conditions.

If a standard ascent trajectory were run with initial estimates of the LEM uncertainty that are ten times greater than those of Case 1, the results are summarized in Case 7 of Fig. 7.30. With the same initial injection errors, which would result in the same uncorrected point of closest approach of 8.4 miles, the guidance system would require four midcourse corrections with a total of 60.6 fps. This figure can be compared with that of Case 1, and illustrates the importance of having a reasonably good estimate of the LEM injection uncertainties. Cases 5 and 6 illustrate that the actual injection errors could be in error by a factor of 3 over those estimated with acceptable results; however, when the LEM injection uncertainty is in error by a factor of 10, unacceptable conditions result as illustrated in Case 7.

Case 8 of Fig. 7.30 illustrates the effect of degraded

radar angle tracking performance. In this case, a 3 mr 1 σ tracking performance was actually used when the guidance system estimated the tracking performance to be 1 mr. By comparing runs 1 and 8 in Fig. 7.30, it can be seen that the degraded radar tracking accuracy required an additional 17 fps in the midcourse ΔV requirement.

Case 9 of Fig. 7.30 shows the effect of the angle uncertainty in the application of the midcourse velocity corrections. In Case 1, it was assumed that all midcourse corrections were applied with an angle uncertainty of 10 mr, as listed in Fig. 7.27. Case 9 of Fig. 7.30 assumes perfect midcourse velocity corrections as called for by the primary rendezvous system, and results in negligible ΔV improvement.

The effects of lunar gravitational uncertainty on the rendezvous guidance system are illustrated in Case 10 of Fig. 7.32. In this simulation, it was assumed that the lunar gravitational constant was in error by one part in a thousand for the standard ascent maneuver of Fig. 7.30. Comparing these two runs, it can be seen that the effects of the lunar gravity uncertainty result in an additional 5 fps velocity requirement during the long range rendezvous phase.

The effects of CM orbital ephemeris errors are illustrated in Case 11 of Fig. 7.32. In this simulation, it was assumed that the CM ephemeris uncertainties were in the order of 9000 ft and 8.2 fps as summarized under Case 11. It should be noted that these were considered to be extreme CM ephemeris errors, and were used to illustrate the effects on the long range rendezvous guidance system. The CM orbital uncertainties were also chosen of such a sign, so that the point of closest approach or miss distance was increased in this case to 16.1 nm, assuming that the LEM injection errors were those of the standard ascent of Case 1. The effects of the LEM injection uncertainty and the CM orbital uncertainties of these particular magnitudes and

	SIMULATION COMMENTS	$[\delta V_{LEM} + \delta V_{CM}]_0$ (fps)	UNCORRECTED MISS (nm)	NUMBER OF CORRECTIONS	FINAL MISS (FT)	TOTAL VELOCITY CORRECTION (fps)
10.	LUNAR μ ERROR ($\mu_{act} = 0.999\mu_{est}$)	9.9	8.8	3	170	32
11.	CM ORBIT ERRORS: $[\delta V_{CM}]_0 = 8.2$fps δX δY δZ $\delta\dot{X}$ $\delta\dot{Y}$ $\delta\dot{Z}$ -8700' -790' -1750' -0.7 -7.6 -2.9	18.1	16.1	3	900	51.3
12.	COMBINED #10 AND #11	18.1	16.4	3	850	54.8
13.	ANGLE ONLY TRACKING α_{est} = 1mr $BIAS_{est}$ = 1mr α_{act} = 1mr $BIAS_{act}$ = 1mr	9.9	8.4	3	170	53.4
14.	ANGLE ONLY TRACKING α_{est} = 1mr $BIAS_{est}$ = 1mr α_{act} = 3mr $BIAS_{act}$ = 1mr	9.9	8.4	3	570	96.1

Fig. 7.32 Long range rendezvous summary (cont).

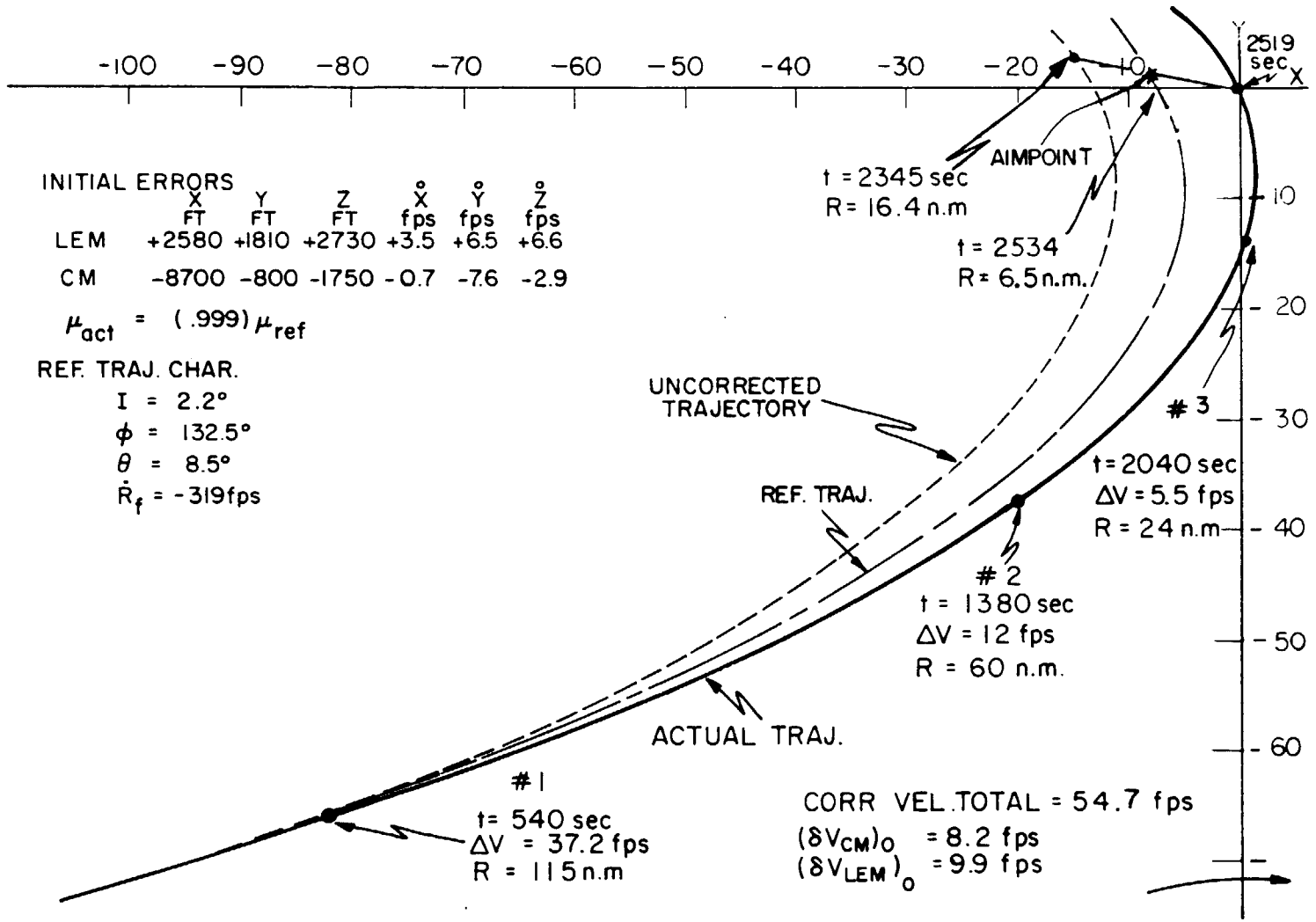

Fig. 7.33 Ascent rendezvous - combined errors - x-y plane trajectory projection.

directions resulted in a midcourse guidance ΔV requirement of 51.3 fps, as illustrated by Case 11 of Fig. 7.32. These effects are further illustrated in Fig. 7.33 which is an ascent trajectory projection in the XY plane for the combined errors of standard LEM injection uncertainties, the CM orbital uncertainties of Case 11, and the lunar gravitation uncertainties of Case 10. In Fig. 7.33, it can be seen that the reference trajectory for the ascent and rendezvous phase does not intersect the CM, but has a point of closest approach of 6.5 nm due to the CM ephemeris uncertainties. The lunar gravitational constant uncertainty also contributes to this error, but in a minor manner which can be shown by comparing the uncorrected miss distances of Cases 10 and 1 of the rendezvous summary tables. The uncorrected trajectory of Fig. 7.33 results in a point of closest approach of 16.4 nm due to the combination of all errors. Three midcourse corrections were again required by the primary G&N system resulting in a total ΔV requirement of 54.7 fps for this particular simulation. The times, ranges, and magnitudes of the velocity corrections are illustrated in Fig. 7.33 and represent a worse than average situation in which the CM and LEM velocity uncertainties were chosen in directions to result in maximum miss distances.

Cases 13 and 14 of Fig. 7.32 illustrate the effects of using angle only tracking from the LEM AOT during the long range rendezvous phase in the event of rendezvous radar failure. In Case 13, an angle tracking accuracy with the combined optics and LEM RCS system was assumed to be 1 mr, and the actual tracking performance by the astronaut using the LEM RCS system was within this level. For the ascent trajectory with its corresponding standard injection uncertainties, the rendezvous maneuver using optical tracking only required a total of 53.4 fps in midcourse corrections, as compared with 27 fps when radar tracking data of equivalent angle performance combined with range rate data was used. This represents an increased

requirement of 26 fps, or essentially double that of the rendezvous radar performance. Case 14 of Fig. 7.32 illustrates the effect of degraded optical tracking to a level of 3 mr 1σ when the guidance system has assumed tracking accuracies of 1 mr. For the standard ascent maneuver, this resulted in a total midcourse ΔV requirement of 96.1 fps. This represents an additional ΔV requirement of 43 fps over the 1 mr tracking accuracy of Case 13, or a 69 fps additional ΔV requirement over the standard ascent trajectory case of Case 1 using the specified rendezvous radar tracking performance. Cases 13 and 14 of Fig. 7.32 were included to illustrate the ΔV penalty associated with optical angle tracking only used in a back-up mode in the event of rendezvous radar failure.

7.4.3 Current Ascent Trajectories

Recent analysis has restricted the out of plane launch conditions of the LEM from the CM orbit to levels of 0.5 degrees instead of the 2.2 degree level previously considered. This restricted out of plane launch condition resulted from recent LEM ΔV and vehicle design requirements. Typical ascent trajectories from these launch conditions are illustrated in Figs. 7.34 to 7.37. Figures 7.34 and 7.35 illustrate the projection of a 0.5 degree out of plane launch condition trajectory on the XY and XZ planes, respectively. This trajectory resulted from the powered ascent trajectory summarized in Figs. 6.8 to 6.11 of Section 6.3 and covers a central angle from injection to aim point of 153.5 degrees. The long range rendezvous guidance technique required 3 midcourse velocity corrections for this trajectory when injected with the standard position and velocity uncertainties listed in Fig. 7.26. The midcourse velocity corrections indicated in Fig. 7.34 are discussed in Section 7.5. The final closing velocity at the terminal rendezvous phase for this trajectory is 140 fps, as indicated in Fig. 7.34.

As mentioned in Section 5.4, there are two possible op-

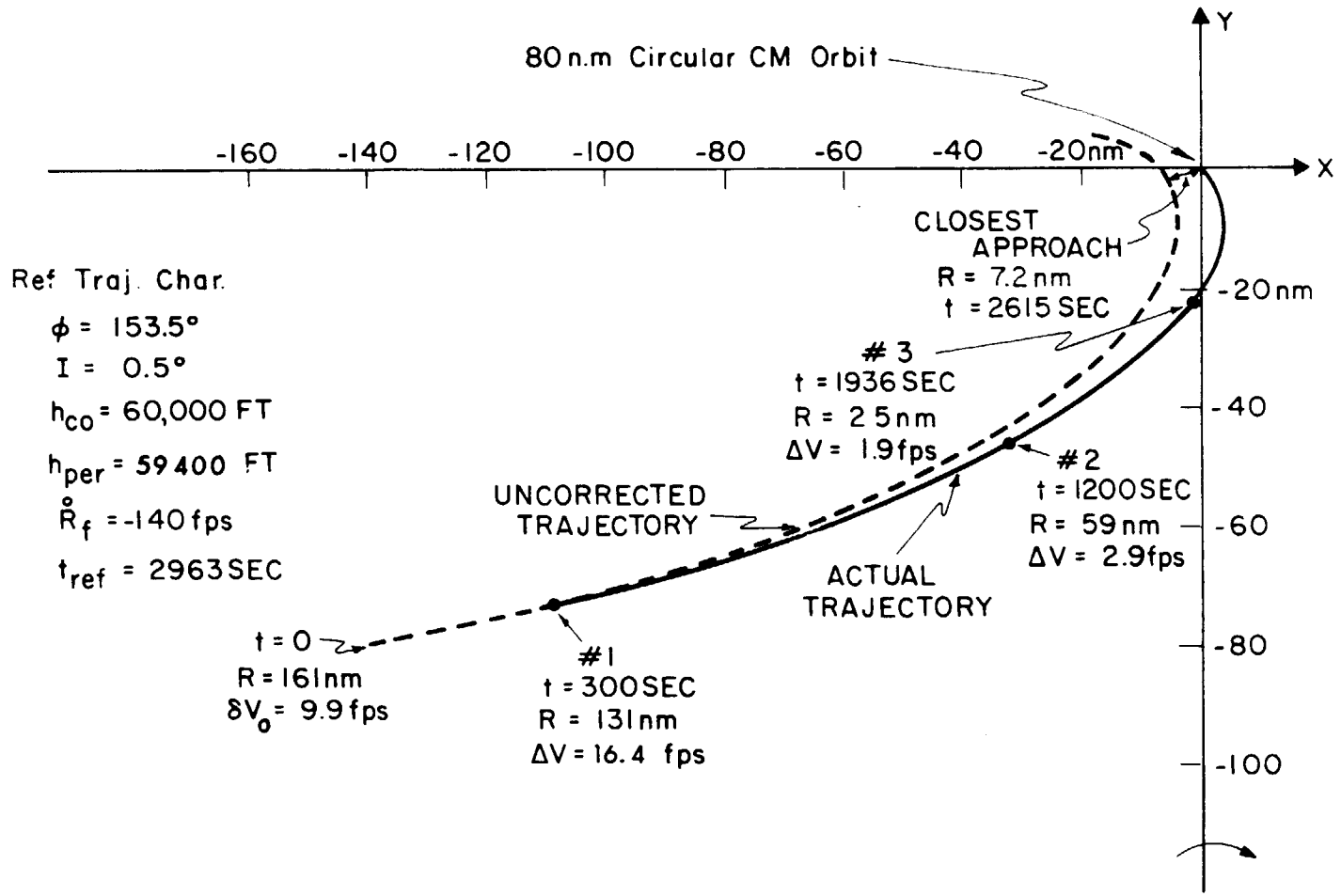

Fig. 7.34 Ascent rendezvous (x-y plane trajectory projection).

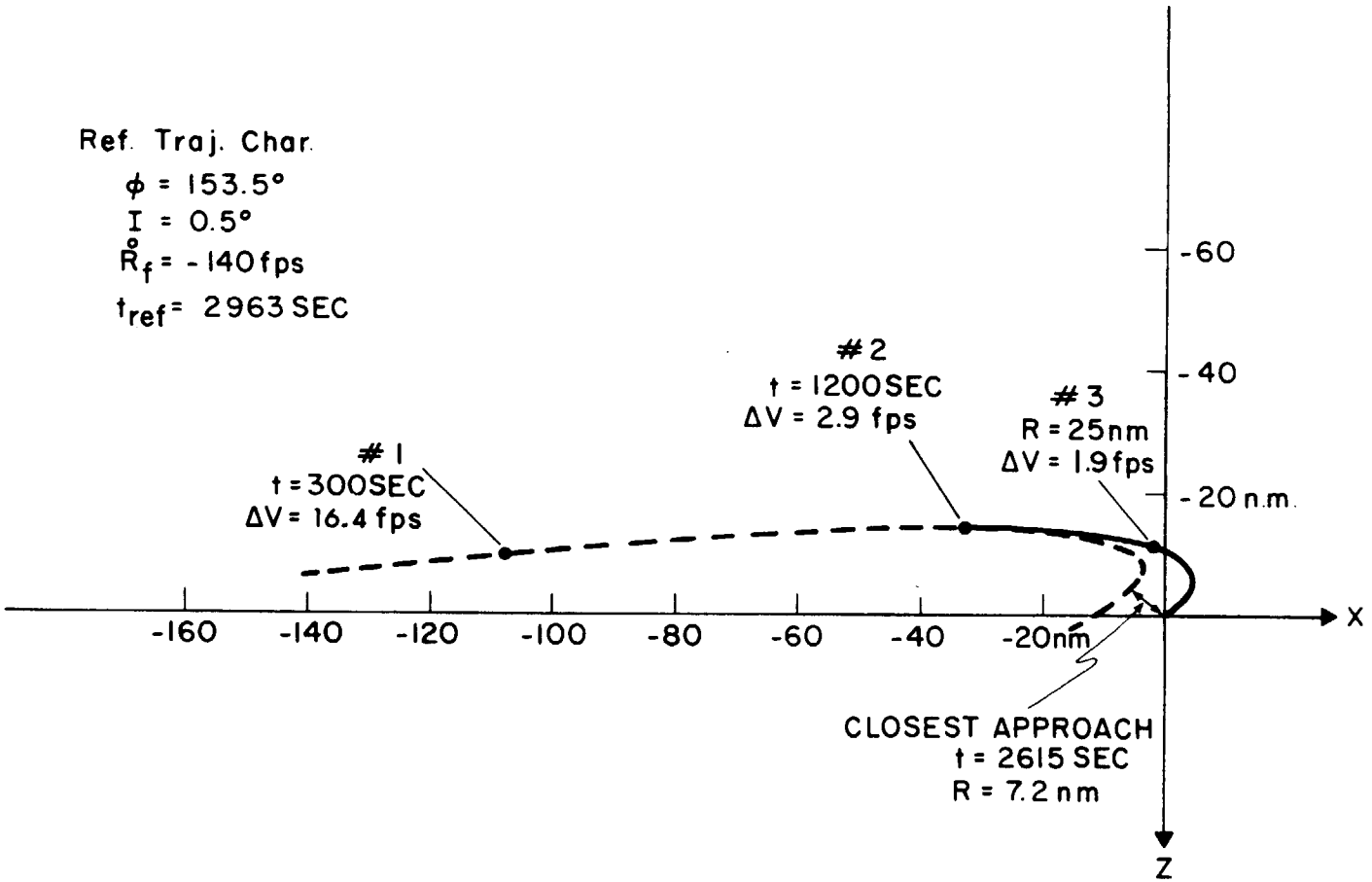

Fig. 7.35 Ascent rendezvous (x-z plane trajectory projection).

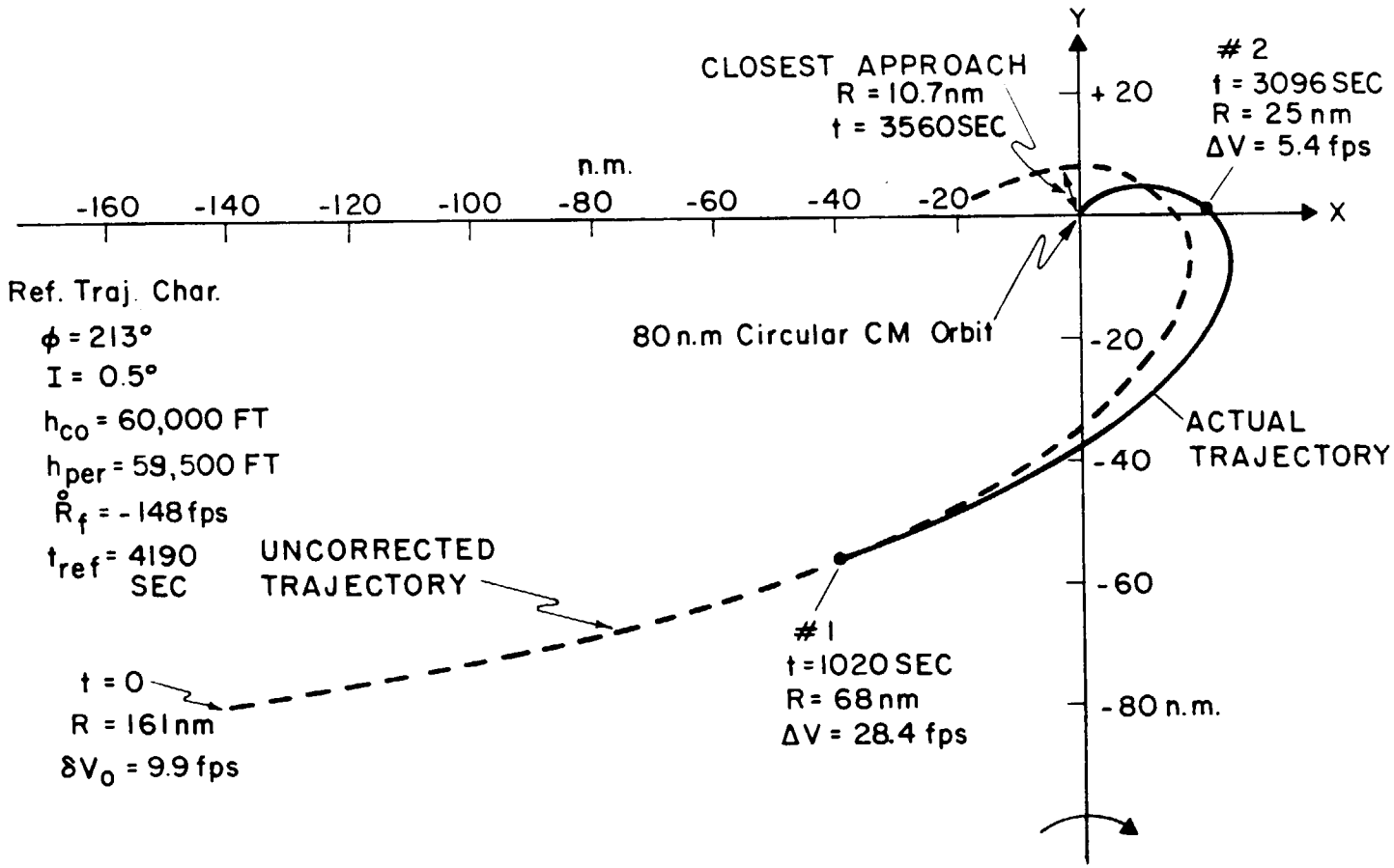

Fig. 7.36 Ascent rendezvous (x-y plane trajectory projection).

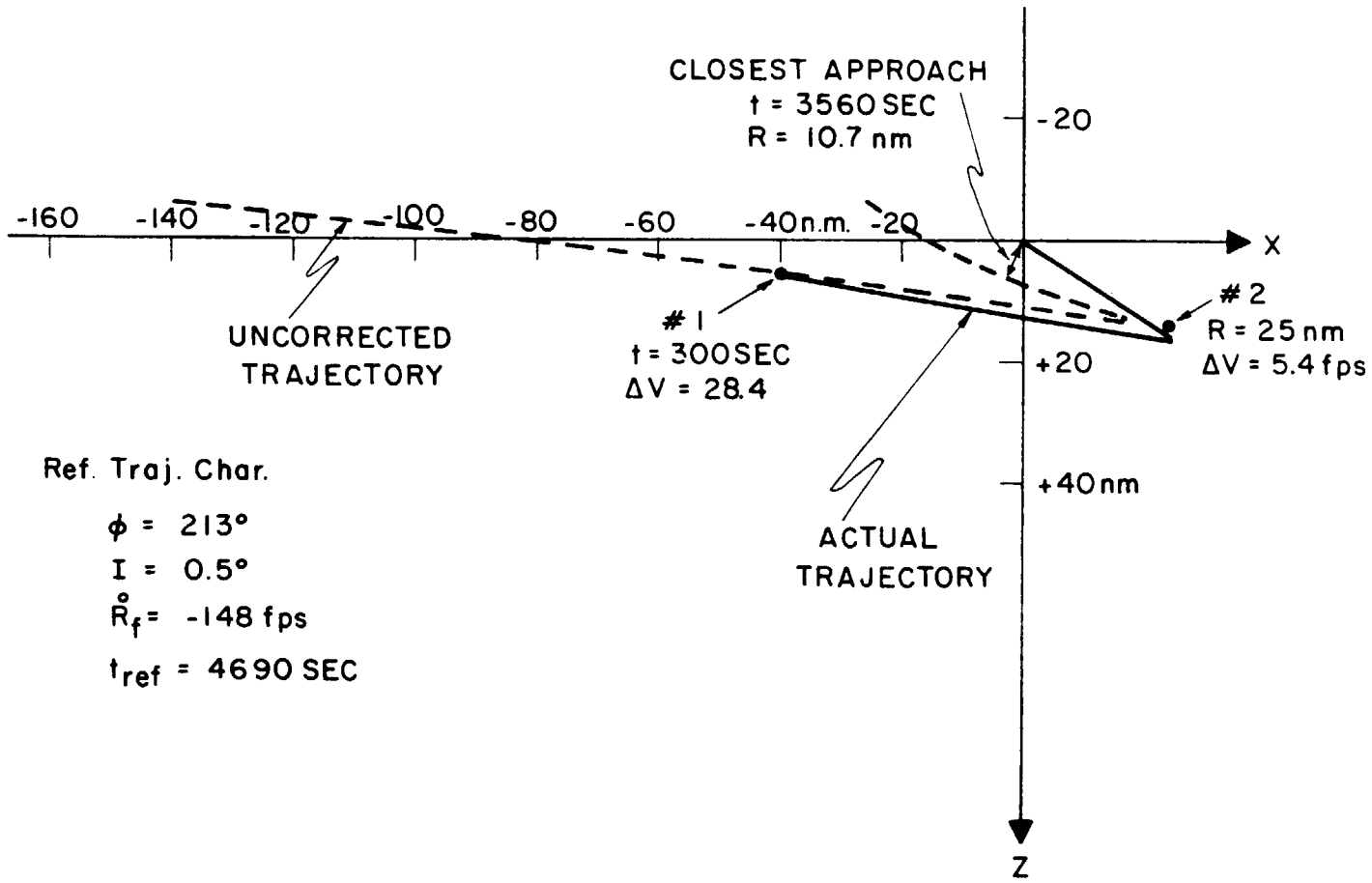

Fig. 7.37 Ascent rendezvous (x-z plane trajectory projection).

timum direct ascent trajectories for a given out of plane condition. For the 0.5 degree out of plane launch condition currently considered, a trajectory covering a central angle from injection to aim point of greater than 180^{o} is illustrated in Figs. 7.36 and 7.37. These figures illustrate the projections of the ascent trajectory on the XY and XZ planes for a trajectory covering a central angle of 213^{o} when injected with standard injection uncertainties. These uncertainties result in a point of closest approach of 10.7 nm. The two midcourse velocity corrections shown in Figs. 7.36 and 7.37 were based on a fixed time schedule which was modified by a $180^{o} \pm 20^{o}$ sector criteria. This midcourse correction criteria and possible improvements to it are discussed in Section 7.5. It might be noted here, however, that midcourse correction timing criteria can be developed that essentially equalize the midcourse ΔV requirement for trajectories covering central angles of greater than 180 degrees to the level of those having central angles of less than 180 degrees.

7.5 Midcourse Velocity Correction Logic

7.5.1 General Comment

A statistical velocity correction (SVC) logic was described in Sections 7.2.4.1 and 7.3. Briefly, the SVC logic calls for implementation of the current velocity correction estimate ($\Delta\hat{\underline{V}}$) when the ratio of the rms magnitude of the uncertainty in $\Delta\hat{\underline{V}}$ to the rms magnitude of ΔV is less than a prescribed threshold. Selection of this threshold was based on two considerations: (1), minimum total ΔV; and (2), minimum number of corrections. With low threshold values, velocity corrections will not be applied until the uncertainty is a small proportion of the estimated correction. This results in a small number of corrections, each of which has a high probability of being accurate. However, since the midcourse ΔV correction increases monotonically with time after injection, the total ΔV expended eventually will increase, as the threshold setting is lowered. On the other hand raising the threshold

setting results in: (1), increased number of corrections; and (2), corrections containing a higher proportion of uncertainty. A threshold setting of 0.3 yields sufficiently low ΔV totals without requiring an excessive number of corrections.

Since the SVC logic is based on ensemble averages of measurement errors and injection errors, it will yield satisfactory results over the entire ensemble while not necessarily being optimum for any paricular condition. Also, since the statistical ratio used is computed in flight, it is not necessary to have different schemes for the wide variety of trajectories possible in the LEM mission.

Although it is obviously desirable to utilize a logic which yields the best results over the ensemble of initial conditions and ascent trajectories, the SVC logic has some disadvantages which make it less desirable than a scheme which utilizes a fixed time schedule of velocity corrections. The following sections will: (1), discuss the disadvantages of the SVC logic; and (2), present a fixed time velocity correction concept.

7.5.2 Disadvantages of SVC Logic

One of the disadvantages to the SVC logic becomes apparant when considering rendezvous trajectories with central angles greater than 180 degrees. For the purpose of this discussion, reference may be made to Fig. 7.38 which shows the midcourse ΔV requirements for two typical abort trajectories with central angles greater than 180 degrees. Of particular interest are the "resonance" peaks occuring for transfer angles in the vicinity of 180 degrees. The reason for these peaks is as follows.

If the central angle from the LEM's current estimated position vector, $\hat{R}_{LEM}$, to the aim point vector $R_{CM}(T_A)$, is in the vicinity of 180 degrees, and $\hat{R}_{LEM}$ is slightly out of the original LEM reference trajectory plane, a prohibitively large plane change may be required if an intercept trajectory is to be established at this point. This, of course, would require an

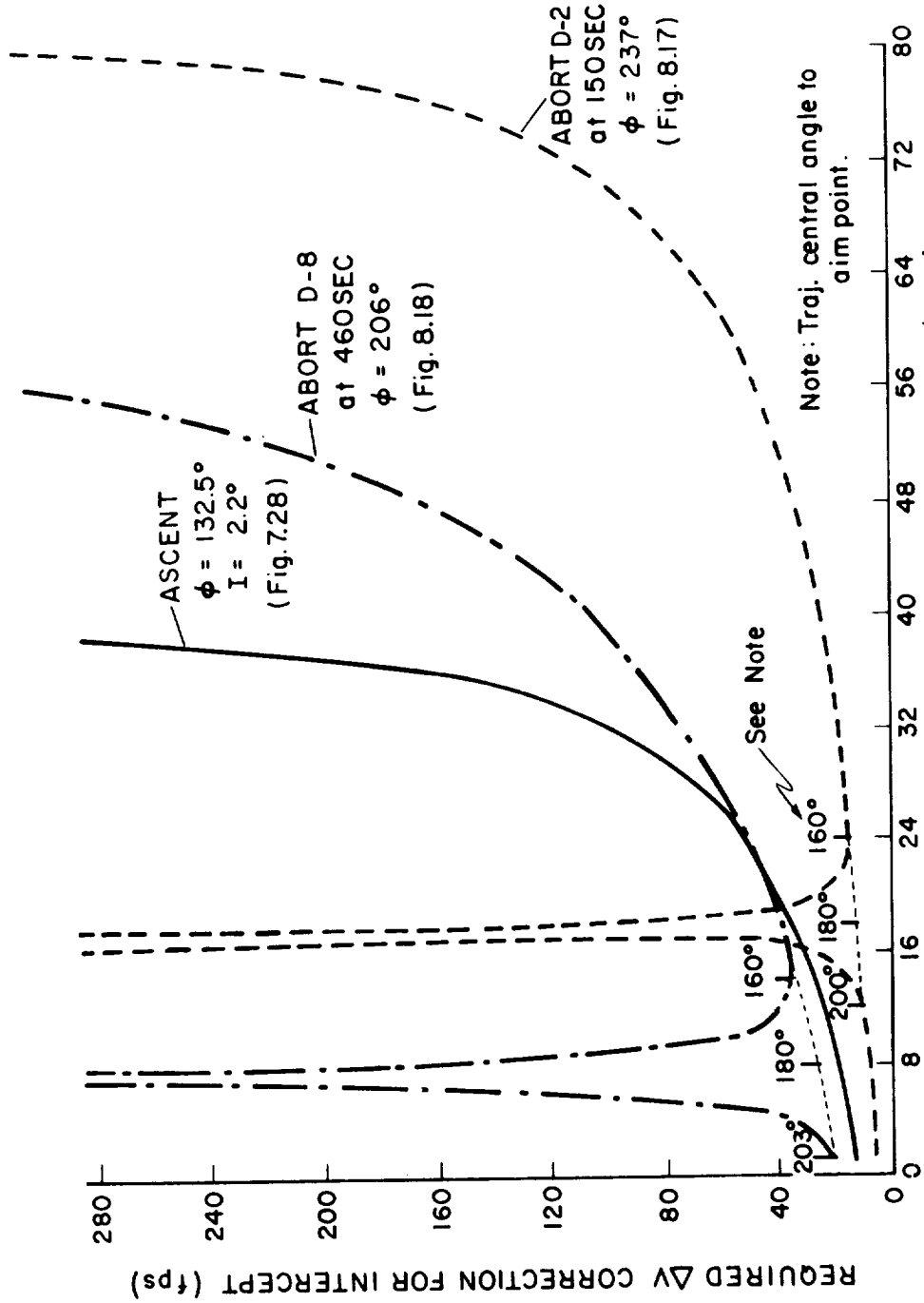

Fig. 7.38 Mid-course correction requirements vs time.

extremely large ΔV, since the LEM velocity vector (which is essentially in the original reference trajectory plane except for small out-of-plane velocity errors) would have to be rotated by approximately the angle of the plane change. This plane change angle is a function of the out-of-plane component of $\hat{\underline{R}}_{LEM}$ and the amount the transfer angle differs from 180 degrees. For the expected errors in position and velocity at injection and expected measurement errors, the out-of-plane component of $\hat{\underline{R}}_{LEM}$ will require exorbitant plane changes in a band of transfer angles from 160 degrees to 200 degrees. Outside this band of transfer angles, the plane change is not significant.

Thus, midcourse velocity corrections, which are based on a computation of the velocity required to establish an intercept trajectory with the CSM at time = T_A (i.e., the solution of Lambert's problem), will require larger values of ΔV within this band than for points on the trajectory which are outside the band yet closer to the intercept point. Therefore, in order to avoid the "resonance" peak, a ΔV penalty is incurred since application of a velocity correction must be delayed despite the fact that the uncertainty in the correction may be well below an acceptable level. This undesirable situation may be avoided by the following technique.

Since the large plane change around 180 degrees is the cause of the ΔV "resonance" peak, the elimination of this plane change must be effected in the guidance concept. The exact solution to the intercept problem demands the large plane change so a less precise solution is required which, while it admittedly will be slightly in error, will not require the exorbitant plane change. Such a solution is found by assuming the cause of the large plane change (the out-of-plane component of $\hat{\underline{R}}_{LEM}$) to be non-existant. Thus, the projection of $\hat{\underline{R}}_{LEM}$ in the original LEM reference trajectory plane is used as the LEM position vector, and Lambert's problem is solved for the velocity required at

this position to intercept the CSM at time = T_A. The small error implicit in this solution is more than compensated for by the savings in ΔV achieved by the earlier application of ΔV now made possible.

This technique provides a means of applying a satisfactory velocity correction in the vicinity of a 180^o transfer despite the fact that R_{LEM} is not in the original reference trajectory plane. However, the SVC logic may not be employed in this band of transfer angles. The reason is that the SVC logic utilizes the rms value of ΔV which, being an ensemble average, will reflect the fact that on the average the LEM error vector will contain an out-of-plane component. Thus, the rms value of ΔV and the rms magnitude of the uncertainty in ΔV will go through the resonance peaks referred to above. The ratio utilized in the SVC logic will therefore not be a meaningful quantity on which to base a decision on the application of a ΔV which, in fact, is computed using the special technique described above. Herein lies a disadvantage of the SVC logic as opposed to a fixed time schedule: the application of ΔV must be delayed until the transfer angle is less than 160 degrees and the statistical ratio again becomes meaningful.

A second disadvantage is the fact that the SVC logic will require more computation time and computer storage than the fixed time schedule. These additional computations would include: extrapolation and up-dating of the X matrix, computation of the C* matrix, rms value of ΔV , and rms magnitude in the uncertainty in ΔV.

A final disadvantage would be in the area of astronaut monitoring. With a fixed time schedule, the astronaut would know beforehand exactly when to apply velocity corrections, whereas with the SVC logic this depends on the particular trajectory which is being flown.

7.5.3 The Fixed Time Velocity Correction Concept

A fixed time velocity correction TC scheme would utilize a predetermined schedule of times at which midcourse velocity corrections would be applied, along with a final correction at 25 nm which would assure conditions that are compatible with the terminal phase of rendezvous. The times selected would yield satisfactory results irrespective of the particular trajectory flown. As mentioned in Section 7.5.1, the SVC logic with a threshold setting of 0.3 will result in low total rms ΔV without an excessive number of corrections, averaged over the ensemble of injection and measurement errors. For any reference trajectory then, the best choice of times for midcourse corrections would be those dictated by the SVC logic, in order to assure satisfactory ensemble performance. However, these times could differ depending on the reference trajectory, and it is desired to obtain a single time schedule for all trajectories in the LEM mission. The approach taken was to select, as closely as possible, the times dictated by the SVC logic for those trajectories in which the timing is most critical. These trajectories are the ones which cover the smallest central angles. This can be seen by referring to Fig. 7.39. The rms magnitude of ΔV required for

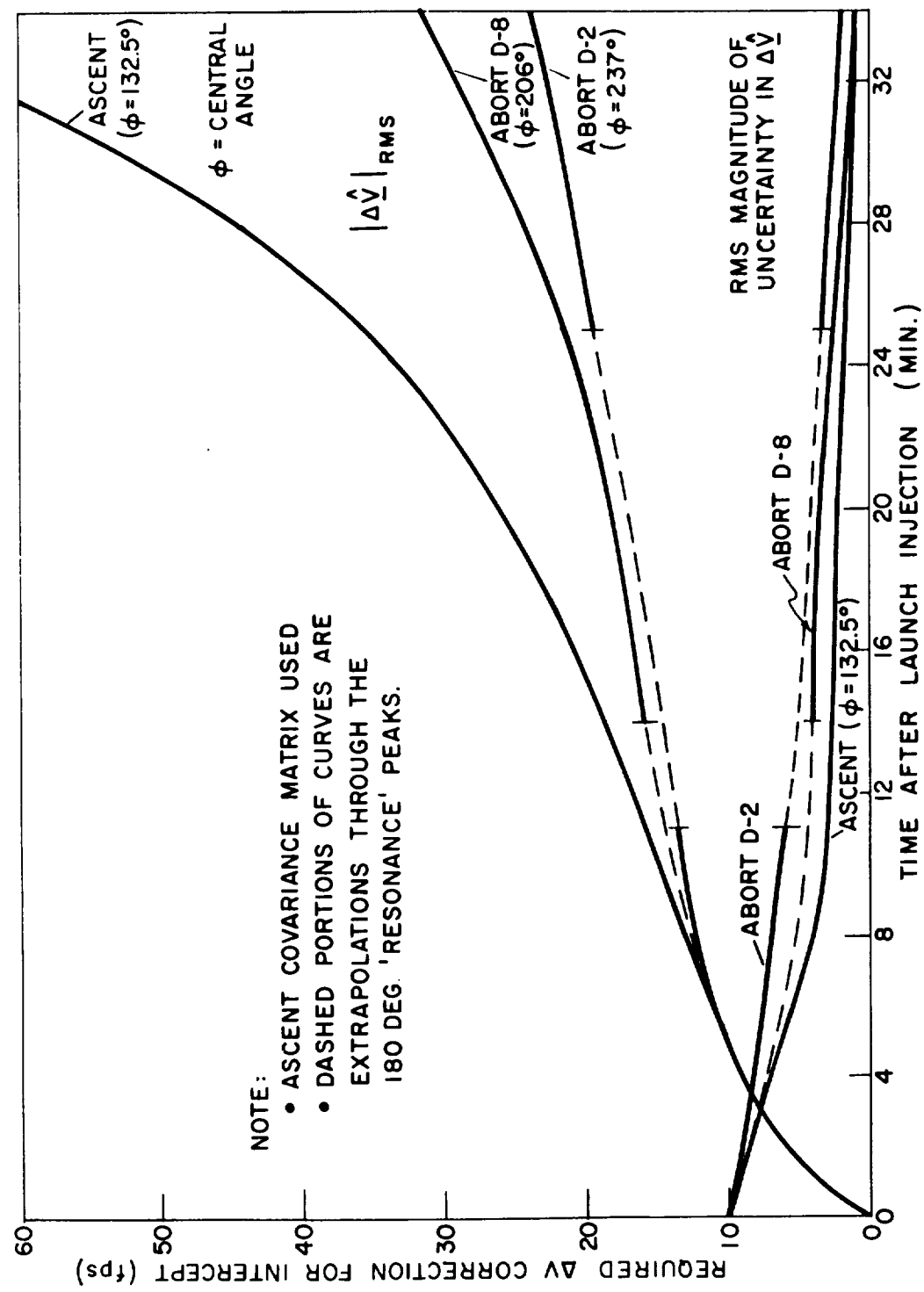

Fig. 7.39 Rms mid-course correction requirements vs time.

intercept is plotted vs time from burnout for three typical reference trajectories. (Note that the same initial covariance matrix was used for these plots to compare the effect of the trajectory on ΔV). It can be seen that as the central angle of the trajectory increases, the slope of these curves decreases. Thus, the trajectories with the largest central angles will be less sensitive to ΔV timing changes than those covering smaller central angles. It can also be seen from the plots of rms magnitude of uncertainty in ΔV in Fig. 7.39 that after about 10 minutes these curves are quite flat. Thus, the errors in ΔV will not be too sensitive to timing changes.

Consequently, on the basis of the above conclusions, the fixed times would be selected as those dictated by the SVC logic for the ascent trajectory of Fig. 7.39. (These times are 9 minutes and 23 minutes). However, the actual times selected are 10 minutes and 25 minutes, to be compatible with another ascent trajectory under consideration ($\phi = 153.5^{o}$, $I = 0.5^{o}$) (see Section 7.4.3) requiring SVC times of 10 minutes and 26 minutes. For the trajectories with larger central angles, there will be appreciable time (and also ΔV buildup) between the 25 minutes correction and the final correction at 25 nm. To prevent excessive ΔV buildup, the fixed time schedule includes corrections at 40 minutes and every 20 minute interval thereafter until the 25 nm point is reached. This could result in, at most, 2 more corrections for the longest trajectories considered. However, a predetermined threshold would be specified (typically 1 fps), below which ΔV would not be applied. These additional corrections would then still be effective in preventing excessive ΔV buildup, without requiring unnecessary engine starts.

A statistical performance study was made to compare the fixed time schedule discussed above with the SVC logic for five typical LEM trajectories. The pertinent results are summarized in the table of Fig. 7.40. An additional time schedule is included

	TRAJECTORY	LOGIC	MID-COURSE CORRECTION					TOTAL RMS ΔV (fps)
			TIME RMS ΔV	TIME RMS ΔV	TIME RMS ΔV	TIME RMS ΔV	RMS ΔV Range=25n.m.	
1	ASCENT ϕ=132° I = 22°	SVC	9 min 13.8 fps	23 min 7.7 fps			5.5 fps	27
		TC	5 min 10.3	20 min 12.1			6.6	29
		TC	10 min 14.6	25 min 8			3.8	27.4
2	ASCENT ϕ= 153.5° I=0.5°	SVC	10 min 13.2	26 min 7.2			2.5	22.9
		TC	5 min 9.6	20 min 9.6			4.7	23.9
		TC	10 min 13.2	25 min 6.7			2.4	22.3
3	ASCENT ϕ=213° I = 0.5°	SVC	17 min † 18.4	28 min 4.6	37 min 1.3		1.7	26
		TC	5 min 10	20 min 7.6	40 min 6.3		1.2	25.1
		TC	10 min 13.5	25 min 5.4	40 min 3.1		1.1	23.1
4	ABORT D-8 ϕ=206° I = 0°	SVC	17 min † 27.1	31 min 5.8			2.4	35.3
		TC	5 min 15	20 min 14.6	40 min 6		0.2	35.8
		TC	10 min 21.5	25 min 6.9	40 min 4.2		0.2	32.8
5	ABORT D-2 ϕ=237° I =0°	SVC	25 min † 10.2	43 min 1.7	71 min 1.4		0.3	13.6
		TC	5 min 2.5	20 min 9.5	40 min 2.8	60 min 0.5	1.2	16.5
		TC	10 min 5.7	25 min 5.7	40 min 1.5	60 min 0.6	1.2	14.5

SVC = STATISTICAL VELOCITY CORRECTION ($\sqrt{\delta U / \delta V} < 0.3$)
TC = FIXED TIME CORRECTIONS
† = DELAYED CORRECTION TO 180 ± 20° CRITERIA

Fig. 7.40 Comparison of mid-course correction criteria (statistical study).

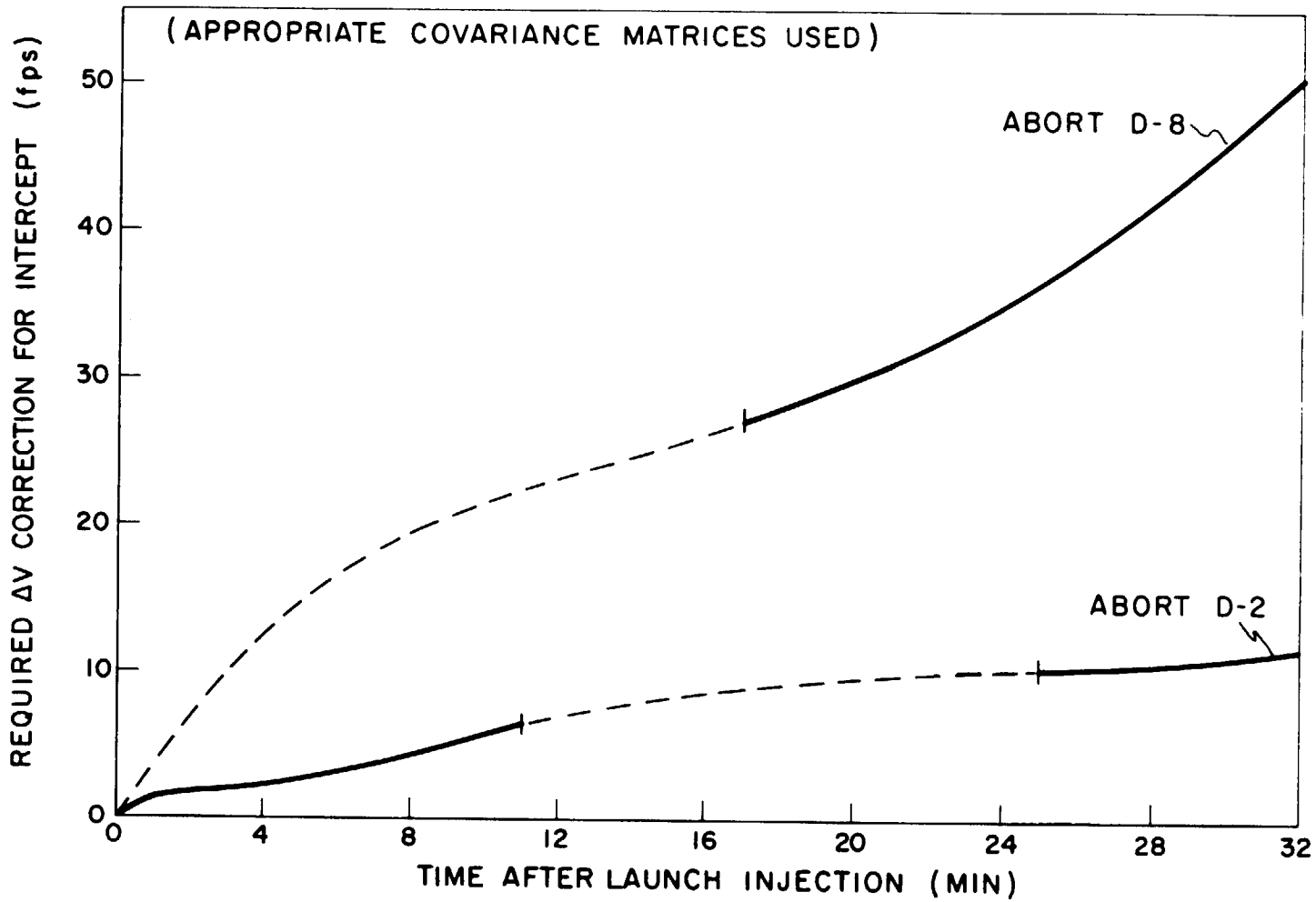

Fig. 7.41 Rms mid-course correction requirements vs time.

(5 minutes, 20 minutes, 40 minutes, etc.), since this particular schedule produced excellent results for trajectories with a specific set of initial conditions. It can be seen, however, from Fig. 7.40, that on an ensemble basis this schedule is not as good as the one selected on the basis of SVC logic. It can also be seen from the table that the selection of 10 minutes and 25 minutes yields results which are essentially identical to the SVC logic for the two ascents (items 1 and 2 of Fig. 7.40). For two of the trajectories with central angles greater than 180 degrees (items 3 and 4 of Fig. 7.40) the TC logic (10 minutes, 25 minutes) yields lower total rms ΔV than the SVC logic as expected, since no delay is required in the vicinity of 180 degrees. This improvement is not noted for the trajectory of item 5. The reason for this is the extremely flat ΔV buildup curve exhibited by this trajectory and shown in Fig. 7.41 where the initial covariance matrix associated with this particular trajectory was utilized. Thus, the delay caused by the 180 degree band cost very little in additional ΔV, whereas this late correction had less uncertainty associated with it than the one at 10 minutes.

Some results of a simulation utilizing specific initial conditions (as opposed to statistical analysis) are presented in Fig. 7.42. The conclusions stated on the basis of the statistical analysis are essentially confirmed by these results. However, for these particular conditions, the TC scheme using 5 minutes and 20 minutes yields the best results. The statistical results do not substantiate that this schedule will, on the average, yield the best results so that no significance should be attached to this single sample. In all cases, the TC scheme effected a savings in ΔV for the trajectories with central angles greater than 180 degrees. (In item 5 the midcourse ΔV total exceeded that for the SVC logic, but the overall total ΔV including rendezvous was less). A ΔV threshold of 1 fps was used for this simulation with the result that a maximum number of corrections applied was four, which occurred only for the ascent trajectory of item 3.

	TRAJECTORY	LOGIC	MID-COURSE CORRECTION					TOTAL MID COURSE ΔV (FPS)	TOTAL ΔV (INCLUDING REND)	FINAL MISS. (FT)
			TIME ΔV	TIME ΔV	TIME ΔV	TIME ΔV	ΔV (RANGE = 25 N.M)			
1	ASCENT $\phi = 132°$ I = 22°	SVC	9 min 16.6 fps	23 min 10.4 fps			0.3* fps	27	341 fps	60
		TC	5 min 17	20 min 3.1			3.3	23.4	337.5	60
		TC	10 min 16.9	25 min 15.7			1.1	33.7	345.4	60
2	ASCENT $\phi = 153.5°$ I = 0.5°	SVC	10 min 16.7	26 min 10.4			1	28.1	158.8	36
		TC	5 min 16.4	20 min 2.9			1.9	21.2	154.2	40
		TC	10 min 16.7	25 min 9.4			1	27.1	158	42
3	ASCENT $\phi = 213°$ I = 0.5°	SVC	17 min † 28.4	(28 / 0.4)* → 30 / 1.0	37* 0.2		1	30.4	174.9	32
		TC	5 min 16.1	20 min 8.1	40 min 1.2		1.4	26.8	169.7	28
		TC	10 min 16	25 min 8.5	40 min 3.1		1.1	28.7	166.2	22
4	ABORT D-8 $\phi = 206°$ I = 0°	SVC	17 min † 35.8	31 min 5.1			1	41.9	147.2	120
		TC	5 min 20.8	20 min 8.8	40 min 5.8		0.1*	35.4	141.4	162
		TC	10 min 22.7	25 min 11.9	40 min 2.6		0.1*	37.2	143.2	162
5	ABORT D-2 $\phi = 237°$ I = 0°	SVC	25 min † 15.7	43 min 1.2	71 min 0.1*		0.2*	16.9	345.4	138
		TC	5 min 2.2	20 min 8.5	40 mi 4.2	60 min 0.1*	0.2*	14.9	338.6	252
		TC	10 min 5.8	25 min 10.4	40 min 1.4	60 min 0.1*	0.2*	17.6	341.3	252

* VELOCITY CORRECTION NOT APPLIED IF $|\Delta V| < 1.0$ fps

† DELAYED CORRECTION TO $180° \pm 20°$ CRITERIA

Fig. 7.42 Comparison of mid-course correction criteria (based on specific initial conditions).

7.5.4 Summary

The fixed time schedule of midcourse velocity corrections appears to be a more satisfactory ΔV application criterion than the statistical velocity correction logic for the following reasons:

1. No ΔV penalty because of necessity to delay ΔV application for trajectories with central angles greater than 180 degrees.
2. Less computer storage and computation time.
3. More satisfactory astronaut monitoring.

The apparent advantage of the SVC logic - completely general with respect to reference trajectory and initial conditions - does not appear to offer a significant advantage over the TC scheme. The time schedule selected - 10 minutes, 25 minutes, 40 minutes, every 20 minutes thereafter (with appropriate ΔV threshold), plus a correction at 25 nautical miles relative range - yields satisfactory results for all five trajectories examined. The type of trajectory is not too critical since the fixed times are selected to satisfy the shortest trajectories, whereas the longer ones (greater central angle) are less critical to timing of corrections. In addition the initial injection errors will not vary considerably from trajectory to trajectory so that the uncertainty level in $\Delta\hat{\underline{V}}$ should be sufficiently low by 10 minutes of tracking. Thus, although the present time schedule of corrections may not be precisely the one selected when the reference trajectories are more firmly established, a slight variation of this schedule should easily make it compatible with the trajectories of the LEM mission.

7.6 Terminal Rendezvous Phase

7.6.1 G&N Operation

The terminal rendezvous phase is initiated at a relative

range of 5 nm between the two vehicles. The previous midcourse rendezvous phase achieved a collision or intercept trajectory that would nominally intercept the CSM at the time of arrival (t_A). The objective of the primary G&N system during the terminal rendezvous phase is to control a series of thrust maneuvers such that the relative velocity is decreased to -5 fps as the range closes to the initial docking range of 500 feet.

The guidance technique for controlling the terminal rendezvous maneuver was described in Section 7.2.4.2, and is essentially a modification of the midcourse rendezvous phase in which a new aim point and time of arrival on the CSM orbit is defined on the basis of some terminal range-range rate criteria. This type of operation is analogous to the translunar midcourse phase when the guidance objective is changed from an aim point at the lunar sphere of influence to a plane and perilune criteria. Terminal rendezvous maneuvers are generally described in a relative line of sight coordinate system in the literature. It should be pointed out that the primary G&N computes the terminal rendezvous velocity corrections in the same lunar centered inertial frame used in the midcourse rendezvous phase. Under nominal operation, the LEM will be on an intercept trajectory after the last midcourse correction (typically made at a range of about 25 nm), and the primary G&N system will command terminal velocity corrections that are essentially entirely along the line of sight which is similar to the conventional line of sight coordinate operation. The guidance system completely controls closing velocity $\dot{R}$ and the trajectory W_{LS} with the shifting aim point concept at each velocity correction. Since the rendezvousing vehicle is held on an intercept trajectory throughout the final phase, the terminal rendezvous maneuver is generally illustrated in a range-range rate (R-$\dot{R}$) phase plane which shows a profile of closing velocity history for the thrust and coast intervals of the maneuver. Phase planes of this type are presented in the following section for typical rendezvous trajectories.

The guidance concept during the thrust maneuvers of the terminal rendezvous phase is a simplified form of the explicit equations described for the powered ascent phase in Section 6.2. In this system, the present LEM position and velocity vectors, $\hat{\underline{R}}_{LEM}$, $\hat{\underline{V}}_{LEM}$, the aim point $\hat{\underline{R}}_{CM}(t_A)$, and the required impulsive velocity correction, $\Delta\underline{V}$, are determined by the tracking radar data and computation summarized in Figs. 7.7 and 7.15 during the coast periods of the terminal phase. The thrust maneuvers are then initiated, directed, and finally terminated so that the LEM will pass through the aim point at the correct time by the explicit guidance concept in the form used during the final 30 seconds of the powered ascent maneuver. These explicit equations are simplified from the form presented in Section 6.2 as follows:

1. Burn out velocity is controlled, but the radial position requirement is relaxed thereby omitting one of the calculations used during the powered ascent.

2. Since the terminal rendezvous powered maneuvers are relatively short and cover a small central angle, the Lambert subroutine will not have to be interrogated after the first few cycles of the explicit ascent equations. The ascent equations can determine the required burn-out velocity components at the predicted burn-out point early in the maneuver provided thrust characteristics of the engine to be used is known.

The terminal rendezvous maneuver will normally be controlled by the LEM RCS jets provided that the initial closing velocity and weight conditions are within the RCS capability. As mentioned in Section 7.2.4.2, under nominal ascent weight conditions, the RCS has a 200 fps velocity capability and the ascent engine would be used in those cases involving higher velocities and vehicle weight conditions to reduce the relative velocity within the RCS capability. Examples of the terminal rendezvous maneuver are presented in the following section.

7.6.2 Terminal Rendezvous Maneuvers.

As mentioned in the previous section, the midcourse rendezvous phase G&N operation will nominally establish an intercept trajectory by the time the vehicle reaches the initial terminal rendezvous range of 5 nm. The fixed range-rate schedules listed in Section 7.2.4.2 have been used for most primary G&N analysis of the terminal rendezvous maneuver. An example of the terminal maneuver for the ascent trajectory shown in Figs. 7.34 and 7.35 of Section 7.4.3 is shown as a R-$\dot{R}$ phase plane plot in Fig. 7.43. This particular ascent trajectory from 0.5 degree out of plane launch conditions resulted in a closing velocity at the initial terminal range (5 nm) or -143 fps. Since this closing velocity is within the RCS capability, the RCS jets were used to control the three thrusting maneuvers required by the following range-rate schedule:

Range (R)	Desired Range Rage ($\dot{R}_d$)
5 nm	-100 fps
1.5 nm	- 20 fps
0.25 nm	- 5 fps

After the first 30 second thrust period using 2 RCS jets (normally the +Z axis jets) tracking data was used to determine a new aim point and timing as described in Figs. 7.14 and 7.15 at the second thrust point (R = 1.5 nm). Tracking and navigation computation is done during the coast intervals (horizontal dashed lines in Fig. 7.43) of the terminal maneuvers. The profile of Fig. 7.43 assumed an initial LEM weight of 4480 lbs and an effective exhaust velocity of the RCS jets of 8700 fps (I_{s_p} = 270 seconds). The terminal maneuver from 5 nm to 500 feet required slightly more than 11 minutes making a total time from ascent injection to initiation of docking of 57 minutes for the trajectory of Fig. 7.34.

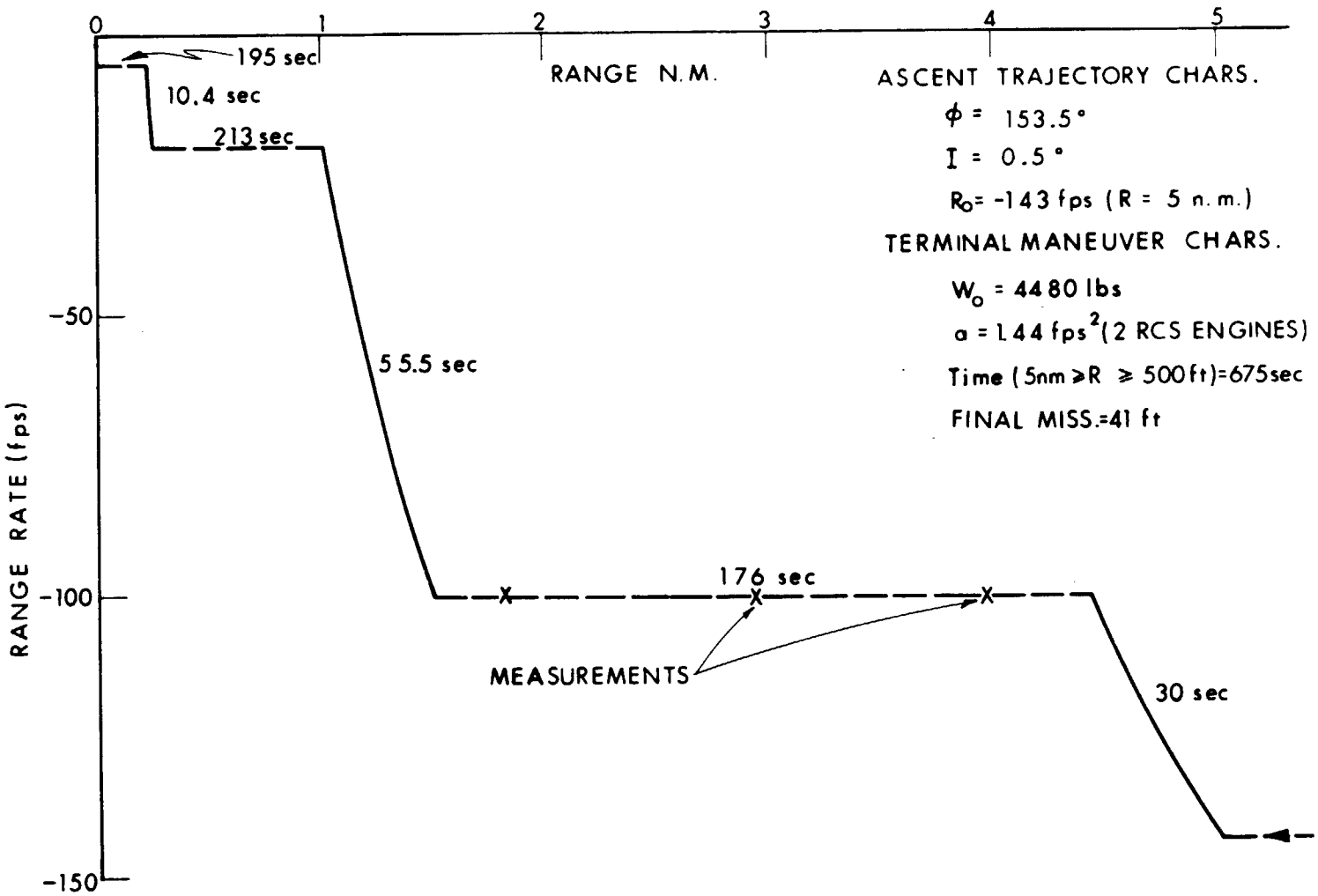

Fig. 7.43 LEM terminal rendezvous R-$\dot{R}$ profile (fixed R-$\dot{R}$ schedule method).

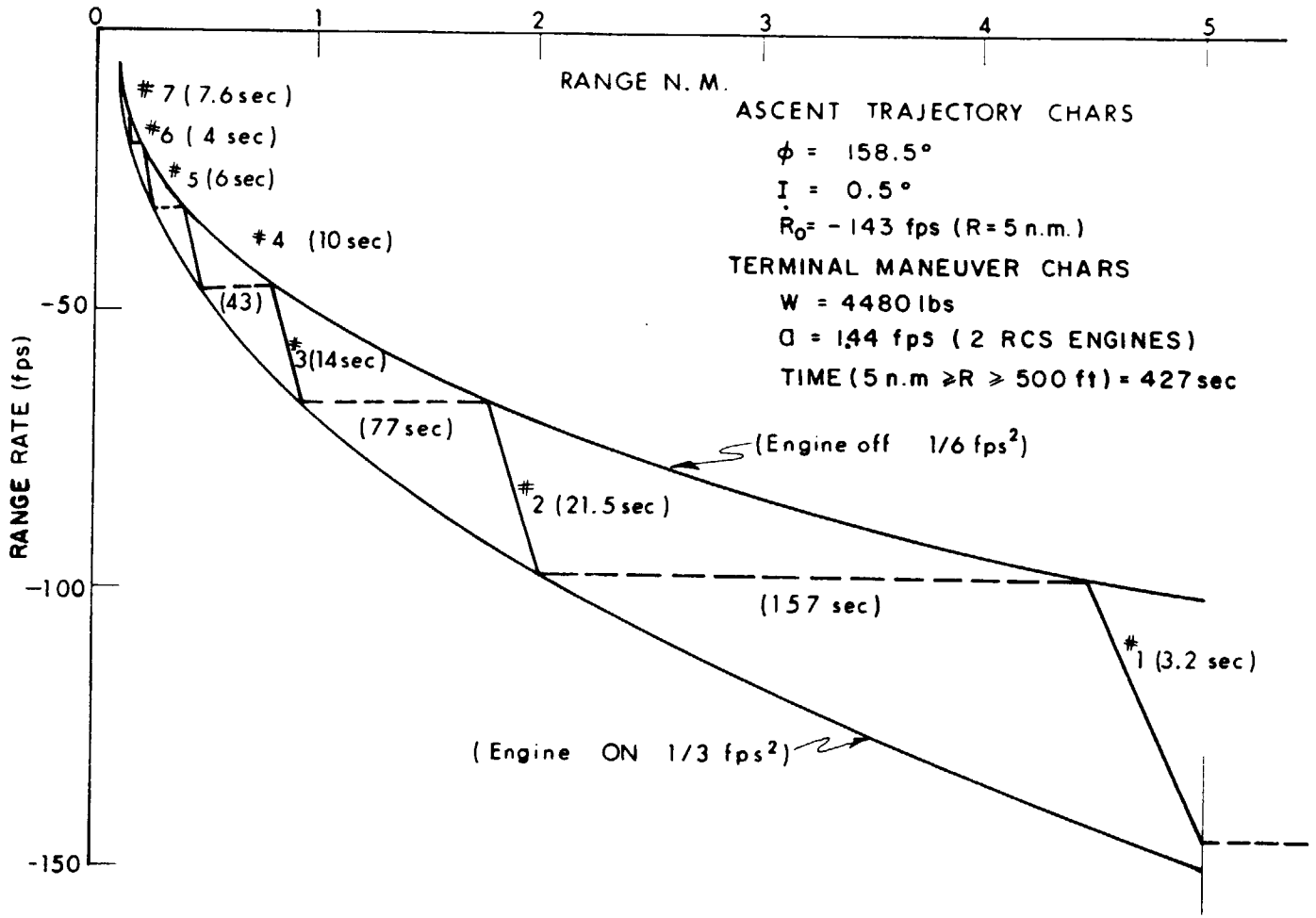

Fig. 7.44 LEM terminal rendezvous for parabolic R-$\dot{R}$ profile.

During the terminal rendezvous phase, the final aim point $\underline{R}_{CM}(t'_A)$ was shifted for each of the three thrust or velocity corrections. In this example, the aim point was shifted a total of 22.4 degrees from the initial midcourse aim point, and had the effect of lengthening the rendezvous by 459 seconds. The terminal miss or closest approach of the terminal maneuver in Fig. 7.43 was 41 feet, if the vehicles were allowed to close at 5 fps after the third and last thrust period.

An alternate terminal R-$\dot{R}$ criteria was listed in section 7.2.4.2 involving a parabolic or constant acceleration engine-on and engine-off criteria. An example of the terminal rendezvous phase using this criteria is shown in Fig. 7.44 for the same ascent trajectory and initial conditions of the example in Fig. 7.43. The engine-on and engine-off criteria was referenced to the desired docking conditions as follows:

$$\text{Engine off:} \quad \frac{(R + 5\ \text{fps})^2}{2(R - 500\ \text{ft})} = \frac{1}{6}\ \text{fps}^2$$

$$\text{Engine on:} \quad \frac{(R + 5\ \text{fps})^2}{2(R - 500)} = \frac{1}{3}\ \text{fps}^2$$

This criteria required seven velocity corrections for the terminal phase as shown in Fig. 7.44. In this example, the seventh or final thrust period was left on until the desired - 5 fps terminal velocity was achieved. The total time for the maneuver was four minutes shorter than that of Fig. 7.43. As mentioned in Section 7.4.2.4, there are many possible R-$\dot{R}$ criteria that could be used for the terminal rendezvous phase. At the present time, the R-$\dot{R}$ schedule of Fig. 7.43 is preferred over the parabolic R-$\dot{R}$ criteria of Fig. 7.44 in the primary G&N operation for the following reasons:

1) Longer coast periods for tracking and computation between velocity corrections, especially at short

ranges.

2) Fewer engine starts and aim point shifts.

3) A preselected thrust initiation schedule as a function of range which would enable astronaut monitoring regardless of initial velocity conditions. The velocity correction ΔV requirement is essentially the same for either $R-\dot{R}$ criterion.

An example of a terminal rendezvous maneuver with initial closing velocities greater than the RCS capability is illustrated in Fig. 7.45. These initial conditions ($\dot{R}_0 = -319$ fps) resulted from the ascent trajectory of Figs. 7.28 and 7.29 which was launched from 2.2 degree out of plane conditions. The same initial weight (4480) lbs) and RCS engine characteristics were assumed, as in the examples of Figs. 7.43 and 7.44,along with the $R-\dot{R}$ schedule requiring three terminal velocity corrections. Since the initial closing velocity at 5 nm exceeds the RCS capability, three cases are illustrated for the first thrust maneuver in Fig. 7.45.

In Case 1, the ascent engine (3500 pounds thrust, $I_{s_p} = 306$ seconds) reduced the closing velocity to the desired -100 fps level in a 8.9 second maneuver, Points A to C in Fig. 7.45. In this case, it was assumed that there was enough propellant in the ascent tanks to provide the 219 fps maneuver. The following two velocity corrections were then achieved by 2 RCS jets (+Z axis) after the vehicle was reoriented during the first 194 second coast interval (C to G).

In the second case of Fig. 7.45, the ascent engine reduced the initial closing velocity to -200 fps at Point B and was then shut off. The LEM was maintained in the same orientation (X axis essentially along the line of sight), and the four -X axis RCS jets were then used to reduce the closing velocity from -200 fps to the desired -100 fps level (B to D of Fig. 7.45). The final two velo-

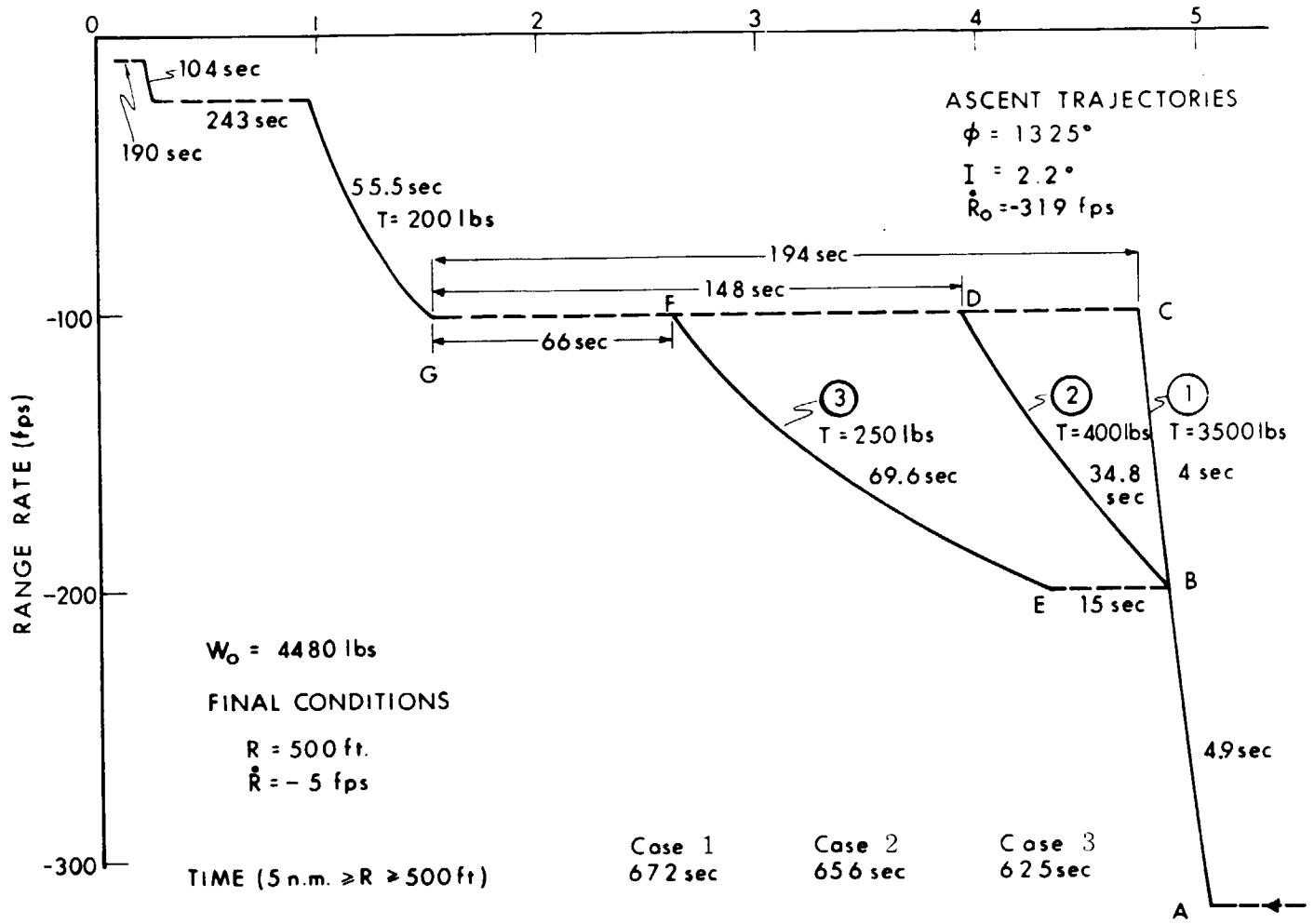

Fig. 7.45 LEM terminal rendezvous (R-$\dot{R}$ phase plane). Fixed R-$\dot{R}$ schedule method.

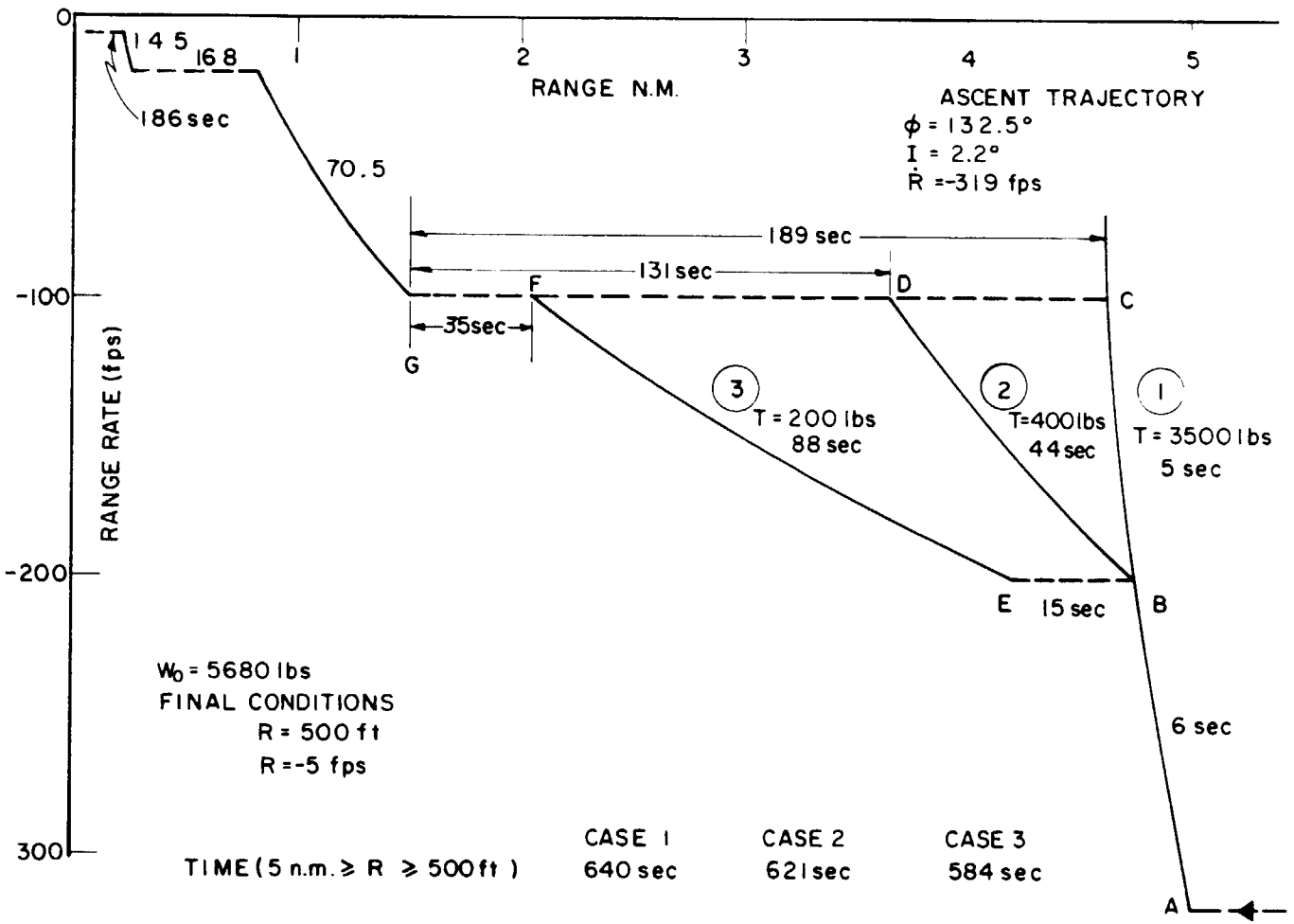

Fig. 7.46 LEM terminal rendezvous maneuver (R-$\dot{R}$ phase plane). High initial weight.

city corrections were again achieved with the two Z axis RCS jets as in Case 1.

The third case shown in Fig. 7.45 terminates the ascent engine when the -200 fps velocity condition is reached (Point B). The LEM was then reoriented 90 degrees during the 15 seconds coast interval (B to E) and the two Z axis RCS jets turned on to control the velocity to the desired -100 fps level (E to F). The final two velocity corrections were the same as in the previous cases.

As shown in Fig. 7.45, the major difference between these three cases is in the first thrust and coast periods. Case 1 resulted in an over-all maneuver that was 47 seconds longer than Case 3. In normal operation, when it is necessary to ignite the ascent engine for the first terminal phase velocity correction, it is desirable to maintain the ascent engine on until its propellant supply is used or shut off by the G&N system after the desired velocity has been achieved (Case 1). When insufficient ascent engine propellant is available to complete the first velocity correction, either Case 2 or 3 of Fig. 7.45 could be used depending upon time or monitoring requirements. In all cases, the final two velocity corrections would be controlled by the +Z axis RCS jets. The total time from injection to initiation of docking for the ascent trajectory of Fig. 7.28, and the Case 1 terminal phase profile of Fig. 7.45 was 51.4 minutes.

More recent estimates of the LEM ascent stage weight conditions at normal rendezvous are higher than that assumed in Fig. 7.45. An initial weight condition of 5680 pounds is shown in Fig. 7.46 for the same ascent trajectory of Fig. 7.45 and 7.28. The three cases of Fig. 7.45 are repeated for this weight condition and it can be seen by comparing these two figures that the major effect is a reduced overall terminal phase time for the 5680 weight condition. The heavier weight LEM requires longer thrust maneuvers with resulting shorter coast periods (especially

the first coast period of Case 3) for the same R-$\dot{R}$ schedule.

7.6.3 Docking and Operations Prior to Transearth Injection

Docking of the LEM and CSM has been assumed to be a completely manually controlled operation requiring no primary G&N operation other than achieving the desired initial conditions of a closing relative velocity of -5 fps at a separation range of 500 feet at the end of the terminal rendezvous phase.

After docking and crew transfer has been achieved, the CSM orbital navigation mode of operation described in Chapter 2 is continued to establish the initial conditions for the transearth injection phase.

7.7 CSM Monitoring Operation

Throughout the LEM midcourse and terminal rendezvous phases, the CSM will monitor the LEM trajectory and velocity corrections with its primary G&N system, which is essentially identical to that of LEM as indicated in Fig. 7.1. The two primary G&N systems will solve the same guidance problem independently, and monitor the results over the inter-vehicle communication or data link. This monitoring problem is currently under study and will be presented in a later report. If the LEM primary G&N system had failed, the CSM primary system would be the first level back-up during the rendezvous phase. Velocity correction commands could be relayed to the LEM over the communication link (Fig. 7.1), or the CSM could perform the retrieval or active rendezvous. If possible, it is desirable to perform the rendezvous maneuver with the LEM to conserve CSM propellant, but the CSM would always be prepared to perform the midcourse and terminal rendezvous maneuvers throughout the rendezvous phase from either ascent or abort injection conditions.

The CSM procedure for commanding LEM velocity corrections during rendezvous, in the event of LEM primary G&N failure, or active retrieval, in the event of LEM propulsion failure, is presented in Chapter 9.

CHAPTER 8

PRIMARY G&N CONTROLLED ABORT MANEUVERS

8.1 General Description

The abort maneuvers considered in this chapter result from conditions other than primary G&N failure between the injection into the descent orbit and the final hover and touchdown on the landing maneuver. Abort conditions which arise after the lunar landing maneuver has been completed result in guidance operation very similar to that described for normal launches and rendezvous in Chapters 6 and 7. Emergency launch considerations have already been discussed in Sections 5.2 and 6.2. In those sections the LEM was required to be injected into a parking orbit whether or not the CSM was within the line of sight tracking. In these cases, the phasing of the two vehicles must be modified by either waiting or changing one of the orbits such that line of sight tracking can be achieved. Once tracking has been established, both the normal rendezvous techniques described in Chapter 7 and aim point determination discussed in Section 8.2 are used for the completing of the abort maneuver. The abort conditions considered in this chapter, however, are restricted to the phases of the mission prior to the time when normal primary G&N system operation is terminated in the landing phase.

The objective of the primary G&N system for these abort cases is to establish a rendezvous trajectory as soon as possible that will result in near minimum time and ΔV requirements. This operation is sometimes referred to as a "quick abort" capability. This capability may be required in the case of life support system failure or extensive radiation. The primary G&N system uses the explicit guidance equations discussed in

Chapter 6 and also the rendezvous guidance technique discussed in Chapter 7 in order to achieve this objective. The abort maneuvers and trajectories considered in this chapter are limited to the LEM vehicle. The CSM will normally monitor the LEM operations as mentioned in Section 7.7. CSM active retrieval operations are described in Chapter 9. The following sections describe typical primary G&N performance for the LEM-powered and unpowered portions of the abort trajectories.

8.2 Abort Conditions Prior to the Landing Maneuver

This phase of operation includes the interval from injection into the descent orbit through the coast phase of the descent trajectory up to the ignition point for the powered landing maneuver. The type of abort operation in this interval is dependent upon the type of descent orbit used for the landing mission.

Aborts from equal period descent trajectories (covered in Section 3.2) are relatively simple since this type of descent orbit is chosen for its natural abort characteristics. If an abort condition arose between injection and perilune of such a trajectory, the powered landing maneuver would not be initiated and the LEM would be allowed to free fall to the intial injection point where a terminal rendezvous maneuver would be performed. Small midcourse corrections may be required in maneuvers of this type. These are dependent upon the injection errors and type of guidance used for the injection maneuver (as summarized in Section 3.2.4 and Fig. 3.10).

The Hohmann type descent trajectories (covered in Section 3.3) do not have the natural abort capability of the synchronous descents, and therefore require powered maneuvers in order to establish abort trajectories over the interval considered. If an abort condition occurred during the coast interval of the Hohmann descent, the primary G&N system would be required to:

1. Determine an appropriate aim point for the abort rendezvous;

2. Execute the powered maneuver in order to establish the rendezvous trajectory;

3. Provide midcourse correction on the rendezvous maneuver; and

4. Control the terminal rendezvous maneuver.

The aim point determination in abort cases of this type is achieved in the same manner as described in Section 5.4 with the logic network shown in both Fig. 8.1 and Fig. 5.6. The CSM and LEM position and velocity vectors are continually updated by the navigation technique, and these state vectors are then used in the network of Fig. 8.1 in order to determine an appropriate aim point based on ΔV and perilune requirements. This operation is identical to that previously described in Chapter 5 with the exception that a single near optimum ΔV point is determined within the perilune criteria by the search or iteration technique represented by the vertical lines in Fig. 5.7. Horizontal or phase angle iteration in order to determine launch interval is not used in this case. Once the aim point and time of arrival on CSM orbit has been determined, the explicit guidance technique described in Section 6.2 is used in order to control the first powered maneuver of the abort trajectory. Typical trajectories for various abort points separated by about 10 minutes along the Hohmann descent trajectory are summarized in Fig. 8.2. In this figure, the LEM is injected on the Hohmann descent at Point A and a condition requiring a quick abort, illustrated by Point B, occurred at some interval between Point A and the perilune P. The resulting abort trajectory central angle, ϕ_2, required injection velocity, ΔV_1, and terminal rendezvous velocity, ΔV_2, are summarized in this figure. It might be noted that the phasing between the two vehicles during the interval A to P of Fig. 8.2 is increasing in such a direction that it makes immediate abort action preferable to waiting for some later time in the descent trajectory, as illustrated in the table of Fig. 8.2.

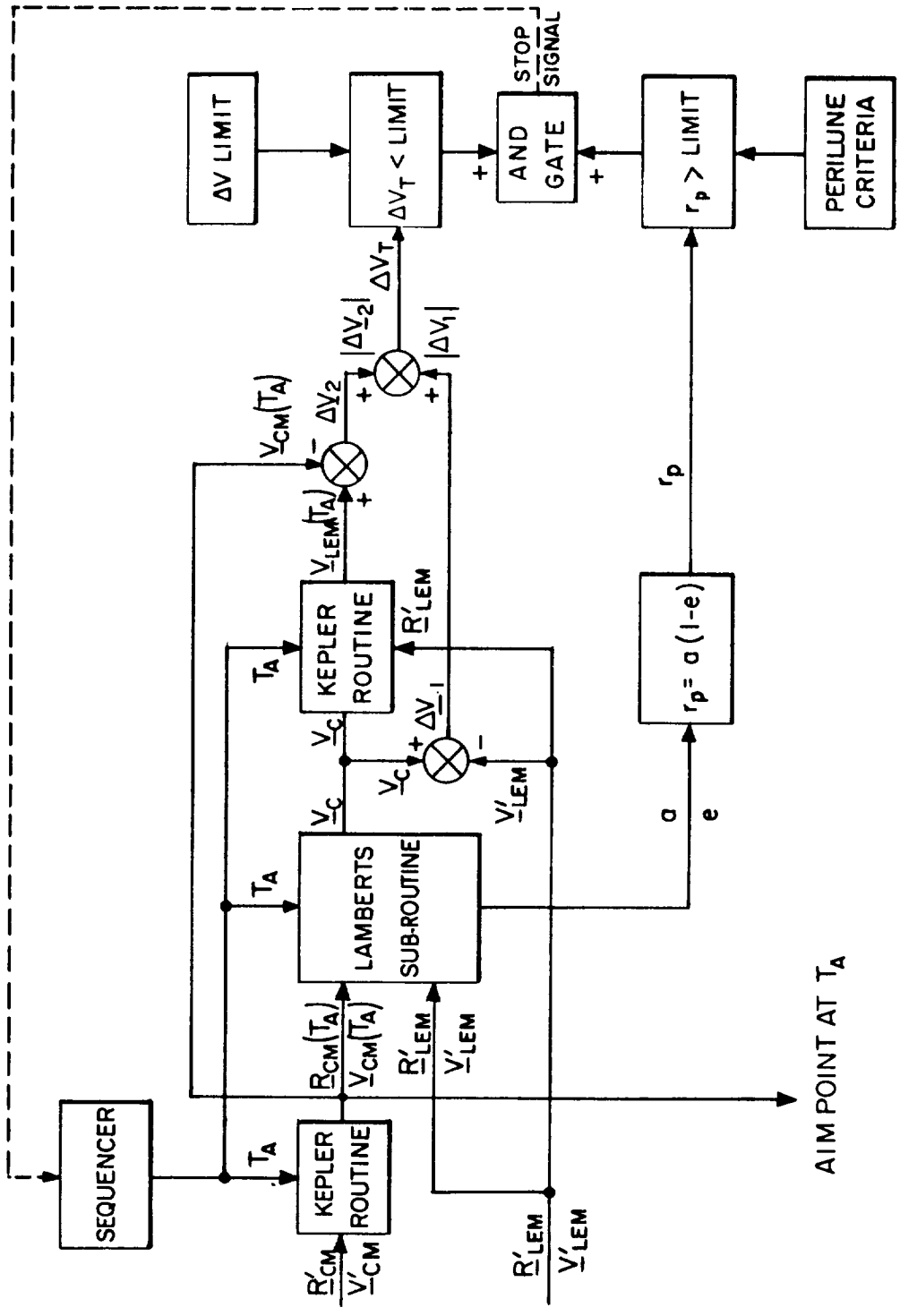

Fig. 8.1 Aim point determination.

The primary G&N operation listed above is carried out on the LEM vehicle and the CSM vehicle. Aim point determination will be checked and verified over the intervehicle communication link, and after the LEM has been injected on rendezvous trajectory, both vehicles will perform the midcourse correction computation described in Sections 7.2 and 7.5. Terminal rendezvous, ΔV_2 of Fig. 8.2, will be achieved by the LEM as described in Section 7.6. Active CSM retrieval cases are described in Chapter 9.

8.3 Aborts During Landing Maneuvers for Hohmann Descents

8.3.1 Typical Powered Abort Maneuvers

General rendezvous trajectories for aborts from a landing maneuver similar to that described in Section 4.3 are summarized in Fig. 8.3. In this figure, the LEM is injected into a Hohmann descent trajectory at Point C and initiates a powered landing maneuver at Point P. Referencing time zero as the initiation of the landing maneuver at Point P, the table of Fig. 8.3 summarizes the required injection velocity, V_{CO}, the free fall central angle, ϕ, the terminal rendezvous impulsive velocity, ΔV_2, and the perilune of the abort rendezvous trajectory for various abort times during the landing maneuver. The abort time of 519 seconds in this figure represents an abort condition after 60 seconds of hover for the landing maneuver. The terminal rendezvous points on the CSM orbit, resulting from aborts during the landing maneuver, are illustrated by the abort rendezvous sector in Fig. 8.3. It was assumed that these abort trajectories were coplanar with the CSM orbit, and that the burnout altitude of the powered abort maneuver was at 50,000 feet with a minimum perilune altitude criterion of 30,000 feet.

The general characteristics of the landing and powered abort maneuvers with the relative phasing of the two vehicles are illustrated in Fig. 8.4. With reference to this figure, the CSM is behind the ignition point of the landing maneuver ($t = 0$) by an angle of 9.4°.

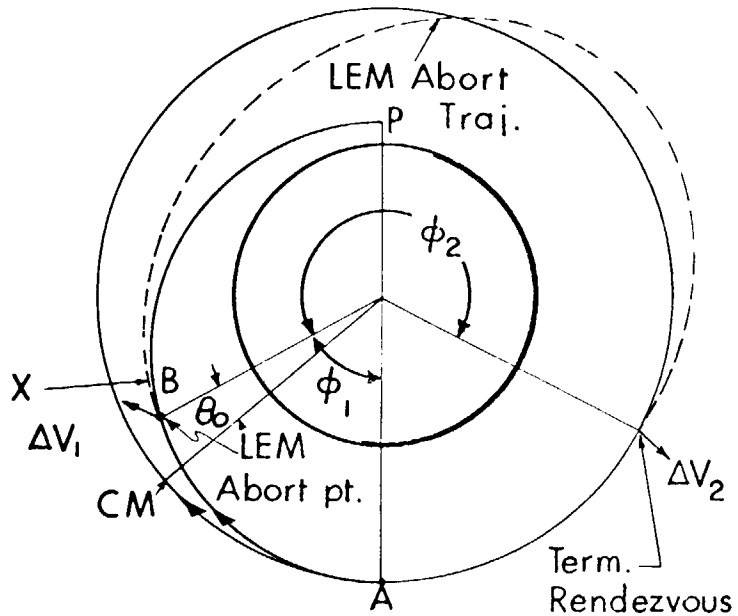

ϕ_1 (deg)	θ_o (deg)	ϕ_2 (deg)	ΔV_1 (fps)	ΔV_2 (fps)	h_{per} (n.m.)
28.9	-0.45	292	124	22	74.1
58.4	-0.37	295	145	94	58.8
88.9	0.68	298	119	207	37.1
120.5	2.9	287	104	293	21.1
153.3	6.3	275	96	354	11.1
175.5	8.9	265	98	377	8.3

Fig. 8.2 LEM abort trajectories prior to lunar landing.

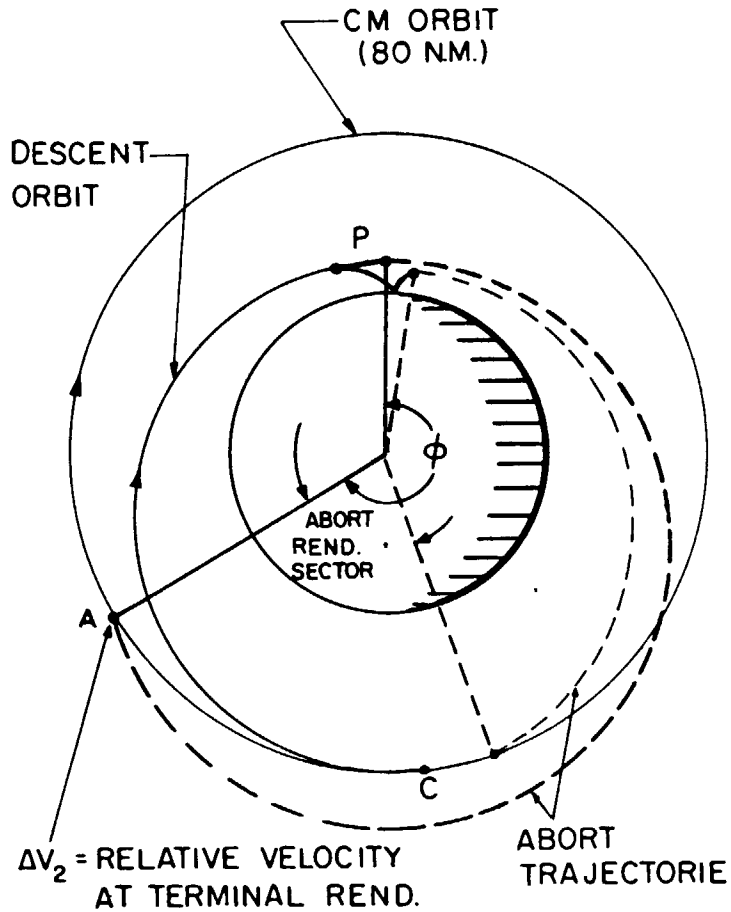

GENERAL RESTRICTIONS

I = 0

h_{co} = 50,000 FT

MIN. h_{per} = 30,000 FT

ABORT TIME (SEC)	ϕ (DEG)	REQUIRED V_{co} (fps)	ΔV_2 (fps)	h_{per} (NM)
0	245	5664	374	5.2
100	250	5670	382	5.9
300	233	5630	294	5.8
459	157	5577	101	5.8
519	191	5580	98	7.7

Fig. 8.3 General abort trajectories during landing maneuvers initiated from a Hohmann descent trajectory.

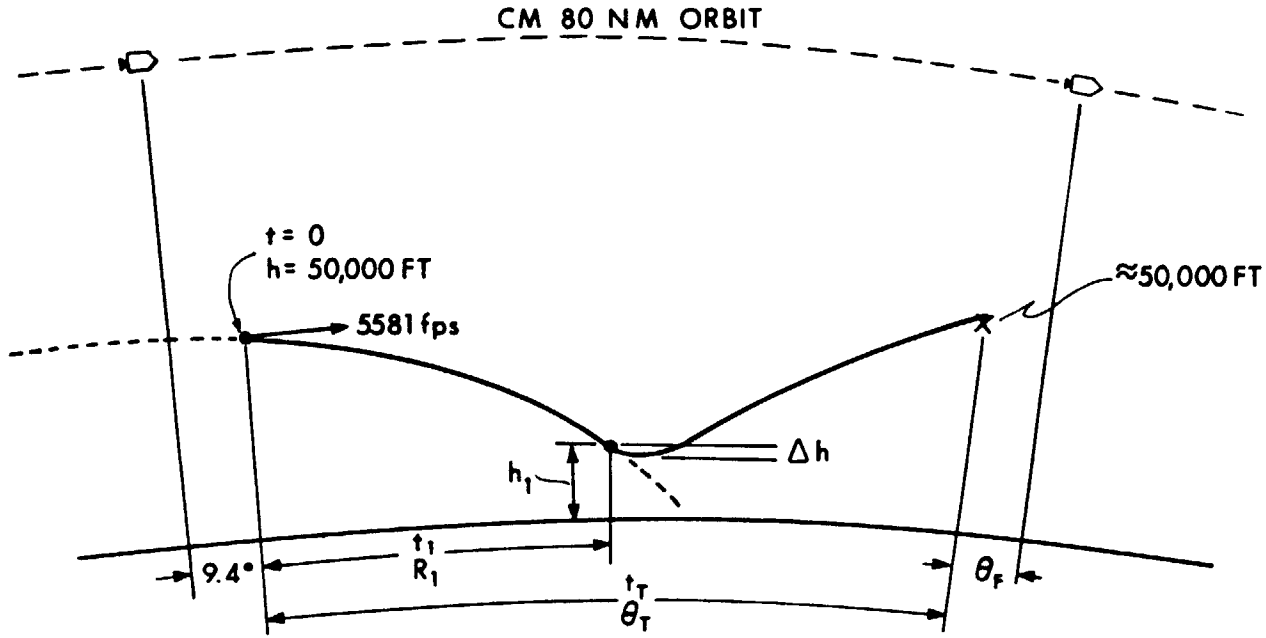

	CASE	t_1 (SEC)	R_1 (NM)	h_1 (FT)	Δh (FT)	θ_T (DEG)	t_T (SEC)	θ_F (DEG)
1	AT PERILUNE	0	0	50,000	0	0.6	11	-9.5
2	DURING DESCENT	150	132	43,200	850	15.1	304	-9.64
3	DURING DESCENT	300	205	19,880	4000	21.7	585	-2.43
4	AT LANDING SITE	459	226	200	0	22.2	810	+8.04
5	AFTER 60 SEC HOVER	519	226	200	0	22.1	870	+10.76

Note: 1. 10 deg/sec Max. LEM attitude rate.
2. LEM staged at abort.

Fig. 8.4 Abort injection conditions (Hohmann descent trajectory).

The cases illustrated in Fig. 8.4 cover typical aborts at times varying from perilune or ignition to a 60 second hover condition. The time t_1 listed in this figure is the point in the landing maneuver at which the abort was initiated at a distance R_1 from the ignition point and at an altitude of h_1. In this figure, it was assumed that the descent stage of the LEM vehicle was staged at the abort time. The primary G&N system controls the landing maneuver phase prior to abort by the explicit equations presented in Section 4.2, and then guides the abort powered maneuver by similar explicit equations presented in Section 6.2. The Δh column of Fig. 8.4 summarizes the altitude loss from the abort point altitude in the landing maneuver when the abort maneuver is controlled by these guidance equations. The following vehicle assumptions are made:

1. No intentional vertical thrust or rise interval is programmed by the guidance equations;
2. The maximum attitude rate of the LEM vehicle is limited to 10 degrees per second;
3. Ascent engine thrust is constant at 3500 pounds (I_{sp} = 306 seconds);
4. Initial ascent stage weight = 8835 pounds.

The total time for the landing and abort-powered maneuvers with the separation angle between the two vehicles at injection on the abort trajectory are summarized in the last two columns in Fig. 8.4. The phase conditions θ_f (a negative sign indicating that the CSM is behind the LEM) result in the abort trajectory sectors illustrated in Fig. 8.3.

8.3.2 Aim Point Determination for Abort Trajectories

The explicit guidance equations for the powered ascent portion of the abort trajectory require the LEM position and velocity vectors and an aim point and time of arrival on the CSM orbit as inputs. It is unknown at the present time if there

will be sufficient computing time during powered phases of the landing and abort trajectories in order to perform the iterative aim point determination computation described in Sections 5.4 and 8.2. A dynamic simulation of the LEM vehicle and LGC is currently being conducted in order to determine the explicit guidance equation cycle time requirements and available computation time during the powered phases of the LEM mission. Assuming that insufficient computation time for aim point determination will exist during the powered maneuvers, an alternate precomputed aim point scheme can be used. Any precomputed aim point technique is complicated by the fact that abort maneuvers during the landing phase can be controlled by either the descent stage, the ascent stage, or some combination. These alternatives result in a wide range of possible acceleration profiles. A relatively simple predetermined aim point scheme could be developed by the following procedure.

Prior to the initiation of the powered landing maneuver, a series of abort times on a reference landing trajectory could be chosen and, estimated abort trajectories determined from these points, assuming that the LEM was staged at the abort point. Under this assumption, the powered abort trajectory would have a reasonably well known acceleration profile which would cover approximately the same central angle and require the same time as the landing maneuver to the abort point in question. From these injection conditions, the relative phasing between the two vehicles could be estimated, and an abort trajectory determined that would be optimized for the maximum perilune altitude. Each abort trajectory would have a terminal rendezvous point on the CSM orbit under these assumptions that could be represented by a time, or time of arrival, on the CSM orbit. A polynomial could then be generated to approximate these times of arrival. These times represent aim points on the CSM orbit as a function of abort times during the landing maneuver. As previously mentioned, this operation would be completed before the LEM initiated the landing maneuver and the time of arrival polynomial stored in the LGC.

If an abort condition occurs during the landing maneuver, the primary G&N system will command the descent engine throttle

to its maximum setting and set the thrust vector at a preselected attitude such as 45 degrees above the horizontal in the direction of the trajectory. During the interval that the LEM is being re-oriented to this new position (10 to 12 seconds for the maximum attiude rate assumed) the LGC interrogates the time of arrival polynomial and then advances the CSM position vector by this time on the basis of its stored ephemeris. By the time the LEM approaches the preselected thrust attitude, the explicit guidance equations have had an opportunity to cycle sufficient times using this aim point that they can direct the thrust attitude of the LEM for injection on an abort trajectory. It might be noted that the chief requirement of this initial powered abort maneuver is to inject the LEM on a safe ascent trajectory that comes as close as possible to the preselected aim point. After injection, the aim point could always be modified or changed during the free fall phase of the midcourse rendezvous phase by the aim point determination technique previously described in Sections 5.4 and 8.2.

The effects of either staging or not staging the LEM vehicle using this preselected aim point procedure are summarized in Figs. 8.5 and 8.6. In Fig. 8.5,the powered landing and abort maneuvers are summarized along with vehicle phasing and injection for two cases. The first case (indicated by the asterisk at the abort time) represents the condition when the descent stage is staged at the abort time and the powered abort trajectory completely controlled by the ascent engine. This is the case for which the precomputed aim point determination is made. The second case illustrated in Fig. 8.5 represents the condition when the descent stage is used to control as much of the powered abort maneuver as possible. The time at which the descent stage is jettisoned is listed in column three of Fig. 8.5 with time referenced to the initiation of the landing maneuver at t = 0. It can be seen in this figure that the descent stage can completely control the powered abort maneuver for an abort initiated prior to 250 seconds

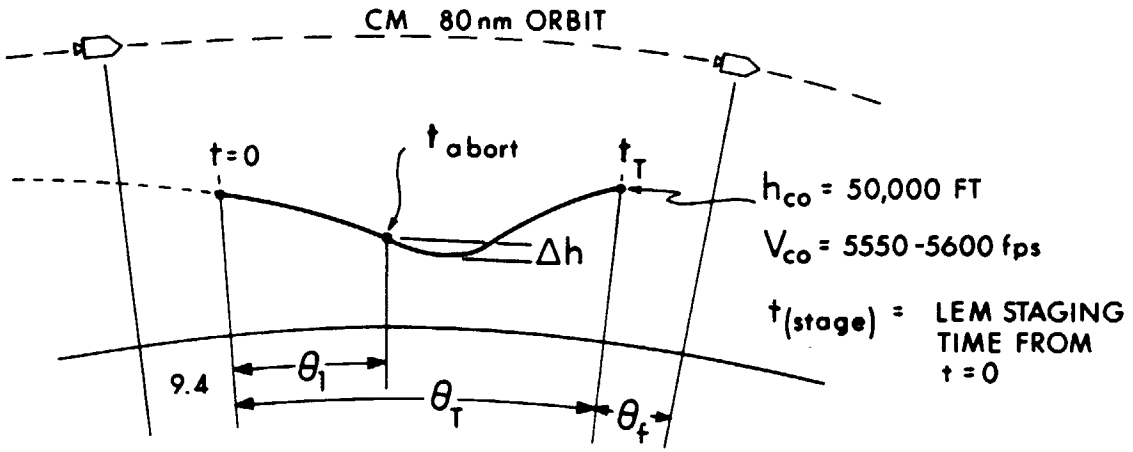

CASE	t(abort) (sec)	θ1 (deg)	t(stage) (sec)	tT (sec)	Δh (ft)	θT (deg)	θf (deg)
ABORT DURING DESCENT PHASE 1	150*	8.1	150	304	850	15.1	-9.64
	150	8.1	–	292	770	14.6	-9.71
ABORT DURING DESCENT PHASE 1	250*	11.6	250	494	3200	20.7	-5.95
	250	11.6	–	444	2100	18.8	-6.57
ABORT DURING PHASE 2	354*	13.4	354	678	3100	22.4	+1.3
	354	13.4	548	600	1300	21.1	-1.17
ABORT AT HOVER POINT	459*	13.8	459	810	0	22.2	+8.04
	459	13.8	603	762	0	22.9	+4.9

*LEM staged at t(abort)

Fig. 8.5 LEM staging effects during abort maneuvers - Hohmann descent trajectory.

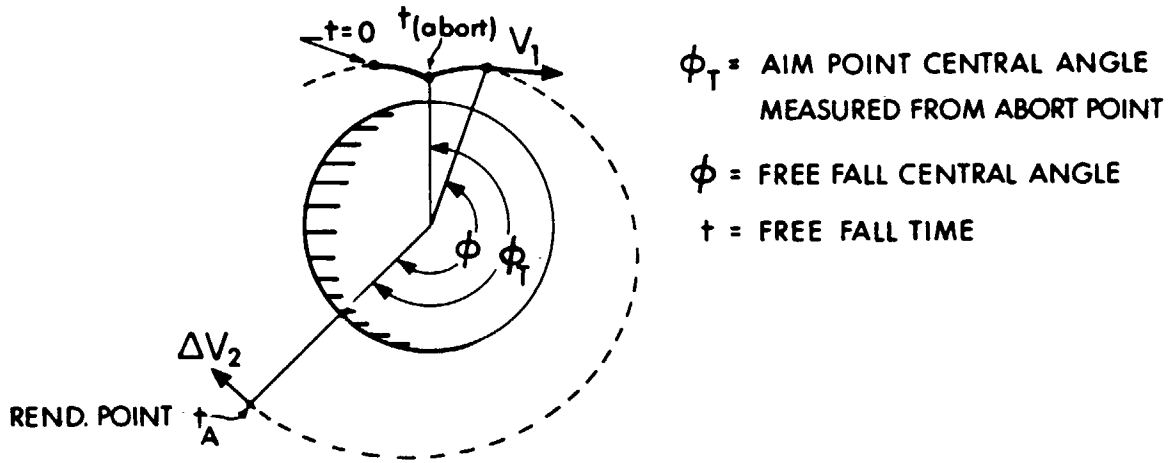

$t_{(abort)}$ (sec)	t_A (sec)	ϕ_T (deg)	ϕ (deg)	$\delta\phi$ (deg)	t (sec)	δt (sec)	V_1 (fps)	ΔV_2 (fps)	h_{per} (ft)
150*	5917	272	265	0.5	5613	12	5676	384	49 650
150	"	"	265.5		5625		5677	384	49750
250*	5906	268	258.5	L9	5412	50	5660	348	49300
250	"	"	260.4		5462		5663	355	49600
354*	5480	246	236.8	1.2	4802	82	5618	246	48670
354	"	"	238.0		4880		5628	275	45350
459*	4897	215	206.9	-0.7	4088	48	5589	145	48920
459	"	"	206.2		4136		5596	187	36650

*LEM staged at $t_{(abort)}$

Fig. 8.6 Abort trajectories for various LEM staging conditions - Hohmann descent trajectory.

along the landing maneuver. The assumptions made in this simulation are identical to those previously listed in Section 8.3.1 with the following additions:

1. Descent engine is shut off and the stage jettisoned immediately, (no time delay) when the LEM weight reaches 11,000 pounds.

2. During the powered abort maneuver using the descent engine, the thrust is set at 10,500 pounds (I_{sp} = 301 sec).

Further simulation results not tabulated in Fig. 8.5 indicate that the descent stage can control abort maneuvers initiated up to 300 seconds along the landing maneuver from the Hohmann descent under these assumptions. This implies that the descent stage could be used in cases where the abort is not due to this engine in order to control aborts over most of the first phase of the landing maneuver, as illustrated in the first two cases listed in Fig. 8.5. With reference to these cases, it can be seen that the phasing of the two vehicles at injection does not vary over one degree between the staged and unstaged cases. The third and fourth cases listed in Fig. 8.5 illustrate the effects of staging the descent stage during the powered abort maneuver. In the abort during Phase 2, the descent stage was used for 194 seconds after the abort point or 548 seconds after initiation of the landing maneuver. The final case listed in Fig. 8.5 involved an abort at the hover point and used the descent stage for an additional 144 seconds of the abort maneuver. Referring to the last two cases of Fig. 8.5, it can be seen that the phasing angle at injection is larger than in earlier abort cases due to staging effects.

Figure 8.6 summarizes the difference between the staged and unstaged powered abort maneuvers when the predetermined aim point technique as described above is used to control the abort maneuver. The time of arrival t_A in the second column of this figure is the output of the polynomial generated prior to the landing maneuver. The central angle of the powered and free fall trajectory is listed under column, ϕ, while the free fall

trajectory central angle is compared under column $\delta\phi$. With reference to this column, it can be seen that the free fall trajectory for those cases in which the LEM was not staged at the abort point covered greater central angles in all cases except that of the hover condition. The free fall time from injection to terminal rendezvous is listed under column t with the difference shown in column δt. Comparing the cases summarized in Fig. 8.6, it can be seen that the case in which the descent stage was used to its capacity in the powered abort always resulted in greater free fall times in order to cover the generally larger free fall central angle. Column V_1 of this figure summarizes the injection velocities required in all cases for achieving the predetermined aim point conditions. It can be seen that there is a small difference in injection velocity magnitude for the cases considered. The terminal rendezvous initial closing velocity conditions for these trajectories are listed in column ΔV_2. The two most important factors in evaluating the predetermined aim point technique are the total ΔV required, $V_1 + \Delta V_2$, and the perilune altitude of the ascent trajectory. Comparing the cases listed in Fig. 8.6, it can be seen that in those cases in which the descent stage was used to its capacity, more total ΔV was required than the case in which the descent stage was jettisoned at the abort time. This is to be expected since the aim points were determined for this latter case, and the additional ΔV requirement for the condition using the descent stage is more than compensated for by the additional ΔV capability maintained by using this stage to its capacity. The perilune altitudes summarized in the last column of Fig. 8.6 indicate that the predetermined aim point technique results in ascent trajectories with adequate perilune conditions, but the minimum criterion is being approached for the abort cases late in the landing maneuver, specifically at the hover point.

The predetermined aim point technique illustrated in this section is one of several possible approaches to the primary G&N operation during the powered abort maneuvers. Final deter-

mination of the approach taken will be made by the expanded simulations currently being conducted.

It might be noted that in the predetermined abort aim point procedure described above, the time of arrival polynomial can only be carried to a point in time at which acceptable injection phasing angles and resulting perilunes exist. After this time, the LEM is forced into a parking orbit operation if an abort is required. This condition will normally only exist after the LEM has landed, but the primary G&N system is kept active in order to control aborts during the next 15 to 30 minutes (see Section 5.2). In this case the emergency launch to parking orbit guidance (see Section 6.2) is used when the limit of the time of arrival polynomial is reached.

The operating margin for the predetermined abort aim point concept described above could be further increased if during aborts using the descent stage the descent engine throttle were always set at a level that approximates the acceleration of ascent stage operation. This abort procedure has not been assumed in the primary G&N analysis, but would result in similar acceleration profiles during abort maneuvers controlled by either stage and also reduce the trajectory differences listed in Fig. 8.6.

8.3.3 Primary G&N Performance

Figures 8.7 through 8.10 summarize error volumes at the injection point for various landing and abort maneuvers. These error volumes were generated by propagating the convariance matrix from the perilune or landing maneuver ignition point (Fig. 3.28) through the powered landing and abort maneuvers to the injection point. The IMU instrument uncertainty was then added to this covariance matrix in order to generate the error volumes shown in the figures. It might be noted that in comparing the error volumes in Fig. 8.10, resulting from a landing and an abort maneuver initiated after 60 seconds of hover, with the error volume for a nominal ascent as shown in Fig. 6.19, the velocity

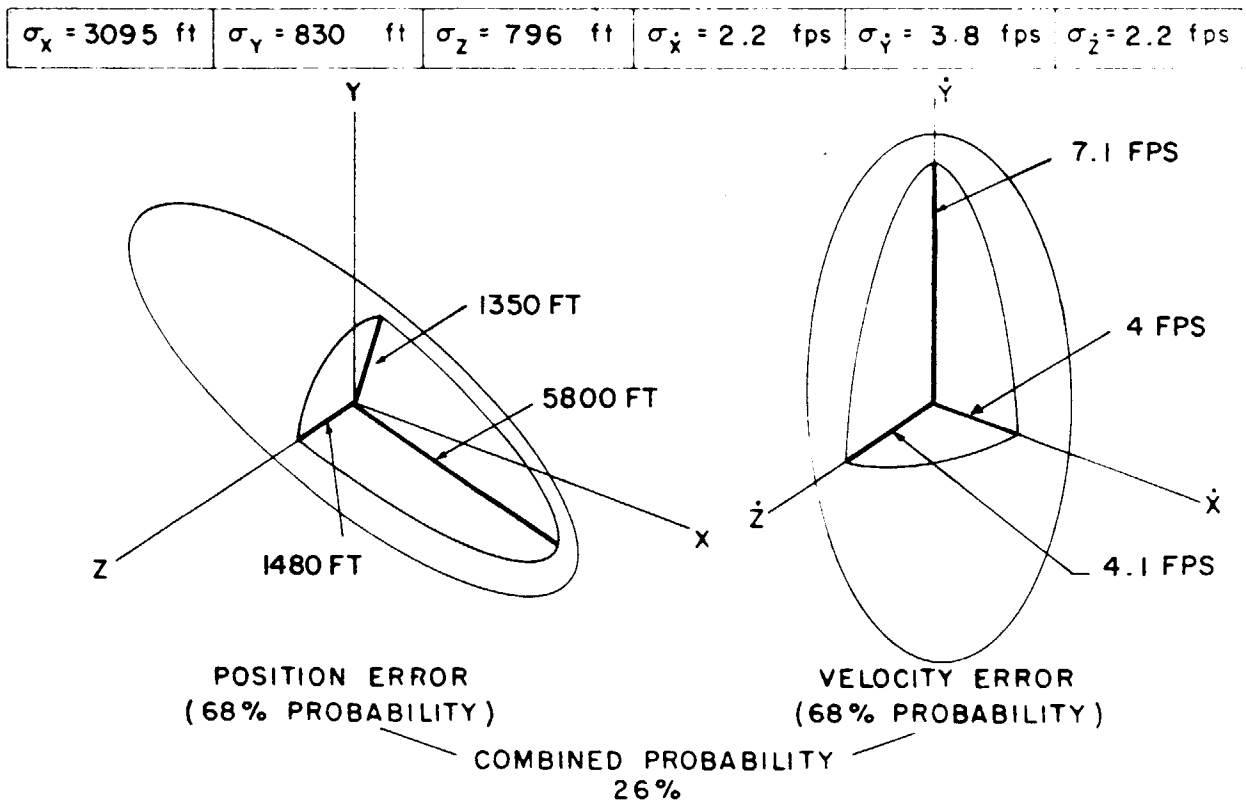

Fig. 8.7 Error volume at burnout of abort initiated at 150 seconds in landing trajectory following Hohmann descent.

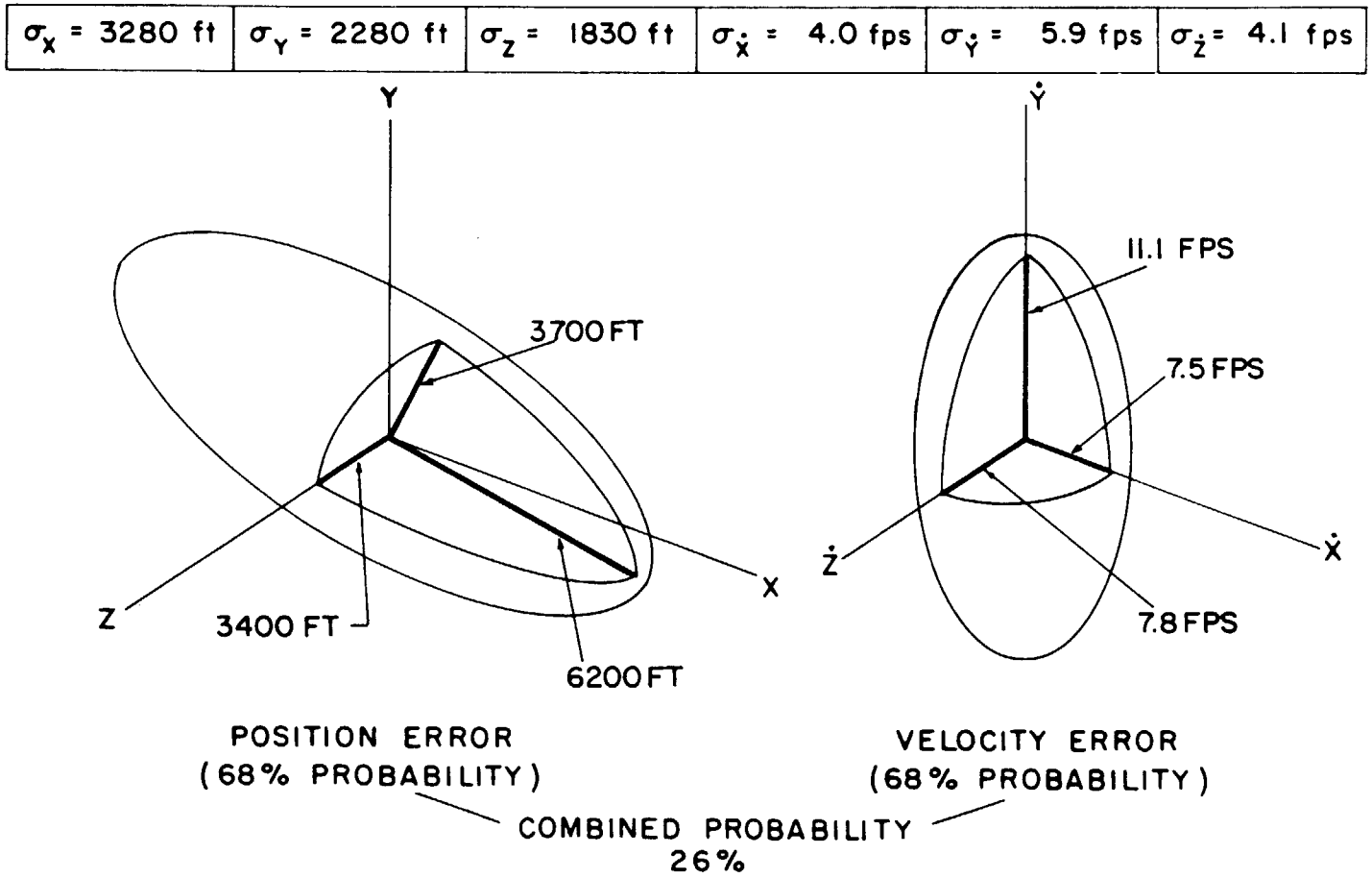

Fig. 8.8 Error volume at burnout of abort at 300 seconds in landing trajectory following Hohmann descent.

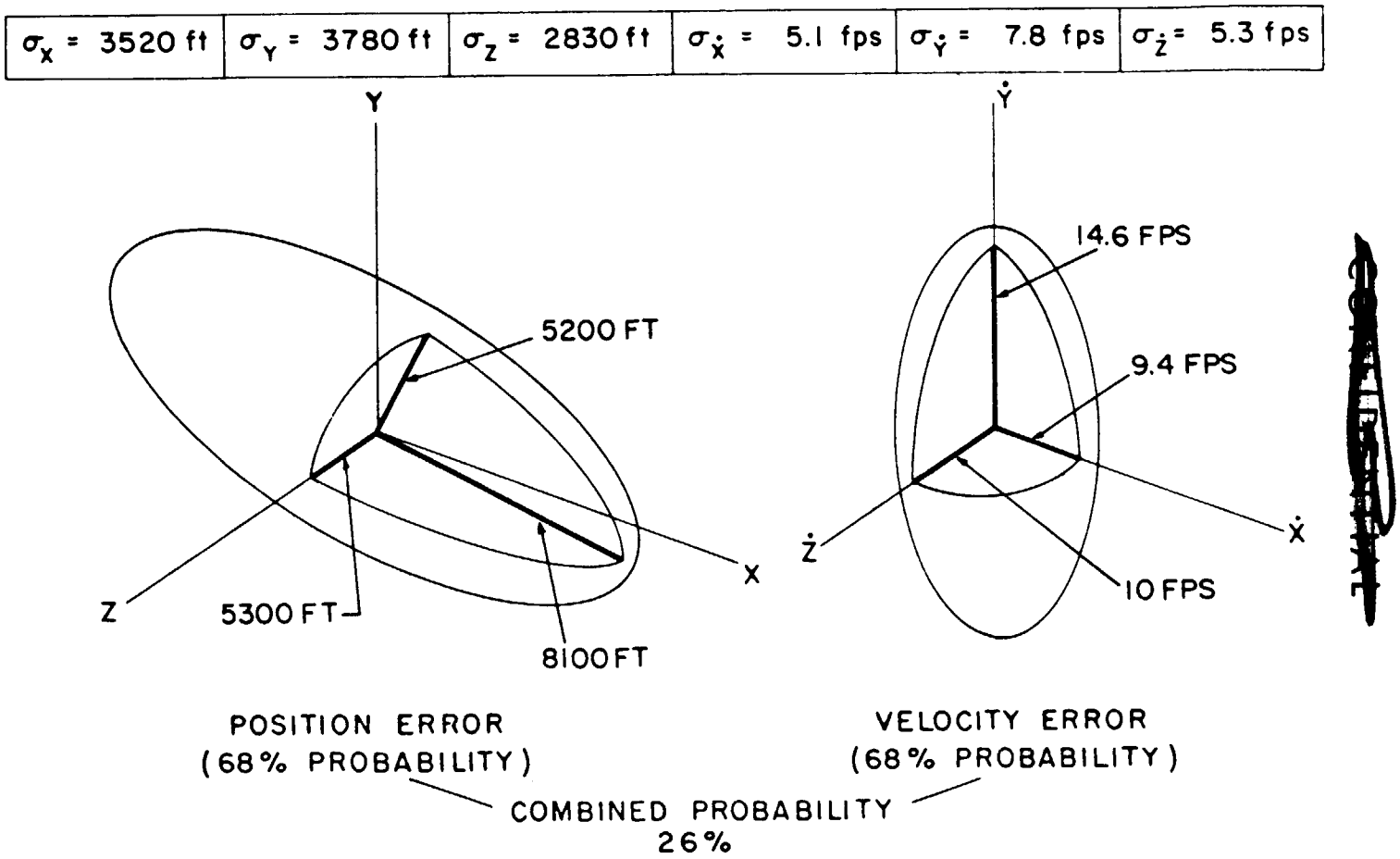

Fig. 8.9 Error volume at burnout of abort from hover point following Hohmann descent.

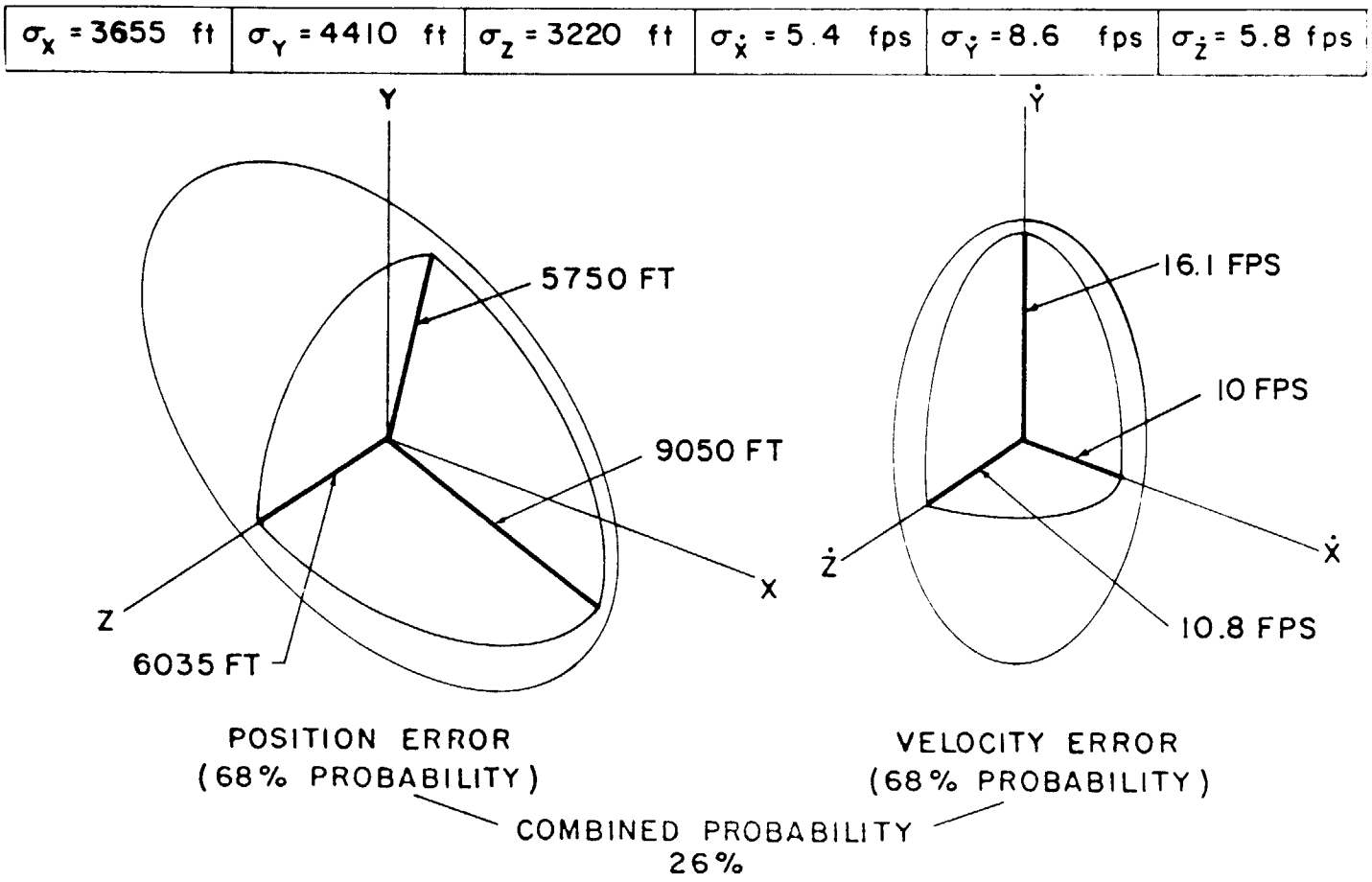

Fig. 8.10 Error volume at burnout of abort after 60 seconds of hover following Hohmann descent

and position components of the abort injection are only slightly larger than those of the ascent injection. This is true even though the powered trajectory of the landing abort maneuver was more than twice the time of the ascent trajectory. This condition arises from the fact that the major error source in the ascent trajectory is due to IMU misalignment at launch initiation as illustrated in Fig. 6.18. In the case of the abort maneuver, the alignment effects tend to cancel since the thrust acceleration profile during the powered abort phase is almost directly opposite to that of the powered landing phase preceding it. This fact thus tends to cancel misalignment effects. The injection uncertainties shown in Fig. 8.10 are primarily due to acceleration bias errors for that portion of the total covariance matrix contributing to IMU performance. A similar effect is illustrated in comparing the abort injection error volume of Fig. 8.8 with that of the landing maneuver error volume from which the abort trajectory initiated in Fig. 4.25. In this comparison, the velocity components $\dot{Y}$ and $\dot{Z}$ are essentially equal, but the $\dot{X}$ component for the abort trajectory is approximately twice that of the landing maneuver, thus indicating that for the abort cases the accelerometer bias effects are becoming dominant over misalignment effects.

The unpowered ascent trajectories after abort injection along with the associated midcourse rendezvous guidance performance for injection of uncertainties similar to those presented in Figs. 8.7 through 8.10 are illustrated in Section 8.5.

8.4 Aborts During Landing Maneuvers from Equal Period Descents

8.4.1 Typical Powered Abort Maneuvers.

Figure 8.11 illustrates the general trajectory characteristics for abort maneuvers during the powered landing phase initiated from an equal period type descent orbit. In this figure, the LEM is injected on synchronous orbit at Point A, and returns to this point for a rendezvous condition if the descent engine is not ignited at Point P. The table of Fig. 8.11 summarizes the general

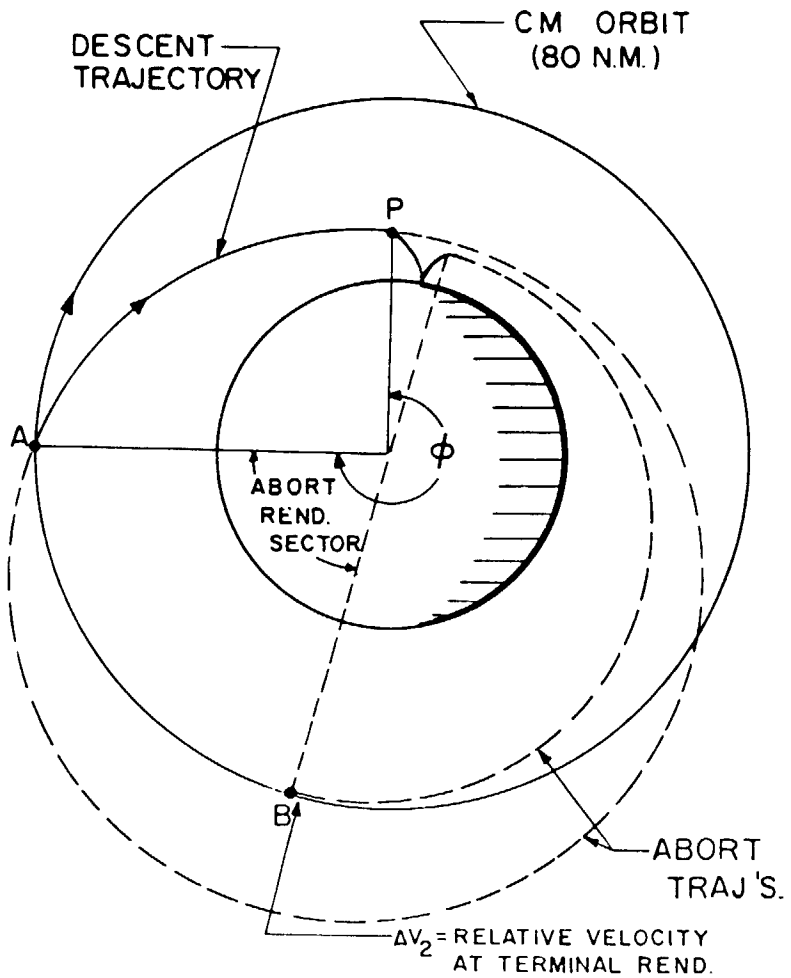

GENERAL RESTRICTIONS

I = 0

h_{co} = 60,000 FT

MIN. h_{per} = 30,000 FT

ABORT TIME (SEC)	ϕ (DEG)	REQUIRED V_{co} (fps)	ΔV_2 (fps)	h_{per} (NM)
0*	266	5671	373	8.3
150	238	5642	342	5.9
300	211	5598	230	5.7
447	191	5572	97	9.0
507	213	5566	103	4.3

*Equilperiod return from 50,000 ft.

Fig. 8.11 General abort trajectories from equal period descent orbit.

trajectory characteristics for aborts initiated during the powered landing maneuver which required 447 seconds to achieve a hover condition. The 507 second abort case of Fig. 8.11 is the 60 second hover condition. With reference to Fig. 8.11, it can be seen that the abort rendezvous sector from this type of landing maneuver ranges from 270 to 180 degrees (Points A to B) measured from the ignition point P of the landing maneuver. The abort injection altitude for the cases summarized in Fig. 8.11 was 60,000 feet, with a minimum perilune condition criterion of 30,000 feet.

The general characteristics and phasing between the two vehicles during the landing and powered abort from the equal period landing conditions are summarized in Fig. 8.12. Results of this figure are very similar to those for the Hohmann landing case of Fig. 8.4. The major difference in the phasing between these two maneuvers is the position of the CSM at the start of the powered landing maneuver: 9.4 degrees behind the LEM in the Hohmann case, and 8.1 degrees in the equal period case. The phasing between the two vehicles at abort injection is summarized in the last column of Fig. 8.12 for the equal period landing and abort cases. The resulting trajectories from these initial injection conditions are similar to those for the Hohmann landing and abort conditions as can be seen by comparing Figs. 8.11 and 8.3.

8.4.2 Primary G&N Performance.

Figures 8.13 through 8.16 summarize the injection error volumes for abort maneuvers initiated during a landing maneuver from equal period descent conditions. These error volumes are for orbital navigation Model #1 and the covariance matrix from which the perilune error volumes of Fig. 3.25 were generated. When compared with ascent and landing trajectory error volumes, the same effects described in Section 8.3.3 for the Hohmann landing and abort injection cases apply for those error volumes of Figs. 8.13 through 8.16.

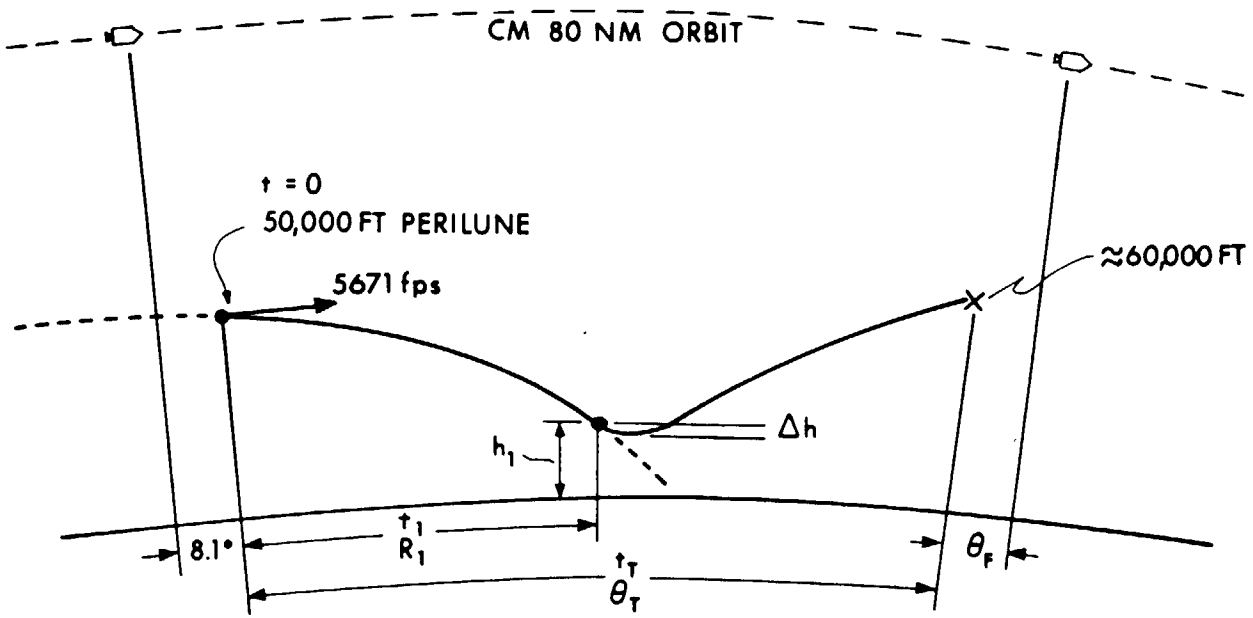

	CASE	t_1 (SEC)	R_1 (NM)	h_1 (FT)	Δh (FT)	θ_T (DEG)	t_T (SEC)	θ_F (DEG)
1	AT PERILUNE	0	0	50,000	0	0	0	-8.1
2	DURING DESCENT	150	116	42,174	1015	14.2	306	-7.0
3	DURING DESCENT	300	180	17,537	4207	20.2	596	+1.1
4	AT LANDING SITE	447	193	200	0	20.0	800	+10.9
5	AFTER 60 SEC HOVER	507	193	200	0	20.0	860	+13.9

Note: 1. 10 deg/sec Max. LEM attitude rate.
2. LEM staged at abort.

Fig. 8.12 Abort injection conditions (equal period descent trajectory).

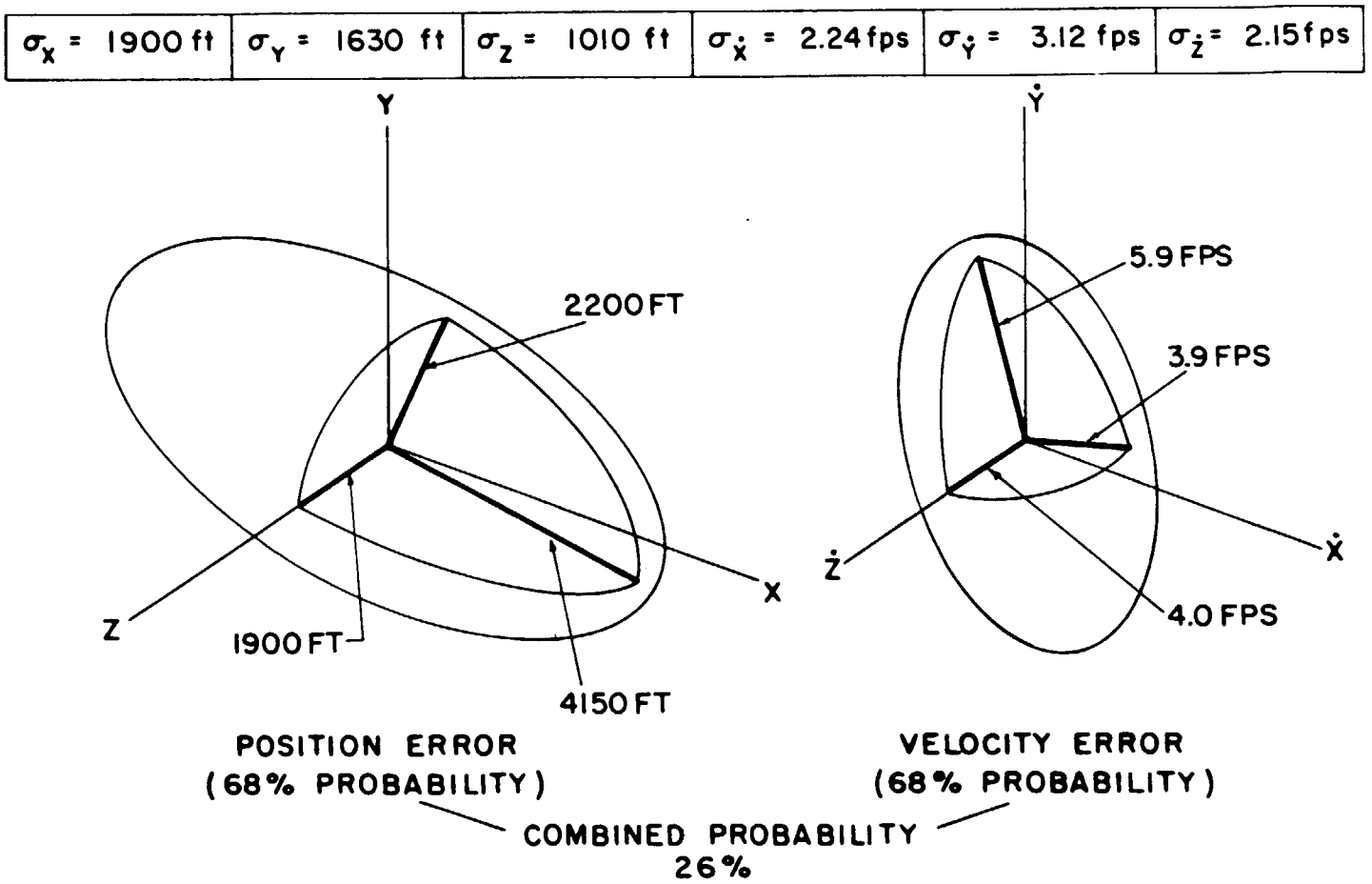

Fig. 8.13 Model 1 landing and abort trajectory. Error volume at burnout of abort from 150 seconds.

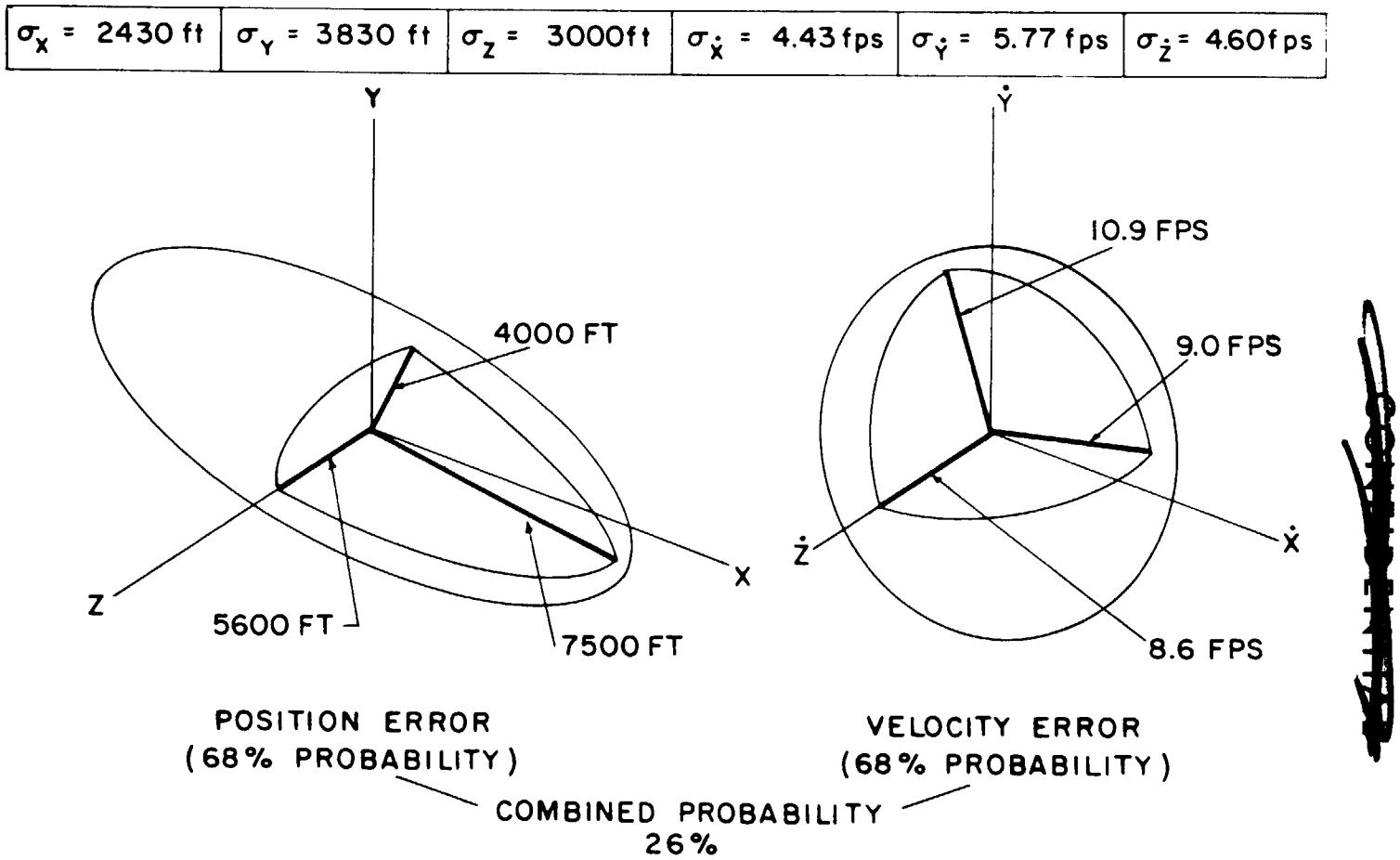

Fig. 8.14 Model 1 landing and abort trajectory. Error volume at burnout of abort at 300 seconds.

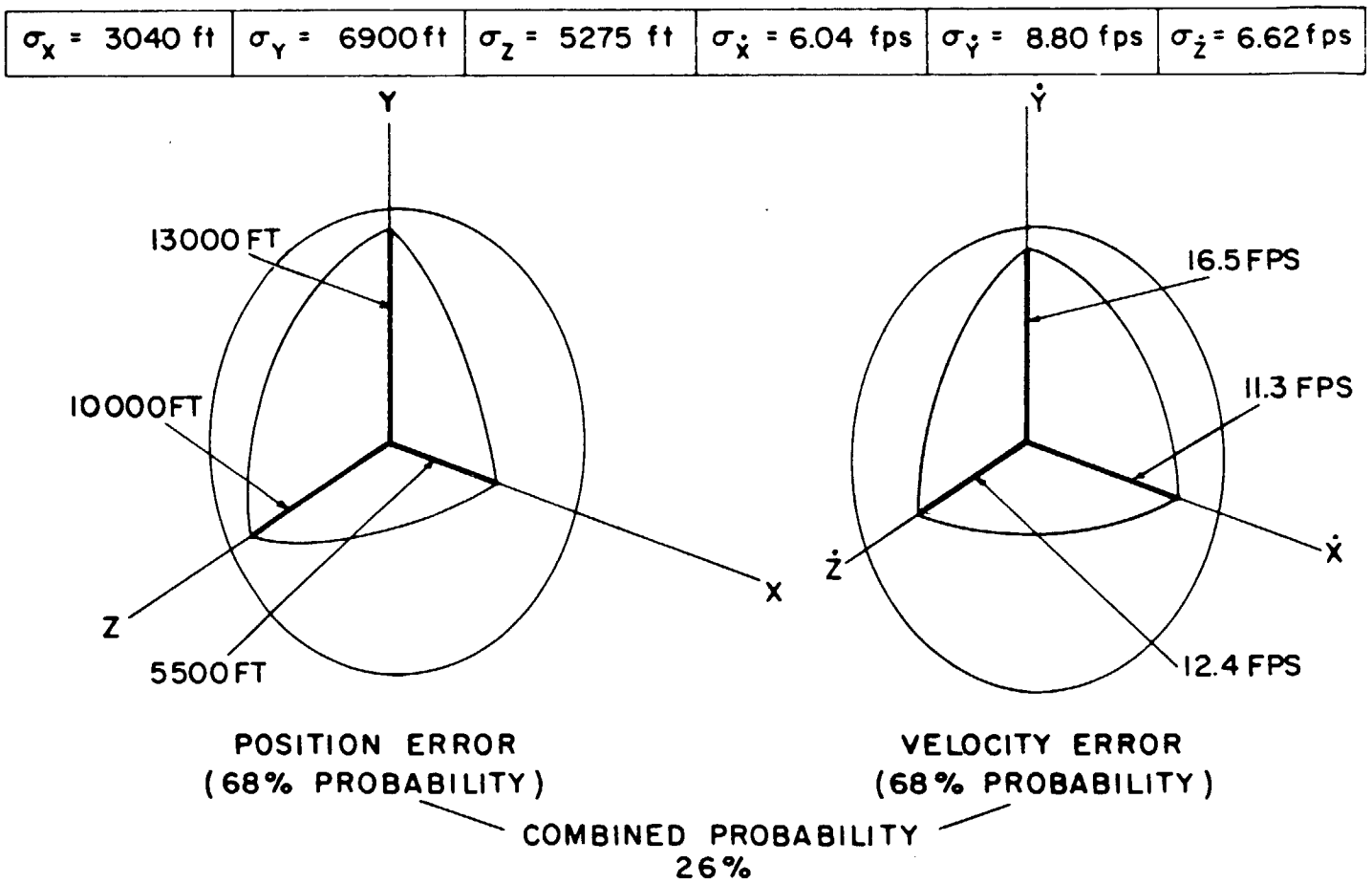

Fig. 8.15 Model 1 landing and abort trajectory. Error volume at burnout of abort at hover.

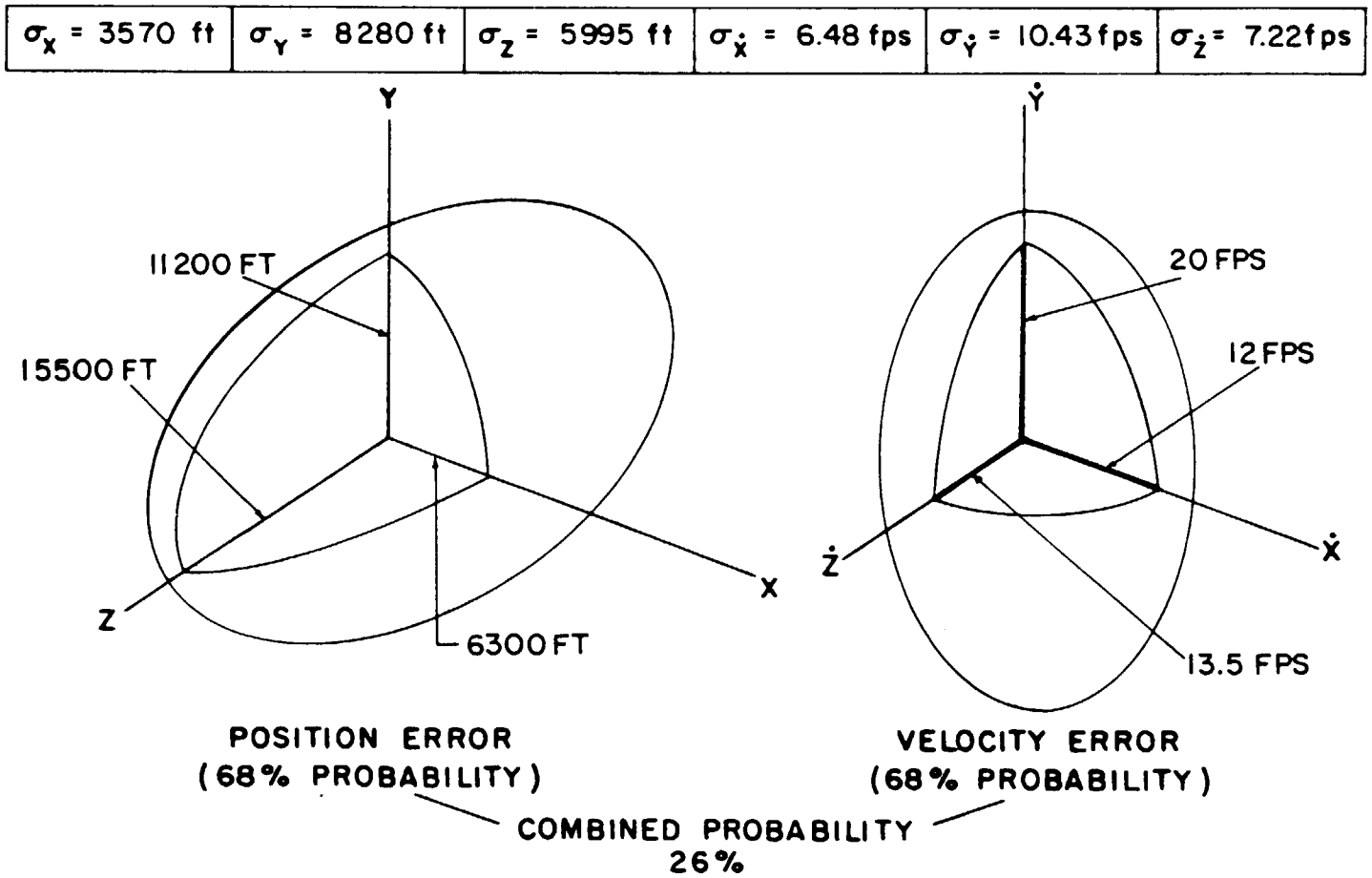

Fig. 8.16 Model 1 landing and abort trajectory. Error volume at burnout of abort after 60 seconds of hover.

8.5 Rendezvous Trajectories from Aborted Landings.

Figure 8.17 is a plot of an abort trajectory which resulted from an abort condition initiated after 150 seconds of the powered landing maneuver from an equal period descent condition. In this case, the LEM was ahead of the CSM by 7 degrees central angle at injection. The rendezvous maneuver covered a central angle of 237 degrees between the injection point and the terminal aim point. The LEM injection errors assumed for this trajectory are listed in Fig. 8.17, and are similar to those in Fig. 8.13 when a positive sign is chosen for all components. The uncorrected trajectory resulting from these injection errors had a point of closest approach to the CM of 12.2 nm as indicated in Fig. 8.17. The rendezvous midcourse guidance technique was used for midcourse velocity corrections in this trajectory and required a total of 17.3 ft/sec in three midcourse corrections. The initial LEM E matrix used in the rendezvous guidance system can be generated for all possible abort conditions from a reference landing trajectory. This involves extensive storage in the LGC, and it is therefore desired to limit the initial LEM E matrices required to those for ascents and abort trajectories. The trajectory shown in Fig. 8.17 used the standard LEM ascent injection matrix (listed in Fig. 7.27) for control of the midcourse rendezvous phase. When comparing this case with that of using the actual LEM injection E matrix for this abort condition, there was negligible difference in midcourse guidance performance. It is therefore concluded that a single LEM E matrix will be used for both ascent and abort conditions. The tracking parameters used for the trajectory of Fig. 8.17 again are those listed previously in Fig. 7.27 for ascent trajectories. With reference to Fig. 8.17, it can be seen that the final or third midcourse correction was applied at a range of 105 miles and resulted in a miss distance of less than 500 feet. In this particular case, a very good first midcourse correction was made at a range of 219 miles, thus resulting in very small second

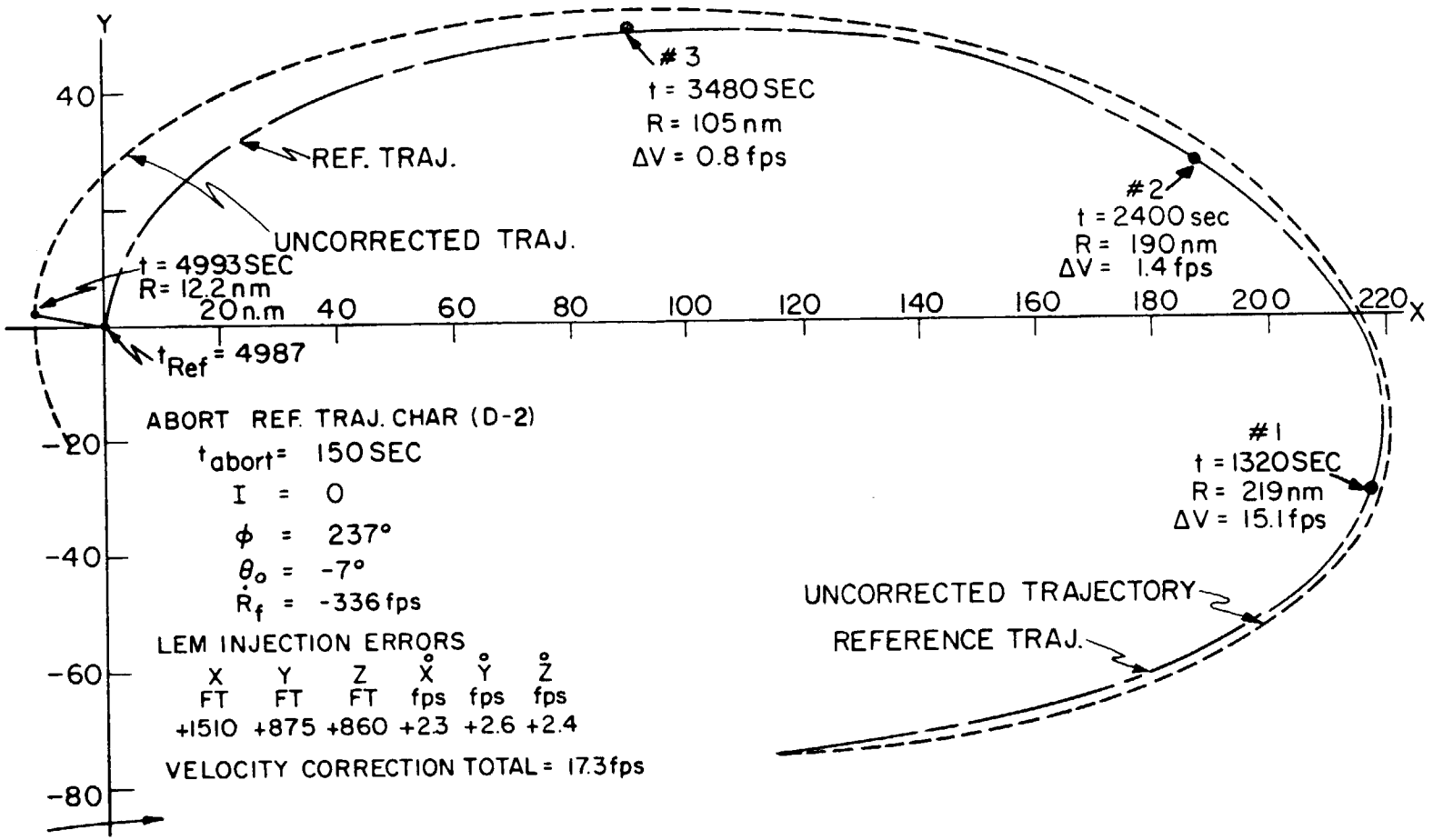

Fig. 8.17 Abort rendezvous trajectory - XY plane projection.

and third midcourse corrections being required. This trajectory illustrates the performance capabilities of the midcourse rendezvous technique at long ranges for the radar tracking performance currently specified. The trajectory of Fig. 8.17 is referred to as abort trajectory D-2 in Section 7.5 which compares fixed time and statistical midcourse correction criteria. The trajectory shown in Fig. 8.17 used the statistical criteria and initial covariance matrices of Fig. 7.27.

A rendezvous trajectory resulting from aborting the landing maneuver during a hover condition is illustrated in Fig. 8.18. After powered abort injection, the phasing between the two vehicles was 12.4 degrees in this case. This phase is greater than that normally associated with the Hohmann type transfer. The trajectory illustrated in Fig. 8.18 assumed the LEM injection errors as listed, thus resulting in an uncorrected point of closest approach of 10.8 nm. This trajectory is plotted from the first midcourse guidance correction point at 125 nm. A total of four midcourse corrections were required for a total of 48.4 ft/sec in order to establish the final intercept trajectory. All system parameters and initial E matrices, with the exception of the injection errors, are the same as those listed in Fig. 7.27. The statistical midcourse correction criteria were used for the trajectory of Fig. 8.18. As a result, the first midcourse correction was delayed until the LEM was within 160 degrees of the final aim point due to the 180 degree $\pm$ 20 degree sector limitation, (as described in Section 7.5). An alternate technique for reducing the midcourse correction ΔV requirement for trajectories of this type has been presented in Section 7.5. This technique can essentially reduce the ΔV requirement from 48.4 ft/sec to 40 ft/sec. The trajectory of Fig. 8.18 is referred to as abort trajectory D-8 in Section 7.5.

The terminal rendezvous maneuver for the abort trajectories is controlled in the same manner as those for the ascent trajectories described in Section 7.6. The trajectories of Figs. 8.17 and 8.18,

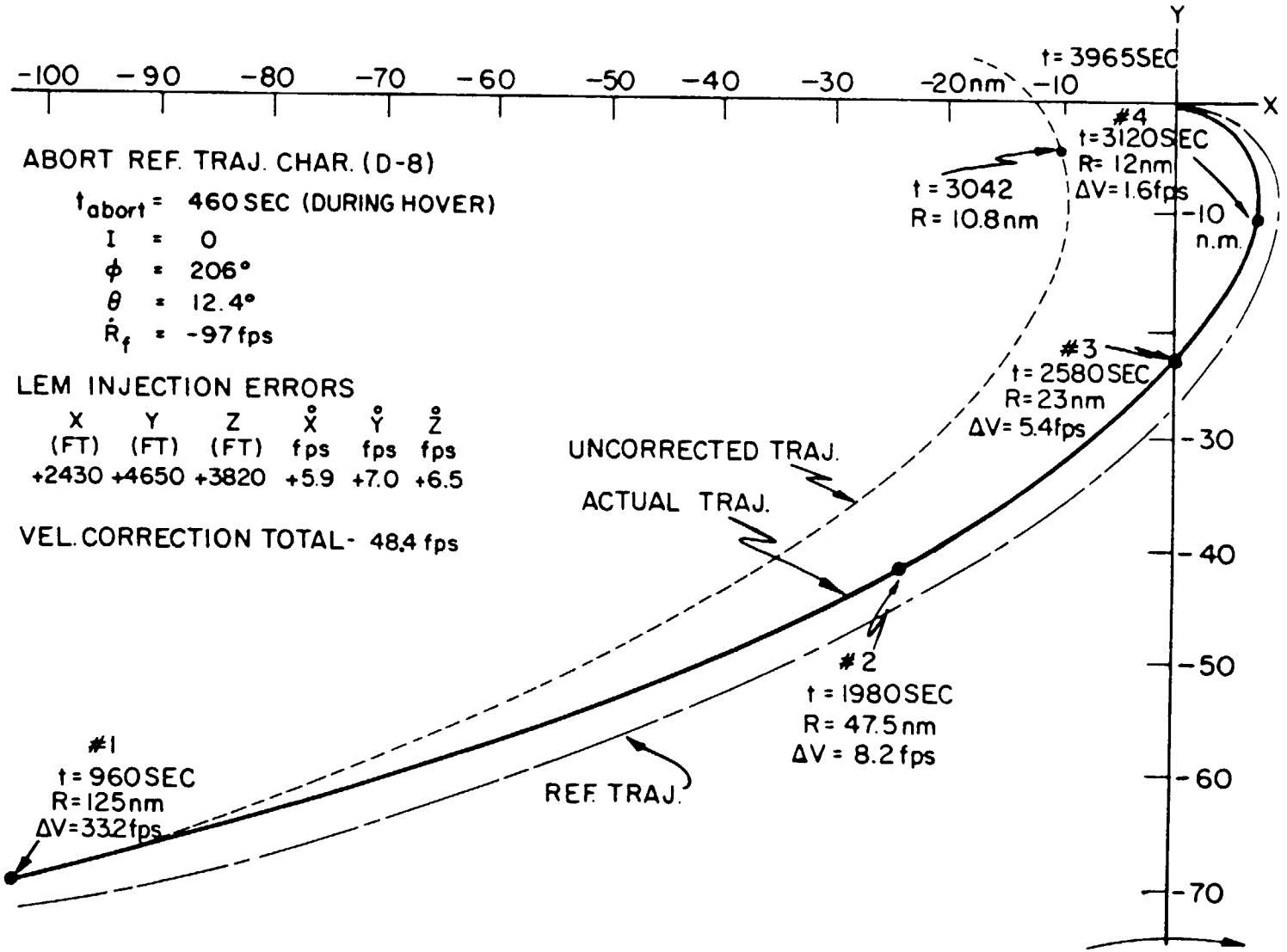

Fig. 8.18 Abort rendezvous trajectory - XY plane projection.

illustrate that the terminal rendezvous closing velocity can vary between 100 ft/sec and over 300 ft/sec. In the case of the trajectory of Fig. 8.17, a high initial closing velocity at the terminal rendezvous phase of 336 ft/sec resulted with a relatively heavy LEM vehicle. This was because the descent stage could perform the complete powered abort maneuver providing this stage was not the cause of the abort condition. In this case, the descent stage or the ascent stage main propulsion system would have to reduce the closing terminal velocity within the capability of the LEM - RCS system during the first velocity correction or thrust period of the terminal rendezvous maneuver. In the abort trajectory of Fig. 8.18, a relatively low closing velocity results. This could be handled by the LEM - RCS system since the descent stage would have been jettisoned relatively early in the powered abort maneuver. In the trajectory case of Fig. 8.18, the first terminal rendezvous thrust maneuver would not be applied since the closing velocity is lower than the desired or prescribed 100 ft/sec velocity condition. A two-thrust terminal rendezvous maneuver would be initiated at a range of 1.5 nm in this case if the $R\text{-}\dot{R}$ criteria presented in Section 7.6 were used.

CHAPTER 9

CSM RETRIEVAL AND LEM BACK-UP OPERATIONS

9.1 Objectives

As mentioned in Section 7.7, the CSM will monitor all unpowered (descent and rendezvous) phases of the LEM mission with its primary G&N system and the navigation technique described in Section 7.2. The monitoring criteria and procedure is currently being developed and will be presented in a future report. The major effort of this monitoring operation will be to determine proper operation of the LEM and CSM primary G&N systems, and to command LEM midcourse and terminal velocity corrections over the inter-vehicle communication or data link in the event of LEM primary G&N failure. If the LEM primary G&N system failed during the powered landing or ascent maneuvers, these powered maneuvers would be controlled by the LEM abort or back-up guidance system to injection. The CSM system would then track the LEM and command required midcourse corrections. This operation is described in Section 9.2.

Another CSM rendezvous requirement is the active retrieval of the LEM in the event of LEM propulsion failure after injection. The primary G&N rendezvous guidance presented in Section 7.2 will be used for this type of operation, and typical retrieval trajectory conditions are presented in Section 9.3.

9.2 CSM Back-up Guidance Operations for the LEM

9.2.1 General Comments

A study was conducted to determine the maximum LEM injection errors that could be permitted and still achieve a rendezvous within the LEM ΔV budget using the CSM midcourse and

terminal velocity commands. It was assumed that the primary G&N system, including the rendezvous radar on the LEM, had failed and that powered ascent was made with the LEM back-up or abort guidance system. Immediately after injection, full use is made of the primary G&N system and the rendezvous radar on the CSM whenever possible to determine the velocity corrections which the LEM should make in order to achieve rendezvous with the CSM. This data is transmitted from the CSM to the LEM by voice or data link.

In this investigation it was not felt necessary to require the LEM to be injected into a clear perilune orbit at the end of the powered ascent phase, since such a requirement unduly restricts the permissible velocity errors at injection. Even with much larger errors, there is sufficient time available after injection before it is necessary for the LEM to correct its orbit so as to insure a safe minimum altitude. This available time can be used to advantage by the primary G&N system on the CSM to determine a velocity correction for the LEM which would not only insure a safe orbit, but also place the LEM on a more optimum trajectory to the CSM.

LEM injection was assumed to take place at an altitude of 50,000 feet with the CSM in a circular orbit of 80 nm altitude. It was assumed that the ΔV budget in LEM main propulsion and RCS tanks to achieve rendezvous was 630 fps after the LEM ascent had been injected with a velocity of 5500 fps.

Three possible abort situations were considered in this study:

1. Emergency launch from the lunar surface with the LEM back-up G&N system when the CSM is not visible (i.e., not within tracking range).
2. Abort from the normal landing phase with the LEM back-up G&N system. Both an early and late abort are considered.

3. Ascent from the lunar surface with the LEM back-up G&N system when the CSM is within tracking limits.

9.2.2 Emergency Launch From the Lunar Surface Under LEM Back-up Guidance Control

In this example, the LEM must leave the lunar surface under control of the back-up G&N system when the CSM is not visible or within radar tracking range. Such would be the case if the LEM primary G&N system had failed and the ascent engine propellant tank developed a serious leak or potential loss of pressurization. The primary goal is to get off the lunar surface and into a safe orbit as soon as possible

At ascent injection (Fig. 9.1), the cut-off velocity (V_{co}) is assumed to be at some positive angle (α_{co}) with respect to the local horizontal. Although the LEM may have injected into an orbit with an unsafe perilune, it is proposed that the LEM be permitted to coast upwards until,at some predetermined time, a velocity correction (ΔV_1) is applied horizontally which would then place the LEM in a safe orbit. The velocity correction (ΔV_1) was arbitrarily selected to be 200 fps, and applied with an angular error (α_1) of ± 5 degrees with respect to the local horizontal.

The range of flight path angles (α_{co}) considered at injection were 0 to 8 degrees. Results are given in Tables 9.1 and 9.2 for cut-off velocities of 5,500 and 5,600 fps, respectively. In each table, the time after injection at which ΔV_1 is applied is the same for all values of α_{co}, and is equal to the time between injection and apolune for the α_{co} = 8 degrees case.

The symbols used in Fig. 9.1 and Tables 9.1 and 9.2 are the following:

H_{co} = injection altitude = 50,000 feet

V_{co} = magnitude of injection velocity

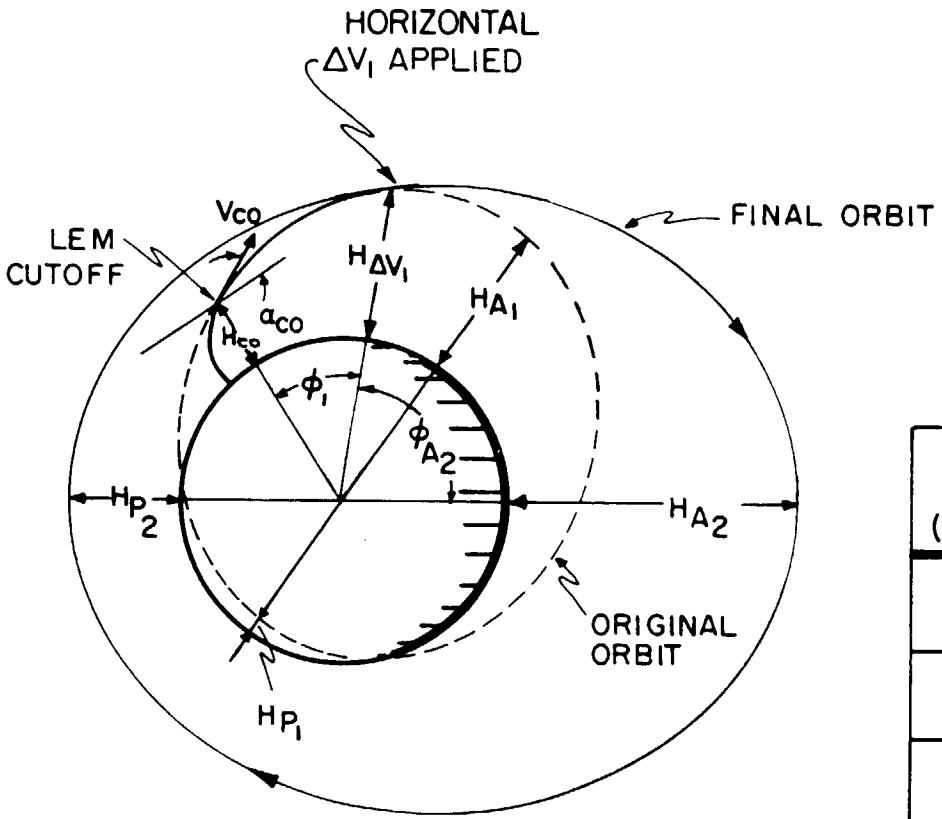

$H_0 = 50,000$ FT

$V_{CO} = 5,500$ FPS

$\Delta V_1 = 200$ FPS
[APPLIED 1865 SECS
AFTER INJECTION]

α_{CO} (DEG)	H_{P_1} (N.M.)	H_{A_1} (N.M.)	H_{P_2} (N.M.)	H_{A_2} (N.M.)
0	8.2	21	16	166
2	-19	49	48	128
4	-52	82	80	91
6	-85	115	52	115

Fig. 9.1 Emergency lunar surface launch (CSM not visible).

TABLE 9.1

Emergency Lunar Surface Launch - CSM Not Visible

Conditions:

H_{co} = 50,000 ft

V_{co} = 5,300 fps

ΔV_1 = 200 fps

t = 1865 secs.

α_{co} (Deg)	H_{p_1} (NM)	H_{A_1} (NM)	ϕ_1 (Deg)	$H_{\Delta V_1}$ (NM)	α_1 (Deg)	H_{p_2} (NM)	H_{A_2} (NM)	ϕ_{A_2} (Deg)
8	-118	148	85	148	0	14.4	148	0
7	-102	131	87	131	-5	32.6	131.3	-5
					5	32.7	131.1	3
6	-85	115	89	115	-5	51.4	114.9	-9
					5	51.7	114.6	3
5	-69	98	91	98	-5	69.9	99.0	-21
					5	70.7	98.1	7
4	-52	82	93	82	-5	79.4	92.1	-132
					5	81.1	90.4	154
3	-36	65	95	65	-5	64.7	109.4	-170
					5	64.8	109.3	172
2	-19	49	97	49	-5	48.5	128.2	-177
					5	48.3	128.5	173
1	-3	33	99	32	-5	32.2	147.2	180
					5	31.8	147.7	173
0	8.2	21	102	16	-5	15.9	166.2	177
					5	15.4	166.9	172

TABLE 9.2

Emergency Lunar Surface Launch - CSM Not Visible

Conditions:

H_{co} = 50,000 ft

V_{co} = 5,600 fps

ΔV_1 = 200 fps

t = 2261 secs.

α_{co} (Deg)	H_{p_1} (NM)	H_{A_1} (NM)	ϕ_1 (Deg)	$H_{\Delta V_1}$ (NM)	α_1 (Deg)	H_{p_2} (NM)	H_{A_2} (NM)	$\circ_{A_2}$ (Deg)
8	-93	196	100	196	0	46.8	196	0
7	-77	180	102	179.6	-5	64.9	179.6	-1
					5	64.6	179.9	6
6	-61	164	104	163.5	-5	83.4	163.6	3
					5	82.4	164.6	13
5	-45	148	106	147.5	-5	101.0	148.4	15
					5	98.3	151.3	30
4	-30	133	109	131.8	-5	113.5	138.3	61
					5	107.1	145.0	71
3	-16	119	112	116.3	-5	107.6	146.5	123
					5	101.6	153.1	114
2	-4	107	114	101.1	-5	93.2	163.4	140
					5	88.5	168.8	132
1	5	98	117	86.2	-5	77.4	181.5	145
					5	73.3	186.5	139
0	8.2	95	120	71.7	-5	61.3	199.8	146
					5	57.6	204.7	142

α_{co} = flight path cut-off angle with respect to local horizontal

α_1 = angular error with respect to the local horizontal in applying ΔV_1 (positive when ΔV_1 is above the local horizontal)

ϕ_1 = central angle from injection to point of ΔV_1 application

ϕ_{A_2} = central angle from point of ΔV_1 application to new apolune (positive if apolune ahead)

$H_{\Delta V_1}$ = altitude when ΔV_1 is applied

H_{p_1} = perilune altitude after injection

H_{A_1} = apolune altitude after injection

H_{p_2} = perilune altitude after ΔV_1 application

H_{A_2} = apolune altitude after ΔV_1 application

t = time after injection when ΔV_1 applied

It is apparent from Tables 9.1 and 9.2 that there is no serious difficulty in establishing a safe orbit for the LEM if the injection flight path angle is anywhere between 0 to 8 degrees and the cut-off velocity is between 5,500 and 5,600 fps. Note that an angular error (α_1) of ± 5 degrees in applying ΔV_1 has very little effect on the final orbit.

One factor should be stressed, however, with respect to this type of abort: the length of time which the LEM may have to stay in orbit before the proper phasing is established with respect to the CSM for rendezvous. This will probably be a problem for most any orbit which the LEM may achieve. No attempt was made to analyze the problem of orbit stay time for the LEM. However, it should be pointed out that range and range rate tracking by earth stations would probably be very useful in

reducing the stay time. It is possible that enough time is available between injection and ΔV_1 application to enable earth tracking to determine a more suitable ΔV_1 to reduce stay time.

The method of attack used in this example is by no means optimum, but does illustrate that a relatively simple scheme can permit sizable injection errors with reasonable crew safety.

Typical ΔV requirements for changing the orbital plane of the LEM one degree are 82 feet per second at apolune and 101 feet per second at perilune, which were determined for the case where $\alpha_{co} = 0^{o}$ and $V_{co} = 5,500$ feet per second.

9.2.3 CSM Primary G&N System for LEM Aborts

Whenever the CSM is within radar tracking range of the LEM, the CSM primary G&N system and rendezvous radar would be used in assisting the LEM in an abort. If the LEM primary G&N system has failed during the normal landing phase or during the lunar stay period, the LEM back-up G&N system is used for powered ascent. After LEM injection the CSM primary G&N system and rendezvous radar are used to determine the LEM orbit and the velocity corrections required by the LEM to achieve rendezvous. Sufficient radar tracking time (typically 10 minutes) exists after LEM injection to determine the LEM's orbit with sufficient accuracy.

Use is made of the aim point minimum ΔV, two-impulse program (Section 5.4) and the statistical midcourse navigation scheme (Section 7.2) to determine the required LEM velocity corrections. The manner in which the midcourse navigation scheme is used in this case is slightly different from that used in previous rendezvous problems (Section 7.4) because of the larger LEM injection errors considered for the abort cases. During normal operation, the time of the first midcourse correction is based

upon the ratio

$$\sqrt{\left(\frac{\text{DELU}}{\text{DELV}}\right)}$$

for the statistical midcourse correction criteria. In the abort situation considered here, however, it has been found that a more optimum approach is first to determine the LEM orbit as in the midcourse navigation scheme, and then to use the aim point determination program to determine the best aim point and time for the first midcourse correction (ΔV_1) before continuing with the regular midcourse navigation scheme. The constraints placed upon the aim point ΔV program were that the total ΔV for rendezvous was not to exceed the assumed ΔV budget (630 fps) and that the perilune altitude after the first midcourse correction was not to be below 50,000 feet, as described in Sections 5.4 and 8.2. All of the aborts covered in this section use this modified midcourse navigation scheme.

In Fig. 9.2, it was assumed that the LEM back-up G&N system has controlled the powered ascent up to injection (LEM cut-off) with a resulting velocity magnitude (V_{co}) and a positive flight path angle (α_{co}). At this point, the central angle between the CSM and the LEM is θ_o. The LEM orbit at injection has an apolune altitude (H_{A_1}) and a perilune altitude (H_{p_1}). After the LEM has moved through a central angle of ϕ_1, the first midcourse correction (ΔV_1) is applied. This correction would be determined by the CSM and transmitted to the LEM. The LEM then proceeds along the new orbit, defined as having an apolune altitude (H_{A_2}) and a perilune altitude (H_{p_2}), until it reaches the point where ΔV_2 is applied in the terminal rendezvous maneuver.

The parameters measured by the radar in the midcourse navigation scheme were range rate and the two gimbal angles defining the line of sight. The 3-sigma radar accuracies were

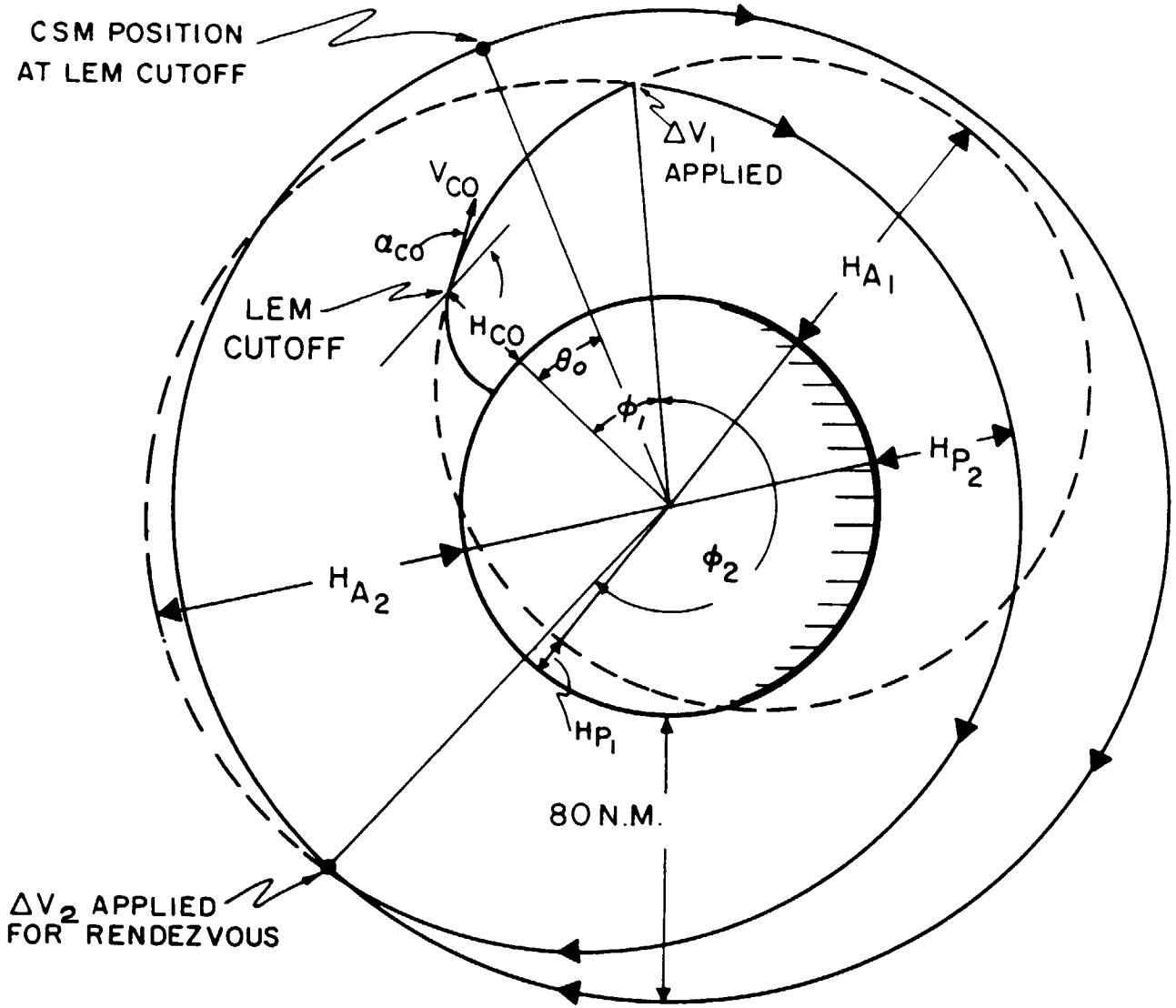

Fig. 9.2 LEM back-up G&N ascents & aborts (CSM within tracking limits).

1% in range rate and 3 milliradians in both line-of-sight angles, as in Section 7.4. These measurements were made every 60 seconds with the preceding accuracies.

During an abort, it was assumed that the LEM will always attempt to inject with a velocity (V_{co}) of 5,500 fps and a positive flight path angle (α_{co}) of 3 degrees. Deviations in the flight path angle of ± 3 degrees with respect to the nominal value (α_{co} = 3 degrees) were considered. For the worst case, which was α_{co} = 6 degrees, a 2 degree out-of-plane velocity component was also considered at injection, resulting from LEM back-up guidance alignment and performance. This inclination of the LEM injection velocity with respect to the desired orbital plane will be indicated in the following tabulated results under the heading (INCL).

9.2.3.1 Aborts From Landing Maneuvers with the LEM Back-up G&N System

Two abort cases were considered for the normal landing phase. The first was an early abort and represents a powered ascent under control of the LEM back-up G&N system from a point along the landing trajectory 300 seconds after perilune ignition. The results for this abort are shown in Fig. 9.3. The second landing abort considered was after hovering 60 seconds (about 500 seconds after perilune ignition). Figure 9.4 summarizes the results for this late abort.

The time (t_{ϕ_1}) in Figs. 9.3 and 9.4 is the time between injection and application of the first midcourse correction. The last column (ΔV_T) in these figures represents the sum of the first midcourse correction (ΔV_1) and the final velocity correction (ΔV_2) for the terminal rendezvous maneuver. ΔV_T is within the assumed budget of 630 fps for all cases. Only one midcourse correction (ΔV_1) was made for each case in the tables. It is probable that one or two more midcourse corrections would be made if the first correction (ΔV_1) does not place the LEM on a

INITIAL CONDITIONS:

CSM IN CIRCULAR ORBIT (ALT. = 80 n.m.)

H_{co} = 50,000 ft.

V_{co} = 5,500 fps

θ_o = 1.4 deg

$t_{(abort)} \approx$ 300 sec AFTER PERILUNE IGNITION

α_{co} (deg)	INCL (deg)	H_{P_1} (n.m)	H_{A_1} (n.m)	ϕ (deg)	t_{ϕ_1} (sec)	ΔV_1 (fps)	H_{P_2} (n.m.)	H_{A_2} (n.m.)	ϕ_2 (deg)	ΔV_T (fps)
0	0	8.2	21	43	780	146	8.6	125	241	450
3	0	35	65	62	1200	126	25	92	140	275
6	0	-85	115	59	1200	270	54	107	313	408
6	2	-84	116	31	600	431	15	81	52	563

Fig. 9.3 LEM back-up G&N controlled early abort.

INITIAL CONDITIONS:

CSM IN CIRCULAR ORBIT (ALT = 80 N.M.)

H_{CO} = 50,000 FT.

V_{CO} = 5,500 FPS.

θ_o = 13.9 DEG

$t_{(abort)} \approx$ 500 sec (60 sec HOVER CONDITION)

α_{CO} (DEG)	INCL (DEG)	H_{P_1} (N.M.)	H_{A_1} (N.M.)	ϕ_1 (DEG)	t_{ϕ_1} (SEC)	ΔV_1 (FPS)	H_{P_2} (N.M.)	H_{A_2} (N.M.)	ϕ_2 (DEG)	ΔV_T (FPS)
0	0	8.2	21	75	1380	96	9.7	80	159	189
3	0	-35	65	121	2400	130	39.5	80	267	184
6	0	-85	115	40	800	506	33.8	80	327	568
6	2	-84	116	59	1200	286	15	109	311	578

Fig. 9.4 LEM back-up G&N controlled late abort.

direct collision course with the CSM. This would be the case if insufficient radar tracking time was used to determine the LEM orbit after injection. However, it has been found that for most abort cases, sufficient tracking time (at least 10 minutes) does exist for determining a ΔV_1 which will place the LEM on a collision course. The maximum miss distances encountered after application of ΔV_1 were found to be about 3 to 4 nm, and would result in additional midcourse corrections for these cases.

To determine the extra amount of midcourse ΔV which would be used to correct for a miss of 4 miles, a simulation run was made for the last case ($\alpha_{co} = 6^o$, INCL. $= 2^o$) in Fig. 9.4 where ΔV_T was the largest requirement encountered. The miss distance after the first correction (ΔV_1) was 3.9 miles. Additional midcourse corrections were required by the G&N system at 4320 and 6000 seconds after LEM injection in order to place the LEM on a collision course. The total ΔV for these two corrections was 16.9 fps. The conclusion drawn from this result is that the extra ΔV required in making midcourse corrections, after the first one has been made, should be no more than 15 to 20 fps and will usually be less.

9.2.3.2 Ascent From the Lunar Surface with the LEM Back-up G&N System

To illustrate the abort case of launch from the lunar surface under control of the LEM back-up G&N system, the launch was so timed as to produce an initial phase angle (θ_o) between the CSM and LEM of 12 degrees at injection. The selection of a 12 degree injection phase angle was not made on an optimum basis, but the results did indicate that the over-all ΔV requirement was better than in the previous cases ($\theta_o = 1.4^o$ and 13.9^o). From all indications, it seems that the central angle (θ_o) can be between 1 to 16 degrees without incurring a ΔV requirement over 630 fps for rendezvous. Later studies should

INITIAL CONDITIONS:

CSM IN CIRCULAR ORBIT (ALT. = 80 N.M.)

H_{CO} = 50,000 FT.

V_{CO} = 5,500 FPS

θ_0 = 12 DEG.

α_{CO} (DEG)	INCL (DEG)	H_{P_1} (N.M.)	H_{A_1} (N.M.)	ϕ_1 (DEG)	t_{ϕ_1} (SEC)	ΔV_1 (FPS)	H_{P_2} (N.M.)	H_{A_2} (N.M.)	ϕ_2 (DEG.)	ΔV_T (FPS)
0	0	8.2	21	56	1020	89	10.5	82	154	198
3	0	-35	65	112	2220	138	47	80	259	183
6	0	-85	115	59	1200	180	9.3	111	333	431
6	2	-84	116	73	1500	194	12	112	301	518

Fig. 9.5 Typical LEM back-up G&N ascent.

indicate the permissible variation in θ_o, and the best value for launch.

The results summarized in Fig. 9.5 for $\theta_o = 12$ degrees are therefore typical for launch from the lunar surface, and it is seen that ΔV_T is well below the assumed budget of 630 fps.

9.3 CSM Retrieval Operations

9.3.1 General

CSM active retrieval will be required in the case of complete LEM propulsion failure. Retrieval will also be required in some cases of partial LEM propulsion failure or excessive LEM ΔV requirements. Two general classes of retrieval conditions were considered in the study presented in this section. These are listed in Fig. 9.6 as retrieval cases for normal LEM ascents and LEM abort cases.

9.3.2 Retrieval After Normal LEM Ascents

The first case considered involved a normal LEM ascent and injection followed by a failure in the LEM RCS such that no midcourse or terminal rendezvous maneuvers could be achieved by the LEM. It might be noted that a complete failure of the LEM RCS would also incapacitate the ascent engine due to no ullage and thrust attitude control. This case is illustrated in Fig. 9.7, and is the ascent trajectory of Fig. 7.28 of Section 7.4. It was assumed that the LEM was injected on this trajectory with the same injection errors summarized in Fig. 7.24. This reference trajectory would normally intercept the CSM orbit at Point A of Fig. 9.7, but due to the injection errors, has a closest approach distance of 8.4 nm as shown by Point A′ of Fig. 9.2. After LEM ascent injection, the CSM tracked the LEM and used the rendezvous guidance technique of Section 7.2 to compute midcourse corrections and terminal rendezvous corrections. In this case the ascent reference trajectory time of arrival was maintained, except that a new aim point was determined on the actual LEM

- NORMAL LEM ASCENTS

  1. LEM INJECTION & MID-COURSE --- CSM TERMINAL RENDEZVOUS

  2. LEM INJECTION --- CSM MID-COURSE AND TERMINAL RENDEZVOUS

- LEM ABORT CASES

  1. ABORT PRIOR TO LANDING MANEUVER INJECTION

     a. Equal period descent trajectory --- CSM terminal rendezvous
     b. Hohmann descent trajectory --- CSM transfer trajectory, mid-course and terminal rendezvous

  2. DIRECT ABORTS DURING LANDING MANEUVER (similar to ascents)

  3. EMERGENCY LAUNCH ABORTS --- LOW ALTITUDE LEM PARKING ORBIT

     a. CSM waiting period for acceptable phasing
     b. CSM transfer trajectory, mid-course and terminal rendezvous

Fig. 9.6 CSM retrieval conditions.

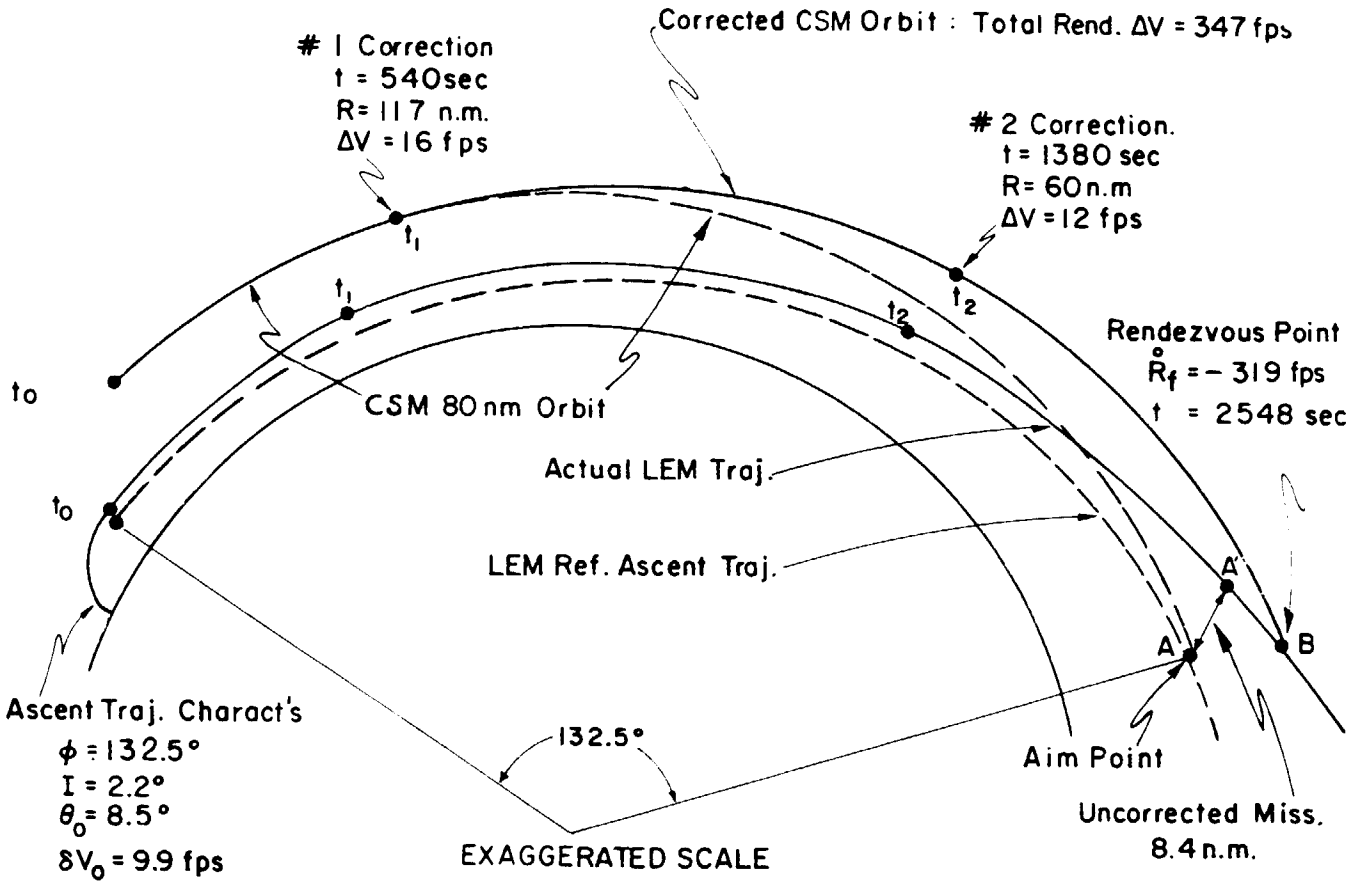

Fig. 9.7 CSM rendezvous after LEM injected on ascent trajectory.

trajectory at this future time (Point B of Fig. 9.7). The CSM then made midcourse corrections to intercept the LEM at Point B. The direct method of computation for this phase would compute required CSM velocity corrections required for this intercept. It was found in this investigation that if the CSM computed the required LEM velocity corrections to intercept the CSM at the original aim point A, the sign or direction of these corrections could be reversed and applied by the CSM to intercept the LEM at Point B with negligible difference in overall ΔV requirement. Since the CSM would normally compute required LEM velocity corrections for monitoring purposes, this second method of computation would be the simplest for the CSM G&N system.

Figure 9.7 indicates that two CSM midcourse corrections were required in this retrieval case. These velocity corrections were determined by the system parameters and initial conditions listed in Fig. 7.27 (statistical correction criteria). One important modification is required in the CSM midcourse computations. Since the service module propulsion system (SPS) must make all midcourse and terminal velocity corrections, the minimum midcourse correction this system can provide is on the order of 10 fps (approximately 0.5 seconds thrust time). The midcourse correction computation of Section 7.2.4.1 was, therefore, modified such that a velocity correction was not made by the CSM unless it was over 10 fps in the case of Fig. 9.7. The two midcourse corrections required a total velocity of 28 fps, which is essentially the same as that required by the LEM for the same trajectory conditions in Fig. 7.28. The terminal rendezvous initial closing velocity for this trajectory was 319 fps, as before.

The terminal rendezvous maneuver for the CSM retrieval is modified from the R-$\dot{R}$ schedule used by the LEM in Section 7.6 because of the SPS characteristics. Only two thrust periods were used, as shown in Fig. 9.8, in order to limit the number of required engine SPS restarts. The range rate-range schedule used in Fig. 9.8 was that listed in Section 7.2.4. The first velocity

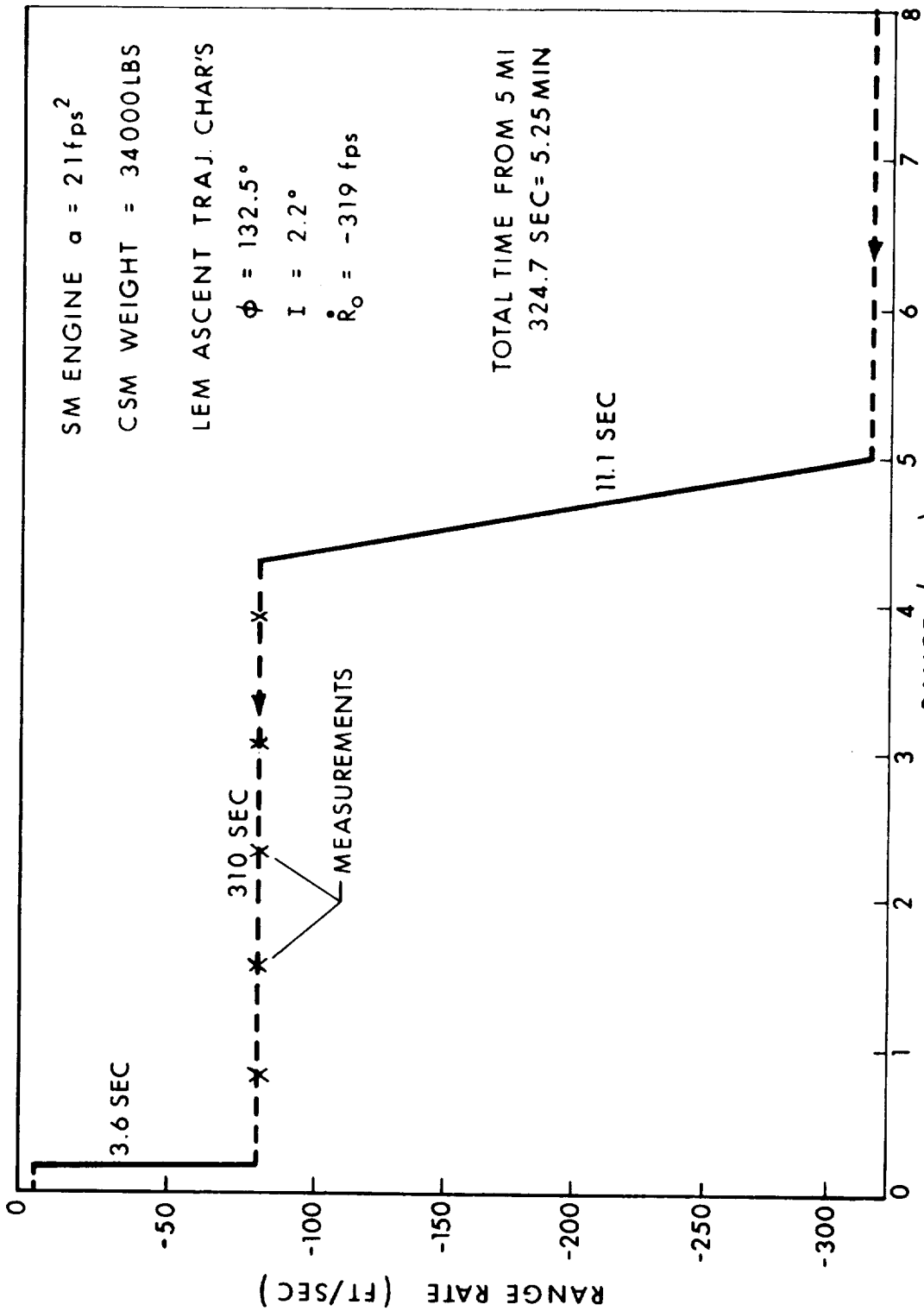

Fig. 9.8 CSM terminal rendezvous maneuver (R-$\dot{R}$ phase plane).
Fixed time of correction method.

correction reduced the closing velocity to 80 fps. The second and final velocity correction reduced the relative velocity to -5 fps at a range of 1000 to 1500 feet in this case. This second velocity correction was purposely kept in the range of 75 fps, so that at least 3 seconds of thrust would be required of the SPS. Current simulations indicate that a shorter burning interval of the SPS would not allow sufficient time for the CSM thrust vector control and G&N systems to stabilize the attitude rate of the CSM at thrust termination. In this case, it was assumed undesirable to have an unpredictable attitude rate at the end of the final rendezvous maneuver, when the relative range was very short and there was no visible monitoring capability by the astronaut. The normal CSM RCS maximum attitude rate is 0.5 deg/sec for reorienting the CSM 180 degrees from the final rendezvous maneuver attitude (-X axis along the line of sight) to the desired docking attitude. This reorientation period could be shortened by using the CSM RCS hand-control mode which has a maximum rate of 5 deg/sec. Final docking was again assumed to be manual with no requirement on the primary G&N system. All CSM controlled terminal rendezvous maneuvers presented in this section assume the two-thrust period schedule shown in Fig. 9.8. Because of 80 fps velocity requirement of the first coast interval, CSM terminal rendezvous maneuvers require approximately half the time (5 to 6 minutes) from 5 nm to 500 feet as those of LEM R-$\dot{R}$ schedule of Section 7.6.

The second retrieval case considered involved normal LEM controlled launch and midcourse corrections, with failure of the LEM system prior to the terminal rendezvous phase. The normal operation in such a case would require the CSM to perform the terminal maneuver at the proper time since an intercept trajectory would have been established by the LEM. It is assumed that the normal CSM attitude just prior to and during the usual terminal rendezvous phase would be such that the line of sight would be near the SCT field of view limit towards the CSM-X axis. A relatively small reorientation (approximately 25 degrees) would then

be needed in case the CSM was required to perform the terminal rendezvous maneuver. In the particular case considered, which is admittedly very unlikely to occur, it was assumed that the CSM did not have time to initiate the terminal rendezvous maneuver and the vehicles were allowed to pass each other. This situation is illustrated in Fig. 9.9. The LEM was injected on the 132.5 degree ascent trajectory (Fig. 7.28) at Point A, with the initial aim point at Point B. The terminal rendezvous was not initiated at 5 nm before B, and the two vehicles were allowed to pass each other and separate to a range of 24 nm during an additional five minutes, as shown by Point C. During this five minute interval, the CSM primary G&N system determined a new aim point (D) by the technique described in Sections 5.4 and 8.2. This new CSM trajectory covered a central angle of 297 degrees with apolune and perilune altitudes of 81.4 nm and 17.25 nm respectively. An initial velocity correction of 220 fps was required to establish this trajectory, which resulted in a terminal closing velocity of 130 fps at point D on the LEM ascent trajectory of 53.9 nm altitude.

The rendezvous trajectory of Fig. 9.9 is illustrated in Fig. 9.10 in the local vertical coordinate system centered in the LEM. This figure only shows the XY or LEM orbital plane projection of this trajectory. It should be noted that this is a non-coplanar problem since the initial LEM ascent trajectory was launched with an out-of-plane condition of 2.2°. The important points to be noted in the trajectory of Fig. 9.10 are that the two vehicles never separated in range over 38 nm, and that no mid-course correction was required. This latter fact is due to low initial uncertainties (prolonged tracking over A to C of Fig. 9.9), and the minimum requirement of 10 fps velocity corrections by the SPS. The terminal rendezvous would be performed by the technique presented in Section 7.6, with the modifications described for Fig. 9.8. The total ΔV requirement for the retrieval case of Fig. 9.9 was 350 fps. The maximum CSM ΔV allocated

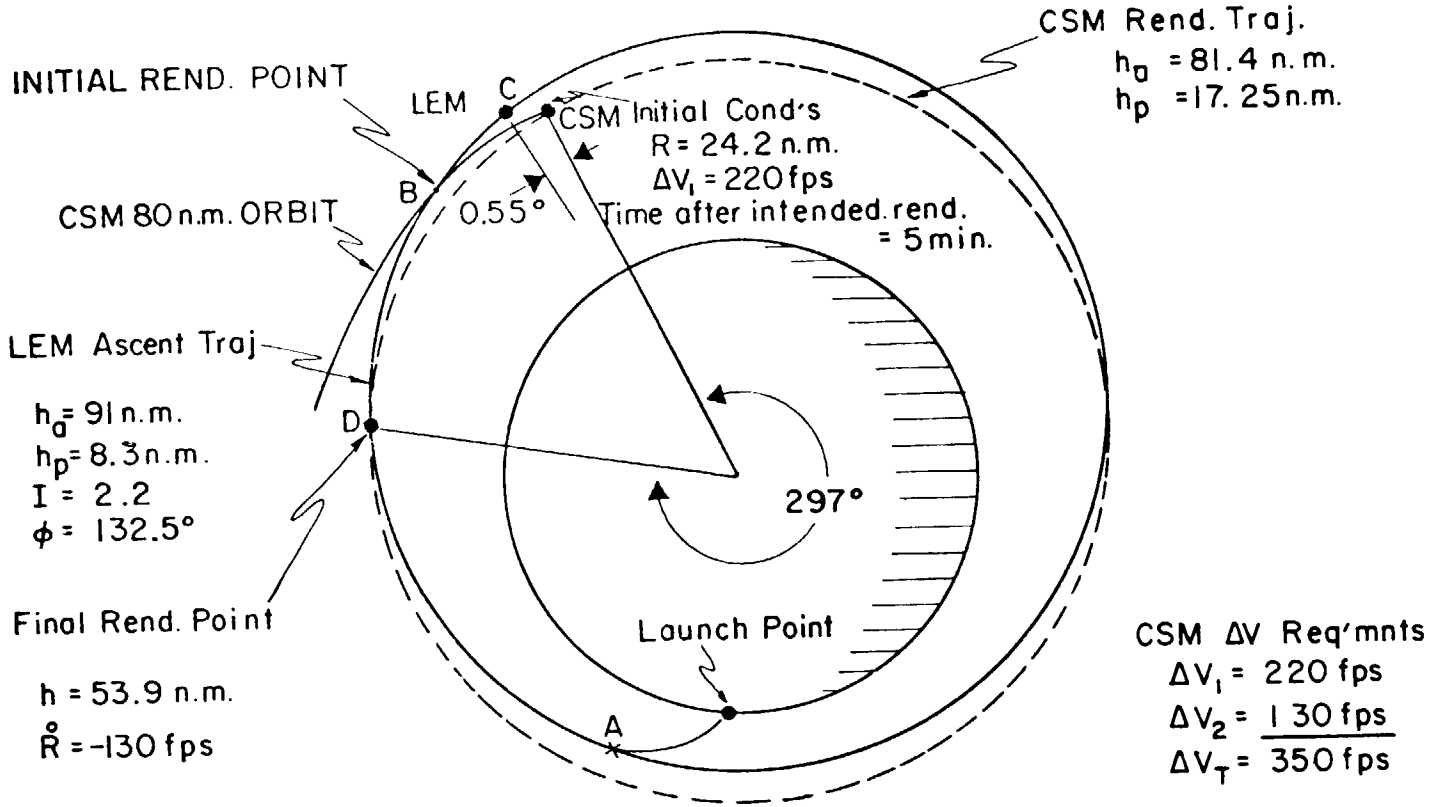

Fig. 9.9 CSM retrieval after aborted terminal rendezvous.

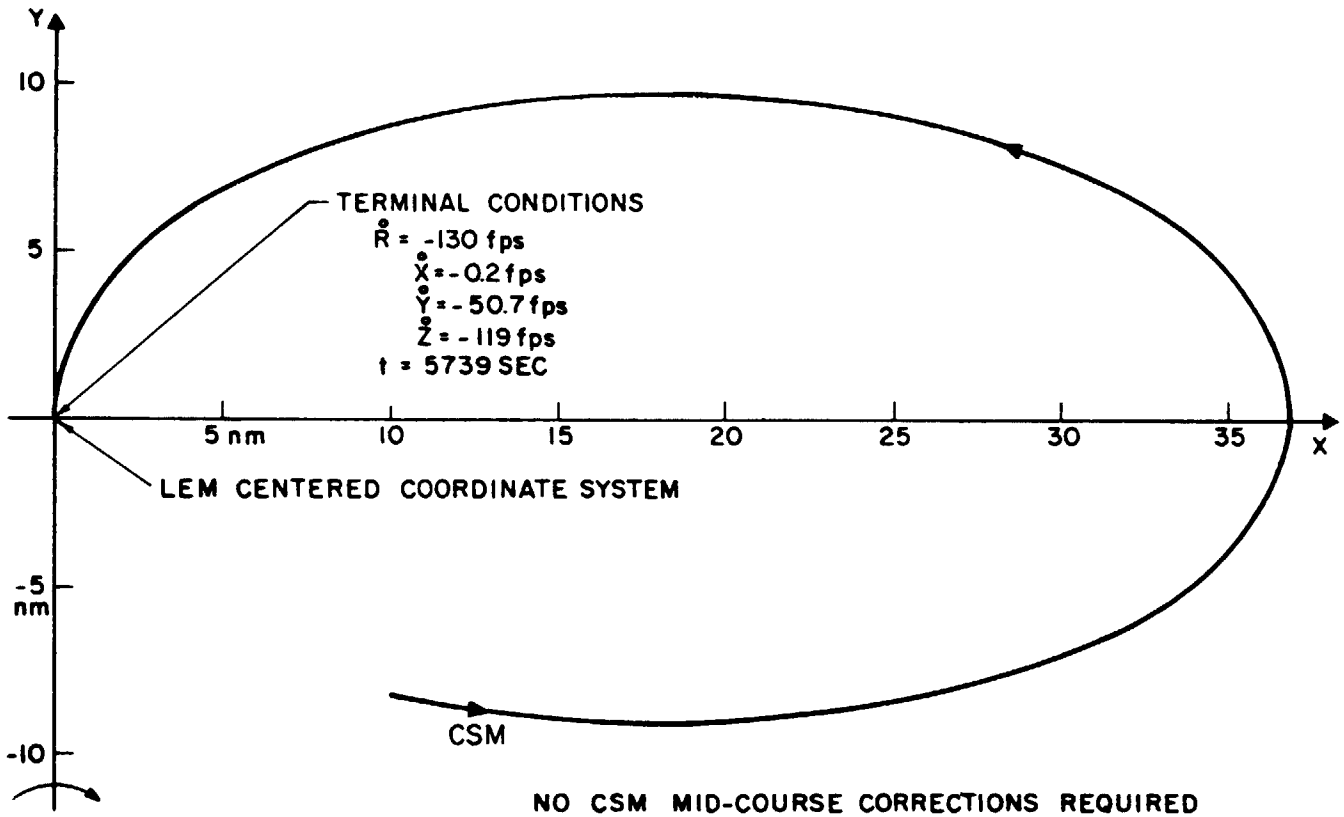

Fig. 9.10 CSM retrieval trajectory after aborted terminal rendezvous(XY plane projection)

for retrieval assumed in this study was 455 fps in the SPS. No translation capability in the CSM RCS was assumed for the midcourse or terminal rendezvous phases.

9.3.3 Retrieval After LEM Abort Cases

9.3.3.1 LEM Aborts Prior to the Powered Landing Maneuver

CSM retrieval of LEM in cases in which the LEM mission was aborted after descent injection, but prior to initiation of the powered landing maneuver, depend upon the type of LEM descent trajectory, as indicated in Fig. 9.6. In the case of equiperiod descent orbits, the CSM merely waits one period, and then performs a terminal rendezvous maneuver. In the case of Hohmann type LEM descent orbits, the CSM must determine and initiate a retrieval or transfer trajectory, perform required midcourse corrections and, finally, the terminal rendezvous. Figure 9.11 illustrates the sector or time interval after LEM injection on a Hohmann descent at Point A where a direct retrieval orbit could be accomplished within the SPS 455 fps ΔV capability. A direct retrieval orbit is defined in this case as a clear perilune orbit that intercepts the LEM with no further velocity corrections other than normal midcourse corrections. This is contrasted to a catch-up or phasing orbit technique which will be described later.

Referring to Fig. 9.11, the CSM could initiate a direct retrieval orbit over a 2886 second interval after LEM descent injection within the 455 fps ΔV limit. Point B' of this figure indicates the position of the CSM at the limiting case. The LEM phasing at this point is 5.6 degrees ahead of the CSM at Point B. This limiting case occurs 600 seconds before the LEM arrives at the perilune or ignition point of the descent orbit. The limiting retrieval trajectory of Fig. 9.11 would be determined by the aim point program of Sections 5.4.and 8.2. In this case, the retrieval trajectory required a 106.5 fps initial CSM velocity maneuver, and resulted in a trajectory that covered 280^{o} with a perilune of

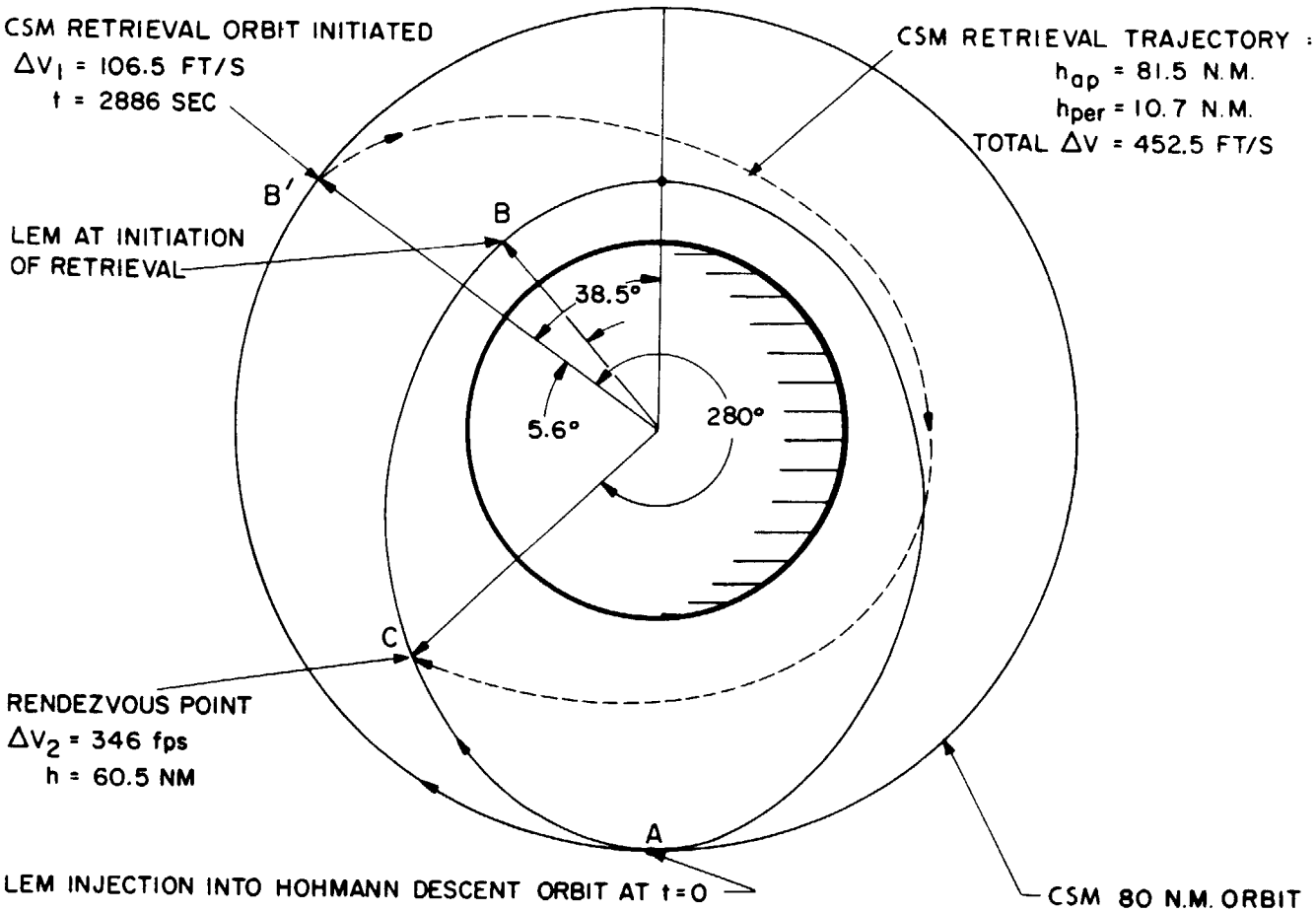

Fig. 9.11 CSM retrieval prior to powered landing maneuver for Hohmann descent trajectory--limit condition for direct retrieval orbit.

10.7 nm and an apolune of 81.5 nm. The terminal rendezvous would occur at Point C and require 346 fps terminal maneuver ΔV. The total CSM ΔV for this retrieval case was very close to the 455 fps limit, and therefore is considered to be the limiting case for direct retrievals after injection, since earlier LEM abort times or CSM initiation of retrieval between A and B' of Fig. 9.11 would require less total ΔV.

CSM retrievals initiated after Point B' of Fig. 9.11, but before the LEM starts the landing maneuver, require a CSM phasing or catch-up orbit procedure as shown in Fig. 9.12. In this example, the CSM retrieval operation was started when the LEM was at the descent perilune, Point B, and the CSM was 9.4 degrees behind at Point B'. No clear perilune direct retrieval orbit could be initiated under these conditions within the 455 fps limit. The procedure used in Fig. 9.12 was to inject the CSM on a Hohmann descent orbit at Point B'. When the CSM reaches the perilune of this catch-up orbit, the LEM is at the apolune of its orbit and the vehicle phasing has reversed from the initial conditions at Points B. At Point C, the CSM initiated its direct retrieval orbit (ΔV = 101 fps) that had an apolune (h_{ap}) of 12.3 nm, and perilune (h_{per}) of 4.6 nm which is the minimum perilune altitude allowed by the aim point determination program. The final rendezvous was made at Point D on the LEM orbit (altitude of 8.37 nm) for a total ΔV requirement of 298 fps independent of nominal midcourse corrections.

In the example of Fig. 9.12, the CSM retrieval orbit could have been initiated prior to the perilune Point C within a time interval of 10 minutes and still have kept the total ΔV requirement below 455 fps. Other CSM catch-up orbits were investigated which had perilunes at Point C higher than 8.3 nm. These higher perilune cases did not improve the total ΔV requirement over the example of Fig. 9.12, however, and were not considered further.

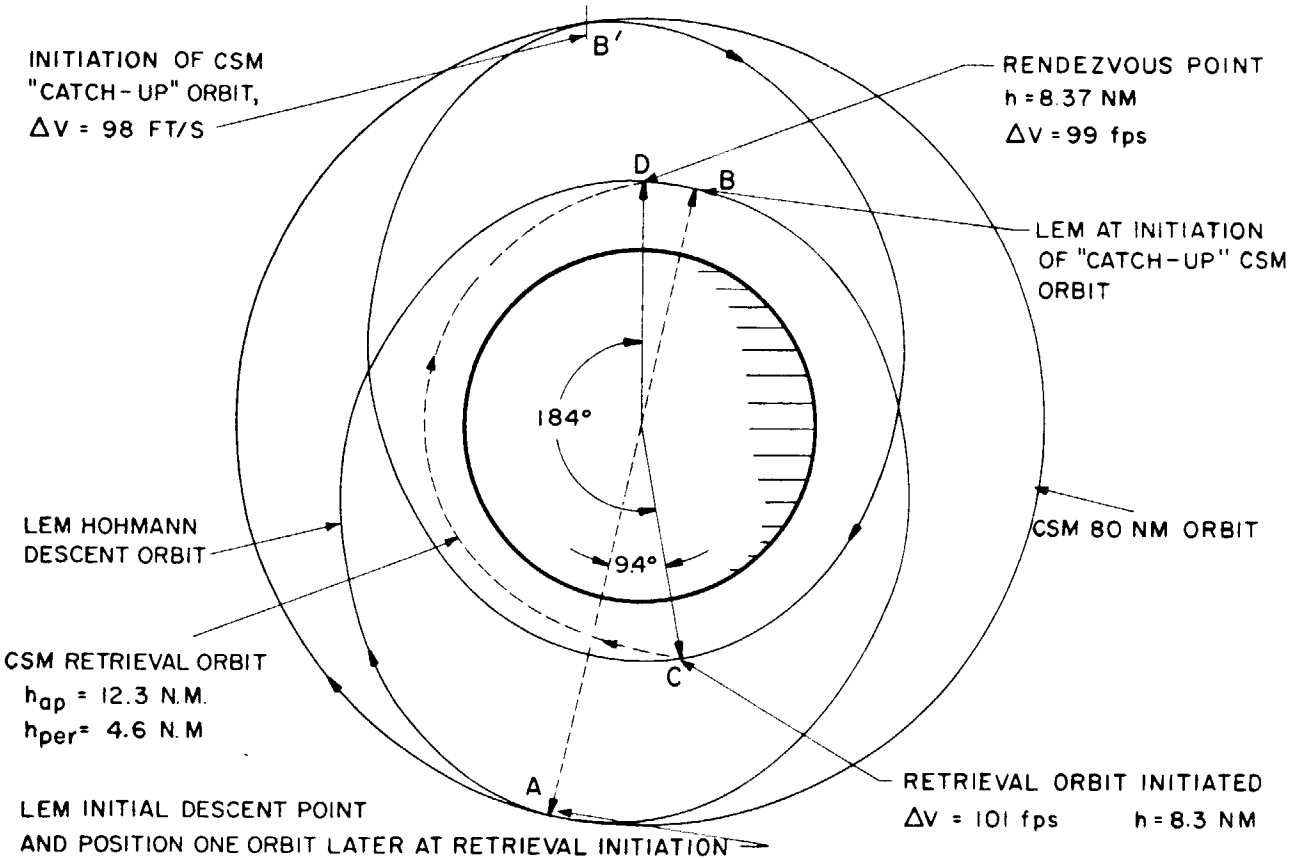

Fig. 9.12 CSM retrieval for LEM abort at the start of landing maneuver (retrieval ΔV req's. = 298 fps).

9.3.3.2 LEM Direct Aborts During the Landing Maneuver

CSM retrieval cases, after the LEM aborted during the powered landing maneuver under control of the LEM primary G&N system, would be very similar to the cases described in Section 9.2 and will not be considered further. This type of situation is not very probable, since it implies a LEM abort due to some condition other than propulsion and then assumes a LEM propulsion failure, or lack of propellant, after abort injection (a possible double failure condition).

9.3.3.3 CSM Retrieval of the LEM in a Parking Orbit

If the LEM were injected into orbit due to energency launch conditions (propellant leaks, etc.), the CSM may not be within radar tracking range at the launch time. As indicated in Fig. 9.6, the CSM must then wait for the vehicle phase to come within tracking range or initiate a catch-up orbit based on MSFN tracking and control. The CSM would then initiate a final retrieval trajectory, perform regular midcourse correction and the terminal rendezvous.

Figure 9.13 illustrates an example of a CSM retrieval of the LEM in a low altitude parking orbit of perilune altitude (h_p) 3.4 nm and apolune altitude (h_a) 15.2 nm. It was assumed that this LEM parking orbit was inclined 2 degrees to the CSM orbital plane because of the combination of out of plane launch conditions and guidance uncertainties. The phasing of the two orbits was allowed to drift to the conditions of Fig. 9.13 at which time the CSM was 8.5 degrees ahead of the LEM and 109 degrees from the intersection or node of the two orbital planes. A retrieval trajectory was initiated at Point 1 of Fig. 9.13, with a velocity correction of 121 fps. It was assumed that the orbital and injection velocity uncertainties in this example were 10 fps. Two CSM midcourse corrections were required as shown in Figs. 9.14 and 9.15 which are the XY an XZ plane projections of the retrieval trajectory plotted on a LEM centered local

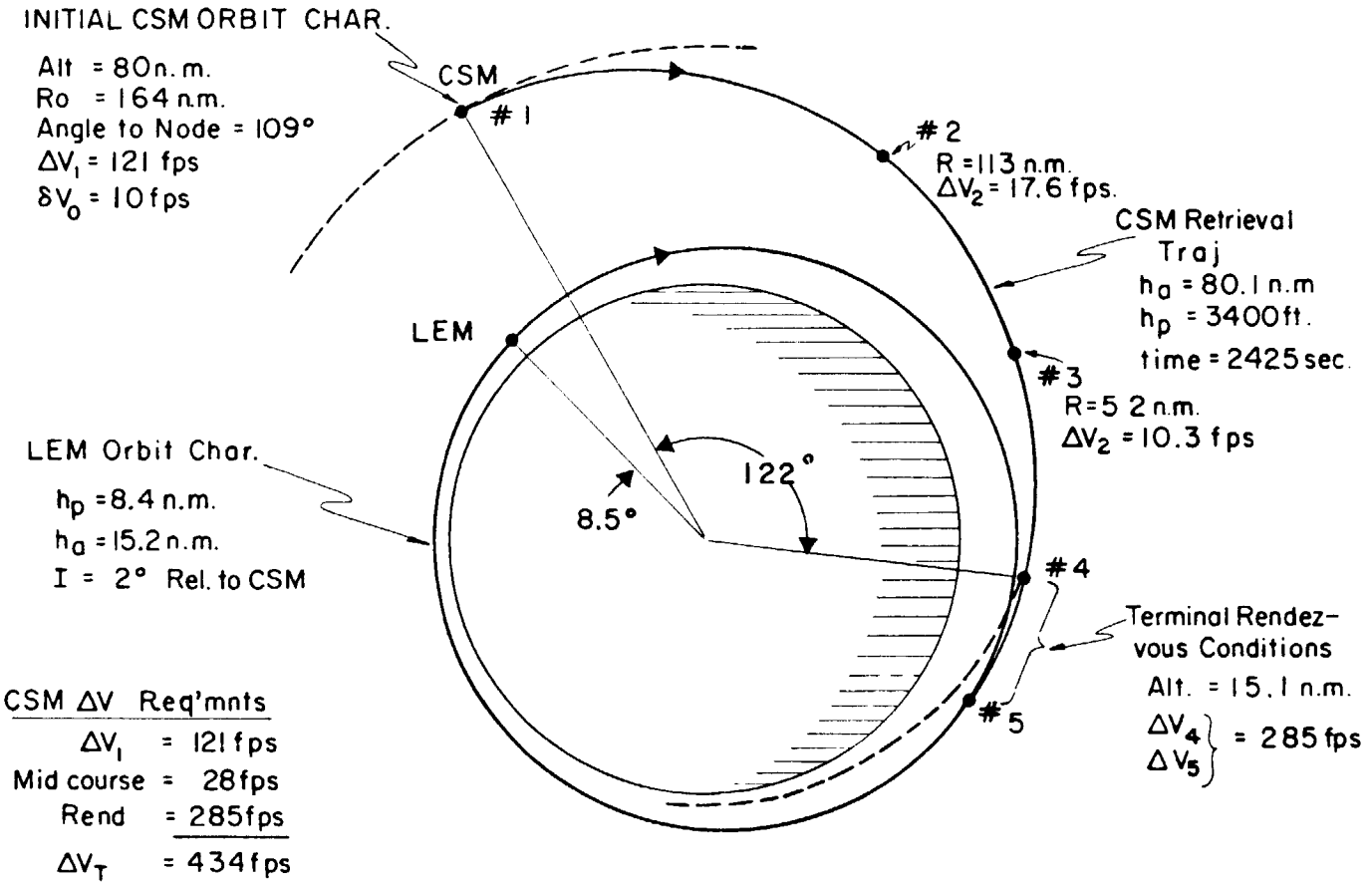

Fig. 9.13 CSM retrieval of LEM in low altitude parking orbit.

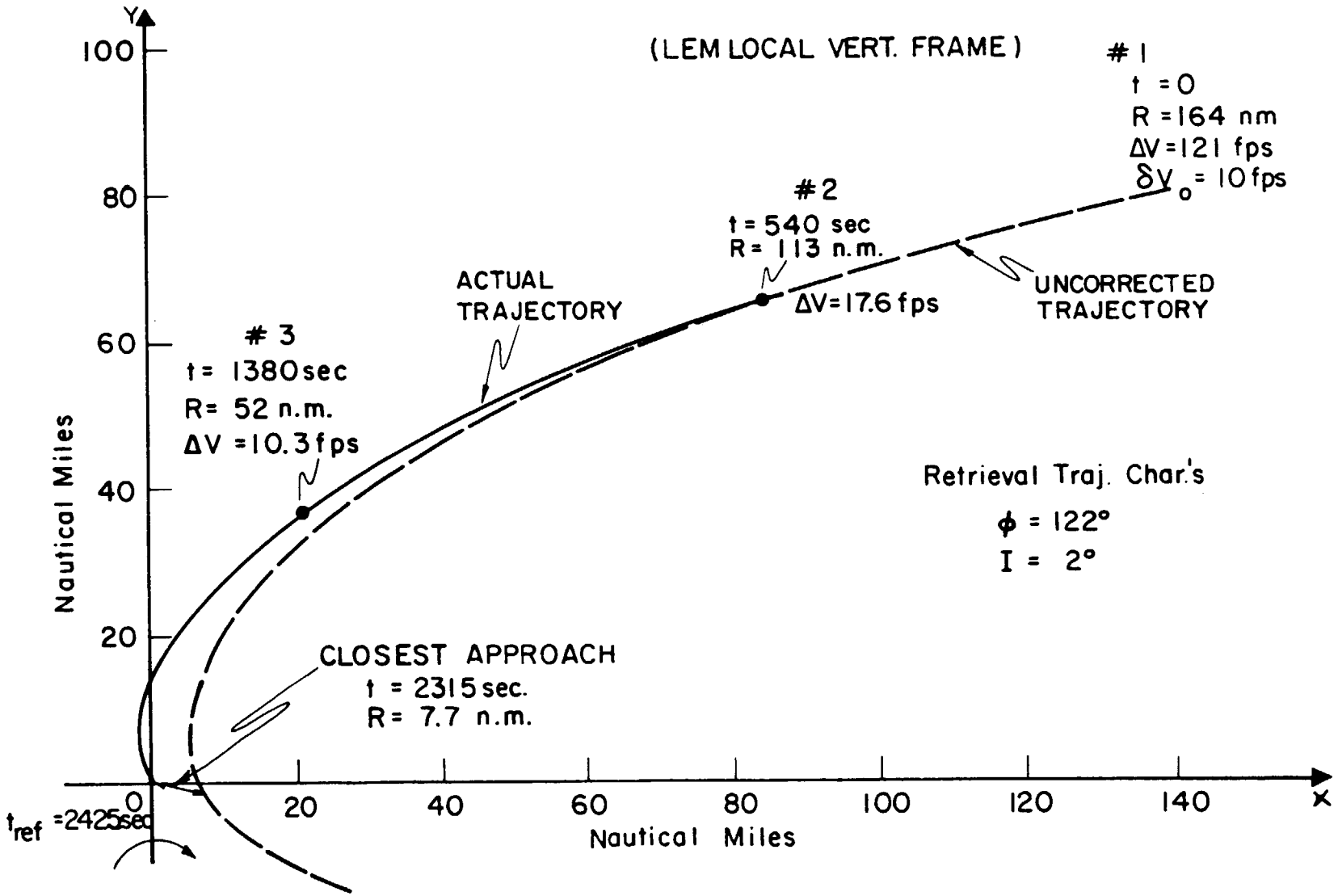

Fig. 9.14 CSM retrieval of LEM in low altitude parking orbit - xy plane trajectory projection.

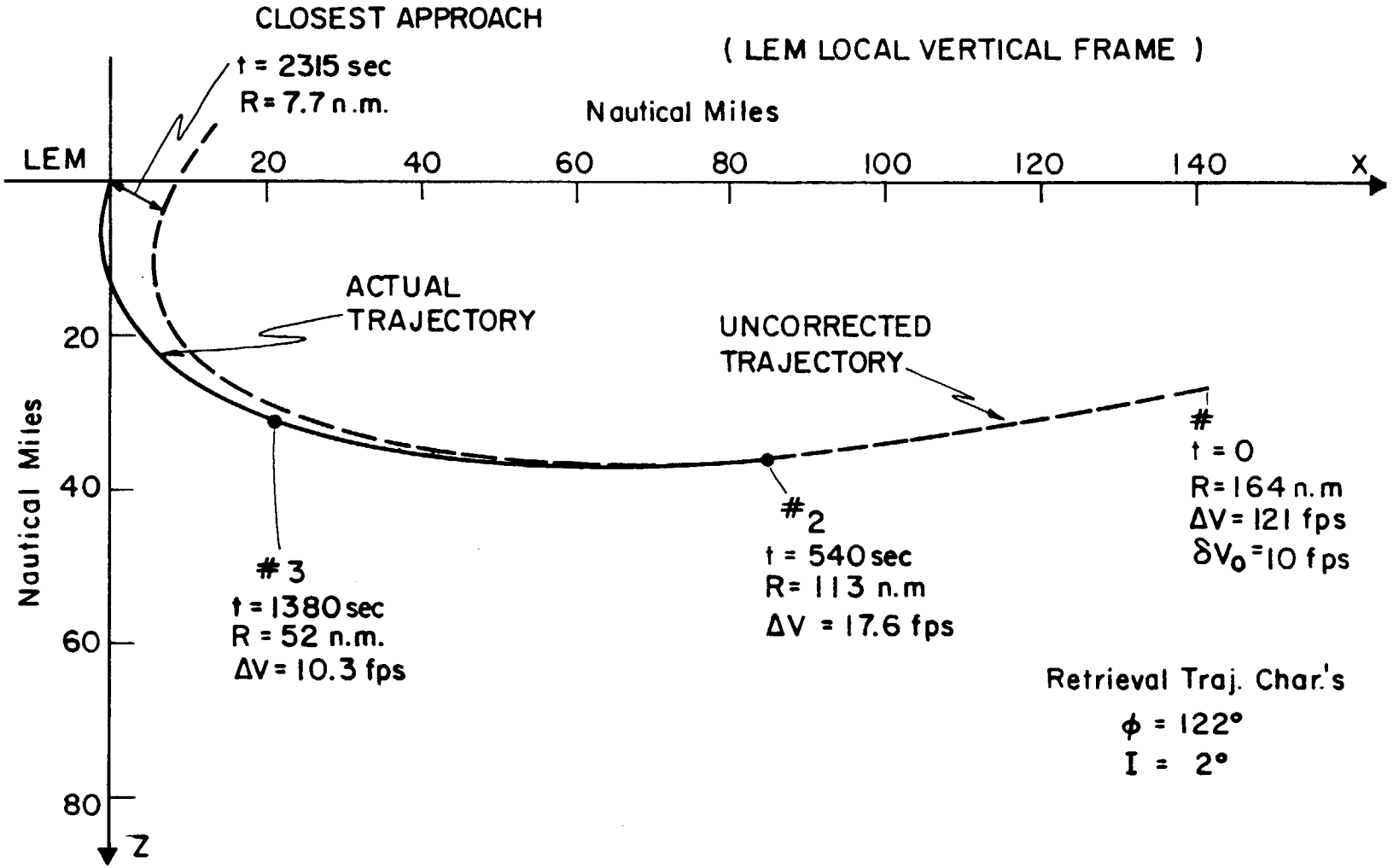

Fig. 9.15 CSM retrieval of LEM in low altitude parking orbit - xz plane trajectory projection.

vertical coordinate system. The uncorrected point of closest approach for this trajectory was 7.7 nm, as shown in these figures. The final terminal rendezvous maneuver, indicated in Fig. 9.13, involved two thrust periods (#4 and #5 of the overall retrieval operation) as described in Section 7.2. The overall retrieval ΔV requirement was 434 fps, a large percentage of which is due to the 2 degree noncoplanar condition in this example. This indicates that the 455 fps allotment will normally be expended for 2 degree out of plane retrievals in low altitude parking orbits, and long phasing or waiting times must be expected in the absence of DSIF directed phasing changes.

It might be noted that the CSM retrieval orbit of Fig. 9.13 does not intersect the LEM orbit at its node with the original CSM orbit, but 13 degrees beyond this point. The perilune altitude of this retrieval orbit is very low (3400 feet), and might be ruled unacceptable. If, however, the CSM achieved the terminal rendezvous at Points 4 and 5 of Fig. 9.13 at an altitude of 15.1 nm, the low perilune would never be reached.

9.4 CSM Operations After Retrieval

CSM primary G&N operations after retrieval and crew transfer would revert to the orbital navigation mode described in Chapter 2 in order to establish initial conditions and timing of the transearth injection maneuver. This would normally be done in the final CSM orbit after the rendezvous and retrieval had been completed, provided that this orbit was high enough so that acceptable landmark and horizon measurements could be made by the CSM optics. If the CSM retrieval was made to a low altitude LEM parking orbit (Section 9.3.3.3), it might be necessary for the CSM to transfer to a higher orbit (i.e. 80 nm) where lower landmark tracking rates (10 mr/sec max) can provide accurate data for the orbit navigation made prior to transearth injection.

APPENDIX A

ERROR ELLIPSOIDS

If $\underline{\xi}$ is an n-dimensional error vector whose components have a probability distribution about a zero mean, then the following matrix C (the covariance matrix) can be defined:

$$C = E\left[\underline{\xi} \cdot \underline{\xi}^T\right]$$

The operator E, (expected value), averages over the n-dimensional probability distribution associated with the $\underline{\xi}$ vector.

If the error distribution is assumed to be Gaussian, then a family of n-dimensional ellipsoids having surfaces of constant probability density can be defined as follows:

$$\underline{\xi}^T C^{-1} \underline{\xi} = K$$

where K is an arbitrary constant.

The error ellipsoid corresponding to the probability p is the ellipsoid E_K for which the probability that $\underline{\xi}$ lies inside E_K is p. It can be shown that the probability is a function of the dimension and the constant K. Hence, given the dimension, and the desired probability the appropriate K can be determined.

The principal axes of the error ellipsoid can be described by the n vectors,

$$\sqrt{\frac{K}{\lambda_i}}\ \underline{x}_i$$

where the λ_i are the eigenvalues of C^{-1} and the $\underline{x}_i$ are the corresponding unit eigenvectors.

The same results can be obtained by computing the eigenvalues and eigenvectors of the matrix C rather than its inverse. In this case the principal axes are described by the n-vectors

$$\sqrt{K \lambda_i}\ \underline{x}_i$$

For the lunar landing and abort studies, the error vector $\underline{\xi}$ is six-dimensional, having three components of position error and three components of velocity error. For these studies a value of K was chosen such that the six-dimensional error ellipsoid contained 68.3% of the error vectors. In addition, two three-dimensional error ellipsoids were computed, one containing only position errors and the other only velocity errors. A value of K was chosen such that the position ellipsoid contained 68.3% of the position errors and the velocity ellipsoid 68.3% of the velocity errors. These three-dimensional ellipsoids can be considered as projections onto position and velocity space of a six-dimensional ellispoid containing 26% of the combined position-velocity errors.

In Table 1, values of K are given for two probabilities (0.6826 and 0.9974, commonly called 1σ and 3σ) and for various dimensions. Table 2 gives factors for converting 1σ ellipsoids of various dimensions to 3σ ellipsoids.

TABLE 1

VALUES OF K FOR p = 0.6826 (1σ) AND p = 0.9974 (3σ) FOR n = 1, 2, 3, 4, 6

n	$K_{1\sigma}$	$\sqrt{K_{1\sigma}}$	$K_{3\sigma}$	$\sqrt{K_{3\sigma}}$
1	1.0000	1.0000	9.0000	3.0000
2	2.2957	1.5152	11.8200	3.4380
3	3.5268	1.8780	14.1565	3.7625
4	4.7195	2.1724	16.2513	4.0313
6	7.0384	2.6530	20.0621	4.4791

TABLE 2

To convert 1σ ($p = 0.6826$) n-dimensional ellipsoids to 3σ ($p = 0.9974$) n-dimensional ellipsoids, multiply major axes by A:

n	A
1	3.00
2	2.27
3	2.00
4	1.86
6	1.69

APPENDIX B

DEVELOPMENT OF THE INTEGRAL OF THE THRUST ACCELERATION, SMOOTHING THRUST ACCELERATION, AND ESTIMATING EFFECTIVE EXHAUST VELOCITY

This appendix contains the development of a useful expression for the thrust acceleration of a constant-thrust, constant-massflow rocket engine. The integral of the thrust acceleration over a given time is also developed. Finally, a filter for smoothing thrust acceleration and estimating effective exhaust velocity is shown.

The fundamental scalar law of motion of a rocket-propelled vehicle is

$$m\, a_T = v_e\, \dot{m} \tag{B. 1}$$

where

$$v_e = g_e\, I_{sp} \tag{B. 2}$$

$$g_e = 32.174 \tag{B. 3}$$

$$\dot{m} > 0 \tag{B. 4}$$

If the mass flow $\dot{m}$ of the rocket is constant

$$m = m_o - \dot{m}\, t \tag{B. 5}$$

and Eq (B. 1) can be re-written as

$$a_T = v_e\, \dot{m}/(m_o - \dot{m}\, t) \tag{B. 6}$$

Dividing numerator and denominator of Eq (B. 6) by $\dot{m}$ yields

$$a_T(t) = v_e/(m_o/\dot{m} - t) \tag{B. 7}$$

It is undesirable to express $a_T(t)$ in terms of m_o and m because these quantities are difficult to measure on board the spacecraft. The quantity $(m_o/\dot{m})$ can be eliminated by evaluating Eq (B. 1) for t = 0 and dividing each side of the result by $\dot{m}\, a_T(0)$.

$$m(0)/\dot{m} = v_e/a_T(0) \tag{B. 8}$$

The quantity $v_e/a_T(0)$ has the dimensions of time. The following symbol is introduced

$$\tau = v_e/a_T(0) \tag{B. 9}$$

The quantity τ is sometimes called the "burnup time" because it is the time it would take a rocket that is all fuel (no structure) to consume itself completely. Thus the expression for the thrust acceleration of a constant I_{sp}, constant mass flow engine is

$$a_T(t) = v_e/(\tau - t) \tag{B. 10}$$

The integral of $a_T(t)$ from t = 0 to t = T_{go} is equal to ΔV

$$\Delta V = v_e \int_0^{T_{go}} dt/(\tau - t) = - v_e \ln (1 - T_{go}/\tau) \tag{B. 11}$$

Equation (B. 11) yields the theoretical or ideal (no gravity, no angle of attack) gain in speed of a rocket-propelled vehicle that burns for T_{go} seconds. This equation can provide the basis for T_{go} prediction. (It was used in making the transition from Eq (6. 36) to Eq (6. 37) in Section 6. 2. 3.)

The steering commands computed from the guidance equations of Chapter 6 are somewhat erratic if the IMU accelerometer outputs are noisy. This problem is made worse when IMU

accelerometer outputs are $\overline{\Delta V}$, which must be numerically differentiated to obtain $\underline{a}_T$. The quantization of ΔV introduces additional noise when ΔV is differentiated. There is a simple and effective method of smoothing thrust acceleration which results in the steering commands being well-behaved. It can be seen from Eq (B. 10) that $a_T(t)$ is inversely proportional to a linear function of time. Consequently, $1/a_T(t)$ is a convenient quantity to smooth.

$$1/a_T(t) = \gamma + \beta t \tag{B. 12}$$

$$\gamma = \tau/v_e \tag{B. 13}$$

$$\beta = -1/v_e \tag{B. 14}$$

Since the reciprocal of $a_T(t)$ is required in the steering law, there is no extra division required by forming $1/a_T$ after taking each accelerometer reading. The procedure is to fit the reciprocals of the a_T measurements to a straight line; i. e., estimate the parameters γ and β from a multitude of $1/a_T$ readings. Because of Eq (B. 14) v_e can be estimated from the $1/a_T$ filtering process.

APPENDIX C

EVALUATION OF THE DERIVATIVES OF H(t) AND h(t) FOR ASCENT GUIDANCE EQUATIONS

The time-to-go predictor derived in Section 6.2.3 required the evaluation of H(0), $\dot{H}(0)$, $H^{(2)}(0)$, etc. When the differentiation is straightforward and no approximations are made the derivatives are given without intermediate steps and without comments.

$$H_o = 1 \tag{C.1}$$

$$\dot{H}_o = -\dot{h}_o / r_D v_e \tag{C.2}$$

$$\ddot{H}_o = \dot{H}_o^2 - \ddot{h}_o / r_D v_e \tag{C.3}$$

$$H_o^{(3)} = \dot{H}_o^3 + 3 \dot{H}_o (-\ddot{h}_o / r_D v_e) - h_o^{(3)} / r_D v_e \tag{C.4}$$

$$H_o^{(4)} = \dot{H}_o^4 + 6 \dot{H}_o^2 \left[-\ddot{h}_o / r_D v_e \right] + 4 \dot{H}_o \left[-h^{(3)} / r_D v_e \right]$$

$$+ 3 \left[-\ddot{h}_o / r_D v_e \right]^2 - h_o^{(4)} / r_D v_e \tag{C.5}$$

(The superscripts in parentheses indicate powers of the differentiation operator).

The derivatives of the specific angular momentum must now be derived.

$$\dot{h}(t) = r\, a_T \cos \alpha \tag{C.6}$$

It is quite satisfactory to approximate Eq(C. 6) as follows

$$\dot{h}(t) \approx r_D a_T \cos \alpha \qquad \text{(C. 7)}$$

This approximation becomes more and more accurate as the vehicle approaches the time of thrust termination. Furthermore, the approximation is reasonable early in the flight because r(t) changes by only a small fraction throughout the flight.

It is easily verified that

$$d\, a_T/dt = a_T^2/v_e \qquad \text{(C. 8)}$$

Hence

$$\ddot{h}(t) \approx r_D (a_T^2/v_e) \cos \alpha - r_D a_T \sin \alpha\, \dot{\alpha} \qquad \text{(C. 9)}$$

$$\ddot{h}(t) \approx \dot{h}(t) (a_T/v_e) - r_D a_T \sin \alpha \dot{\alpha} \qquad \text{(C. 10)}$$

The only approximation made in Eq (C. 9) is the assumption that $r(t) = r_D$. This approximation results in the elimination of many terms which do not contribute very much to the prediction.

$$h^{(3)}(t) \approx 2\ddot{h}(t) (a_T/v_e) - r_D a_T \cos \alpha\, (\dot{\alpha})^2$$

$$- r_D\, a_T \sin \alpha \ddot{\alpha} \qquad \text{(C. 11)}$$

At this point is is convenient to introduce another approximation. The approximation is not necessary; but it introduces a great deal of simplification without a large sacrifice in accuracy

$$\ddot{\alpha}(t) \approx 0 \qquad \text{(C. 12)}$$

Then

$$h^{(3)}(t) \approx 2\ddot{h}(t)\, (a_T/v_e) - r_D a_T \cos \alpha (\dot{\alpha})^2 \qquad \text{(C. 13)}$$

$$h^{(4)}(t) \approx 3h^{(3)}(t)\,(a_T/v_e) + r_D a_T \sin\alpha\,(\dot{\alpha})^3 \qquad \text{(C. 14)}$$

Now the $h^{(n)}(t)$ must be evaluated at $t = t_o$, the current time.

$$d\,a_T/dt\Big|_{t=t_o} = a_{To}^{\,2}/v_e = a_{To}/\tau \qquad \text{(C. 15)}$$

The $h^{(n)}(0)$ are,

$$\dot{h}_o = r_D a_{To} \cos\alpha_o \qquad \text{(C. 16)}$$

$$\ddot{h}_o = \dot{h}_o/\tau - r_D a_{To} \sin\alpha_o (\dot{\alpha}_o) \qquad \text{(C. 17)}$$

$$h_o^{(3)} = 2\ddot{h}_o/\tau - \dot{h}_o \dot{\alpha}_o^{\,2} \qquad \text{(C. 18)}$$

$$h_o^{(4)} = 3\,h_o^{(3)}/\tau + r_D\, a_{To} \sin\alpha_o (\dot{\alpha}_o)^3 \qquad \text{(C. 19)}$$

Finally, the expressions for $h_o^{(n)}$ should be substituted into Eqs (C.1 - C. 5), and any possible algebraic simplifications carried out. Among the algebraic simplifications which result is the canceling out of all r_D's. This is not surprising because the approximations made are equivalent to stating that

$$d\,v_\theta/dt \approx a_T \cos\alpha \qquad \text{(C. 20)}$$

which is an approximation of

$$dv_\theta/dt = a_T \cos\alpha - \dot{r}\, v_\theta/r \qquad \text{(C. 21)}$$

This approximation is quite good because the ignored term is very small compared to $a_T \cos\alpha$.

REFERENCES

Chapter 1

1.1 MIT Instrumentation Laboratory Staff, System Status Report, MIT Report E-1142 (Rev. 18), March 1964, (C).

1.2 D.G. Hoag, M.B. Trageser, A Progress Report on the Apollo Guidance System, MIT Report R-388, December 1962, (C).

1.3 D.G. Hoag, Apollo Guidance and Navigation - A Problem in Man and Machine Integration, MIT Report R-411, April 1963, (C).

1.4 E.M. Copps, D.A. Koso, K. Nordtvedt, M.B. Trageser, The Horizon Photometer and Other Earth Parking Orbit G&N Measurements, MIT Report E-1353, May 1963, (C).

1.5 A.C. Spark Plug, Apollo G&N Equipment Familiarization Manual for CSM, Report ND-1021037, March 1964, (U).

1.6 A. Hopkins, R. Alonso, H. Blair-Smith, Logical Description for the Apollo Guidance Computer (AGC 4), MIT Report R-393, May 1963, (C).

1.7 A.L. Hopkins, Design Concepts of the Apollo Guidance Computer, MIT Report R-408, June 1963, (U).

1.8 E. Hall, General Characteristics of the Apollo Guidance and Navigation Computer, MIT Report R-410, May 1963, (C).

REFERENCES (Cont)

Chapter 1

1.9 R. Alonso, A.L. Hopkins, Apollo Guidance Computer, MIT Report R-416, August 1963, (U).

1.10 D.G. Hoag, Consideration of Apollo IMU Gimbal Lock, MIT Report E-1344, April 1963, (C).

1.11 Grumman Aircraft Engineering Corporation, Lunar Excursion Module Familiarization Manual, GAEC Report LMA 790-1, January 1964, (U).

1.12 Grumman Aircraft Engineering Corporation, Navigation and Guidance Subsystem Rendezvous Radar/Transponder and Landing Radar Sections Design Control Specification For, GAEC Report LSP-370-2A, November 1963, (C).

1.13 MIT Instrumentation Laboratory Staff, Radar Requirements for Primary Guidance and Navigation Operation, MIT Report R-404, April 1963, (C).

1.14 J.A. Strasser, Four-Beam Landing Radar Set for LEM, Electronics, Vol. 36, No. 6, February 7, 1964, (U).

Chapter 2

2.1 F.D. Grant, Command Module G&N System Performance for the Manned Lunar Landing Mission, MIT Guidance Monitor System Note #6 Rev. 1, March 19, 1964, (C).

2.2 R.H. Battin, A Statistical Optimizing Navigation Procedure for Space Flight, MIT Report R-341, Sept. 1961, Revised May 1962, (U).

Chapter 2

2.3 G. M. Levine, Application of Midcourse Guidance Technique to Orbit Determination, MIT Report E-1261, Dec. 1962, (U).

2.4 E. Denezza and M. Dittrick, Orbit and Landmark Determination During Lunar Orbit, MIT Thesis T-342, June 1963, (U).

2.5 D. W. Gilbert "Lunar Landmark Accuracy," Letter SGE (AC) to MIT dated October, 2, 1963, (U).

Chapter 3

3.1 R. H. Battin, A Unified Treatment of Powered Flight Guidance, MIT Space Guidance Analysis Memo #37, March 8, 1963, (U).

3.2 R. H. Battin, Universal Formulae for Conic Trajectory Calculations, MIT Report R-382, Sept. 1962, (U).

3.3 B. G. Sokkappa, Analytical Description of CSM Powered Flight Phases, MIT Space Guidance Analysis Memo #13-64, Feb. 1964, (U).

3.4 MIT Report R-404 (see 1.13)

3.5 GAEC Report LSP - 370-2A (see 1.12)

Chapter 4

4.1 J.G. Herriot, Methods of Mathematical Analysis and Computation, John Wiley & Sons, Inc., 1963, pp. 36-39.

4.2 D.G. Shepard, The Effect of Retrorocket Exhaust on Visibility During Lunar Touchdown, MIT Report R-391, Dec. 1962, (U).

Chapter 5

5.1 MIT Report R-404 (see 1.13)

5.2 S.J. Madden, Jr., Orbital Element Variation for a Body in Orbit Around the Moon, MIT Report R-387, July 1963, (U).

5.3 E.C. Lineberry, Comparison Between Direct Ascent and Parking Orbit Mode for Lunar Orbit Rendezvous, NASA MSC Memo for Chief, Mission Analysis Division, Dec. 30, 1963, (U).

Chapter 6

None

Chapter 7

7.1 D. Baker, N. Sears, J. Suomala, R. White, Lunar Orbit Determination by Star Occultations and MSFN Tracking, MIT Report E-1429, Sept. 1963, (U).

Chapter 7

7.2 MIT R-341 (see 2.2)

7.3 MIT R-404 (see 1.13)

7.4 E.S. Muller, Summary of b-Vectors for Radar Measurements, MIT Space Guidance Analysis Memo #43, May 7, 1963.

7.5 D.W. Gilbert, "Definition of LEM Terminal Rendezvous Model," Letter SGE(PMK) to MIT dated Dec. 3, 1963, (U).

DISTRIBUTION LIST

Internal

R. Alonso
J. Arnow (Lincoln)
D. Baker
R. Battin
E. Blanchard
P. Bowditch
A. Boyce
R. Boyd
R. Brown
P. Bryant
G. Cherry
E. Copps
R. Crisp
W. Crocker
G. Cushman
J. Dahlen
E. Duggan
J. Dunbar
K. Dunipace (MIT/AMR)
R. Euvrard
J. B. Feldman
P. Felleman
S. Felix (MIT/S & ID)
J. Flanders
J. Fleming
G. Fujimoto
L. Gediman
R. Goss
F. Grant
Eldon Hall
D. Hanley
W. Heintz
E. Hickey
D. Hoag
A. Hopkins
F. Houston
L. B. Johnson
M. Johnston
B. Katz
A. Koso
M. Kramer
W. Kupfer
A. Laats
A. LaPointe
J. Lawrence (MIT/GAEC)
T. Lawton
D. Lickly
R. Magee
G. Mayo
J. McNeil
R. McKern
R. Mudgett
James Miller
John Miller
J. Nevins
G. Nielson
J. Nugent
J. O'Connor
E. Olsson
C. Parker
W. Patterson
R. Phaneuf
J. Rhode
K. Samuelian
P. Sarmanian
W. Schmidt
R. Scholten
E. Schwarm
J. Sciegienny
N. Sears (15)
D. Shansky
J. Shillingford
W. Shotwell (MIT/ACSP)
T. Shuck
J. Sitomer
E. Smith
W. Stameris
J. Suomala
W. Tanner
R. Therrien
W. Toth
M. Trageser
R. Weatherbee
R. White
L. Wilk
R. Woodbury
W. Wrigley
D. Yankovich
B. Young
Apollo Library (1)
MIT/ IL Library (6)

External

(ref. PP1-64; April 8, 1964)

P. Ebersole (NASA/MSC)	(2)
W. Rhine (NASA/RASPO)	(1)
S. Gregorek (NAA S&ID/MIT)	(1)
T. Heuermann (GAEC/MIT)	(1)
AC Spark Plug	(10)
Kollsman	(10)
Raytheon	(10)
WESCO	(2)
Capt. W. Delaney (AFSC/MIT)	(1)

NAA RASPO:	National Aeronautics and Space Administration Resident Apollo Spacecraft Program Office North American Aviation, Inc. Space and Information Systems Division. 12214 Lakewood Boulevard Downey, California	(1)
FO:	National Aeronautics and Space Administration, MSC Florida Operations, Box MS Cocoa Beach, Florida 32931 Attn: Mr. B. P. Brown	(3)
HDQ:	NASA Headquarters 600 Independence Ave., SW Washington, D. C. 20546 MAP, E. T. Sullivan	(6)
AMES:	National Aeronautics and Space Administration Ames Research Center Moffett Field, California Attn: Library	(2)
LEWIS:	National Aeronautics and Space Administration Lewis Research Center Cleveland, Ohio Attn: Library	(2)
FRC:	National Aeronautics and Space Administration Flight Research Center Edwards AFB, California Attn: Research Library	(1)
LRC:	National Aeronautics and Space Administration Langley Research Center Langley AFB, Virginia Attn: Mr. A. T. Mattson	(2)
GSFC:	National Aeronautics and Space Administration Goddard Space Flight Center Greenbelt, Maryland Attn: Manned Flight Support Office Code 512	(2)

MSFC:	National Aeronautics and Space Administration George C. Marshall Space Flight Center Huntsville, Alabama Attn: R-SA	(2)
GAEC:	Grumman Aircraft Engineering Corporation Bethpage, Long Island, New York Attn: Mr. A. Whitaker	(1)
NAA:	North American Aviation, Inc. Space and Information Systems Division 12214 Lakewood Boulevard Downey, California Attn: Mr. R. Berry	(1)
GAEC RASPO:	National Aeronautics and Space Administration Resident Apollo Spacecraft Program Officer Grumman Aircraft Engineering Corporation Bethpage, L. I., New York	(1)
ACSP RASPO:	National Aeronautics and Space Administration Resident Apollo Spacecraft Program Officer Dept. 32-31 AC Spark Plug Division of General Motors Milwaukee, Wisconsin Attn: Mr. L. J. Lewandowski	(1)
WSMR:	National Aeronautics and Space Administration Post Office Drawer MM Las Cruces, New Mexico Attn: BW 44	(2)
MSC:	National Aeronautics and Space Administration Manned Spacecraft Center Apollo Document Control Group Houston 1, Texas 77058	(45)
	Mr. H. Peterson Bureau of Naval Weapons c/o Raytheon Company Foundry Avenue Waltham, Massachusetts	(1)
	Mr. C. Caminiti USAF - Quality Assurance 111 East 16th Street New York 3, New York	(1)
	Mr. H. Anschuetz UASF Contract Management District AC Spark Plug Division of General Motors Milwaukee, Wisconsin 53201	(1)